THE GEOLOGY, GEOCHEMISTRY AND U-Pb GEOCHRONOLOGY OF THE STOG'ER TIGHT GOLD PROSPECT BAIE VERTE PENINSULA, NEWFOUNDLAND

JAHANDAR RAMEZANI

THE GEOLOGY, GEOCHEMISTRY AND U-Pb GEOCHRONOLOGY OF THE STOG'ER TIGHT GOLD PROSPECT BAIE VERTE PENINSULA, NEWFOUNDLAND

by

Jahandar Ramezani

A thesis submitted to the School of Graduate Studies in partial fulfilment of the requirements for the degree of Master of Science

Department of Earth Sciences

Memorial University of Newfoundland

December 1992

St. John's Newfoundland

ISBN 0-315-96064-7

Canada

ABSTRACT

The Baie Verte Peninsula in Newfoundland is the locus of numerous gold occurrences and showings. The great majority of these epigenetic gold prospects are located in the vicinity of the Baie Verte Line, the major structural feature of the Peninsula, and its second (and higher) order splays. The Stog'er Tight prospect, the subject of this study, is a mesothermal, shear-hosted, gold occurrence which is located within the Point Rousse Ophiolite Complex, north of the Scrape Thrust, and to the east of the Baie Verte Line.

Gold mineralization in the Stog'er Tight prospect is hosted by a variety of subextrusive, gabbroic sills which have intruded a volcanic (and pyroclastic) sequence. The crystallization age of the Stog'er Tight gabbro is constrained by U-Pb zircon geochronology to be 483 +3/-2 Ma. The chemical composition of the Stog'er Tight gabbro and associated early volcanic lithologies reflects a progressive transition from island-arc to MORB and OIB-dominated magmatism, analogous to that in modern oceanic back-arc basins. The mineralization is structurally controlled and is characterized by pervasive and systematically zoned hydrothermal alteration. Four distinct alteration zones are identified based on dominant mineral assemblages. These include the chlorite-calcite zone, ankerite-sericite zone, chlorite-magnetite zone and the red albite-pyrite (+ gold) zone. The latter, which represents the highest intensity of alteration and gold mineralization, formed between an early episode of ductile deformation (D_E) and

a subsequent brittle-ductile (D_L) phase, within the D_I shear zones of the area.

Gold was precipitated as a result of shear zone-induced infiltration of fluids which reacted with the Fe-rich phases of gabbro to destabilize the gold-bearing complexes. Hydrothermal alteration involved progressive CO_2, S and K metasomatism as well as significant LILE, REE, HFSE and Th enrichments. These enrichments imply that the mineralizing fluids were in equilibrium with (or derived from) enriched continental crustal sources, as opposed to the commonly depleted oceanic rocks.

The hydrothermal alteration in the Stog'er Tight prospect has a U-Pb zircon age of 420 ±5 Ma. The mid-Silurian age of this hydrothermal zircon implies that gold mineralization in the Stog'er Tight prospect occurred at a final stage of Early Silurian orogenic activity in the Baie Verte Peninsula.

ACKNOWLEDGEMENT

This project could not have been initiated, or completed, without the help and concern of several individuals and organizations. First of all, I am deeply grateful to my supervisors, Mark Wilson and Greg Dunning, for providing me with a spectacular project to work on, and for their support, enthusiasm and thoughtfulness all through my attendance at Memorial University. They instilled in me a respect for science that is based upon sound observation, precision in work and careful interpretation. Their attention often went beyond the student-advisor relationships and it was a great pleasure for me to work with them. Noranda Exploration Company is gratefully acknowledged for providing access to their property, drill-cores, field-camp facilities and maps, and funding for analytical work. Financial support was received from a variety of sources including the Memorial University of Newfoundland Graduate Fellowship, Natural Sciences and Engineering Research Council grants to G. Dunning and M. Wilson and funding from Noranda Exploration Company. Brian Fryer is also thanked for his financial support for field work during the first year of the project.

I owe special thanks to my friends, colleagues and officemates, David Ritcey and Jim Weick, for their companionship during the years at school. David Ritcey helped me immensely with logistics in the field (especially when I was not mature enough to drive a rented vehicle!) and also at times that we had to prepare for a talk in the last few minutes. My special gratitude is due to Benoit Dube from Quebec Geoscience Centre and Alan Huard from Noranda Exploration Company for many useful discussions in the field and for familiarizing me with the subject. I also thank George Jenner, Brian Fryer, and Toby Rivers (Department of Earth Sciences) and Scott Swinden (Newfoundland Department of Mines and Energy) for their comments and advice.

Beverly Chapman, Daryl Clarke, Pamela King and Henry Longerich are thanked for their support and help with XRF and ICP-MS analyses. ICP-OES analyses at the Department of Mines and Energy were carried out by Chris Finch who is specially thanked. Undergraduate students Roger Marsh and Krista Parsons are also thanked for their field assistance.

Last but not the least, I would like to thank my parents who have been a constant source of emotional and financial support for me, and I appreciate their attention, encouragement and thoughtfulness during all those years at school.

TABLE OF CONTENTS

FIGURES

TABLES

CHAPTER 1: INTRODUCTION

1.1 MESOTHERMAL GOLD DEPOSITS

Gold deposits are widely dispersed in time and space, from Archean cratons to the modern orogenic belts. They also occur in a variety of geologic settings and in virtually all types of rocks. About 2/3 of all the gold produced in the world has been extracted from alluvial placers such as the giant Witwatersrand paleoplacer deposit. Gold is also produced as a by-product of many volcanogenic massive sulphide (VMS) and porphyry systems, which are the major sources of syngenetic gold. The vast majority of epigenetic Au-Ag vein deposits are associated with mesothermal and epithermal systems, while shear-hosted mesothermal gold deposits are second only to placers, in terms of cumulative production (Keays & Skinner, 1989).

Despite the diverse geologic settings and rock associations of gold deposits, they do not seem to be uniformly distributed throughout geologic history. Two distinct metallogenic periods have been defined. The first is the Late Archean Era, during which the great deposits of the greenstone belts and the Witwatersrand were produced, and the second is Phanerozoic, which starts

in the Mesozoic and continues to the present. The latter incorporates the widespread gold deposits of the North American Cordillera and Southwest Pacific. The Proterozoic and Paleozoic deposits are notably sparse, indicating a long time gap between the two metallogenic epochs (Keays & Skinner, 1989).

Mesothermal Au-Ag vein deposits are preferentially associated with major cross-cratonic structures, which normally can be traced at surface for several hundreds of kilometres. Two of the best-documented examples within the Superior Province of Canada are the Destor-Porcupine, and Kirkland Lake-Cadillac-Bouzan fault systems in the Abitibi Subprovince. Shear-hosted mesothermal Au-Ag systems are characterized by: 1) brittle-ductile mode of deformation, 2) a diverse variety of host rocks, 3) a diagnostic element association consisting of enhanced concentrations of LILE (large ion lithophile elements), B, W, As, Sb, Se, Te, Bi, Mo, and systematically low abundances of Cu, Pb and Zn, 4) alteration dominated by quartz, albite, carbonate, muscovite, pyrite and tourmaline, and an absence of advanced argillic alteration, 5) ambient mineralization temperatures of $\approx$300°C (up to 450°C) and $P_{fluid} \geq P_{lithostatic}$, 6) Au/Ag ratio averaging 5 and, 7) restricted ranges of $\delta^{18}O$ quartz, $\delta^{13}C$ carbonate and Sr and Pb isotopic signatures within individual deposits, albeit with a geographic provinciality (Kerrich, 1989a & 1990). The epithermal Au-Ag deposits, in contrast, are distinguished from mesothermal deposits by their dominant brittle deformation of host rock, minor or no carbonates, the presence of advanced argillic alteration, temperatures generally $\leq$ 300°C, P

$_{fluid} = P_{lithostatic}$, Au/Ag ratio $\leq$ 5 and $\delta^{18}O$ quartz values conspicuously lower than those of mesothermal deposits. Their mutual differences reflect a strong depth discrimination between mesothermal and epithermal environments (Kerrich, 1989a).

The study of modern geothermal systems has provided important insights into the genesis of epithermal gold deposits. The epithermal systems are usually driven by hot, high-level magmatic bodies that generate upwelling plumes of magmatic and/or meteoric water. The genesis of mesothermal gold deposits, however, has perhaps been the most controversial of any kind of gold deposit. Several models have been proposed for the origin of mesothermal Au-Ag vein systems, including, lateral secretion, exhalative processes, multistage exhalative-remobilization, tonalite-trondhjemite-granodiorite magma suites, oxidized felsic magmas, lamprophyres, mantle degassing-granulitization, meteoric water circulation, and focused discharge of metamorphic fluids (see Kerrich, 1990 and references therein). Nevertheless, mesothermal gold deposits of all ages, from Archean to Cenozoic, have similar structural, mineralogical and geochemical characteristics, implying a singular, rather than multiple, genetic process (Kerrich, 1990).

The largest mesothermal Au-Ag deposits occur in Archean greenstone belts of present North and South American (*e.g.* Superior Province), Australian (Yilgarn Block), South African, Indian and Russian shield areas. The greenstone belts, such as those in the Archean Superior Province, include variably deformed and low-grade metamorphosed sequences of dominantly volcanic

lithologies. These supracrustal sequences are composed of tholeiitic-komatiitic to calc-alkaline volcanic rocks overlain by flyschoid, turbiditic sedimentary rocks, and are interpreted as allochthonous, island-arc sequences. The supracrustal sequences have been intruded by syn- to post-volcanic, granitoid plutons (*e.g.* Corfu *et al.*,1989) and, together, they comprise "granitoid-greenstone terranes". The latter generally intervene with belts of metasedimentary and tonalitic (high-grade) gneisses, which are separated from granitoid-greenstone terranes by major crustal structures. The widely accepted models for the tectonic evolution of granite-greenstone belts involve successive accretion of oceanic terranes (and outboard continental fragments) by subduction at destructive continental margins, concomitant with arc magmatism and with the outward progradation of the arc-trench system which results in advancement of the magmatic arc into previously accreted material. Major crustal underplating by arc magmatism and/or tectonic crustal thickening during collisional events, followed by late tectonic uplift, have also been incorporated in the more recent models (see Hoffman, 1990). Proterozoic granite-greenstone terranes, despite subtle differences, share many tectonic characteristics with the Archean analogues. The well-preserved, Paleozoic belts in central Newfoundland and eastern Australia also resemble the granite-greenstone terranes, though whether identical processes were involved in the tectonic evolution of the older belts remains unclear.

Precise geochronologic studies in greenschist-facies domains of the greenstone belts have indicated that there is a close temporal relationship

between granitoid plutonism, deformation, peak of regional metamorphism and late uplift in most areas (see Chapter 9). Accordingly, the great majority of genetic models for the greenstone gold deposits involve subduction-driven accretion, deformation and metamorphism as the result of collisional tectonism and cratonization (Keays & Skinner, 1989), though there is a general consensus that gold mineralization occurred relatively late in the evolution of the greenstone belts. Recent direct dating of various gold-related hydrothermal minerals by different isotopic techniques suggests that, in general, gold might be significantly younger than any of the related geologic events (see Chapter 9). This late timing often raises the question of whether or not gold mineralization should be considered as an integral part of the last stages of greenstone belt evolution.

Mesozoic and younger mesothermal gold deposits of the North American Cordillera (*e.g.* Mother Lode of California and Juneau of southeastern Alaska) share many of the geologic characteristics of their Archean equivalents. The Cordillera consists of allochthonous terranes and oceanic crustal fragments accreted to the North American continent, in addition to the Proterozoic and Paleozoic continental margin miogeoclinal sedimentary units. Regional-scale, deep seated, strike-slip faults which bound the allochthonous terranes exert the most important control on the Cordilleran mesothermal deposits. Also, no direct association is observed between mesothermal gold mineralization and any kind of magmatism in these deposits (Keays & Skinner, 1988). The conjunction of terrane accretion, subduction, metamorphism, transpression, magmatism, uplift,

and late-kinematic mesothermal gold has also been documented in the Cordillera (Kerrich & Wyman, 1990).

1.2 GOLD METALLOGENY IN NEWFOUNDLAND

Gold has been traditionally produced in Newfoundland as a by-product of volcanogenic (syngenetic) massive sulphide (VMS) deposits. VMS deposits are most abundant in lower Paleozoic volcanic and volcaniclastic sequences of Newfoundland Dunnage Zone. Buchans, Rambler and Duck Pond-Tally Pond are among the largest of these gold-bearing VMS deposits (Tuach *et al.*,1988).

The 1980's were marked by a substantial increase in exploration for epigenetic gold in Newfoundland. These economically significant deposits incorporate a variety of alteration/mineralization styles and environments (Tuach *et al.*,1988), though they are all characterized by low sulphide (and base-metal) contents when compared to syngenetic gold deposits. Scattered epigenetic gold occurrences have been discovered in the Precambrian rocks of the Newfoundland Avalon Zone, as exemplified by the Hickey's Pond Prospect on the Burin Peninsula. They are generally characterized by high-alumina (pyrophyllite), silica, sericite and argillic alteration, and are inferred to have been produced by Late Hadrynian, high-level, epithermal-fumarolic systems (Huard & O'Driscoll, 1985).

The great majority of epigenetic gold occurrences in Newfoundland, however, are concentrated in the Cambro-Ordovician rocks of the Central

Volcanic Belt (Dunnage Zone), genetically related to, and structurally controlled by, major faults and lineaments of the Appalachian Orogen (Tuach, 1988; Dubé, 1990). The association of gold mineralization with major fault systems, and also the contrasting structural influence on its genesis, are especially well represented by examples from the western and eastern boundaries of the Dunnage Zone (Dubé, 1990; Evans, 1992).

Dubé (1990) divided the gold-only deposits of Newfoundland into two major types: a) disseminated stratabound sulphide gold deposits, and b) mesothermal vein type deposits. The former type, as represented by the Hope Brook mine in southwestern Newfoundland, contains disseminated gold associated with abundant sulphide in stratabound mineralized zones. Although the Hope Brook deposit is located within a major deformation zone (Cinq Cerf fault zone), it seems to be more deformed by the fault zone than being genetically related to it (Dubé, 1990).

The mesothermal (vein type) deposits, in contrast, are the most common type of gold-only mineralization in Newfoundland, and these share many features with the typical Archean lode gold deposits. They have strong genetic relations to structural deformation. Dubé (1990) further subdivided these deposits into 1) quartz vein type, and 2) altered wallrock type mineralization. Most of the shear-hosted mesothermal gold deposits in the Western Dunnage Zone, such as the Cape Ray deposit, fall in the first category. Gold mineralization in the Cape Ray deposit occurs in sulphide-rich quartz veins hosted by shear zones (Main Zone) and also in veins and stockwork hosted by

the Windowglass Hill granite (Wilton, 1983). The Main mineralized zone is located in an oblique splay of the main Cape Ray fault.

Quartz vein-hosted mesothermal gold deposits are abundant in the western White Bay area (*e.g.* Browning Mine), Baie Verte Peninsula (*e.g.* Deer Cove) and the Springdale Peninsula (*e.g.* Rendell-Jackman). All prospects are closely associated with major geologic structures (*e.g.* Doucers Valley Fault, Baie Verte Line and Green Bay Fault), but are localized in second and third-order structures subparallel to the main lineaments. In general, mineralization occurs in extension veins and stockwork breccias hosted by brittle to brittle-ductile structures (Dubé, 1990).

In the altered wallrock type of mesothermal gold deposits, quartz veins are a minor component (5%) and mineralization occurs mainly in the altered host rock(s), which are replaced by secondary minerals such as iron carbonate, sericite, albite and pyrite. The only reported example of this type in Western Newfoundland is the gabbro-hosted Stog'er Tight gold prospect on the Baie Verte Peninsula (Dubé, 1990; this study).

Structurally controlled, epigenetic gold occurrences have also been discovered in the eastern Dunnage zone, including those in the Victoria Lake, Bay d'Espoir and eastern Notre Dame Bay areas. These are generally hosted by Paleozoic rocks, and both epithermal and mesothermal styles of mineralization have been identified (Evans, 1992). Intense Fe-carbonate, silica, sericite, pyrite and arsenopyrite alteration in a variety of host rocks, along with widespread As and Sb anomalies, are characteristic of many mesothermal deposits in the

eastern Dunnage Zone. Gabbroic rocks, lithologically similar to those in the western Dunnage Zone, are suggested to be the most prolific host to mesothermal gold mineralization in that area (Evans, 1992).

1.3 SCOPE AND PURPOSE OF THE STUDY

The subject of this study, the Stog'er Tight gold prospect, occurs within the Lower Paleozoic oceanic rocks of the Baie Verte Peninsula, at the northern terminus of the North American Appalachian Orogen. The Baie Verte Peninsula has long been a centre of mineral exploration and production. Since 1864, the peninsula has been host to nine producing mines of base and precious metals and asbestos (Hibbard, 1983). Several precious metal occurrences have also been discovered in the area, over the past decade. All of the mines and the majority of mineral showings occur within the ophiolitic and/or closely associated rocks of the peninsula.

In the last two decades, the Baie Verte area has also been the subject of extensive academic research, as it provides an excellent example for the application of plate tectonic models to ancient orogens such as the Appalachians (*e.g.* Williams & St-Julien, 1982; Hibbard, 1983 and Jamieson, 1992). The most significant tectonic feature of the Baie Verte Peninsula is the juxtaposition of two contrasting lithotectonic units, the Fleur de Lys belt and the Baie Verte belt, along the Baie Verte Line (Chapter 2). This feature, which is attributed to Paleozoic accretionary tectonism along the North American

eastern continental margin, has rendered the Baie Verte Peninsula a favourable environment for epigenetic gold mineralization. The area around the northernmost land exposure of the Baie Verte Line (known as the Baie Verte flexure), in particular, is the locus of several shear-hosted gold occurrences, such as the Albatross, Dorset, Pine Cove, Deer Cove and Stog'er Tight prospects. These prospects are structurally related to the Baie Verte Line or its second- and higher-order splays like the Scrape Thrust and the Deer Cove Thrust (Dubé, 1990). The genesis of these occurrences and their relation to the geologic evolution of the area, would have significant implications for gold metallogeny in the Baie Verte Peninsula, as well as in the Western Newfoundland.

This work presents an integrated geologic, geochemical and isotopic study on the nature and genesis of gold mineralization in the Stog'er Tight prospect, Baie Verte Peninsula. The geometry, petrology and age of the Stog'er Tight gabbro, the main host to mineralization, have been determined, based on field observations, petrography, geochemistry and U-Pb zircon geochronology. Petrography and a variety of mineral identification techniques were employed to define the different mineral assemblages produced as a result of hydrothermal alteration associated with gold mineralization. The chemical effects of the progressive alteration of the host gabbro were then assessed, using major and trace element geochemistry of the alteration assemblages. Finally, the age of hydrothermal alteration (and gold mineralization) was constrained by U-Pb dating of appropriate hydrothermal mineral phases. Overall,

this study aimed to specifically tackle the following problems:

1) the origin and geologic setting of the Stog'er Tight host gabbro,

2) the physicochemical conditions of the alteration-mineralization process(s),

3) the mechanical and chemical controls of the host rock on gold deposition and,

4) the timing of the gold mineralization event with respect to the host rock formation, metamorphism and deformation.

The final goal of the present thesis was to integrate the results of this study with available geologic and geochronologic data from other areas, in order to establish a genetic model for gold mineralization in the Stog'er Tight deposit, in the context of tectonic evolution of the Baie Verte Peninsula.

The relatively simple structure of the Stog'er Tight deposit, the singularity of its host rock, and its widespread and consistent hydrothermal alteration, make this deposit favourable for an alteration study. The numerous drill-holes available for this study have constrained the geometries of the gabbro sills and the alteration/mineralization intervals, and have recovered several complete sections across the alteration zones. Furthermore, the identification of hydrothermal zircon in the strongly altered gabbro has permitted the direct age determination of the alteration/mineralization event, and can be regarded as the most significant feature of the Stog'er Tight deposit.

The results of this integrated study allow a general comparison between the Stog'er Tight deposit and some of the most typical and best-studied mesothermal gold deposits of the Archean Eon, in terms of mineralization processes and tectonic setting. Essentially, the geological settings of Phanerozoic mesothermal gold deposits are better constrained, as compared to those of their Archean counterparts, mainly because of questionable plate tectonic processes in Archean. The northwestern sections of Newfoundland's Central Volcanic Belt and the Baie Verte Peninsula, in particular, represent a structural cross-section from the allochthonous oceanic terranes (Dunnage Zone) to the continental margin platform and basement (Humber Zone, see Chapter 2). Comparisons between mesothermal gold occurrences in such well-defined geologic settings and the classical Archean lode gold deposits can examine, and further refine, models involving gold mineralization in Archean settings, and their applicability to gold metallogeny in younger orogens such as the Appalachians and the Cordilleras.

1.4 METHODS AND PROCEDURES

This thesis project started with mapping of major lithologic units and hydrothermal alteration in outcrops and trenches, together with examination of drill-cores, in the eastern Stog'er Tight prospect area. More than 4000 meters of drill-core were carefully logged and all of the 14 trenches in the study area were mapped. A total of 266 thin-sections were prepared from selected trench

and drill-core samples for petrography. Mineral identification was performed using mainly conventional optical (petrographic) methods, and was further enhanced by scanning electron microscope semi-quantitative analysis and by X-ray powder diffractometry on separated mineral fractions.

Whole-rock samples of different rock types and from a variety of hydrothermal alteration assemblages were analyzed for major and trace element contents by standard methods of atomic absorption spectrophotometry (AAS), inductively coupled plasma optical emission spectroscopy (ICP-OES), X-ray fluorescence spectroscopy (XRF), and inductively coupled plasma mass spectrometry (ICP-MS).

The concentrations of major oxides lighter than phosphorus (SiO_2, Al_2O_3, MgO and Na_2O) were measured by AA at Memorial University Department of Earth Sciences, or by ICP-OES at Newfoundland Department of Mines and Energy, as the precision of XRF analyses for these elements are relatively low. No standard or duplicate analyses were included in the AAS results, so that the precision and accuracy of its analyses, though suggested to be better than those of XRF, are not clear. The precision of ICP-OES analyses, as indicated by duplicates, are approximately 0.4% RSD for SiO_2 and are better than 0.25% for Al_2O_3, MgO, and Na_2O.

The major elements TiO_2, CaO, MnO, K_2O and P_2O_5, as well as trace elements Cr, Ni, Sc, V, Cu, Zn, S, Rb, Sr, Nb, Zr, and Y were analyzed by an ARL 8420 X-ray fluorescence spectrometer at Memorial University Department of Earth Sciences. In general, the precision for TiO_2, Sr and Zr is better than

0.4%, for V, Y and Nb it is about 1.2%, and for Rb it is better than 3%.

The concentrations of Ba, Hf, Th and the rare earth elements (REE) were measured by ICP-MS at Memorial University Department of Earth Sciences. Samples were dissolved using the sodium peroxide sinter method, the analytical technique of which is described in Longerich *et al.* (1990). Briefly, the precision for Ba, Hf and Th is approximately 4% RSD, and for REE it is between 4 and 2%. For samples without ICP-MS data, the Ba, Th and Ce values were taken from lower-precision XRF analyses (see Appendices II & III).

Finally, the U-Pb age determinations for this study were based on the improved isotope dilution method and the measurement of isotopic ratios by the thermal ionization (solid source) mass spectrometer. The detailed analytical procedures are described in Chapter 9.

1.5 LOCATION AND ACCESS

The Stog'er Tight gold prospect, known as the Bradly-North property, was a joint venture by Noranda Exploration Co.(Ltd.) and Impala International Resources (at the time of this study). It is located at the northern part of the Baie Verte Peninsula, at latitude 49°58' north and longitude 56°04'west, on the Baie Verte NTS map sheet (12 H/16). Access to the Stog'er Tight prospect is along the Baie Verte Highway (410), La Scie Highway (414) and Ming's Bight Road (418). An unpaved road (known as the Deer Cove Road) that branches off the Ming's Bight Road about 1.5 km southwest of the community of Ming's Bight passes by the property. Two logging roads and a network of trails provide

access to drill-holes and trench outcrops of the Stog'er Tight prospect.

The mineralized zones of the Stog'er Tight prospect are located along the northern flank of a gentle, ENE-WSW trending rise. The rise is at most 600 ft above sea level and is bordered to the north by a subparallel depression that encloses Fox Pond and Camp Pond. Surface exposure is generally poor in the area and the bedrock is mostly buried under dense forest and swamps.

The Stog'er Tight property consists of 4 mineralized zones (Fig.1-1) that from east to west are: the Magnetic Zone, Stog'er Tight Zone, Gabbro Zone (including its east and west extensions) and the Cliff Zone, with a total strike-length of 1500 m. This study has focused on the Stog'er Tight and Magnetic Zones that cover an area of 0.14 km^2, at the east-central part of the prospect (Fig.1-1).

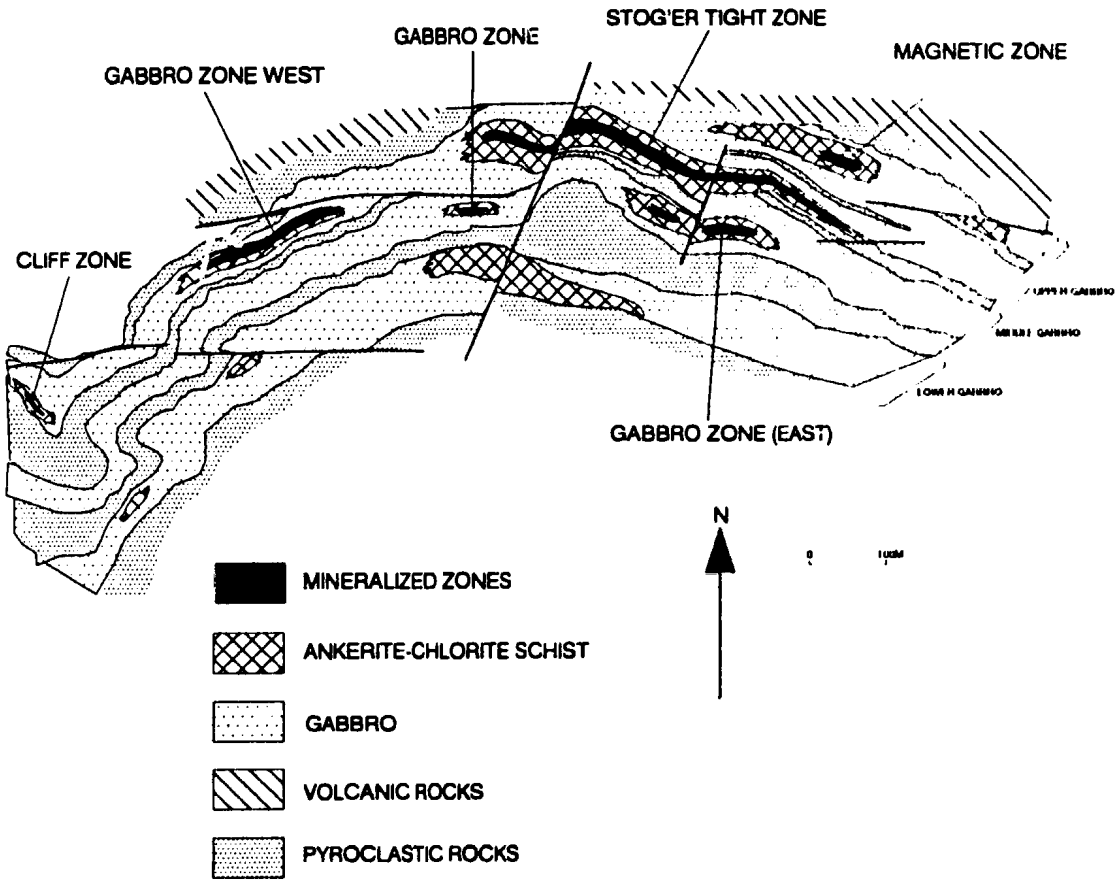

Figure 1-1: Simplified geological map of the Stog'er Tight prospect.
(After Kirkwood & Dubé, 1992)

1.6 EXPLORATION HISTORY

Gold was first discovered in Stog'er Tight area in 1987, when the exploration activities were heavily focused on the nearby Deer Cove prospect (Noranda Exploration-Galveston Resources). Preliminary prospecting directed by soil geochemistry discovered gold mineralization in an unmapped gabbro body which now comprises the Gabbro Zone of the Stog'er Tight deposit. Diamond drilling indicated very restricted mineralization in this zone. However, the identification of this new style of mineralization in the area focused the exploration efforts and led to the July, 1988 discovery of a significantly larger zone of mineralization, the Stog'er Tight Zone. The zone has a WNW-ESE extension, dips moderately north and was systematically trenched for over 450m along its strike. Channel samples up to 23.0g/t Au over 7.0m, and grab samples up to 115.3g/t Au were returned (Huard, 1990). Further exploration discovered the Magnetic Zone and the Cliff Zone at the eastern- and westernmost parts of the property.

Diamond drilling on the property to date exceeds 8000m in 80 holes, and indicates that the average ore grade is 5.5g/t Au over 4.5m. The highest measured ore grade in drill-core is 68.0g/t Au over 0.6m.

CHAPTER 2: REGIONAL SETTING AND GENERAL GEOLOGY

2.1 INTRODUCTION

Newfoundland is part of the Appalachian Orogen of Eastern North America. Rocks of the Appalachian Orogen, in general, range in age from late Precambrian to early Mesozoic; the Middle Ordovician and older lithologies show sharp contrasts in thickness, facies, and structural style in different parts of the orogen. This realization has led to several subdivisions of the Canadian Appalachians into distinct stratigraphic-tectonic zones which are mainly based upon the well-exposed coastal section of northeast Newfoundland (Williams, 1979 and references therein). The subdivision of widest usage is that of Williams (1979), which includes the Humber, Dunnage, Gander and Avalon zones, from west to east, across the orogen (Fig.2-1).

The generally accepted model for the development of the Canadian Appalachians involves the generation and subsequent destruction of a late Precambrian-Early Paleozoic Iapetus Ocean (Wilson, 1966; Dewey, 1969; Williams, 1979) which once separated the Laurentia and Gondwana continents. Thus, the Humber Zone records the development and destruction of an Atlantic-

type continental margin off Eastern North America which was underlain by Grenville basement; the Dunnage Zone represents vestiges of Iapetus Ocean (including island arc sequences), and the Gander and Avalon zones are interpreted as ancient continental margin and platform (Pan-African), which lay to the east of Iapetus. The Dunnage, Gander and Avalon zones are interpreted as three contrasting suspect terranes (megaterranes) of the Appalachian Orogen (Williams and Hatcher, 1983), the exact geologic relationships of which to the North American miogeocline (Humber Zone) are uncertain. Large-scale structural breaks separate these terranes from each other and from the miogeocline.

The major phase of tectonic deformation which led to the closure of Iapetus ocean, the destruction of its continental margins, and the emplacement of oceanic allochthons onto the North American continental margin, is attributed to the Middle to Late Ordovician Taconic Orogeny. Along the eastern margin of the Humber Zone and adjacent parts of the Dunnage Zone, the Taconic Orogeny is manifested by west-facing structures (*e.g.* Baie Verte-Brompton Line) associated with plate collision and ophiolite obduction.

The tectonic style of the Silurian-Devonian development of the Appalachian Orogen contrasts with that of Cambrian and Ordovician times (Williams, 1979). This period is marked by plutonism, metamorphism and deformation which cannot be directly related to the earlier Paleozoic zonation and the structural trends of the orogenic system. The major phase of post-Taconian tectonism in Newfoundland has been traditionally interpreted as Acadian Orogeny (Early Devonian). However, a widespread orogenic event of

Silurian age has been identified which post-dated the Taconian Orogeny, though it was complete prior to the Devonian (Acadian) deformation (Karlstrom et al.,1982; Dunning et al., 1990). Silurian Orogeny involved magmatism, metamorphism, deformation and the generation of terrigenous sediments from the uplifted orogenic belt.

2.2 DUNNAGE ZONE

The Dunnage Zone (also called the Central Volcanic Belt) is a wide composite terrane of the Newfoundland Appalachians (maximum 150 km). It is noted for its Ordovician ophiolite suites and volcanic rocks which are highly variable and distinctive across the northeast coastal section. The boundary of the Dunnage zone with the Humber Zone (miogeocline) to the west is the Baie Verte-Brompton Line. The Ordovician or earlier(?), dominantly metaclastic rocks of the Gander Zone are subdivided into three subzones (Gander Lake, Mount Cormack and Meelpaeg, Fig.2-1), which occur to the east and within the Dunnage Zone (Williams et al., 1988). In southwest Newfoundland, zonal relationships are complicated, the Dunnage Zone is narrow and the whole area is affected by numerous intrusions, as well as high grade regional metamorphism.

In central and northeastern Newfoundland, the Dunnage Zone is dominated by thick and structurally disrupted sequences of mafic to felsic volcanic rocks, volcaniclastic rocks and ophiolite suites. These rocks represent vestiges of the Iapetus ocean, which were accreted to the ancient North

American continental margin during Ordovician time and were subjected to deformation (*i.e.* folding and strike-slip faulting) due to later orogenic events (*e.g.* Williams, 1979, Kean et al.,1981). The thick volcanic and volcaniclastic sequences were generally interpreted by earlier workers (Bird & Dewey, 1970) to represent ancient island arcs formed upon the oceanic crust by subduction, prior to the final plate collision and ocean basin closure. Accordingly, the earlier models for the tectonic history of central Newfoundland assumed a simple, two-stage history: 1) the early opening of Iapetus in the Late Precambrian and Early Cambrian as recorded by the formation of MORB-like ophiolite suites, and 2) the subsequent closing of the ocean by eastward subduction (Bird & Dewey, 1970) in the Ordovician, concomitant with the development of overlying marine volcanic/volcaniclastic sequences of island arc affinity. However, more recent studies have revealed greater complexity in the tectonic history of the oceanic rocks in the Newfoundland Dunnage Zone.

Precise geochronological data from a number of ophiolite suites in central Newfoundland (*e.g.* Bay of Islands, Annieopsquotch, Betts Cove, Pipestone Pond and Coy Pond complexes; Dunning & Krogh, 1985) clearly indicate that the ophiolite sequences cover a narrow age range in the Early Ordovician. Further detailed geochemical and geochronological studies have revealed that at least three of the arc-related volcanic/volcaniclastic sequences, including the Victoria lake Group (Dunning et.al.,1987; Dunning et.al., 1991), Little Port Complex (Dunning & Krogh, 1985) and the Twillingate Trondhjemite predate the earliest known ophiolitic rocks in central Newfoundland. These undoubtedly

indicate that arc magmatism was widespread in Iapetus for a considerable time period prior to the generation of the ophiolites now preserved in the Dunnage Zone. Moreover, it is shown that many of these arc-related sequences, in fact, incorporate variable source components and record complex magmatism in both island arc and non-arc settings (Jenner & Fryer, 1980; Swinden *et al.*,1990) which is comparable to magmatism in the modern back-arc environments. Together, these data have formed the basis for a recently held notion that the Newfoundland Dunnage Zone does not record the opening of the major ocean basin of the Iapetus, but rather the generation and destruction of a complex series of island arc-related peripheral basins, at the margins of Iapetus.

The ophiolite-based sequences of the Dunnage Zone appear to be allochthonous relative to the adjacent Humber and Gander zones. The Late Precambrian basement rocks that occur to the south of the Dunnage Zone in southeastern Newfoundland, together with the Precambrian rocks of the adjacent Avalon Zone, are interpreted as parts of a larger Pan-African crustal block that was first juxtaposed with Iapetan deposits (Dunnage) in the early Paleozoic (O'Brien et al., 1991). The northeast Newfoundland seismic line, together with marine reflection profiles of the Canadian Appalachians indicate that a western crustal block (Laurentian) meets, or almost meets, an eastern crustal block (Pan-African?) beneath the central Dunnage Zone. The Red Indian Line may be the surface projection of that deep crustal suture.

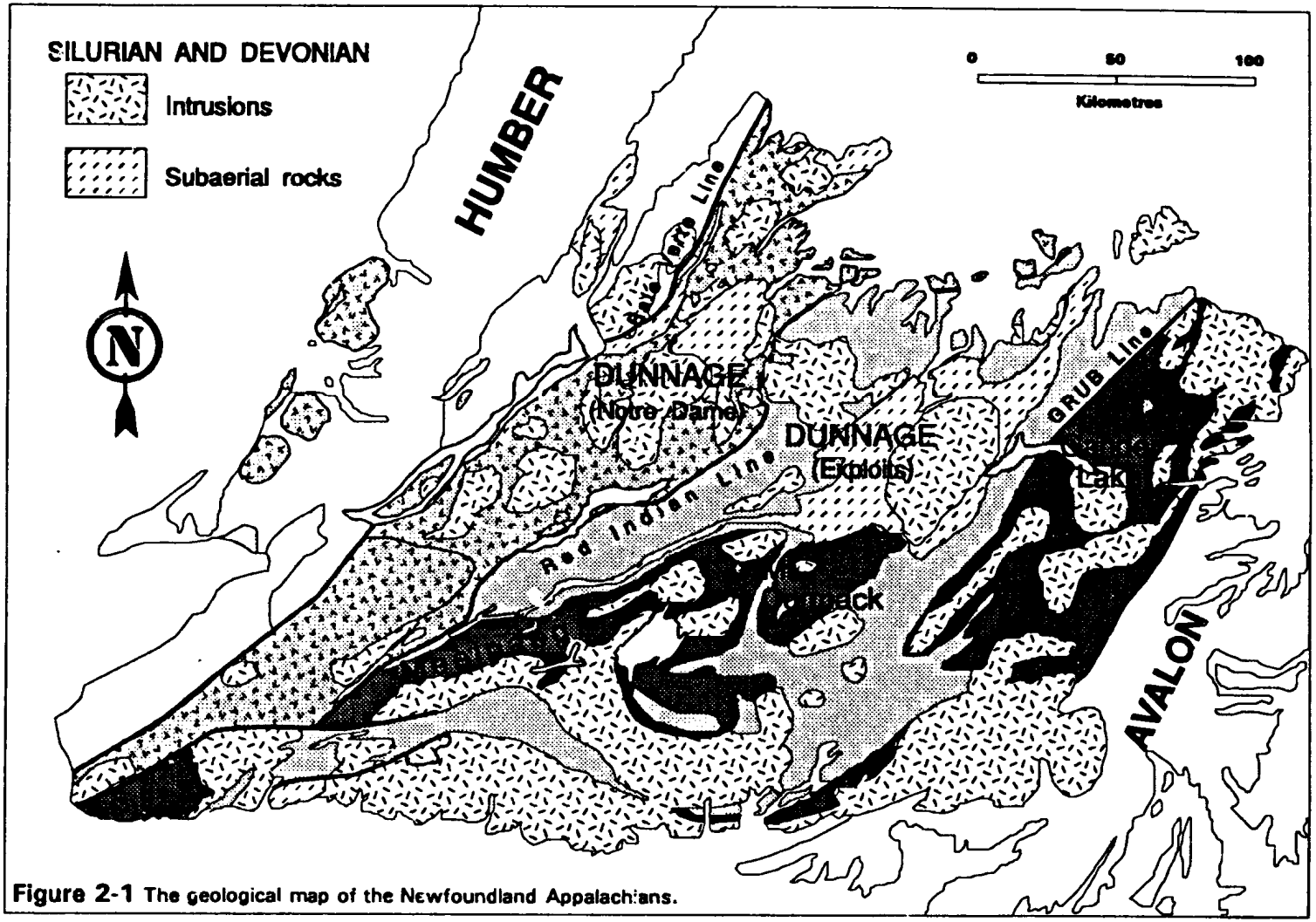

Figure 2-1 The geological map of the Newfoundland Appalachians.

2.3 BAIE VERTE PENINSULA

Baie Verte Peninsula is located along the rugged north coast of Newfoundland, and represents the northernmost land exposure of the Appalachian Dunnage Zone (Fig.2-1). The Baie Verte Peninsula exposes rocks of both the Humber and Dunnage Zones. A continuous and relatively well-exposed contact between the Paleozoic margin of North America and the ancient oceanic vestiges of Iapetus, *i.e.* the Baie Verte Line, is exclusive to this area. Regardless of its structural and lithologic complexities, the Baie Verte Line is the most prominent and fundamental structural feature of the Baie Verte Peninsula (Fig. 2-2). The Line divides the peninsula into two contrasting lithologic terranes. These are termed informally the Fleur de Lys Belt which lies to the west and north of the Line, bordered by the Baie Verte Belt to the east and south (Hibbard, 1983).

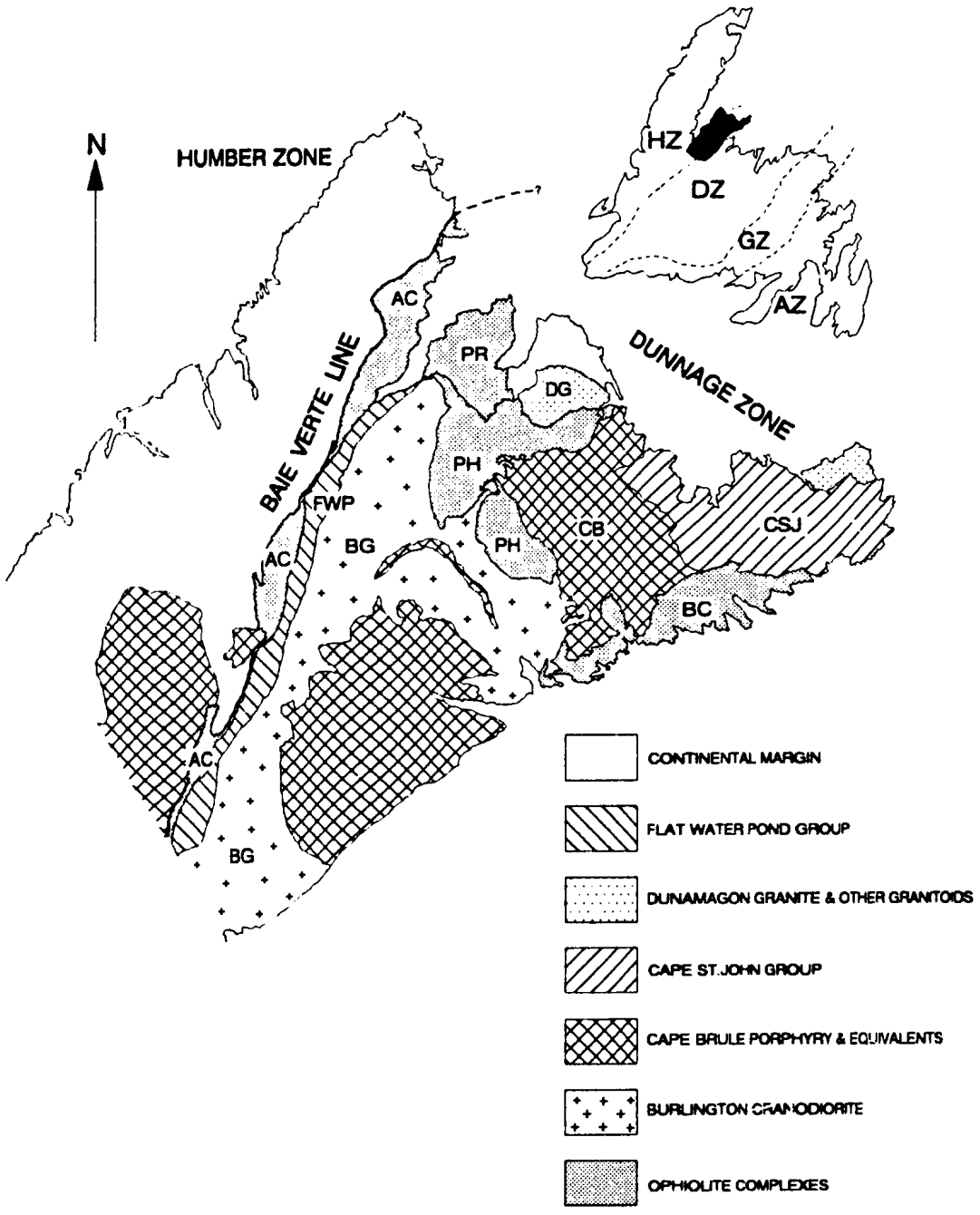

Figure 2-2: Geological map of the Baie Verte Peninsula

2.3.1 Fleur de Lys Belt

The dominantly metamorphic suites of rocks which constitute the Fleur de Lys Belt are interpreted as the miogeocline and the underlying basement of the Paleozoic North American continental margin (Humber Zone). The Fleur de Lys Belt consists of three lithologically distinct units including a local basement, a metaclastic cover sequence and post-kinematic granitoid intrusions. The complex structural geology of the Fleur de Lys Belt records a relatively continuous history of deformation and metamorphism. Hibbard (1983) grouped the structures into four deformation phases, the earliest of which only affected the basement, while the other three affected the entire sequence, with local variations in intensity.

The structural basement occurring at the core of the Fleur de Lys Belt is represented by migmatites, banded gneisses, metaconglomerates, and psammitic to semi-pelitic schists of the East Pond Metamorphic Suite. The migmatitic gneisses of the East Pond Metamorphic Suite are interpreted as the Grenvillian crystalline basement upon which the continental margin was constructed (*e.g.* Church, 1969; de Wit, 1980). The basement is overlain by the sequence of pelitic to psammitic schists, metaconglomerates and metabasites, interpreted to represent the Late Precambrian to Early Cambrian sedimentary rocks deposited during the early stages of the rifted margin. Mafic dykes present in the suite have been attributed to the phase of continental rifting which led to the formation of the Iapetus ocean (*e.g.*Church, 1969).

The cover sequence unconformably overlying the East Pond Metamorphic Suite is known as the Fleur de Lys Supergroup, and is composed of psammitic, semipelitic and graphitic schists, marble, chloritic schist and amphibolite. The supergroup has been considered to represent the metamorphosed distal equivalent of the lower Paleozoic platform rocks of western Newfoundland deposited on the continental slope and rise during the later stages of margin development.

Both the East Pond Metamorphic Suite and the Fleur de Lys Supergroup were post-tectonically intruded by a granitoid batholith termed the Wild Cove Pond Igneous Suite. Other minor granitic intrusions in the Fleur de Lys Belt are considered to be satellites of the latter.

Metamorphic rocks of the Fleur de Lys Supergroup contain abundant and widely distributed garnet and albite porphyroblasts with complex pre- and post-porphyroblast metamorphic fabrics which indicate a multiphase tectonic history (Kennedy, 1971, 1975). Textural evidence implies generally that the peak of metamorphism was reached late in the tectonic history of the supergroup (*e.g.* Bursnall and de Wit, 1975). Similar, constant porphyroblast-matrix relationships in different stratigraphic units of the Fleur de Lys Supergroup imply that various rock units were already juxtaposed prior to the peak metamorphic conditions which produced the porphyroblasts, and probably indicate that metamorphism resulted from relaxation of a thermal anomaly following initial burial of the continental margin by overriding thrust sheets (Jamieson and Vernon, 1987).

Deformational fabrics and matrix-porphyroblast textural relationships have

played an important role in tectonic interpretation of the Fleur de Lys Supergroup, in the absence of precise isotopic ages. The earliest deformation and metamorphism of the Fleur de Lys Supergroup has been attributed to the Taconian (Middle Ordovician) obduction of the oceanic allochthons over the clastic rocks of the North American continental margin (*e.g.* Bursnall and de Wit, 1975; Hibbard, 1983). Also, a major episode of post-Taconic, presumably Acadian (Devonian), metamorphism was inferred by de Wit (1976), based on the interpretation that porphyroblast growth post-dated the main episode of deformation. Dallmeyer (1977) obtained $^{40}Ar/^{39}Ar$ cooling ages from the western Fleur de Lys Supergroup, ranging from 420 ±10 to 386 ±5 Ma for hornblende and from 381 ±5 to 366 ±5 Ma for biotite, which were incompatible with the Taconian age of metamorphism. On the other hand, the post-kinematic dioritic to granitic rocks of the Wild Cove Pond Igneous Suite have been considered to be of Devonian age (Wanless et al., 1972) and thus deemed to bracket the youngest possible age of the metamorphism. Recent geochronologic results (Dunning and Cawood, unpublished data), however, indicate a major phase of Silurian metamorphism (and magmatism) in the Fleur de Lys Belt, in reasonable accordance with the acquired Silurian hornblende ages for peak metamorphism. In summary, the present bulk of evidence suggests that the western Baie Verte Peninsula was subject to a poly-phase deformation and metamorphism (with a possible Middle Ordovician to Early Devonian age span), though the peak of metamorphism was reached in Silurian time.

2.3.2 Baie Verte Belt

The rocks of the Baie Verte Belt constitute the western margin of the Dunnage Zone (Notre Dame Subzone). They are in significant contrast with those of the Fleur de Lys Belt to the west and north. The Baie Verte belt is composed of three major geologic elements, including 1) ophiolitic basement, 2) volcanic cover sequences, and 3) a variety of mafic to felsic, but largely granitoid, intrusions (see Fig.2-2).

2.3.2.1 Ophiolitic Basement

The ophiolitic affinity of the mafic-ultramafic assemblages on the eastern portion of the Baie Verte Peninsula was first noted by Neale (1959). Four geographically distinct but somewhat correlatable ophiolitic assemblages are recognized on the peninsula, including the Advocate (Kidd, 1974; Bursnall, 1975), Point Rousse (Norman & Strong, 1975; Kidd et al., 1978) and Betts Cove (Upadhyay, 1973; Coish, 1977) Complexes, and the Pacquet Harbour Group (Gale, 1973). The ophiolitic sequences of the Baie Verte Belt are either incomplete or dismembered (Hibbard, 1983). Despite the geographic separation, variable internal relationships and structural complexity, a similar origin is proposed for the ophiolite complexes of the Baie Verte Peninsula and of the Humber Zone, based on stratigraphic, geochemical and structural data (*e.g.* Bursnall and de Wit, 1975; Hibbard, 1982).

The presumed single oceanic slab that comprised the ophiolite complexes of the Baie Verte Peninsula displays the general stratigraphy of the oceanic lithosphere, including an ultramafic member, cumulate and intrusive gabbroic

rocks, mafic sheeted dyke complex, and pillowed mafic volcanic rocks (Hibbard, 1983). The slab is overlain stratigraphically by somewhat younger sequences of dominantly mafic volcanic and volcaniclastic rocks. The following describes the major similarities and contrasts between the ophiolite complexes of the Baie Verte Belt.

The Advocate Complex is intensely dismembered and structurally disrupted, and occurs as a discontinuous strip along the Baie Verte Line. The Complex displays a polyphase history of alteration, metamorphism and deformation. The Betts Cove Complex is the farthest from the Baie Verte Line and, despite the lack of an ultramafic tectonite member, is the most intact ophiolite on the peninsula. It is uniformly metamorphosed to the lower greenschist facies which is documented as ocean floor metamorphism (Coish, 1977). The Point Rousse Complex represents a complete but dismembered ophiolite with ophiolitic units which are lithologically very similar to those of the Advocate and Betts Cove Complexes. The sequence of variably deformed and metamorphosed volcanic and volcaniclastic rocks, mafic dykes and gabbro with ambiguous stratigraphy, which collectively constitute the Pacquet Harbour Group, appears to be quite distinctive from other ophiolite complexes on the peninsula; there is an apparent lack of ultramafic and cumulate gabbro members in this group. The ophiolitic lavas of the Pacquet Harbour Group, Betts Cove Complex and the Point Rousse Complex contain highly magnesian boninitic basalts (Norman & Strong, 1975; Gale, 1973; Upadhyay, 1973; Hibbard, 1983) that are mutually correlative. The boninitic lavas become progressively more

magnesian towards the easterly Betts Cove Complex (Hibbard, 1983).

The only direct age constraint on the ophiolite complexes of the Baie Verte Peninsula is from the Betts Cove Complex. A U-Pb zircon age of 488.6 +3.1/-1.8 Ma was obtained from a sample of Betts Cove Gabbro (Dunning & Krogh, 1985). Nevertheless, the exact age of obduction of the oceanic slab and emplacement of the ophiolitic suites (Baie Verte Belt) over the continental margin rocks (Fleur de Lys Belt) at the Baie Verte Peninsula is not well constrained. This tectonic event has been traditionally attributed to the Taconian orogeny (de Wit, 1980; Hibbard, 1983), mainly based on the structural and metamorphic history of the peninsula, and also by analogy to comparable stratigraphic relationships known elsewhere in Newfoundland.

Presently, there are two relevant, but indirect, lines of evidence for the Ordovician emplacement of the ophiolite complexes of the Baie Verte Peninsula. First, the $^{40}Ar/^{39}Ar$ ages from the metamorphic aureoles of the Bay of Islands Complex (469 ±5 Ma, Dallmeyer & Williams, 1975, recalculated with new decay constant from published data) and the St. Anthony Complex (489 Ma, Dallmeyer, 1977) indicate that the obduction of the oceanic crust occurred in the Early to Middle Ordovician, and at least 14 Ma after the crystallization of the ophiolitic intrusive rocks.

Secondly, an area of about 2000km^2 in western and southwestern Dunnage Zone is underlain by Late Ordovician, calc-alkaline, syntectonic tonalitic rocks (*e.g.* Southwest Brook Complex) which intrude and locally enclose the Ordovician ophiolitic rocks (Annieopsquotch Complex), as well as

the continental margin metaclastic rocks of Fleur de Lys type (Dunning et.al., 1989). These foliated biotite- and hornblende-bearing tonalites, trondhjemites and granodiorites have conspicuous island-arc geochemical signatures and are interpreted to have been generated during a collision event which involved attempted eastward subduction of the continental margin beneath the overriding oceanic slab (Taconian Orogeny, Dunning et.al., 1989).

Despite this age evidence, the exact stratigraphic and structural relations between the Baie Verte ophiolite complexes and the Humber Zone allochthons are not well established. Moreover, there is presently no known Ordovician syntectonic intrusion on the Baie Verte Peninsula (G.R. Dunning, personal comm.). Consequently, there is no direct evidence in support of Taconian ophiolite emplacement from the Baie Verte Peninsula.

2.3.2.2 Volcanic Cover Sequence

The volcanic cover sequence overlying the ophiolitic rocks of the Baie Verte Peninsula is represented by the mafic volcanic and volcaniclastic rocks of the Snooks Arm Group which conformably overlie the Betts Cove Complex, the Point Rousse cover sequence and the upper portions of the Pacquet Harbour Group. The cover rocks of the Advocate Complex are in unconformable contact with the underlying ophiolitic rocks and appear to be significantly different than the other three cover sequences.

The Snooks Arm Group consists of two mainly volcaniclastic formations (Bobby Cove and Balsam Bud Cove Formations) and two dominantly pillow lava

formations (Venams Bight and Round Harbour Formations) with a total thickness of more than 2000m (Upadhyay, 1973). The sedimentary/pyroclastic units are dominated by andesitic tuff, andesitic agglomerate and flysch with subordinate greywacke, argillite, chert and conglomerate. The entire sequence is metamorphosed to the lower greenschist facies. Abundant diabase sills, and plugs, dykes and sills of silicic composition intruded the group. The Snooks Arm Group denotes contemporaneous volcanism and deep-water sedimentation directly over the oceanic crust. Based on a detailed geochemical study of the Snooks Arm Group, Jenner and Fryer (1980) suggested that these rocks may have formed in either an oceanic island setting or as part of a back-arc basin. A fossil age of Middle Arenigian was reported for the Snooks Arm Group (Snelgrove, 1931).

The Snooks Arm Group has many similarities to Point Rousse cover sequence which conformably overlies the Point Rousse Complex (Chapter 3). The group is also comparable lithologically and geochemically with portions of the Pacquet Harbour Group.

2.3.2.3 Intrusive Rocks

A number of intrusions crosscut the rocks of the Baie Verte Peninsula. These plutons are mainly granitoid, though associated dioritic to gabbroic rocks are not uncommon. The major intrusive elements of the Baie Verte Belt, from southwest to northeast, are: the Burlington Granodiorite (Neale, 1958; Hibbard, 1983), Dunamagon Granite (Baird, 1951), Cape Brule Porphyry and its southerly

equivalents (Neale, 1967; DeGrace et al.,1976), and the La Scie Intrusive suite (Cockburn, 1971; DeGrace et al.,1976). The latter includes the La Scie Granite, Seal Island Bight Syenite and the Reddits Cove Gabbro. These intrusions have been traditionally grouped into two Early Ordovician (Burlington Granodiorite and Dunamagon Granite) and Siluro-Devonian suites. However, recent geochronologic data from the igneous suites of the Baie Verte Peninsula (Dunning and Cawood, unpublished data) have revealed Silurian ages for the Burlington Granodiorite and the Dunamagon Granite, as well as for the Cape Brule Porphyry and the Seal Island Bight Syenite.

2.3.3 Baie Verte Line

The tectono-stratigraphic zones of the northern Appalachians are generally bounded by major fault structures (*e.g.* Baie Verte-Brompton Line, Gander River Ultramafic Belt, Dover-Hermitage Bay Fault, see Fig.2-1). The Baie Verte-Brompton Line is one of the major structural breaks of the Appalachian Orogen and is defined largely by mafic-ultramafic complexes of ophiolitic origin. Stratigraphic relations and radiometric ages indicate that these oceanic rock bodies are Early Ordovician in age and are mutually correlative. The Baie Verte-Brompton Line is traceable along most of the length of the Appalachian-Caledonides system (Williams, 1978). The ophiolite complexes at Baltimore, Maryland and New York, and small mafic-ultramafic bodies along the Highland Boundary Fault in the British Caledonides occur in a structural setting

interpreted to be analogous to Baie Verte-Brompton Line in the Canadian Appalachians (Williams and St-Julien, 1982). The overall sinuous trend of the Baie Verte-Brompton Line along the Appalachian Orogen is interpreted to reflect the original shape of the continental margin bounded by rifts and transform faults.

In west-central Newfoundland, the Baie Verte-Brompton Line (here noted Baie Verte Line for simplicity) is a continuous structural zone which represents the boundary between the oceanic volcanic suites of the Dunnage Zone to the east, and the multi-deformed metaclastic rocks of the Humber Zone to the west. It is interpreted as a tectonic zone of Ordovician ophiolite emplacement along the western margin of North America. Post-Ordovician tectonic phases have accentuated this structural feature and are responsible for steep attitudes along its length (Williams and St-Julien, 1982). The Baie Verte Line is locally buried under Silurian-Devonian and Carboniferous cover rocks.

On the Baie Verte Peninsula, the Baie Verte Line is essentially defined by the presence of discrete outcrops of the Advocate ophiolite complex. The Advocate Complex is bounded to the west by the metaclastic rocks of the Fleur de Lys Supergroup and greenschists and amphibolites of the Birchy Complex. To the east it is bounded by the basal conglomerates of the Flat Water Pond Group. The Advocate complex has a steep northeast-trending foliation in most places (subparallel to the Baie Verte Line) and is cut by numerous shear zones. The local occurrence of a garnetiferous amphibolite near the base of the complex suggests local development of a Bay of Islands-type metamorphic

aureole beneath the Advocate complex. This implies the emplacement of rocks by tectonic transport along the Baie Verte Line.

The area to the west of Baie Verte Line is underlain by the high grade gneisses and migmatites of the East Pond Metamorphic Suite (Grenvillian?) that are overlain by thick metaclastic sequences of late Precambrian to Early Ordovician age (Fleur de Lys Supergroup). The latter is metamorphosed to greenschist and amphibolite facies and is affected by polyphase deformation. Near the Baie Verte Line, the Fleur de Lys Supergroup consists mainly of greenschists and amphibolites which comprise the Birchy Complex. The protoliths of the Birchy Complex are believed to be of ophiolitic origin (similar to those of the Advocate Complex), although the complex has been subject to the same deformations that affected the Fleur de Lys metaclastic rocks to the west (*i.e.* post-emplacement metamorphism). The occurrence of ophiolitic melanges beneath the ophiolites of the Baie Verte Line (*e.g.* Coachman's Melange of the Birchy Complex) and their similarity to Humber Arm and Hare Bay melanges in Western Newfoundland imply the westward transport of ophiolite complexes across the Fleur de Lys terrane, probably from a root zone at or near the Baie Verte Line.

The area to the east of Ming's Bight is underlain by psammitic and semi-pelitic schists and metaclastic rocks of the Ming's Bight Group which is interpreted to be the same lithostratigraphic unit as the Fleur de Lys Supergroup, though the former is located to the east of the Baie Verte Line. Structural breaks analogous to the Baie Verte Line are also indicated between

the Ming's Bight metaclastic rocks and the nearby ophiolitic lithologies at Ming's Bight and near Pacquet Harbour. These have caused complexities regarding the structure of the Baie Verte Line at its northern extremity. It has been proposed that the Baie Verte Line changes its course from a northward trending straight line, to a 'Z' shaped line projecting northeastward near Pacquet Harbour. Therefore, the Fleur de Lys psammites of the Coachmans Harbour and the Ming's Bight psammites at Ming's Bight are suggested to be equivalent and interpreted to form the opposing limbs of a tight flexure which wraps around the Point Rousse Peninsula (Hibbard, 1982).

To the east of Baie Verte Line, the basal conglomerates (olistostromes) of the Flat Water Pond Group are faulted against the Advocate Complex to the west. The distinctive types of clasts in the Flat Water Pond Group (granitic rocks, serpentinite, virginite, pelitic schist, etc.), together with other structural evidence, suggest that these volcanic and sedimentary rocks were deposited upon an orogenically disturbed oceanic crust subsequent to the emplacement of ophiolite complexes.

CHAPTER 3: STRATIGRAPHY AND LITHOLOGY OF THE STOG'ER TIGHT AREA

3.1 INTRODUCTION

The Stog'er Tight Au Prospect is located within a sequence of dominantly oceanic rocks that belong to the Point Rousse Complex. The Point Rousse Complex encompasses the mafic and ultramafic rocks of a complete but dismembered ophiolite and its cover sequence, that outcrop on the Point Rousse Peninsula between Ming's Bight and Baie Verte. The complex is considered to have the form of a broad, tectonically bounded, generally east-trending synclinorium with ophiolitic plutonic members occurring to the north and south of the centrally located cover sequence (Fig.3-1). The ophiolitic components are confined to structural blocks bounded by dominantly northwest-dipping high angle and thrust faults. The dominant lithologic units in the Stog'er Tight prospect area are mafic volcanic, pyroclastic, volcaniclastic and mafic intrusive rocks.

3.1.1 Point Rousse Ophiolite

All of the components of an ophiolite suite are present in the Point

Rousse Complex, including serpentinized ultramafic rocks, gabbro and metagabbro, sheeted dikes and pillow lava (Fig.3-1). The ophiolitic units of the Point Rousse Complex are lithologically very similar to those of the Advocate and Betts Cove Complexes (Hibbard, 1983).

The ultramafic rocks include harzburgite and lherzolite with subordinate dunite and pyroxenite, and are serpentinized to variable extents. Steatitization and carbonatization (dominantly magnesite) of the ultramafic rocks are also common in the complex. Cumulate ultramafic units occur in the transition zone between non-cumulate ultramafic rocks and the overlying gabbros, however, their lower contact with the non-cumulate rocks is not exposed, except where it is faulted.

Gabbros in the Point Rousse Complex are generally medium-grained (1-2 mm) and equigranular with well-preserved textures. They are characterized by a conspicuous absence of opaque minerals (Kidd et al., 1978). The rare to subordinate orthopyroxene in the gabbros is almost invariably altered, while some clinopyroxene has remained fresh.

Cumulate gabbros with graded compositional layering are identified in a few localities. The contrasting layers range in composition from feldspathic clinopyroxenite to anorthositic gabbro and locally display a strong gneissic foliation coplanar with the layering. This foliation is interpreted to have formed as a result of deformation at high, sub-magmatic temperatures, as opposed to the deformation associated with the regional cleavage and thrusting (Kidd et al., 1978). Pod-like dikes or sills of pegmatitic gabbro, 1-20 cm thick, which cut the

layering, are common in the layered gabbros.

Medium-grained homogeneous clinopyroxene gabbro is found between the layered gabbros and the sheeted dike unit. This gabbro does not show any grain-size or compositional variation. The transition from gabbro to sheeted diabase dykes is associated with an upward increase in the proportion of sheeted dykes complemented by a decrease in the proportion of interstitial gabbro screens. There are also small amounts of medium-grained, brecciated sodic leucogabbro or trondhjemite found within this transition zone. The trondhjemite is essentially quartz-free and consists of albitized plagioclase and minor actinolite after hornblende. The total thickness of layered and homogeneous gabbro is at least 600m, and locally can be more than 850m (Kidd et al., 1978).

The sheeted dyke complex consists of fine-grained, homogeneous, strongly altered diabase with intersertal to slightly ophitic texture. They are commonly well defined by their chilled margins and internal flow laminations, and range from 10cm to 1m wide; most are between 20 and 50cm wide. Wholly undeformed, one hundred percent sheeted dyke sequences are observed in a number of localities at the coastal margins of the Point Rousse Peninsula. The dyke attitudes are variable from east-west to north-south in different coastal sections. A minimum thickness of 350m is reported for the 100% sheeted dyke complex. The transition from the sheeted dykes to pillow lavas is characterized by the appearance of pillow lava screens between the dykes, followed by an increase in lava proportion (Kidd et al., 1978).

Ophiolitic pillow lavas, apart from those in screens between sheeted dykes, are only locally identified. These pillow lavas are aphyric, variolitic, strongly altered and contain minor pillow breccia. Some maroon chert occurs in boudinaged beds and interstitial to pillows. Geochemical analyses (Norman and Strong, 1975) have shown that the pillow lavas of the Point Rousse Complex have low K and Ti contents, typical of oceanic tholeiitic rocks. A large group of pillow lava samples, however, are characterized by high Mg, Ni and Cr, and low K, Ti, Ba, Zr, Sr and Y, which is comparable to those in basaltic komatiites (boninites).

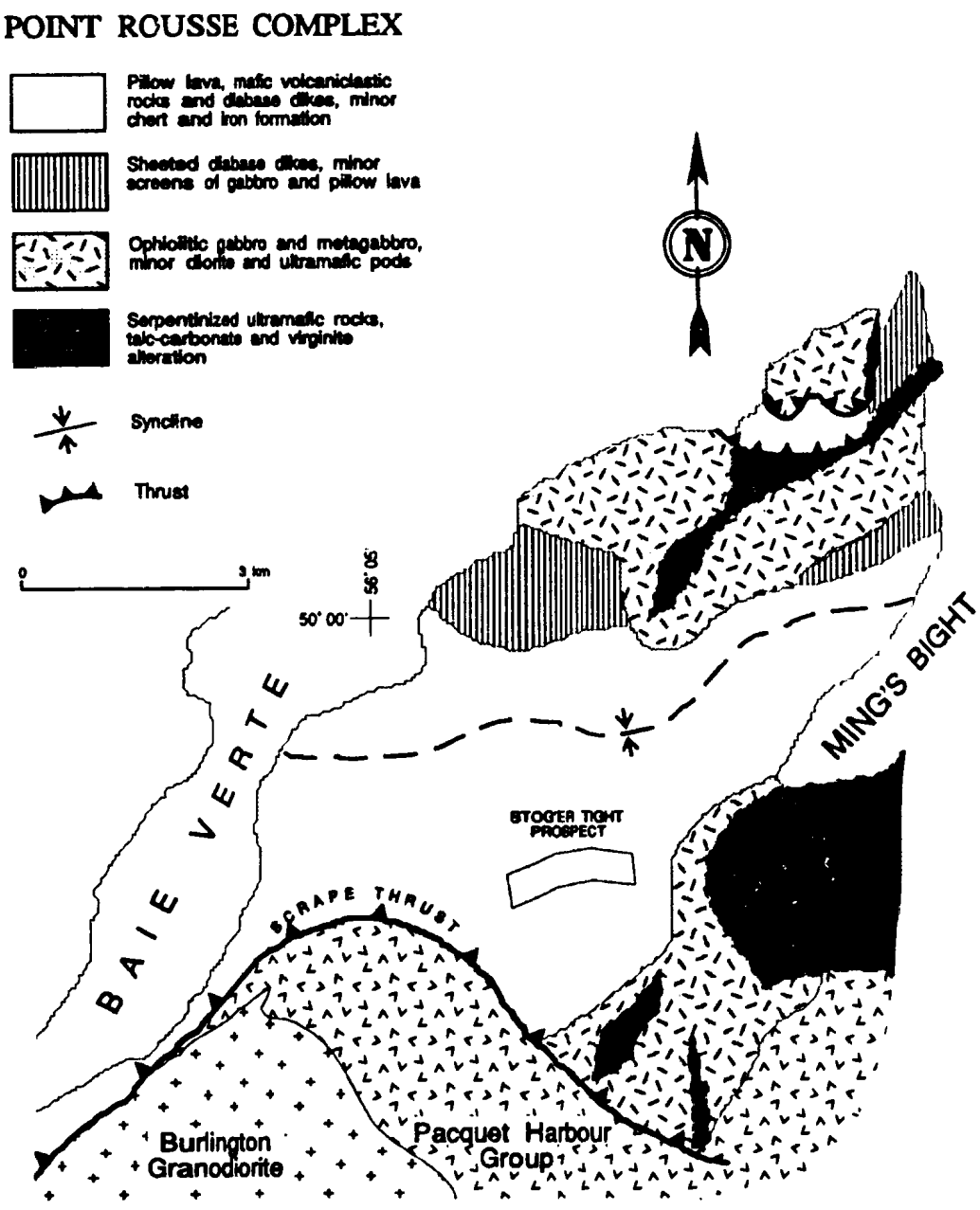

Figure 3-1: Geologic map of the Point Rousse Complex (after Hibbard, 1983)

3.1.2 Point Rousse Cover Sequence

A continuous sequence of mafic volcanic and sedimentary rocks overlie conformably the ophiolitic volcanics of the Point Rousse Complex (Norman and Strong, 1975; Kidd et al., 1978). The cover sequence is composed of mixed pillow lavas, mafic pyroclastic rocks and volcaniclastic rocks with a general east-west trend and a moderate northerly dip. These rocks outcrop between two ophiolitic terranes of the complex, as well as in a thrust sheet of deformed pillow lavas and greenschist in the northern part of the peninsula (between Deer Cove and Devil's Cove Pond, Fig.3-1). Basal conglomerates with abundant mafic volcanic and volcaniclastic fragments occur in the northern section of the central terrane of cover rocks. In addition, this section contains epiclastic units, minor argillite, a variety of tuffs and thin mafic sills. Burgundy coloured chert interlayered with magnetite-rich layers, form typical iron formation and outcrop in the area of the old Goldenville Mine. The southern portion of the cover sequence contains mainly pillow lava and pillow breccia, mafic pyroclastic rocks and volcaniclastics. The change in facing directions of the volcanic and pyroclastic beds along the coast of Baie Verte is considered as the evidence for a regional east-west trending syncline in the cover rocks. Field relationships suggest that there are major facies changes both laterally and vertically through the cover sequence.

A variety of late mafic dykes (and sills) intrude the cover and the ophiolitic portions of the Point Rousse Complex. They are reported as diabase

dykes, plagioclase porphyritic diabase, porphyritic dolerite and leucocratic gabbro (Hibbard, 1983). Kidd et al. (1978) also noted a rare variety of thin but continuous, late dykes which consist of purplish buff, fine-grained dolerite containing titanaugite. They suspected that these dykes are not part of the general ophiolite complex and mentioned the probability that they belong to a wholly younger event.

3.2 DESCRIPTION OF ROCK UNITS IN STOG'ER TIGHT

The Stog'er Tight gold prospect is located within the southern portion of central terrane of the Point Rousse cover sequence (Fig.3-1). The sequence of rocks at the prospect area consists mainly of mixed pyroclastic and volcaniclastic rocks, and effusive volcanic rocks (including pillow lava) with a general WNW-ESE strike and northerly dip. This volcanic/pyroclastic sequence is cut by a series of subparallel gabbroic sills which host the four main mineralized zones of the Stog'er Tight deposit (see Fig.3-2 and Appendix V). The Stog'er Tight Gabbro therefore refers to a multiple mafic intrusion which was intruded conformably into the cover sequence, subsequent to the accumulation and lithification of the enclosing volcanic and pyroclastic rocks. Kirkwood and Dubé (1992) mapped the Stog'er Tight gabbro as three distinct sills within the pyroclastic sequence, including a southernmost gabbro, a middle gabbro and an upper or northernmost gabbro sill (see Fig.2-2). According to their notion, the area of the present study incorporates the upper gabbro sill of the Stog'er Tight prospect. Therefore, the descriptions and interpretations of

this study are based chiefly on the lithologic, petrographic and geochemical characteristics of the upper gabbro, which is the host of gold mineralization in the Stog'er Tight and Magnetic Zones.

The following sections describe the stratigraphic, lithologic and petrographic features of the main rock units in the prospect area. The detailed petrography and mineralogy of the Stog'er Tight gabbro are presented in chapter 5.

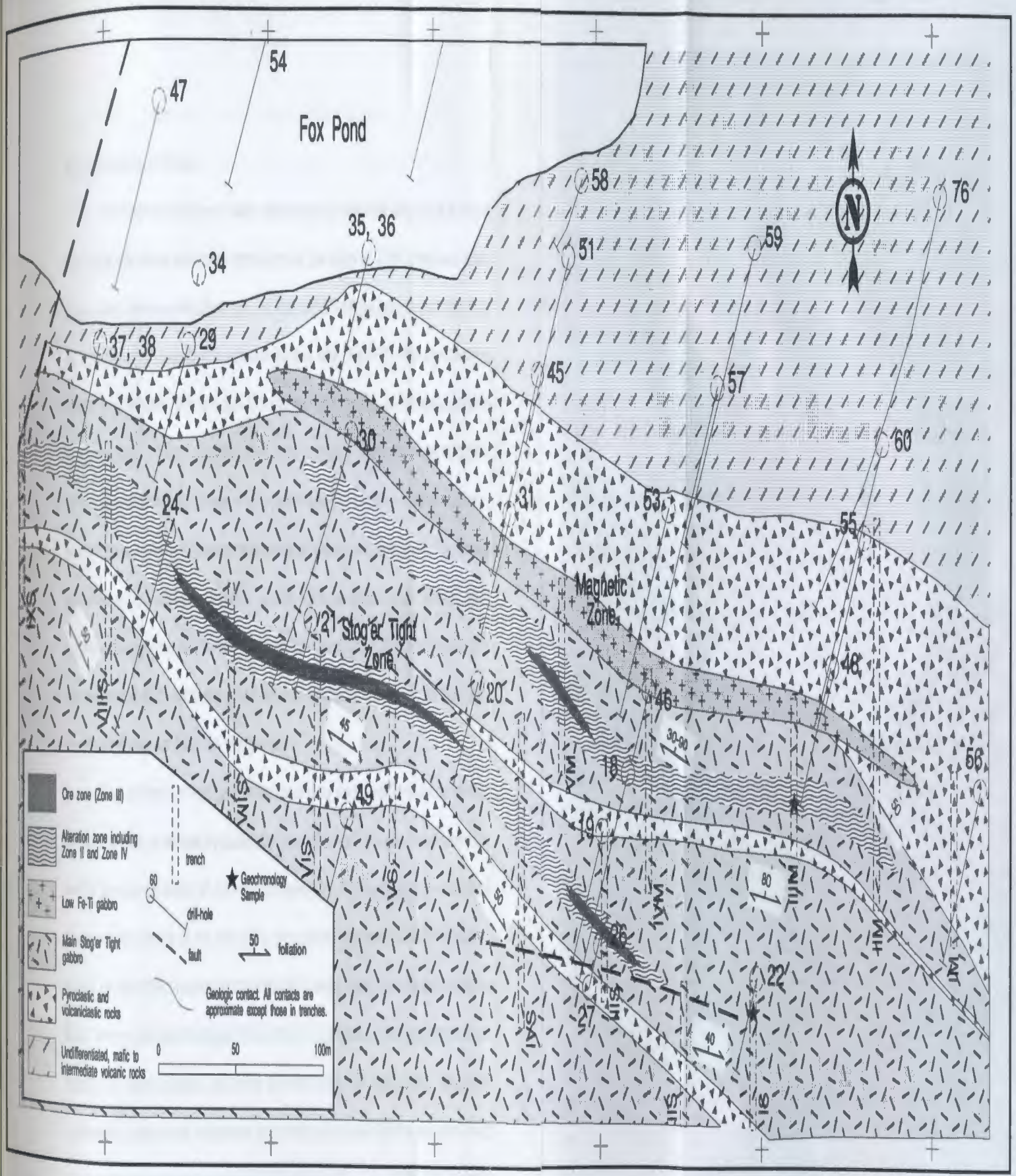

Figure 3-2: Geologic map of the study area (eastern Stog'er Tight Prospect), compiled from Noranda Exploration Company's base map.

3.2.1 Pyroclastic Rocks:

Pyroclastic rocks are a major constituent of the rock sequence and are the most abundant extrusive component in the Stog'er Tight prospect area. They occur stratigraphically at the top and bottom of the gabbro unit and also as screens interstitial to the separate gabbro sills (Fig.3-2). The pyroclastics range in grain-size from ash-tuff to lapilli-tuff and locally, pyroclastic breccia (agglomerate). Thinly bedded (3-10cm) variably deformed pyroclastics composed of alternating beds of ash- and lapilli-tuff outcrop on the southern end of trench IIIM and also at both ends of trench IIIS (Fig.3-3). Trench IM exposes an 8 meters interval of similar tuffs in gradational contact with volcaniclastic rocks. All the beds strike southwest (110-130°) and dip steeply northeast (60-83°). Intervals of tuff and/or pyroclastic breccia occur in almost all of the drill-cores from the study area.

Fine-grained ash tuffs are characterized by a delicate lamination which, in hand sample, is defined by successive alternation of light-green and greenish-white laminae (or beds) of different composition. This lamination is a primary depositional feature of the ash tuffs; the whitish laminae probably represent layers of abundant vitroclastic material which were subsequently devitrified to fine, amorphous assemblages. Characteristic pyroclastic fabrics are evident locally in coarse-grained ash-tuffs and especially in lapilli-tuffs. Relics of vitroclastic, spherulitic, vitrophyric and rarely, pumiceous fabrics are preserved in a number of relatively undeformed tuff samples (Fig.3-4). Pyroclastic breccia

is predominantly made up of subrounded fragments of volcanic origin.

Chlorite, silica, feldspar and calcite are the major crystalline mineral constituents of the tuffs, whereas fibrous actinolite, epidote/clinozoisite and titanite occur in variable proportions in specific samples (*e.g.* BN18-B1 and BN53-34). Coarse crystal-vitric-ash-tuffs are characterized by abundant feldspar phenoclasts up to 2mm long.

The most prominent textural feature of the medium- to coarse-grained tuffs in thin section is the presence of dense, cloudy patches of amorphous Fe-Ti oxides (and/or hydroxides?) which commonly show a lineated wavy texture (Fig.3-4). These semi-opaque patches usually incorporate a variety of fibro-radial textures such as spherulites and open-space fillings which have been replaced by alteration minerals. Fe-Ti oxides are normally released and rhythmically accumulated along the margins of vitroclastic fragments (*i.e.* glass shards and pumiceous vitric lumps), during the process of devitrification of basaltic glass into palagonite, smectites and zeolites (Fisher & Schmincke, 1984). Late-stage, low-grade metamorphism of the tuffs in the area resulted in ultimate transformation of the devitrification products (palagonite and zeolites) into chlorite, epidote, carbonate and silica. The presence of abundant amorphous oxide wisps with strong preferred orientation in the least deformed lapilli-tuffs probably indicates that the original vitroclastic fragments were flattened and compressed upon deposition as hot particles (eutaxitic fabric), a process somewhat similar to that in the young welded pyroclastic flow deposits. Identical textural relationships and alteration/metamorphic history have

been outlined for some Archean hyaloclastic deposits (Dimroth & Lichtblau, 1979).

Subrounded lithic clasts of various sizes (up to 70mm or more) and lithologies are a significant component of the lapilli-tuffs and are the dominant constituent of the pyroclastic breccia. The majority of lithic fragments were derived from a variolitic mafic volcanic rock which shows plagioclase phenocrysts and abundant vesicles in a felty groundmass of strongly altered feldspar microlites (Fig.3-5). Other types of small, aphanitic, lithic fragments occur in subordinate amounts in the lapilli-tuffs. In the pyroclastic breccia, large, closely packed, lithic fragments are welded by ash-size vitroclastic material. Besides the wide range of grain-size variations in the pyroclastic rocks, the lithic fragments in the breccias are conspicuously well-sorted. This indicates that the fragments were transported sufficiently by the fluid media, prior to deposition and lithification, and therefore the rock is *not* a pillow breccia.

3.2.2 Mafic to Intermediate Volcanic Rocks:

Undifferentiated volcanic (effusive) rocks, including pillow lavas and massive flows, cover the area to the north and northeast of the Stog'er Tight gold prospect and occur at the top of the gabbro/pyroclastics sequence (Fig.3-2). Almost all of the drill-cores recovered from north of the Magnetic Zone show significant intervals of volcanic lithology (see Appendix V). These drill-cores show successive occurrences of medium-grained volcanic rocks (pillow cores?), separated by thin intervals of fine-grained, strongly altered material (altered

pillow margins?). Unfortunately, field exposures of the volcanic unit are limited to only a few localities (trenches IM and IIM), mainly because of the restriction of surface trenching to the zones of gold mineralization. Trench IM exposes a 16m interval of fine-grained mafic rock with structures resembling flattened pillows (Fig.3-6). The lack of solid field evidence (*e.g.*indisputable pillow structures, flow units, etc.), along with strong deformation and recrystallization have caused a major problem in identification and further classification of the effusive volcanic rocks in the area.

The volcanic rocks are characterized in hand sample by a uniformly aphanitic fabric and medium to dark green colours on fresh surfaces. Two of the collected samples (BN18-B3 and 90723-B1), however, show a distinct porphyritic fabric with plagioclase phenocrysts up to 2mm in diameter (Fig.3-7). Undeformed and relatively unaltered effusive volcanics are distinguished from pyroclastic lithologies by: 1) the apparent lack of lamination or bedding, 2) absence of the clastic fabrics and, 3) the paucity of Fe-Ti oxides in the groundmass, if any.

The mineralogy of the volcanic rocks consists of the metamorphic assemblage sodic plagioclase ($\geq$45%), actinolite ($\leq$25%), chlorite ($\approx$15%), epidote and titanite. In thin section, the aphanitic groundmass is typically comprised of small feldspar microlites that are interwoven in an irregular fashion (felty texture), or else show preferred orientation (trachytic texture). The groundmass is nonetheless extremely susceptible to shear deformation, and readily recrystallizes into fine-grained, undifferentiable quartz-albite-chlorite

assemblages. In porphyritic varieties, the microlitic groundmass is wrapped around the phenocrysts (Fig.3-7). The chlorite has a pale-green colour and is non-pleochroic under the microscope. This variety of chlorite is distinctive from those in the gabbroic rocks and in the alteration zones associated with mineralization. Mafic volcanic samples 90723-B1 (trench IM, eastern Stog'er Tight) and BN54-B5 (drill-section 105+00W, western Stog'er Tight) show a striking difference in the modal abundance of actinolite. This suggests that the mineralogy and presumably, the geochemistry of the rocks, are variable throughout the volcanic unit.

3.2.3 Volcaniclastic Rocks:

Thinly laminated, variously coloured and strongly magnetic volcaniclastic rocks occur within the volcanic/pyroclastic sequence, mostly in the northeastern part of the Stog'er Tight area. They are closely associated with the laminated ash-tuffs, such that they can be regarded as local facies variations in the pyroclastic unit. Trench IM exposes a 3 meter interval of largely fragmental magnetic volcaniclastic rocks that grade southwards into typical lapilli-tuffs (Fig.3-8). Bedding in the volcaniclastic rocks is defined by alternating beds or laminae of pyroclastic and sedimentary derivation, which range in thickness from less than a millimetre to a few centimetres. Magnetite occurs almost invariably in the sedimentary beds (Fig.3-9).

The volcanogenic component of the volcaniclastic rocks essentially consists of devitrified vitroclastic tuff of mafic composition, as indicated by the

abundance of amorphous Fe-Ti oxides in the tuffaceous beds. Lithic fragments similar to those in the lapilli-tuffs are also observed in some medium-grained pyroclastic layers (*e.g.* sample BN18-B7). Chlorite, calcite and epidote alteration are common in the volcaniclastics, while the epidote alteration appears to be prevalent in the strongly magnetic intervals.

Medium to fine-grained, siliceous sedimentary layers are interbedded with tuffaceous beds in the volcaniclastic rocks. They are basically composed of poorly sorted, sub-angular quartz grains ranging in size from very coarse silt to medium sand. Other constituents of the sedimentary layers include chlorite, calcite, chert and locally, fine-grained aggregates of crystalline Fe-oxide (goethite?). Magnetite occurs as individual, inclusion-free euhedra up to 0.7mm in diameter that locally constitute as much as 70 percent of the sedimentary interbeds (sample BN67-A23).

Overall, the Stog'er Tight volcaniclastic rocks seem to have originated from remobilized volcanogenic debris and terrigenous detritus, which were transported by turbidity currents and were deposited in a deep-sea pelagic environment. These deposits have the characteristics of volcaniclastic aprons forming around seamounts and oceanic volcanic islands. Iron-rich, variegated (=variously coloured) sediments with almost similar characteristics are also reported from highly saline and oxygen-poor marine environments at the floor of Red Sea (Friedman and Sanders, 1978).

3.2.4 Gabbro

The Stog'er Tight gabbro is a multiple intrusion which outcrops as an arc-shaped body with a general northerly dip and a uniformly variable strike, from ESE at the eastern end (Magnetic Zone), to SW at the West Gabbro Zone (Fig.3-2). The contacts of the gabbro against the country rocks (pyroclastics) are normally visible, fine-grained, chilled margins and are generally conformable with the internal bedding of the volcanic/pyroclastic lithologies. Several relatively continuous screens of pyroclastic rocks subdivide the gabbro unit into separate, subparallel sills. Kirkwood and Dubé (1992) mapped the Stog'er Tight gabbro as three distinct sills within a pyroclastic unit. Accordingly, the entire area of this study which includes the mineralized Stog'er Tight and Magnetic Zones, incorporates only the northernmost or upper gabbro sill (Fig.3-2). However, detailed mapping of the Stog'er Tight gabbro in outcrop and particularly, in drill-core (Appendix V), has revealed local discontinuities in the sills. Thus the upper gabbro sill can be viewed as an assemblage of several interconnected gabbro sills which are separated by narrow pyroclastic partitions.

The unaltered and unsheared gabbro is readily distinguishable from volcanic/volcaniclastic lithologies in outcrop (and in drill-core), by its phaneritic fabric and its inhomogeneous texture. Nevertheless, the most distinctive feature of the Stog'er Tight gabbro in hand sample is the abundance of white to creamish wisps of leucoxene (Fig.3-10)(see chapter 5). The conformable intrusive contacts between the gabbro and the pyroclastics are well exposed in trenches IM, IIM, IIIM, IIIS and IVS, as well as in most of the logged drill-cores.

In a few instances, however, the intrusive nature of the contacts was obscured by shear deformation. The true thickness of the host gabbro sill in the study area is highly variable between 11m in drill-core BN88-20 (section 103+00W) to about 70m in drill-core BN89-60 (section 101+00W). This implies that there is an overall (but irregular) increase in the thickness of gabbro from west to east.

Crosscutting relationships between different gabbro sills are observed in a number of surface exposures, as evidenced by the local development of fine-grained chilled margins within the gabbro unit. The crosscutting features are best exposed in the trenches IVM, IVS and VIIS. Lithologic contrasts between adjacent gabbro sills are best observed in the eastern Stog'er Tight where a relatively small sill with limited lateral extent occurs stratigraphically above the main, mineralized gabbro body (Fig.3-2). The small gabbro sill is distinguished from the main gabbro in hand sample by its considerably lower Fe-Ti oxides content.

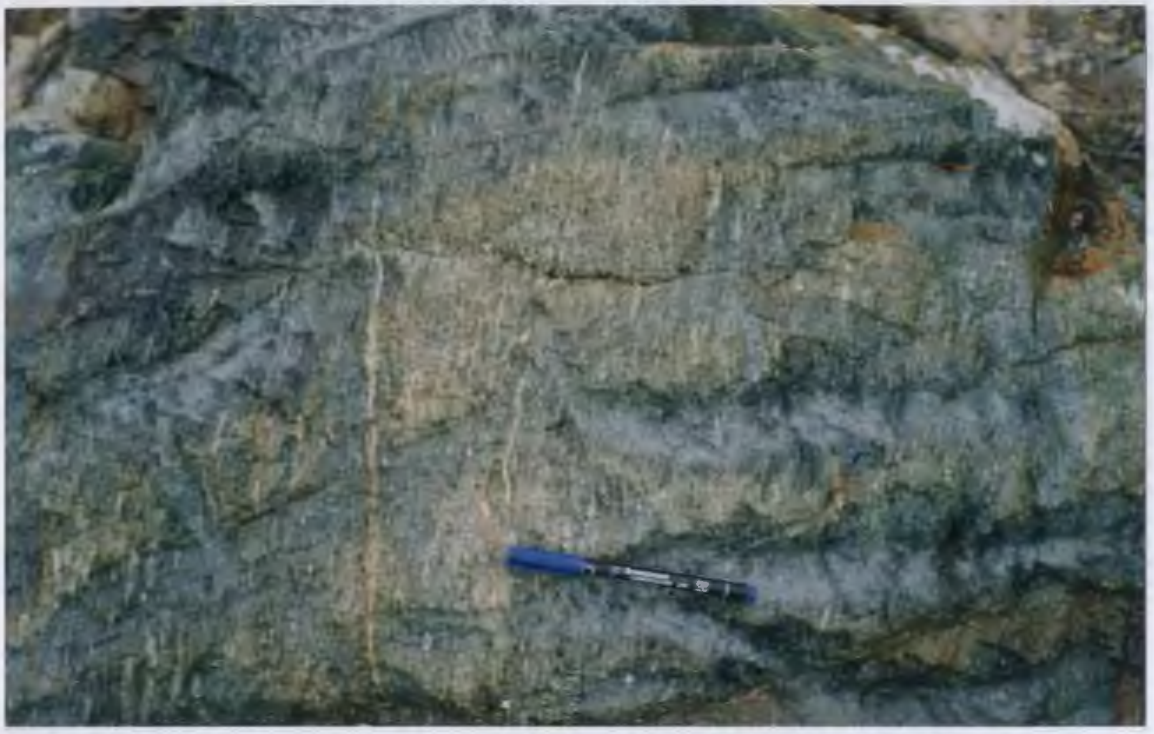

Figure 3-3 Trench outcrop of a pyroclastic rock (ash-tuff) including stretched lapilli. The rock foliation is vertical in the picture.

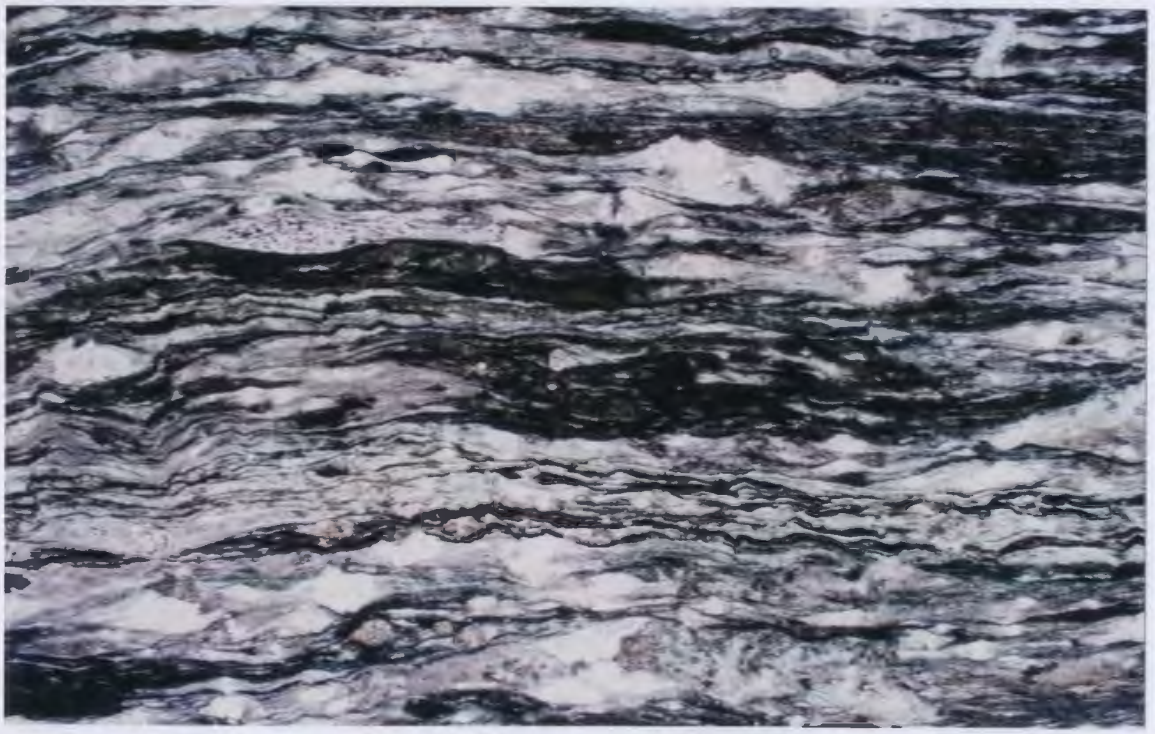

Figure 3-4 Photomicrograph of a fine-grained tuff with pumiceous fabric. Relict spherulites are observed within the dark bands at the center (x25).

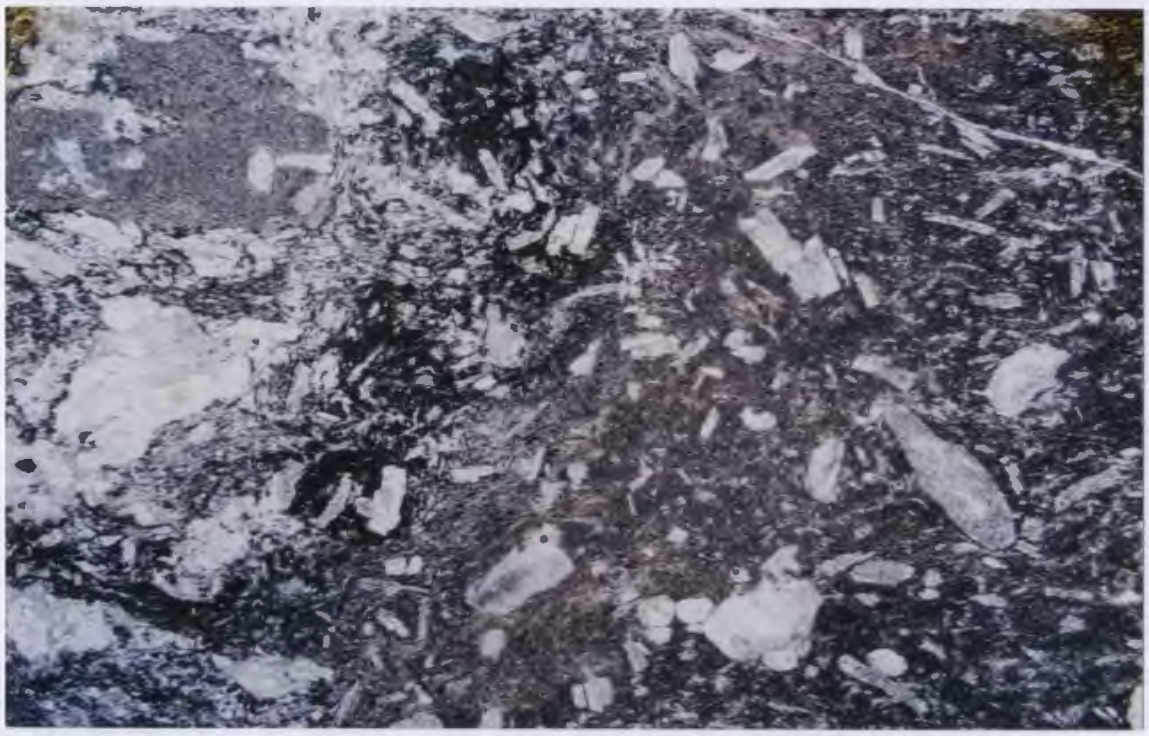

Figure 3-5 Photomicrograph of a pyroclastic breccia showing a porphyritic, lithic clast (right) within a matrix of vitroclastic material (x14).

Figure 3-6 Trench outcrop of a mafic volcanic rock with structures resembling flattened pillows (Trench IM).

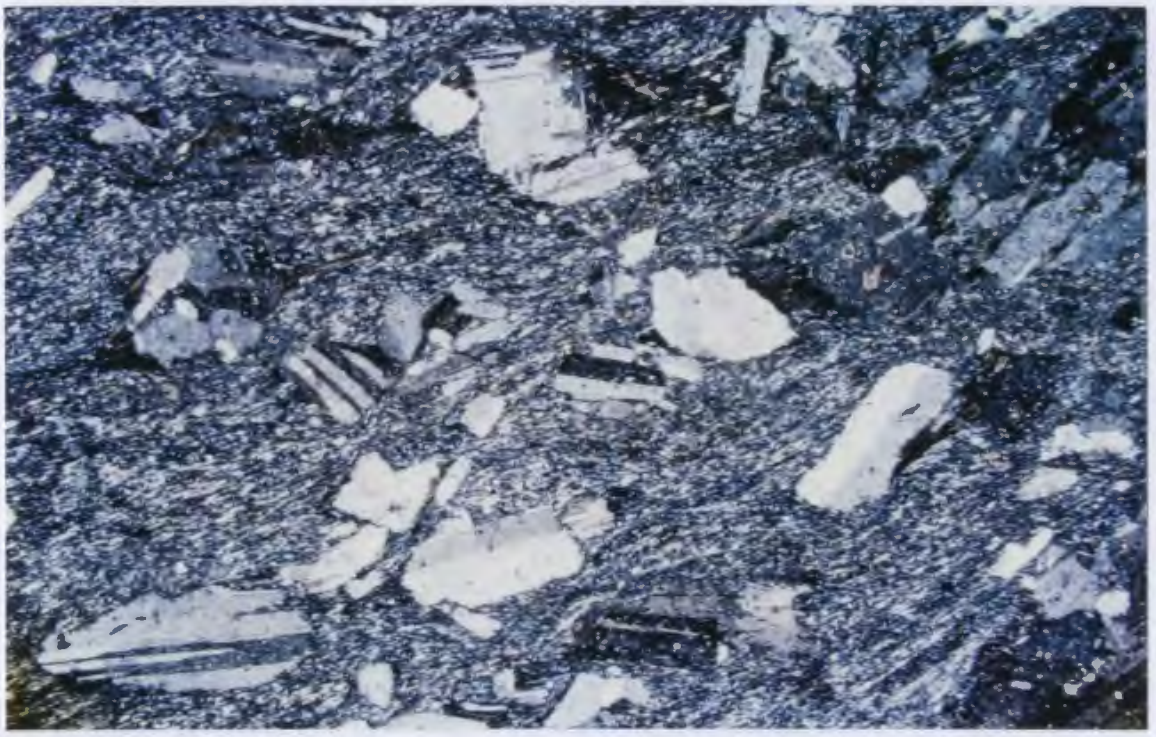

Figure 3-7 Photomicrograph of a volcanic (effusive) rock with distinct porphyritic fabric of twinned plagioclase phenocrysts in a groundmass of plagioclase microlites (xpol. x14).

Figure 3-8 Trench outcrop of magnetic volcaniclastic rocks (Trench IM).

Figure 3-9 Photomicrograph of a thinly-bedded volcaniclastic rock with alternating magnetite-rich laminae (x14).

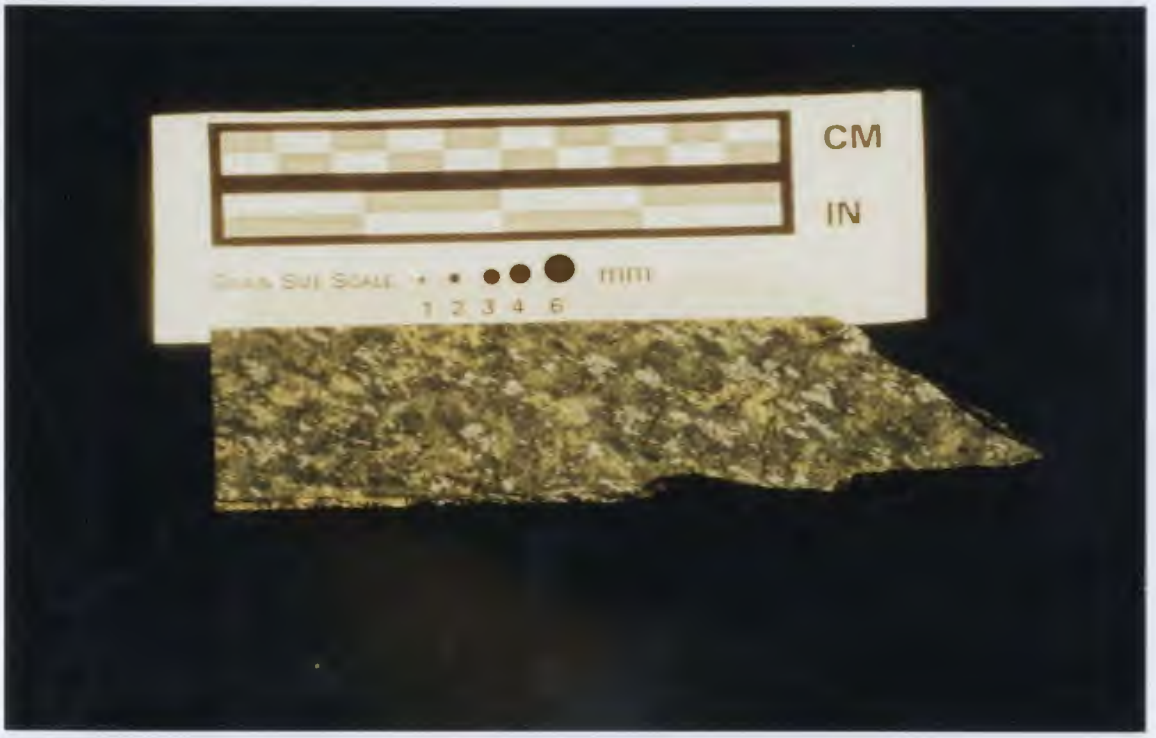

Figure 3-10 Drill-core sample of gabbro showing whitish wisps of leucoxene.

CHAPTER 4: STRUCTURAL SETTING

4.1 INTRODUCTION

Gold mineralization in the Stog'er Tight deposit is structurally controlled by a series of subparallel shear zones which cut the gabbro sills along most of their length. The shear zones are associated with strong deformation, veining and hydrothermal alteration in the host lithologies. Understanding the mechanisms by which ore deposition has occurred in the Stog'er Tight deposit, and the timing of the alteration/mineralization event(s), requires a knowledge of various deformational styles in the main geologic elements of the area. The following review of the structural setting is based on the work of Hibbard (1983) at the regional scale.

Hibbard (1983), subdivided the Baie Verte Peninsula into six tectonic blocks, including: 1) the Western Orthotectonic Block, 2) the Transition Block, 3) the Eastern Orthotectonic Block, 4) the Paratectonic Block, and 5) two geographically isolated blocks represented by the Horse Island and Granby Island rocks. The Point Rousse Complex as well as the great majority of the lithologic units in the Baie Verte Belt (east of the Baie Verte Line), are included

in the Paratectonic Block.

The intensity of deformation and metamorphism in the Paratectonic Block appears to be significantly less than that in the Orthotectonic and Transition Blocks (Hibbard, 1983). Most of the rocks display a single penetrative fabric, and are metamorphosed to lower greenschist facies. The main fabric in the block is a slaty cleavage or foliation (S_M) which is commonly subparallel to bedding, in the layered sedimentary and volcanic rocks. Minor folds (F_M) associated with the S_M fabric have been reported from a few areas, such as the Flat Water Pond Group and the Bobby Cove Formation. Locally throughout the block, the S_M fabric was affected by a later deformation, D_L, which is manifested as a S_L crenulation fabric and/or F_L minor folds in some areas (Hibbard, 1983). The D_E fabric associated with the westward obduction of ophiolites over the Fleur de Lys terrane is absent from the Paratectonic Block.

The Point Rousse Complex is located at the northwesternmost area of the Paratectonic Block. One of the most prominent tectonic features of the Point Rousse Complex is a nearly east-trending major syncline which was identified in the central terrane of the Point Rousse cover sequence (Fig.3-1) and is interpreted as a close-to-tight F_M fold overturned slightly to the southeast (Hibbard, 1983). The S_M fabric associated with the F_M syncline is well developed in the layered volcanic and volcaniclastic rocks of the complex. The structural pattern of the Point Rousse Complex is also dominated by northwest-dipping reverse faults which are interpreted as high angle thrust faults (Norman and Strong, 1975). These faults appear to be subparallel to the axial plane of the

major syncline and, therefore, coeval with the formation of S_M in the area, though structural relationships are locally more complex (*e.g.* the Three Corner Pond area).

The Point Rousse Complex was emplaced to the south over the Pacquet Harbour Group along the north-dipping Scrape Thrust (Fig.3-1). This structural feature appears to have been coeval with a larger tectonic event in the Baie Verte Peninsula, which involved overthrusting of the Eastern Orthotectonic Block (*e.g.* Ming's Bight Group) by the Paratectonic Block along the Scrape Thrust system and the accentuating of the Baie Verte Line along the virginite fault (Hibbard, 1983). The structural features associated with this tectonic phase are characterized by an eastward structural polarity, as opposed to the general north-south trend of the earlier (Ordovician?) structures related to continental collision and ophiolite obduction along the Baie Verte Line. Hibbard (1983) attributed these late, east-trending structures to Acadian tectonism on the peninsula. He suggested that the "Acadian event" may be related to the combined effects of uplift of the Fleur de Lys terrane and the initiation of northward movement of the Baie Verte Belt against the east limb of the Baie Verte Flexure. Accordingly, the widespread D_M deformation in the Point Rousse Complex (formation of the F_M syncline and S_M foliation) could possibly have been coeval with the juxtaposition of the Point Rousse Complex and the Pacquet Harbour Group along the Scrape Thrust, as indicated by their similar polarities. Nevertheless, U-Pb dating of the hydrothermal phases associated with the S_M shear zone (this study) provides evidence that this major tectonic

event (or at least the D_M phase in the Point Rousse Complex) occurred in the Silurian, considerably earlier than the Acadian (Devonian) orogeny.

4.2 STRUCTURE OF THE STOG'ER TIGHT DEPOSIT

The Stog'er Tight gold prospect is located on the southern limb of the regional syncline of the Point Rousse cover sequence (Fig.3-1). This part of the sequence is dominated by the mafic volcanic, pyroclastic and volcaniclastic rocks. The structures within the prospect area are essentially characterized by a well developed regional cleavage subparallel to the lithologic contacts and bedding in layered rocks. The regional cleavage (and the contacts) was subsequently affected by at least one later major deformational stage.

Kirkwood and Dubé (1992) performed a detailed structural study on the Stog'er Tight gold deposit. Much of the following discussion is a summary of that study. Kirkwood and Dubé (1992) assigned the structures in the Stog'er Tight deposit to three deformational generations termed D_1, D_2 and D_3. Accordingly, the first phase of deformation (D_1) involved intense ductile shearing which produced the regional foliation (and its related stretching lineation) in the rocks, and was presumably associated with the regional easterly-trending syncline of the Point Rousse Complex. The second event (D_2) produced south-verging asymmetric folds and axial planar, high-angle faults with roughly east-west orientation. The D_1 and D_2 structures were affected by late NNE- to NE-trending broad open folds (D_3), which clearly refolded the earlier folds. The authors suggested that the hydrothermal alteration and associated

mineralization of the host gabbro is late-D_1 and pre-D_2.

Based on the coaxial nature of the D_1 and D_2 structures, Kirkwood and Dubé (1992) also proposed an alternative structural interpretation for the Stog'er Tight deposit. This second interpretation incorporates both D_1 and D_2 structures into a single and progressive deformational episode, D_I, which was followed by a late D_{II} event (synonymous to D_3). The detailed alteration history of the deposit described in the present study strongly supports the progressive deformation model.

D_I Event

The D_I deformation is characterized by a regional and widespread S_E (early) fabric; a well developed north-dipping foliation that also contains a characteristic L_E downdip stretching lineation (Kirkwood and Dubé, 1992). The D_I deformation was probably associated with the generation of the large-scale, easterly-trending, regional syncline of the Point Rousse Complex and the disposal of the rocks in the Stog'er Tight area on the southern limb of the syncline.

In the Stog'er Tight area, the S_I foliation is best developed in the layered pyroclastic and volcaniclastic rocks. In the deformed vitroclastic ash-tuffs, the foliation is subparallel to the pyroclastic lamination or bedding, such that the distinction between the primary flow fabrics and the superimposed foliation is difficult. The fabric is more distinct in the lapilli-tuffs, where it is manifested as strained lithic fragments (Fig.3-3). The S_I foliation in the Stog'er Tight gabbro

is defined by flattened and slightly lineated chlorite and leucoxene wisps, and is absent or only weakly developed, away from the zones of shear deformation. Near major shear zones, however, the gabbro foliation intensifies and ultimately grades into a strong mylonitic foliation (schistose gabbro). The true width of the D_I shear zones is variable and ranges from a few centimetres to more than 8 metres in drill-core.

The early episode of the D_I event (D_E) was dominated by a ductile deformational regime. The most prominent indications of such early ductile phase are: 1) the considerable width of the shear deformation zones, 2) the near absence of brittle structures (*e.g.* extensional veins) and, 3) the widespread generation of mylonitic rocks (*e.g.* phyllonites), in association with this phase. Following the early D_E ductile phase, the D_I event was continued by a late deformational episode (D_L) which had brittle-ductile affinities and was more localized spatially compared to the D_E phase. The D_L deformation is characterized by the development of quartz-carbonate-albite ($\pm$chlorite) veins and mesoscopic, E- to SE-trending, asymmetric (kink) folds, which folded the S_E-L_E fabric (Kirkwood and Dubé, 1992). Within the main D_I shear zones, the superimposition of D_L (brittle-ductile) deformation on the earlier S_E-L_E (ductile) fabric resulted in the development of a prominent cataclastic fabric concomitant with strong chloritic alteration (see Chapter 7).

Virtually all of the D_I structures (including both D_E and D_L structures) reflect a north-over-south thrust movement which was subparallel to, and presumably coeval with, the large-scale block displacement along the Scrape

thrust (D_M thrusting). Structural and textural evidence also imply that gold mineralization in the high-grade alteration zone of Stog'er Tight was essentially confined to D_I shear zones, and was associated with a late-D_E to early-D_L episode of deformation (see chapter 6).

D_{II} Event:

The D_{II} deformation is characterized by the development of broad-open, regional, NNE- to NE-trending anticlines and synclines (F_{II}) which clearly affected the D_I inclusive structures (Kirkwood and Dubé, 1992). Late-stage brittle faults that displace D_I structures as well as the mineralized zones, could also be related to this event. The D_{II} phase had its maximum deformational effects on the east and southeastern parts of the general Stog'er Tight prospect area (*e.g.* Cliff Zone, Fig.1-1). Nonetheless, the semi-sinuous trends of the mineralization zones and the lithologic contacts in the study area can be attributed to D_{II} folding. The possible relation of the D_{II} event to the D_L deformation in the Paratectonic Block (Hibbard, 1983) is not presently clear.

4.3 VEINS STRUCTURES

Different generations of hydrothermal, quartz-dominated veins occur in the alteration/mineralization zones, as well as in the various unaltered and undeformed rocks of the study area. The strongly foliated (schistose) rocks associated with shear zones, in particular, are characterized by abundant veins of variable thickness. Crosscutting relationships are not uncommon to these

veins, and are observed in several trench outcrops (*e.g.* trench IIIS).

Kirkwood and Dubé (1992) recognized four dominant vein types with different attitudes in the general Stog'er Tight area, termed Va, Vb, Vc and Vd. Types Va and Vb were interpreted to represent the main mineralized veins, while Vc and Vd types were described as veins with no significant gold content. The authors also assigned different mineralogic assemblages to the main vein types including quartz-ankerite-chlorite-pyrite (Va), quartz-ankerite-pyrite (Vb) and quartz-carbonate (Vc). However, the present work indicates that there is no evidence of significant hydrothermal alteration and gold mineralization directly associated with any vein type, in the outcrops of the study area (Stog'er Tight and Magnetic Zones). In particular, *no* pyrite (and thus gold) is found to be present *inside* the quartz-bearing veins in the Stog'er Tight and Magnetic Zones. Textural characteristics of mineralized samples in drill-core nonetheless indicate that Au-bearing pyrite occurs frequently (but not ubiquitously) at the margins of some ductile quartz-albite-ankerite veins, within the strongly altered host gabbro. The latter are shear-parallel, replacement veins (see chapter 6) that are conspicuously dissimilar to the Va- and Vb-type extensional veins described by Kirkwood and Dubé (1992).

4.4 SUMMARY

The Stog'er Tight gold prospect is a shear-hosted mesothermal gold occurrence. Gold mineralization and the associated hydrothermal alteration were structurally controlled by a series of ductile shear zones hosted by gabbro sills.

The shear zones were presumably generated as a result of widespread deformation, folding and thrusting of the Point Rousse Complex, that took place somewhat later than the emplacement of the oceanic slab over the continental margin (Ordovician?). Two fundamental deformational events were identified in the Stog'er Tight area. The early event (D_I) was a progressive deformational event that consisted of an early ductile episode (D_E) followed by a late brittle-ductile phase (D_L). Evidence of the ductile to brittle transition is recorded in the fabrics of strongly deformed and altered rocks, in the D_I shear zones. Textural and petrologic evidence confirm that gold deposition occurred late in the D_E ductile episode, prior to the ductile-brittle transition. Gold-bearing pyrite is present inside the altered host rock and appears to be in relation with syndeformational (replacement) quartz-albite-ankerite veins. The inclusive D_I structures and fabrics were subsequently affected by a later (D_{II}) deformational event which is responsible for the present configuration of the lithologic units and the mineralized zones in the Stog'er Tight deposit.

CHAPTER 5: PETROGRAPHY OF THE STOG'ER TIGHT GABBRO

5.1 INTRODUCTION

Fine- to medium-grained, dominantly mesocratic rocks that constitute the multiple intrusions (sills) of the Stog'er Tight prospect, were generally identified as gabbro, based on mesoscopic criteria. As these rocks, despite their variable geochemical properties, appear to have many lithologic and petrographic similarities, they are herein collectively termed *gabbro*. Kirkwood and Dubé (1992), in their structural study of the Stog'er Tight gold prospect suggested that it is hosted by *differentiated* gabbroic sills. They identified two distinct lithologic units within the northernmost or upper gabbro body (area of this study), mainly based on megascopic field criteria. These were referred to as leucogabbro and ferro-leucogabbro units which were distinguished by their different modal abundances of Fe-Ti oxides. However, the petrographic and geochemical results of this study indicate that the apparent macroscopic contrasts within the individual gabbro bodies are essentially due to grain-size variations, and the modal and chemical compositions of the gabbro vary over a relatively narrow range across the sills. The general term Stog'er Tight Gabbro

is therefore retained in this chapter, though the compositional variabilities (Chapter 7) among individual gabbro sills should by no means be overlooked.

5.2 MINERALOGY

The mineralogy of the Stog'er Tight gabbro is best recognized away from zones of shear deformation and fine-grained lithologic contacts, where the penetrative foliation (S_1) and alteration effects are minimal or even absent. The pre-alteration mineralogy of gabbro has an assemblage of plagioclase (60-45%), amphibole (30-45%), titanomagnetite (7-20%) and epidote ($\leq$5%). The accessory minerals (<5%) are chlorite, calcite, titanite and apatite. Although the abundance of amphibole in these rocks is more consistent with the modal composition of diorites, the chemical analyses of the present work strongly suggest a gabbroic composition for the intrusive rocks of the Stog'er Tight deposit (see Chapter 6 and Appendix II).

Commonly, plagioclase and amphibole grains (up to 4mm and 7mm in diameter, respectively) constitute the isotropic framework of the rock with other minerals occurring as either interstitial grains or as replacements. Centimetre-scale patches of coarse-grained, pegmatitic gabbro locally occur within the massive, medium-grained (aplitic) gabbro. An ophitic fabric of large amphibole grains partially enclosing plagioclase prisms is a typical textural feature of the pegmatitic gabbro in thin section (samples BN19-02 and JR91590, Fig.5-1). Granular and intergranular fabrics are common in the medium-grained gabbro. Locally, plagioclase laths are grouped together in discrete clusters that produce

a glomeroporphyritic fabric (*e.g.* sample 91814-B5).

5.2.1 Plagioclase

Plagioclase occurs in the gabbro as interlocked prisms up to 4mm long. It is characterized by prominent polysynthetic twins, and is altered to varying degrees to fine-grained epidote and less commonly, sericite. Crystallographic measurements on twinned plagioclase grains (Michel-Levy's method) from the best preserved gabbro samples indicated that the plagioclase has an albitic composition (<10% An), which was confirmed by SEM semi-quantitative analyses and XRD measurements as well (samples BN19-03 and BN60-A9). Nevertheless, the presence of abundant epidote in association with albite denotes that the original igneous plagioclase must have had significant amounts of Ca in its composition (see section 5.3.1).

5.2.2 Amphibole

Amphibole is present as dark-green laths up to 7mm long and is prominently intergrown with plagioclase (ophitic fabric) in the coarse-grained, pegmatitic gabbro. In thin section, subhedral to euhedral prisms of amphibole are characterized by a pale greenish-yellow colour, very weak pleochroism, first to lower second order interference colours (maximum = second order blue) and inclined extinction. Most prisms are terminated by frayed margins, which are asbestiform aggregates of fine-grained acicular amphibole. The petrographic and optical properties of the amphibole are consistent with those of actinolite. The

dominance of actinolite (low-Al amphibole, as opposed to Al-bearing hornblende) in the Stog'er Tight gabbro is also verified by SEM and XRD analyses (*e.g.* samples BN60-A9 and BN19-03). However, two gabbro samples from the eastern Stog'er Tight, one from a trench outcrop (JR91590) and the other from drill-core (BN67-A22), contain green amphibole with strong pleochroism and high extinction angles, characteristic of hornblende (Fig.5-2). Sample BN67-A22, in particular, contains small relics of pleochroic amphibole (hornblende) surrounded by actinolite along the grain margins (Fig.5-3). SEM analyses have clearly shown that the pleochroic interiors of the grains (hornblende) have considerably higher Al and Fe, and lower Si, Mg and Ca contents, compared to the actinolite-dominated rims (see Appendix 1). These textural and compositional features imply that there are replacement (and/or overgrowth) relationships between hornblende and actinolite. Both amphiboles contain abundant minute inclusions of zircon and titanite.

Intrusive gabbroic rocks with analogous mineralogy and field relationships have been reported from other parts of the Point Rousse Peninsula (*e.g.*, north of Stog'er Tight, and north of the Deer Cove adit), to contain hornblende (K. Deveau, personal comm.,1992). It is notable that no relict pyroxene has yet been observed in the Stog'er Tight gabbro and the associated rocks.

5.2.3 Titanomagnetite

Igneous magnetite that contains abundant exsolution lamellae of ilmenite (commonly termed titanomagnetite) is a characteristic constituent of the Stog'er

Tight gabbro. It occurs in all levels of the gabbro body, ranging in size from 0.3 mm to ≈ 1 cm, and is variably altered to leucoxene. Leucoxene is a secondary, semi-opaque assemblage of very fine-grained Ti-oxides (and silicates) which may include titanite, rutile and/or anatase. In the unaltered gabbro, titanomagnetite is surrounded by round, massive lumps of leucoxene which have replaced the titanomagnetite at the grain margins and also along the exsolution lamellae within the grains (Fig.5-4). The alteration of the primary titanomagnetite along a series of well oriented, planar lamellae creates visible patches of white to creamish leucoxene with characteristic skeletal patterns. SEM analyses indicate that the leucoxene lumps in the unaltered gabbro (*e.g.* sample BN61-03) are essentially composed of cryptocrystalline titanite aggregates.

The areal distribution of leucoxene in the gabbro, within and outside the alteration zones, strongly suggests that the conversion of titanomagnetite to titanite-bearing leucoxene predated the hydrothermal alteration associated with the gold mineralization in Stog'er Tight. The relative immobility of Ti and the high chemical resistance of Ti-bearing minerals under hydrothermal conditions render the leucoxene resistant to the effects of hydrothermal alteration (see Chapter 8).

5.2.4 Epidote

Epidote has a wider distribution than amphibole in the gabbro. It ranges in grain-size from very fine-grained, dust-like inclusions inside the plagioclase

prisms, to single epidote grains as large as 0.6mm (*e.g.* sample BN60-A9) and is characterized by a pale-yellow colour. SEM analyses of epidote are given in Appendix 1. The second common mode of occurrence of epidote in the gabbro is as coarse-grained, polycrystalline porphyroblasts up to 2mm in diameter which locally display polygonal shapes (Fig.5-5). These porphyroblasts occur along the plagioclase grain boundaries and within the intergranular spaces. Some quartz occurs locally in association with these porphyroblasts, and both epidote types are closely associated with plagioclase (albite). There are also discrete veins within the massive gabbro, which are characterized by intensive epidote alteration. In these zones, plagioclase is totally replaced by epidote such that the actinolite pseudomorphs occur in a matrix entirely composed of medium-grained, recrystallized epidote.

5.2.5 Chlorite

The occurrence of chlorite is common to low-grade metamorphic rocks (greenschist facies), and to the Stog'er Tight gabbro, in particular. However, chlorite is present only as a minor constituent (as inclusions within actinolite) where the gabbro is well preserved. In thin section, flaky aggregates of chlorite with pale olive-green to dark brown anomalous birefringence form small wisps that internally replace the actinolite grains (Fig.5-6). This chlorite (type A) is distinct from other types of chlorite (B-C) associated with hydrothermal alteration of the gabbro (see Chapter 7). In the slightly altered (but undeformed) gabbro, actinolite is partially to totally replaced by chlorite forming

pseudomorphs after actinolite. SEM analyses indicate that chlorites in the Stog'er Tight deposit have a generally high (>20 wt%) Al content (see Appendix 1). Chlorite A, in particular, has a FeO/MgO ratio of about 1.8, which is notably lower than those in the hydrothermal chlorite (3.5 to 4.6) in the chlorite-magnetite alteration zone (see Chapter 7).

5.3 METAMORPHISM

The albite-actinolite-epidote mineral assemblage of the Stog'er Tight gabbro is a characteristic metamorphic paragenesis, while the field and textural relationships (*e.g.* chilled margins, isotropic igneous fabrics, etc.) strongly suggest that the gabbro was originally emplaced as a series of planar, igneous bodies intruding the stratified country rocks. These observations provide important insights to the igneous and metamorphic history of the host gabbro.

5.3.1 Metamorphic Assemblage

Figure 5-7 demonstrates mineral and whole-rock chemical compositions from the Stog'er Tight Gabbro, compared to the average compositions of the common metamorphic mineral phases. The mineral composition data are from SEM semi-quantitative analyses (see Appendix 1). The albite-actinolite-epidote-chlorite assemblage corresponds to a low metamorphic grade (greenschist facies) and the plotted whole-rock analyses are consistent with the modal abundances of these minerals in the Stog'er Tight Gabbro (*e.g.* paucity of

chlorite in the unaltered gabbro). The presence of chlorite and actinolite, in particular, are diagnostic of low grade metamorphism and the formation of Fe-rich epidote (rather than clinozoisite) reflects the Fe-rich composition of the mafic source rock(s). The albitic composition of the plagioclase and the predominance of actinolite over hornblende in the gabbro, place this mineral assemblage in the lower greenschist facies, within the estimated temperature range of 350 to 450°C (Winkler, 1979).

The well-preserved mineral textures can be used to constrain the mineralogic composition of the Stog'er Tight gabbro prior to its metamorphism. The close textural association of Ca-bearing epidote to metamorphic albite suggests that both have been derived from a pre-existing calcic plagioclase. In the case of actinolite and hornblende, the interpretation of phase relations is equivocal. Aluminous hornblende is stable over a wide range of high and medium metamorphic grades, while it reacts to form actinolite under low grade (retrograde) metamorphic conditions. Alternatively, hornblende can be formed from actinolite by prograde metamorphism. Thus, hornblende in the Stog'er Tight Gabbro can be either the precursor or a product of the actinolite. Nevertheless, the abundance of coarse actinolite with pseudomorphous igneous fabrics (*e.g.*ophitic), and the almost ubiquitous occurrence of chlorite patches *within* the actinolite pseudomorphs (Fig.5-6) suggest the transformation of original hornblende to actinolite, with the excess Al of the former stabilizing the aluminous chlorite.

Accordingly, the Stog'er Tight gabbro can be interpreted as a mafic to

intermediate, shallow level, intrusive rock which was originally composed of calcic plagioclase, aluminous hornblende, and titanomagnetite, plus subordinate amounts of titanite and probably apatite. The gabbro along with its country rocks was subjected to metamorphism at low grade (lower greenschist) conditions after crystallization.

5.3.2 Type of Metamorphism

Perhaps the most prominent feature of metamorphism in the Stog'er Tight gabbro is that it was not associated with any considerable deformation in the rock. The regional penetrative cleavage (S_1) and its associated anisotropic fabrics, such as the L_1 stretching lineation and the shear zone mylonitic fabrics, have apparently overprinted the retained igneous fabric of the gabbro (metagabbro). Moreover, the porphyroblastic fabric that is indicative of syntectonic recrystallization and stress-induced metamorphic mineral growth, is entirely absent from the undeformed metagabbro. This evidence has significant implications for the tectonic setting and the metamorphic regime of the Stog'er Tight Gabbro and associated rocks.

The metamorphic features of the Stog'er Tight gabbro (and also the surrounding rocks) are conspicuously different than those formed during burial metamorphism. The latter often involves partial to complete mineralogic and textural reconstitution of the rocks (*e.g.* crystalloblastic fabric) over a broad area, due mainly to hydrostatic stresses at low metamorphic grades (Best, 1982). Such effects are essentially absent from the rocks in the study area. In

addition, the regional-scale metamorphism associated with orogenic belts and convergent tectonic regimes (such as the Appalachians) is characterized by well developed tectonite (anisotropic) fabrics as a result of imposed non-hydrostatic stresses. These fabrics include regional foliation, lineation, folding and thrusting. Although these structural features are locally present in the Point Rousse Complex, the Stog'er Tight metagabbro generally lacks any of these tectonite fabrics and the observed deformation post-dates the major metamorphic phase in the area. Furthermore, the sporadic outcrop of hornblende-metagabbro in close spatial association to the actinolite-metagabbro, and also the local occurrence of intensely epidotized vein systems in the massive gabbro, suggest that metamorphism in the study area was a distinct patchy phenomenon, rather than a pervasive, regional event. All these features imply that metamorphism of the Stog'er Tight Gabbro was not related to orogenesis, but was a result of sub-sea-floor hydrothermal processes that presumably affected the whole Point Rousse Cover Sequence.

Sub-sea-floor metamorphism takes place in the vicinity of ocean-floor spreading centres, within several hundred kilometres of the mid-ocean rifts. This distance corresponds to rocks as old as 10 Ma. Metamorphism occurs as the result of convective circulation of heated seawater through the hot, newly formed oceanic crust at low pressures. Low grade metavolcanics and metagabbros with preserved relict igneous fabrics (isotropic greenstones) are common products of the sub-sea-floor metamorphism (Best, 1982). This type of metamorphism is patchy (even on the thin section scale) and is commonly

associated with veins of secondary metamorphic minerals. In addition, the chemical exchange during seawater-rock interaction at elevated temperatures can precipitate calcite, silica, magnetite, sulfides, etc. at shallow levels. In the Stog'er Tight area, the presence of small massive sulphide lenses within the volcanic/pyroclastic sequence, and also the occurrence of magnetite interbeds and chert in the volcaniclastic rocks are further indications of sub-sea-floor metamorphism.

5.4 DEFORMATION OF GABBRO

The microstructural transition from the albite-actinolite-epidote-metagabbro (undeformed) to the intensely deformed gabbro in the shear zones is commonly associated with extensive hydrothermal alteration and widespread formation of new mineral phases (see chapter 7). The latter have generally obscured the textural relationships and deformational fabrics of the pre-existing mineral grains. However, isolated sections of the shear zones which have not been subjected to pervasive alteration, demonstrate the microstructural transformation accompanying deformation of the Stog'er Tight gabbro. Accordingly, the progressive shear deformation in the gabbro can be categorized in terms of intensity into three successive stages. It is notable that these three progressive stages correspond to the same deformation event (regional D_1 event, see Chapter 4) and are only distinctive in terms of microstructural development.

The earliest stage of deformation in the gabbro is recognized only in thin

section and is characterized by a weak foliation fabric of mineral grains. The strained plagioclase (albite) grains contain internal subgrains with slightly displaced crystallographic orientations. Small-scale kinks crosscut the plagioclase grains and new, fine-grained, polygonal quartz and albite (neocrysts) are formed along the kinks and at the grain/subgrain boundaries (Fig.5-8). The deformation of actinolite is characterized by the formation of fibrous (acicular) actinolite along the grain boundaries and in areas of more intense strain.

The second stage of deformation is marked by the well developed mesoscopic foliation and lineation in the rock. It involves progressive mylonitization of the plagioclase megacrysts and the concomitant development of fine-grained, strain-free quartz-albite (-chlorite) aggregates which enclose the relict porphyroclasts. Actinolite is partially to totally replaced by polycrystalline aggregates of chlorite, that locally show pseudomorphous grain-shapes after actinolite. The foliation is mainly defined by stretched wisps of chlorite and especially, leucoxene. Calcite porphyroblasts are locally formed within the foliated groundmass. Overall, the destruction of the original fabric of the protolith by syntectonic recrystallization produces a protomylonite in this stage (Fig.5-9).

Towards the centre of the shear zones, the final stage of gabbro deformation is associated with the progressive transformation of the protolith to homogeneously fine-grained, recrystallized quartz-albite-chlorite aggregates. This process results in the widespread formation of orthomylonite and finally ultramylonite (Fig.5-10). Fractured and stretched leucoxene porphyroclasts are

the only constituent of the protolith that ultimately survive the intense mylonitization of this stage. The mylonitic groundmass, chlorite aggregates and the leucoxene wisps have all been strongly lineated and dragged parallel to the foliation. As a result, the produced ultramylonite has a well-developed schistosity (Fig.5-11).

The successive phases of deformation and their corresponding microstructures discussed above clearly indicate that the gabbro deformation was dominated by mylonitization processes. It is now widely accepted that mylonites, in general, form as the products of ductile deformation, dynamic strain recovery and syntectonic recrystallization of the country rocks, as opposed to clastic milling and brittle breakage (*e.g.*Bell & Etheridge, 1973; Wise et al.,1984). This indicates that ductile shearing was responsible for the majority (if not all) of the observed deformational fabrics in the Stog'er Tight gabbro.

5.5 SUMMARY

Detailed petrographic studies indicate that the Stog'er Tight gold deposit is hosted by mesocratic gabbro and dioritic gabbro sills. Gabbro is interpreted to have been composed of the assemblage calcic plagioclase, amphibole (aluminous hornblende?) and titanomagnetite, plus subordinate amounts of titanite and/or apatite. Subsequent low-grade metamorphism resulted in the (*in situ*) transformation of the gabbro to an albite-actinolite-epidote (-chlorite) greenstone. This process is attributed to sub-sea-floor metamorphism. The

metamorphosed gabbro and the associated rocks were subsequently subjected to an episode (or episodes) of ductile deformation which was locally associated with progressive mylonitization and/or hydrothermal alteration in the corresponding shear zones

Figure 5-1 Photomicrograph of plagioclase (grey) and actinolite (amber) in pegmatitic gabbro showing ophitic fabric. Note that the actinolite in the picture is a single grain (xpol. x14).

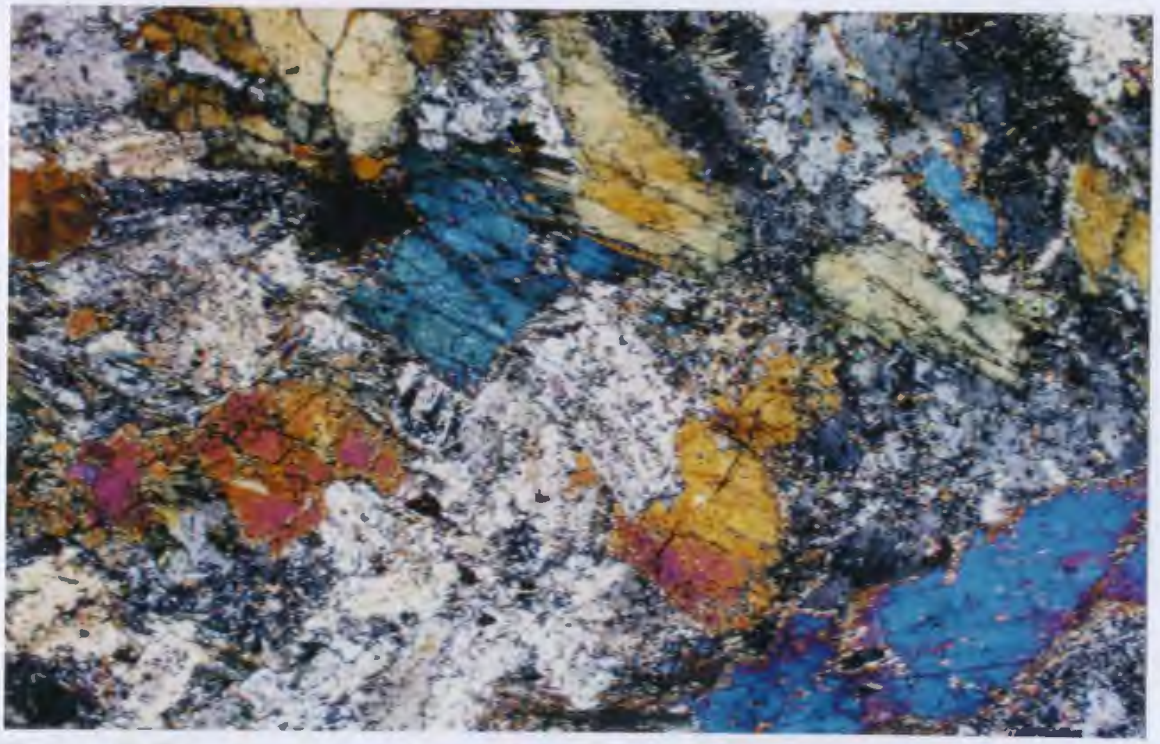

Figure 5-2 Photomicrograph of hornblende (birefringent) in coarse-grained gabbro (sample JR9150, xpol. x25).

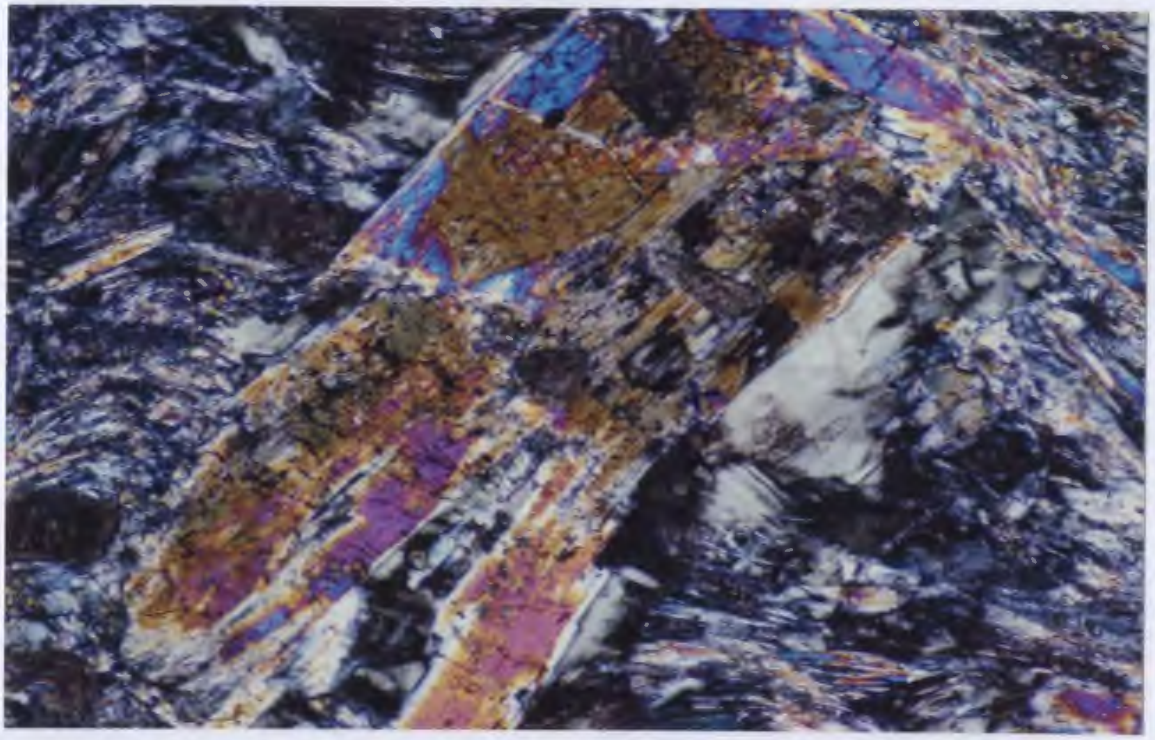

Figure 5-3 Photomicrograph of relict hornblende (yellow-brown) rimmed by actinolite (vivid) along the grain boundaries. Note the acicular actinolite in the matrix (xpol. x100)

Figure 5-4 Photomicrograph of a large leucoxene grain in contact with hornblende (green) in coarse-grained gabbro. Note the relict titanomagnetite (opaque) within the grain (x25).

Figure 5-5 Photomicrograph of an epidote polycrystalline porphyroblast (birefringent) surrounded by plagioclase in the gabbro (xpol. x25).

Figure 5-6 Photomicrograph of large gabbro actinolite grains (birefringent), internally replaced by chlorite wisps (dark brown) (xpol. x25).

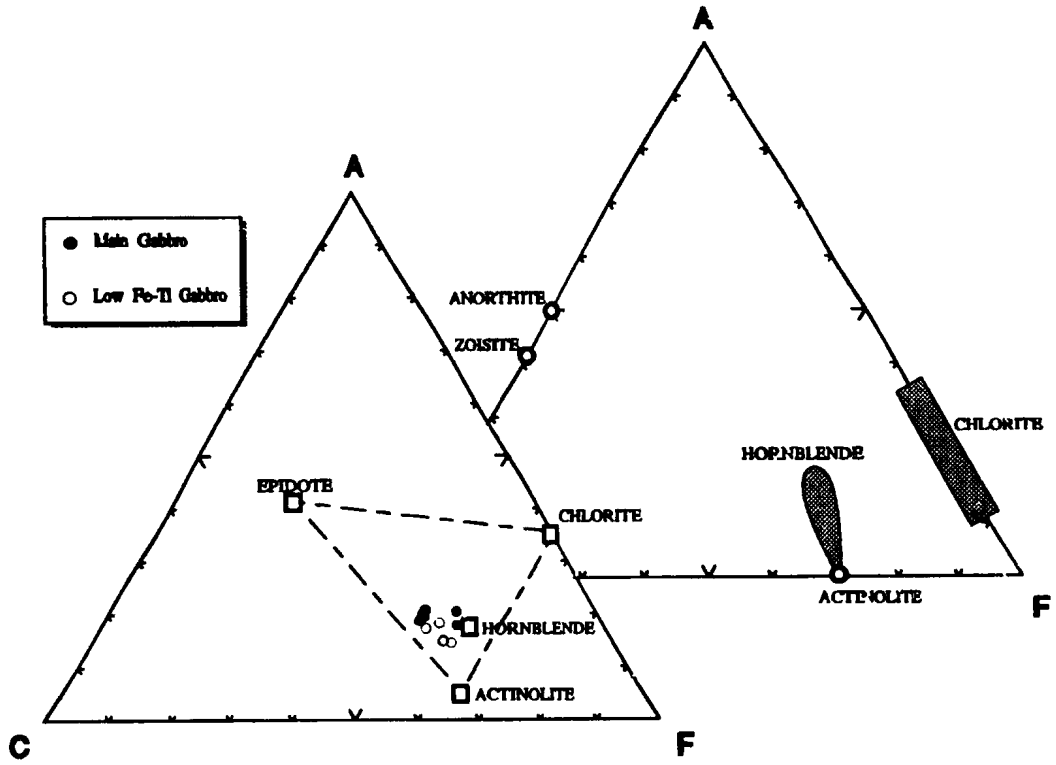

Figure 5-7 ACF diagram showing the analyzed mineral and whole-roc : compositions for the Stog'er Tight gabbro. The typical mineral compositions are from Winkler (1979).

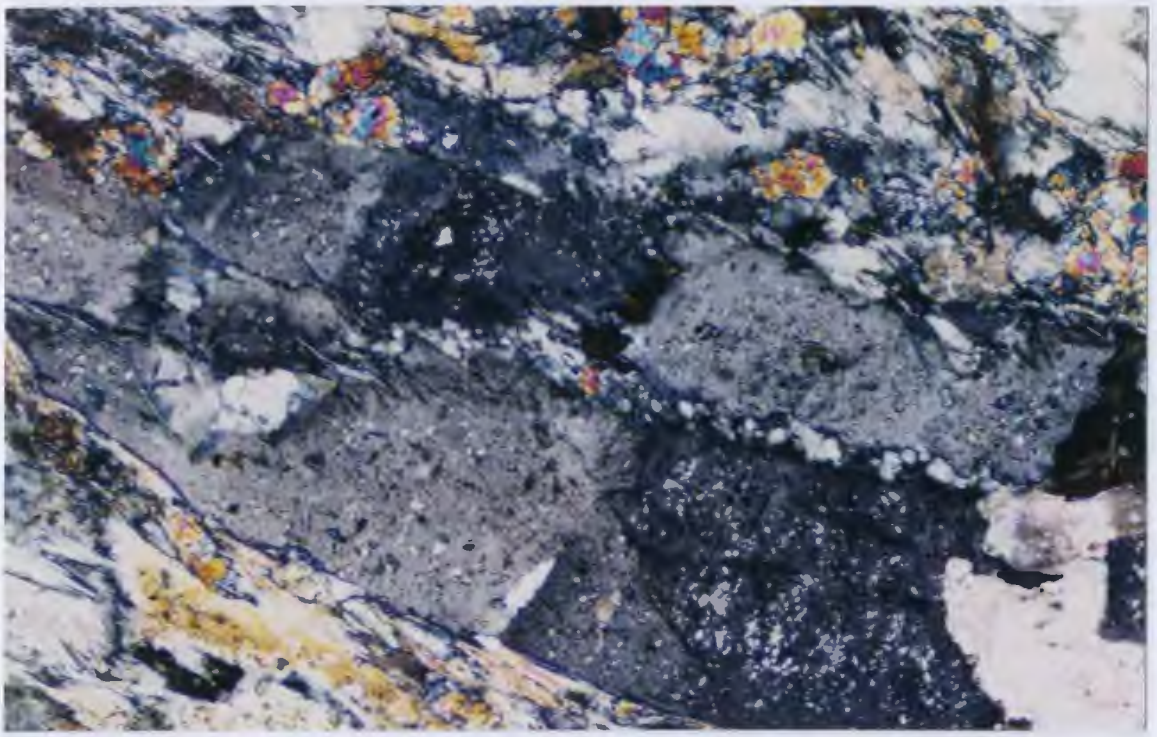

Figure 5-8 Photomicrograph of a strained plagioclase in a weakly deformed gabbro. Note the occurrence of displaced subgrains with variable extinction in plagioclase (xpol. x100).

Figure 5-9 Photomicrograph of a moderately deformed gabbro illustrating the formation of a protomylonite (xpol. x25).

Figure 5-10 Photomicrograph of an ultramylonite showing the intensity of mylonitic deformation in the gabbro. Note the stretched plagioclase relics in the middle.

Figure 5-11 Comparison between undeformed gabbro (above) and the strongly sheared gabbro (below) in hand sample. Note the development of schistosity in the deformed variety.

CHAPTER 6: GEOCHEMISTRY OF GABBRO AND VOLCANIC ROCKS

6.1 INTRODUCTION

Field and petrographic studies have indicated that the mylonitic shear deformation, high-grade hydrothermal alteration and the associated gold mineralization have all been preferentially developed in the Stog'er Tight Gabbro. Although the preferential shear deformation may be explainable by the mechanical and rheological properties of the host lithologies, the prominent association of gold mineralization to the altered gabbro raises the classical question of compositional influence of host rock on mineralization. Understanding the physicochemical conditions of fluid-rock interaction in the context of deformation/alteration processes, moreover, requires a knowledge of the tectonic environment prior to, and during the mineralization event. Consequently, the geochemical characteristics and petrogenesis of different rock units in the area, as well as their spatial and temporal variations, are of particular importance to this study. In this chapter, geochemistry is used to place necessary constraints on a) the petrogenesis and possibly the tectonic setting of the various lithologic units in the study area with emphasis on the

Stog'er Tight Gabbro and, b) geochemistry of the gabbro as a reference or starting point in evaluating the superimposed geochemical effects of the progressive hydrothermal alteration (see chapter 7).

6.2 GEOCHEMICAL DATA

6.2.1 Selection of Samples

A total of 48 samples from different rock types (including altered and unaltered samples) have been analyzed for major and trace elements (the analytical methods and their specifications are described in Chapter 1). The stratigraphic, lithologic and petrographic characteristics of the major rock units are referred to in Chapters 3 and 5. ICP-MS trace element analyses (including REE) were performed on a subset of 26 samples, and the results were plotted on mantle-normalized (spider) diagrams. In this chapter, 20 of the analyzed unaltered samples that best represent the major lithologic units were selected for geochemical presentation. Geochemical data for these samples are given in Appendices II and III.

Samples of the main Stog'er Tight Gabbro (MGAB) that hosts the mineralization zones were collected from a broad area in order to cover the whole range of compositional variation of gabbro (within the limits of the study area). All of the selected samples are from drill-core with the exception of sample 91822-3 (geochronology sample) which was collected from a trench

outcrop. The small, low Fe-Ti gabbro sill (LFTG) which occurs at the top of the main gabbro was systematically sampled and analyzed to assess the compositional variations between separate gabbros and also the possible fractionation trends within the individual sills. The LFTG samples were all selected from drill-hole BN89-55 (drill-section 101+00W) that has recovered a complete section through the sill, from the top to the bottom chilled margins.

The sample set of this chapter includes 4 volcanic (effusive) and 3 pyroclastic rocks (Appendices II and III) that were collected from different stratigraphic levels of the sequence and represent variable rock types within the volcanic/pyroclastic unit (VPU). Two of the pyroclastic samples (BN53-01 and -02) are laminated ash-tuffs, the third sample (BN18-B3) is a crystal-tuff with plagioclase phenoclasts. All three samples are free of lithic fragments. The volcanic samples were selected after careful petrographic examinations and only the least altered samples with well preserved volcanic fabrics (*e.g.* microlithic groundmass) were chosen for geochemistry. The volcanic sample BN54-B5, in particular, is from a drill-core interval that shows pillow-like structures.

All of the rocks in the Stog'er Tight area have undergone lower greenschist-facies (sub-sea-floor) metamorphism (see chapter 5). In addition, a large portion of these rocks have been subjected to shear deformation and/or hydrothermal alteration. Consequently, the chemical composition of the rocks is likely to have been changed significantly due to elemental mobilization and transportation during the metamorphic/hydrothermal processes. The onset of hydrothermal alteration is commonly associated with strong chlorite alteration

followed by introduction of sericite (muscovite) in the rocks. The geochemical results from the hydrothermally altered rocks (chapter 7) indicates that sericite alteration is marked by noticeable compositional variations in the altered rock. Therefore, the compositional effects of hydrothermal alteration can be compensated for by careful petrographic examination of the prospective samples and rejection of those with significant sericite (and chlorite) alteration.

Most of the major elements, such as SiO_2, Na_2O and K_2C, and the great majority of low field-strength elements (LFSE: Cs, Rb, Ba, Sr, etc.) except Th, appear to be mobile under a variety of conditions, including low-grade metamorphism (e.g. Coish, 1977). The application of these elements to this geochemical study is unlikely to give meaningful results. In contrast, it is generally accepted that the high field-strength elements (HFSE: Y, Zr, Nb, Hf, Ta, Ti and P), Th, the transition metals (TE: Sc, V, Cr, Co and Ni) and the rare earth elements (REE) are essentially immobile during weak to moderate alteration/metamorphism of crystalline rocks under low fluid/rock ratio conditions (*e.g.* Pearce & Cann, 1973; Shervais, 1982; Wood et al., 1979). The petrogenetic interpretations of this study are essentially based on the concentrations of these immobile elements in the rocks.

It is notable that the majority of geochemical plots used herein for tectonic interpretation were originally designed for the study of mafic (to intermediate) volcanic rocks that are generally presumed to represent the melt (magma) compositions. Application of these diagrams to the geochemical analysis of intrusive rocks like gabbros will thus be of questionable validity.

Nevertheless, field evidence indicates that the Stog'er Tight gabbro was emplaced as a series of shallow intrusions with limited volumes. Therefore, unless a large magma chamber at depth fed these sills, processes such as open-system crystal fractionation and wallrock assimilation are unlikely to have significantly affected the chemistry of the gabbro under these conditions.

6.2.2 Data Presentation

The degree to which magma composition has been affected by various fractionation processes is of prime interest to any petrologic study. The parameter which is frequently used as an indicator of magmatic fractionation is Mg# (100MgO/[MgO + FeO]). However, because of the mobile character of Fe and Mg under metamorphic conditions, and especially the low precision of XRF measurements for Mg, this parameter has not been used in this study. Zr (a HFSE) has been commonly used as an independent fractionation index for mafic volcanic rocks (*e.g.* Pearce & Norry, 1979; Shervais, 1982). Figure 6-1 illustrates the systematic covariation of Zr and Ti for different rock suites in the study area (MGAB, LFTG and VPU). The geochemically evolved samples of each suite are characterized by higher Zr contents, which is consistent with their lower abundances of mafic minerals. The geochemical data are plotted on the Zr/Ti versus Nb/Y discrimination diagram of Winchester & Floyd (1977) (Fig. 6-2) on which the rocks all fall within the subalkaline field. Almost all of the analyzed samples plot inside or close to the andesite/basalt field. The Zr/TiO_2 ratio (vertical axis on the diagram) is defined as a sensitive index of differentiation

as it reflects the overall decline of TiO_2 content in the differentiated rocks. In contrast, the Nb/Y ratio (horizontal axis) has been denoted as an indicator of alkalinity (Pearce & Cann, 1973; Winchester & Floyd, 1977). Figure 6-2 therefore implies that 1) the Stog'er Tight intrusions range in composition from subalkaline gabbro to dioritic gabbro, 2) MGAB and LFTG are not simply related by magmatic differentiation, but they are distinctive in terms of alkalinity and, 3) volcanic (effusive) members of VPU cover a wide range of composition from basalt to a relatively alkaline andesite.

The Zr-Zr/Y diagram of Pearce and Norry (1979) is used to discriminate between the MGAB, LFTG and VPU suites and to assign possible tectonic settings to each rock suite (Fig.6-3). This diagram shows that all of the MGAB samples plot inside the field of within-plate basalts. The VPU ranges from depleted island arc basalts (tholeiites) to strongly enriched andesites which plot out of the designated fields. The interpretation of LFTG on this diagram is somewhat controversial as the samples from this suite plot somewhere between the MORB and intraplate basalts fields. The diagram clearly shows that the MGAB and LFTG samples lie along two subhorizontal but separate trends which are defined by different Zr/Y ratios. The evolved (differentiated) samples of each suite have shifted to the right (higher Zr content) along these trends. In contrast, the plot of rocks on a Zr versus Nb diagram (Fig.6-4) indicates that the Zr-Nb co-variation (with fractionation) appears to be consistent for all three rock suites.

Shervais (1982) formulated a tectonic discrimination diagram for modern

and ophiolitic volcanic rocks based on the relative abundances of the incompatible transition metals V and Ti (also a HFSE). The rock suites under study were plotted on a similar diagram (Fig.6-5) and the results were compared to the modern analogues. MGAB and LFTG all tend to plot between Ti/V ratios of 20 and 50 which define the field of MORB, while MGAB tends to have higher Ti/V ratios than LFTG. Regarding the VPU, the most depleted members of the suite (tholeiitic basalts) are characterized by high V and low Ti contents and lie inside the field of island arc lavas. Other members of the VPU including the strongly enriched andesites are conspicuously lower in V and plot within the MORB field (see below for interpretation).

Interpretations on the petrogenesis and tectonic setting of the rocks in the Stog'er Tight deposit area can be best made with reference to primitive-mantle normalized, extended, rare earth element plots (spider diagrams, see appendix IV for normalizing factors). The customized plots of this study (Figures 6-6a to 6-6d) include in addition to REE, the immobile HFSE, and Th as the only representative of LFSE. According to these plots, VPU contains some samples with calc-alkaline affinity, while others are depleted tholeiites. In addition, the gabbro units show variable degrees of LREE enrichment.

6.2.3 Interpretation of Results

All of the rocks analyzed for petrogenetic study are characterized by Nb/Y ratios less than 1 (Fig.6-2), indicating their non-alkalic affinity. The TiO_2

contents of the gabbroic rocks have systematically increased with fractionation (*i.e.* Zr enrichment, Fig.6-1), with the exception of the most evolved member of the MGAB suite (sample 91822-3) which shows slight Ti depletion despite its high Zr content. This geochemical behaviour is characteristic of the tholeiitic rock series (Miyashiro & Shido, 1975). The depleted (most primitive) members of the VPU tend to follow the same tholeiitic fractionation trend, though a significant compositional gap exists between these and the other analyzed samples. The rest of VPU members exhibit Ti depletion with fractionation (Fig.6-1) similar to that in the evolved tholeiitic and/or calc-alkaline series rocks.

The Zr, Nb and Y plots of Figures 6-3 and 6-4 imply that the MGAB and LFTG are distinctive in terms of Zr/Y ratios, whereas the Zr/Nb covariation (Fig.6-4) appears to be quite consistent for all of the rocks under study (including VPU). Pearce and Norry (1979) postulated that the variations in Zr/Y ratio could be explained in one of several ways: a) a systematic source heterogeneity, b) variations in the degree of partial melting of a garnet-lherzolite source, c) progressive melting of a single source or, d) fractional crystallization in which garnet is an important crystallizing phase. Presently, there is no evidence for deep-seated partial melting or fractional crystallization which could have possibly launched the garnet-liquid fractionation in the rock suites under study (*e.g.* no Yb or Lu anomaly in REE patterns). Arc magmas, in general, are suggested to have originated from the uppermost 100 km or at most 200 km of the mantle (Gill, 1984), well above the stability field of garnet. Moreover, it has been suggested that Zr/Nb ratio is insensitive to partial melting (or fractional

crystallization) and most of its variations can be attributed to source heterogeneity (Pearce & Norry, 1979). Consequently, the distinctiveness of Zr/Y ratios in conjunction with the consistency of Zr/Nb ratios in all three rock suites can be explained by the episodic partial melting of a single (but not necessarily homogeneous) source material. This interpretation, however, seems to be more applicable to the MGAB and LFTG suites rather than the VPU rocks.

The petrogenetic affinities and possible tectonic setting of the VPU could be modelled with reference to the Ti-V diagram of Shervais (1982) (Fig.6-5). Most arc-related tholeiitic rocks have Ti/V ratios ≤ 20 and therefore are distinctive from MORB on the Ti-V plot. In general, the more evolved rocks of the oceanic arc tholeiite suite are characterized by titanomagnetite fractionation (Miyashiro & Shido, 1975; Shervais, 1982). The fractionation of titanomagnetite (and hornblende) in the final stages of crystallization results in a drastic reduction in Ti and V concentrations and tends to increase the Ti/V ratio, so that the evolved arc-related rock may eventually plot inside the MORB field. The effects of titanomagnetite fractionation are even more evident in the calc-alkaline series rocks which are characterized by progressive Ti (and V) depletion throughout their evolution. Figure 6-5 shows that the most primitive members of VPU (arc tholeiites) have significantly variable V concentrations and plot in the field of island-arc volcanics, whereas the rest of VPU samples are shifted towards higher Ti/V ratios. The VPU can therefore be interpreted as a suite of arc-related extrusive rocks which range in composition from tholeiitic basalts to calc-alkaline andesites. This is probably suggestive of a transition

from tholeiitic to calcalkaline magma genesis in the source of these rocks.

It has long been pointed out that the volcanic rocks erupted in the modern island-arc settings are characterized by an under-abundance of HFSE and enrichment of the LFSE relative to the light REE (LREE) (*e.g.* Pearce & Cann, 1973; Wood et al.,1979). The HFSE depletion is more apparent in the case of highly incompatible elements such as Nb and Ta (high La/Nb and La/Ta ratios), whereas Hf, Zr and Ti depletions are not considered as a ubiquitous signature (Salters & Hart, 1991). Numerous studies have also indicated that more evolved products of calc-alkaline arc volcanism show pronounced HFSE signatures (including Zr and Hf depletion), though in these cases fractionation of minerals like zircon and Fe-Ti oxides can be involved. Accordingly, a negative Nb anomaly and positive Th anomaly on the extended REE plots of this study is regarded as a sufficiently reliable criterion for the identification of arc-related rocks.

The mantle-normalized trace-element patterns of the three rock suites under study-MGAB, LFTG and VPU-are mutually distinctive (Fig.6-6). MGAB is characterized by inclined REE patterns, moderate LREE enrichment ($La_N/Yb_N = 3.0\text{-}3.3$) and distinctive Th negative anomaly (Fig.6-6a). This pattern is characteristic of many MORB-type basalts and is almost identical to that of the E-type MORB (enriched MORB) of Sun and McDonough (1989). The most evolved member of MGAB (sample 91822-3) is conspicuously enriched in both light and heavy REE and plots above others, between the fields of E-MORB and alkali basalt (OIB). This sample also shows a distinct negative Ti anomaly that

is consistent with its highly fractionated tholeiitic affinity.

The LFTG suite features relatively flat REE patterns and slight LREE enrichment ($La_N/Yb_N = 1.6$). These rocks, in particular, are characterized by slight, negative Nb and Ti anomalies (Fig.6-6b). This feature in conjunction with the obvious lack of any negative Th anomaly discriminates the LFTG suite from the typical MORB. The LFTG signature can therefore be interpreted to be transitional between island-arc and relatively enriched MORB. As the analyzed LFTG samples were collected across an individual sill, the parallel variations in the REE patterns and the progressive Ti depletion can well be explained by limited shallow-level fractionation during crystallization. The parallel trace element variations in MGAB, by analogy, can be attributed to the same fractional crystallization effects.

Unlike the gabbroic rocks, the VPU represents a suite of highly variable volcanic and pyroclastic rocks that range in geochemistry from slightly LREE-depleted to strongly LREE-enriched end members. Nevertheless, all of the VPU samples display prominent negative Nb and positive Th anomalies characteristic of island-arc volcanic rocks (Fig.6-6c). The arc tholeiites of the suite are characterized by a general LREE depletion ($La_N/Yb_N = 0.7\text{-}0.8$) and represent the most depleted rocks known in the area. In contrast, the calc-alkaline andesites have steep REE patterns and are strongly enriched in LREE ($La_N/Yb_N = 15.6\text{-}20.6$). The HFSE depletion in the enriched andesites involves not only the strongly incompatible elements Nb and Ta, but the more compatible Zr, Hf and Ti, as well (Fig.6-6c). These features are consistent with the evolved calc-

alkaline character of these rocks. The pyroclastic samples of the VPU plot in the field between the depleted and enriched end members, featuring slight LREE enrichment and negative Nb and Ti anomalies (Fig.6-6d). The extended REE patterns of VPU are therefore consistent with the transitional tholeiitic - calc-alkaline magmatism in the island arc source of these rocks.

6.3 PETROGENESIS AND TECTONIC HISTORY

The above discussion indicates that the relatively limited area which underlies only the eastern part of the Stog'er Tight gold prospect (study area) includes a number of mutually distinctive lithologic units with significantly different geochemical characteristics. The Stog'er Tight Gabbro (MGAB), in particular, features E-MORB to OIB geochemical signature which are not in accord with the evident island-arc affinity of the enclosing volcanic/pyroclastic rocks. The progressive transition from island-arc volcanism to MORB- and OIB-dominated magmatism in the area, therefore, is not consistent with a simple intra-oceanic island arc model.

Arc magmas, in general, are chemically complex and contain variable contributions from subducted oceanic crust, overlying mantle wedge, and the crust (sialic or oceanic) through which the magmas ascend. All three sources are themselves variable in composition. Gill (1984) provided geochemical and isotopic evidence from the Fijian rocks (an intra-oceanic arc and back-arc basin)

that both MORB and OIB sources coexist in the uppermost mantle above the subducted lithosphere. The opening of back-arc basins (the Lau and North Fiji Basins) by rifting within the last 3 Ma has gradually removed the Fiji arc from proximity to the subducting lithosphere. This arc-rifting episode involves a distinct alkali olivine basalt volcanism that is characterized by high TiO_2 contents (1.6 to 2.8%) and resembles OIB both in trace element and isotopic respects (Gill, 1984). Accordingly, the MORB/OIB-related trace element characteristics of the Stog'er Tight Gabbro as well as its spatial and temporal relationships to the corresponding island-arc volcanic rocks can be correlated to those of the Fijian alkali basalts. A similar tectonic setting could also be inferred by analogy for the Stog'er Tight Gabbro.

Volcanic sequences with rock-types analogous to those in Stog'er Tight are known from other parts of the Baie Verte Peninsula (*e.g.* Snooks Arm Group) as well as the Central Volcanic Belt of Newfoundland (*e.g.* Wild Bight Group). The upper stratigraphic levels of the Arenigian Snooks Arm Group (see Chapter 2) that overlies the Betts Cove Complex are dominated by LILE-enriched tholeiites. These volcanic rocks apparently lack the island-arc geochemical signatures and are interpreted to have been formed in an oceanic island or back-arc basin setting (Jenner & Fryer, 1980). The early to middle Ordovician volcanic, subvolcanic and epiclastic rocks that comprise the Wild Bight Group in Central Newfoundland include rocks with both arc and non-arc affinities (Swinden et al., 1990). The alkalic to LREE-enriched (non-arc) tholeiitic volcanic rocks that overlie - and their equivalent subvolcanic rocks which

intrude - the arc-related volcanic products of the group are interpreted to record a late stage of back-arc basin development following the arc-rifting episode (Swinden et al.,1990). The suite of strongly LREE-enriched non-arc tholeiites (type N-II) of the Wild Bight Group, in particular, has many geochemical features in common with the Stog'er Tight main gabbro.

Proposing a feasible petrogenetic model for the Stog'er Tight Gabbro and the associated rocks, however, is restricted by the fact that the presented data are from a limited area which represents only a small fraction of the Point Rousse Volcanic Cover Sequence. Thus, the results of the present study, while suggestive, may not be extendable to include the whole rock sequence and a regional tectonic model based on these results will be of questionable value.

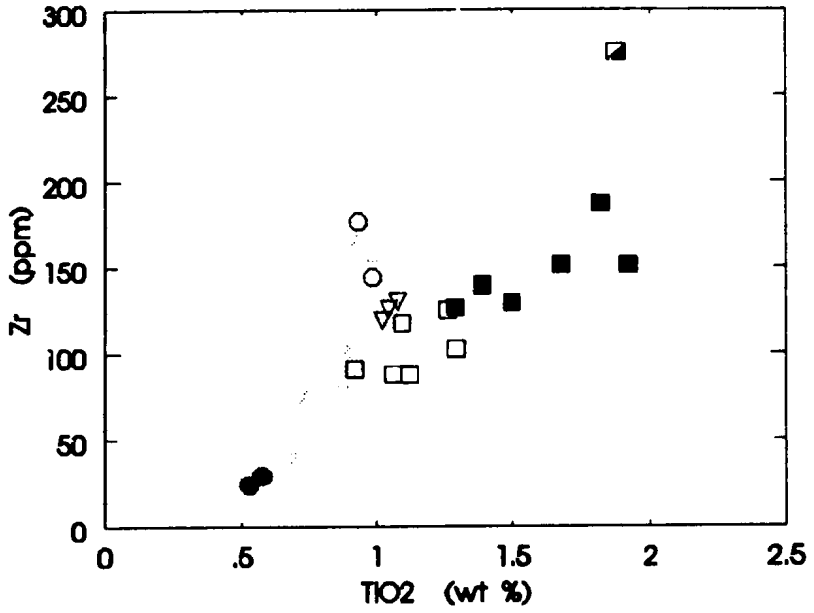

Figure 6-1 Ti-Zr diagram for analyzed samples of LFTG (open squares), MGAB (solid squares), and the gabbro geochronology sample (half-filled square). VPU samples are shown by circles (volcanic rocks) and triangles (pyroclastic rocks).

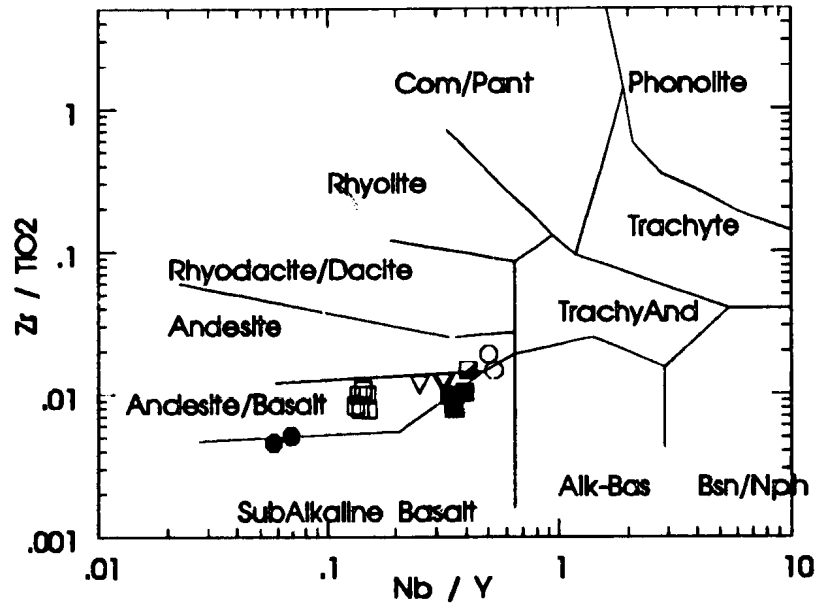

Figure 6-2 Nb/Y-Zr/Ti diagram after Winchester & Floyd (1977). Symbols as in Figure 6-1.

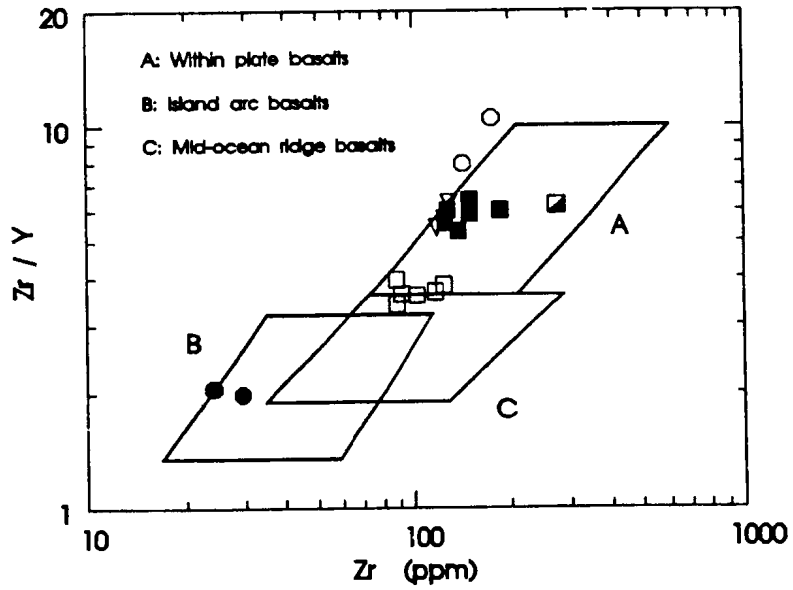

Figure 6-3 Zr-Zr/Y diagram after Pearce & Norry (1979). Symbols as in Figure 6-1.

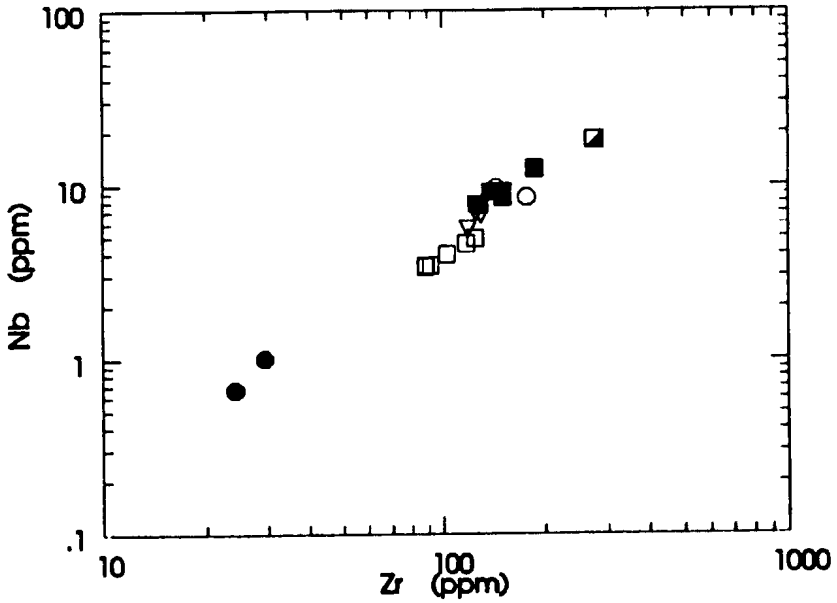

Figure 6-4 Zr-Nb diagram for samples of three rock suites (LFTG, MGAB and VPU). Symbols as in Figure 6-1.

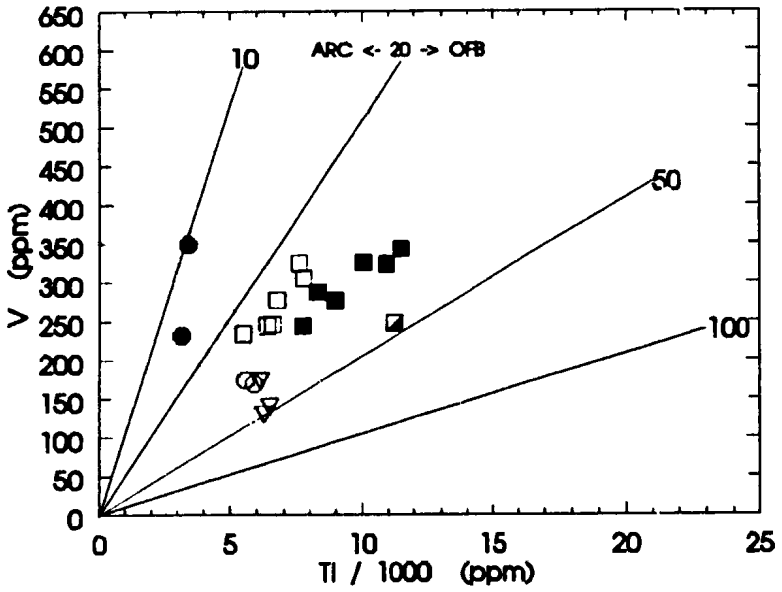

Figure 6-5 Ti-V diagram after Shervais (1982). Symbols as in Figure 6-1. The shaded area marks the field of VPU samples.

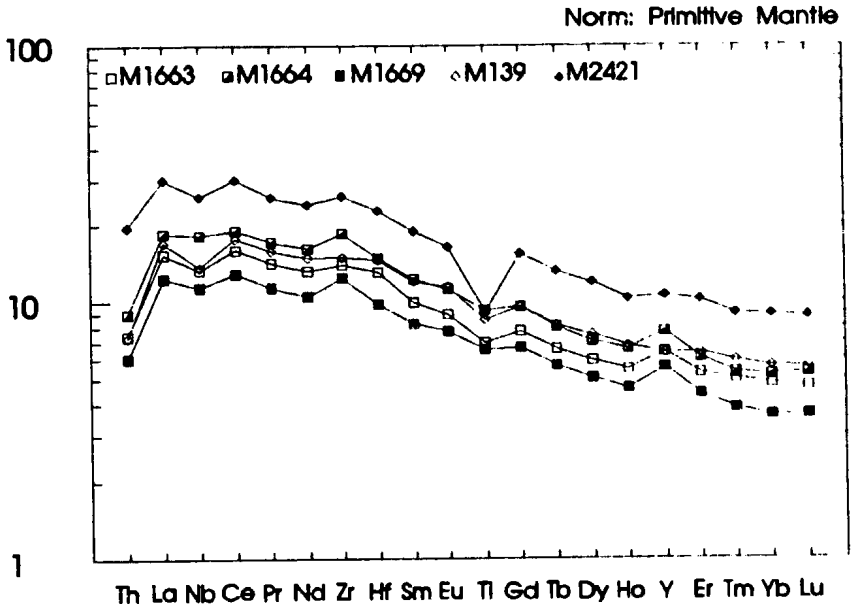

Figure 6-6a Extended REE plots of MGAB samples. See Appendix II for sample specifications.

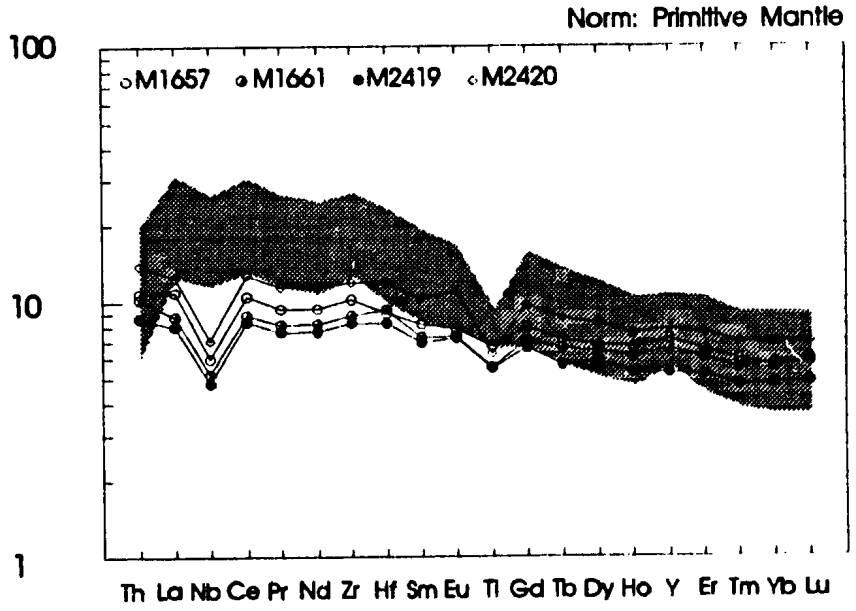

Figure 6-6b Extended REE plot of LFTG samples. The shaded area represents the field of MGAB composition illustrated in Figure 6-6a.

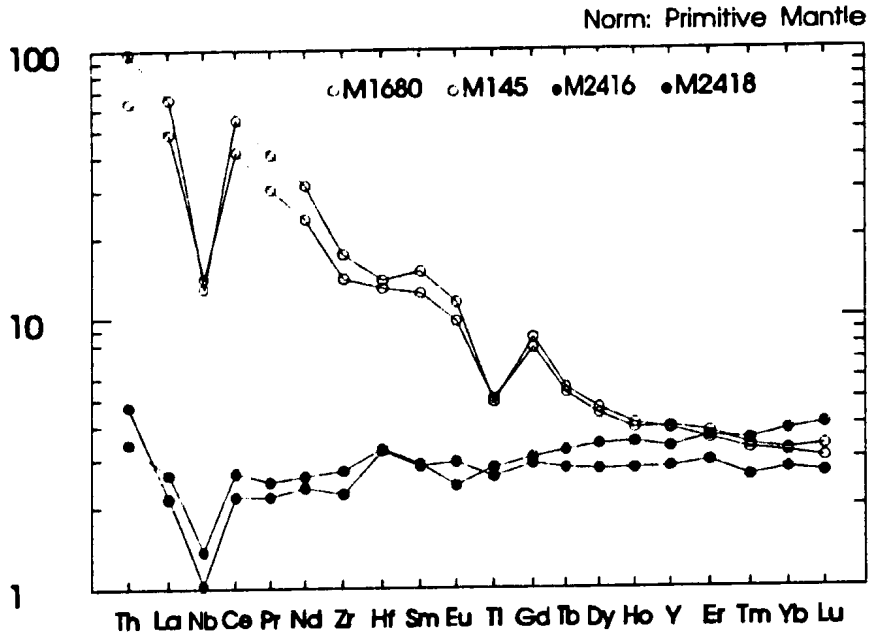

Figure 6-6c Extended REE plots for the volcanic (effusive) samples of VPU.

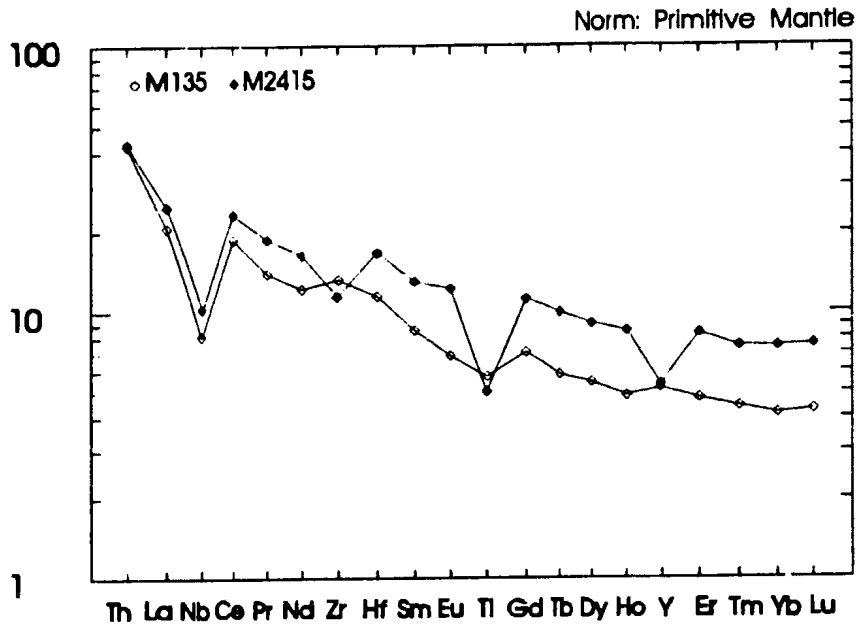

Figure 6-6d Extended REE plot of the pyroclastic samples of VPU.

CHAPTER 7: HOST ROCK ALTERATION AND GOLD MINERALIZATION

7.1 INTRODUCTION

Gold mineralization in the Stog'er Tight deposit is ubiquitously associated with extensive hydrothermal alteration of the host rocks. This close spatial association suggests that the gold precipitation and the host rock alteration were caused by similar processes and therefore correspond to the same geologic event(s). The hydrothermal alteration is marked by fundamental compositional changes in the rocks, the effects of which are visible at the outcrop scale. The alteration/mineralization processes were generally accompanied by ductile deformation of the rocks (see section 5.4), though the effects of intense shear deformation are not evident in the high-grade hydrothermal alteration (and mineralization) zones.

The area under study includes two elongate and subparallel mineralized sections which extend along the strike of the main gabbro sill at the easternmost part of the Stog'er Tight prospect area (see Fig.3-2). These are named the Stog'er Tight Zone and the Magnetic Zone (Chapter 1) of the Stog'er Tight Gold Prospect (Huard, 1990). Mineralization occurs almost exclusively

within the Stog'er Tight gabbro, and is therefore stratabound. It also coincides with the map-scale zones of shear deformation that are best developed in the gabbro bodies. Both Stog'er Tight and Magnetic Zones feature extensive hydrothermal alteration of the enclosed rocks, though gold mineralization is only weakly and locally developed in the Magnetic Zone. Notwithstanding the spatial distinction of the Stog'er Tight and Magnetic Zones at surface (see Figure 3-2), none of the drill-holes recovered from the study area show two convincingly separate major mineralized intervals at depth (Appendix V). This suggests that the Magnetic Zone may only be a near-surface offshoot or splay of the Stog'er Tight mineralization zone.

7.2 HYDROTHERMAL ALTERATION

Gold mineralization zones in the Stog'er Tight deposit are typically bounded by broad alteration envelopes that exhibit consistent mineralogic zoning relationships. The maximum observed width of the alteration zone is 36.5m (drill-hole BN89-29, section 105+00W) and its average width is about 13m (see Appendix V). The hydrothermal alteration has produced a variety of alteration assemblages that overprint the earlier metamorphic assemblage of the gabbro described in Chapter 5. Different mineral assemblages occur systematically with increasing distance from the central high-grade ore zones. Four different alteration zones have been defined on the basis of mineralogy and named according to their characteristic mineral assemblages. These include the

chlorite-calcite zone, ankerite-sericite zone, red albite-pyrite(+gold) zone, and the chlorite-magnetite zone. Figure 7-1 is an idealized schematic illustration of the alteration sequence (zonation) in the Stog'er Tight deposit. A series of typical samples from these alteration zones are shown in Figure 7-2. Most alteration zones are separated by distinct and well-defined boundaries which mark the transition from one alteration type to another. These boundaries therefore represent the reaction fronts between different mineral assemblages. The following describes the mineralogic and textural characteristics of each alteration zone.

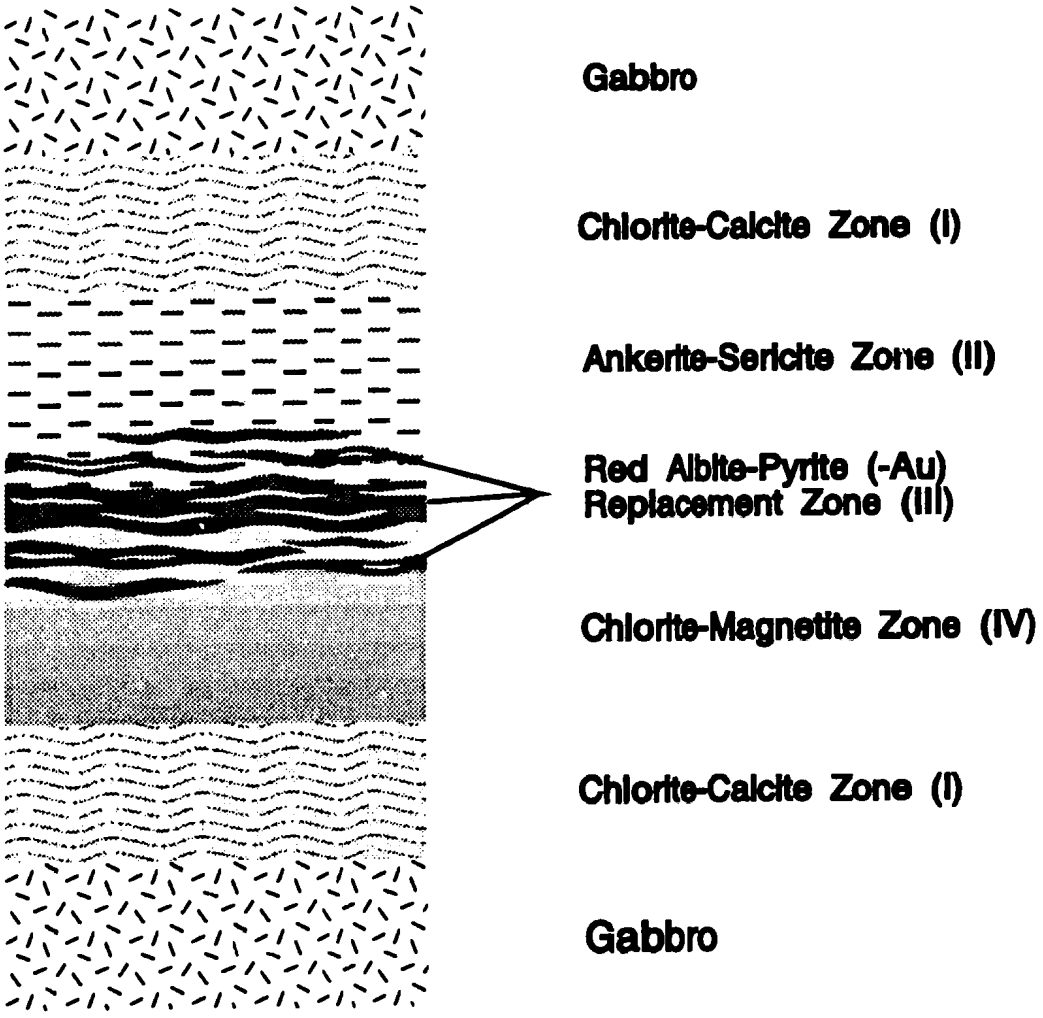

Figure 7-1 Alteration sequence in the Stog'er Tight deposit.

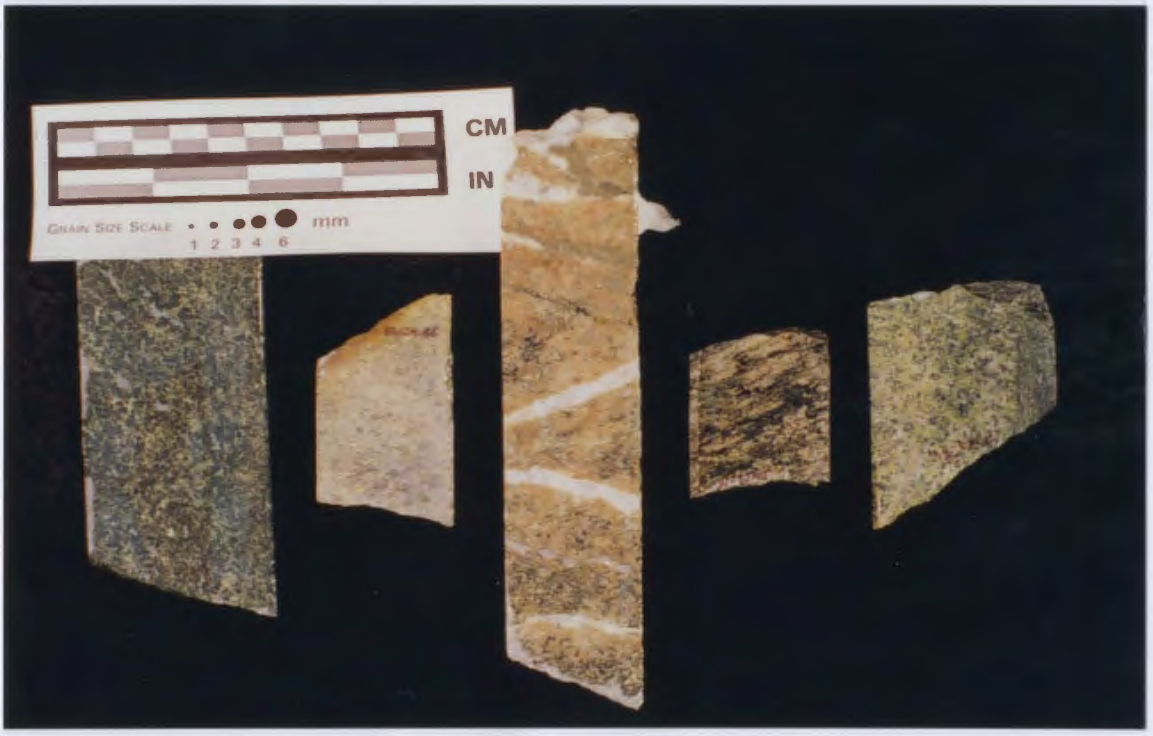

Figure 7-2 Drill-core samples of gabbro. From left to right: actinolite gabbro (unaltered), ankerite-sericite zone, red albite-pyrite zone, chlorite-magnetite zone, and epidote-rich gabbro (unaltered).

7.2.1 Zone I: Chlorite-calcite zone

This zone represents the lowest intensity of alteration and occurs furthest from the central Au-bearing structures. The exact areal distribution of this alteration zone is not clearly known, as it extends beyond the limits of the main shear zones. The onset of hydrothermal alteration is marked by the progressive breakdown of actinolite (see section 5.2.2) into chlorite resulting in round pseudomorphous domains of chlorite that are indistinguishable from the original actinolite in hand sample (*e.g.* sample BN24-02). The chlorite commonly contains minute but abundant inclusions of rutile.

Calcite is a characteristic mineral of this alteration zone. It is evenly distributed in the rock with grain-sizes up to 2 mm and it may constitute up to 10% of the rock. Despite its random distribution, calcite is more closely associated with leucoxene and chlorite, both of which occur locally as inclusions in it. The occurrence of calcite also corresponds to a considerable decrease in the abundance of epidote. Leucoxene is generally similar to that in the unaltered gabbro (skeletal, titanite-dominated) and is not significantly affected by alteration, though massive leucoxene lumps are locally coated by fine-grained, acicular rutile. The presence of minor rutile marks a transition from a titanite-dominated type of leucoxene to a rutile-rich (acicular) variety characteristic of hydrothermally altered gabbro. Apatite also occurs as fractured and partially resorbed grains up to 1 mm in diameter in this zone.

The mineralogic transformation from the unaltered gabbro (metagabbro) to a chlorite-calcite alteration assemblage can be represented by the following reaction equation:

$$3Ca_2(Mg,Fe)_5Si_8O_{22}(OH)_2 + 2Ca_2(Al,Fe)_3Si_3O_{12}(OH) + 10CO_2 + 8H_2O \rightarrow$$

actinolite epidote

$$3(Mg,Fe)_5Al_2Si_3O_{10}(OH)_8 + 10CaCO_3 + 21SiO_2$$

chlorite calcite

7.2.2 Zone II: Ankerite-sericite zone

Towards the central Au-bearing sections, the chlorite-calcite zone grades into a second distinct alteration assemblage which is characterized by pervasive carbonate and sericite alteration. This transition is marked by a pronounced colour change, from greyish-green to a bleached creamish-yellow (Fig.7-2). Hand specimens contain visible chlorite and leucoxene wisps within a light-coloured groundmass of carbonate and sericite.

Abundant, subhedral to anhedral carbonate is disseminated uniformly throughout the rock. It has variable grain-sizes (up to 1.5 mm) and has an average modal abundance of about 50%. Acid tests on selected thin sections, as well as XRD analyses, have indicated that the carbonate in this zone is ankerite (Fe-rich dolomite). The ankerite commonly contains albite, sericite and rutile inclusions and typically surrounds relict chlorite wisps. Fine-grained

muscovite (sericite) occurs as small (>0.4 mm), evenly distributed, discrete or clustered flakes and is commonly intergrown with ankerite (Fig.7-3).

The ankerite-sericite zone is characterized by the total absence of epidote and a significant decline in the abundance of chlorite. Relict chlorite occurs as elongate patches up to 2 mm long that show a variety of interference colours under microscope, though purplish birefringence (anomalous) is the most common. Samples BN60-A6 and BN60-25 have patches of chlorite containing minute rutile and abundant ilmenite inclusions (Fig.7-4). These inclusions suggest that the chlorite (type B) is closely associated with the alteration of titanomagnetite in this zone, and is different than the inclusion-free chlorite (type A) that is pseudomorphous after actinolite in Zone I. SEM analyses also indicate that chlorite B has a higher FeO/MgO ratio ($\approx$2.9) than chlorite A (see Appendix I). Skeletal leucoxene is dominated by fine, acicular rutile aggregates, while massive titanite-rich interiors have been only locally preserved (Fig.7-5). Apatite is also present in variable amounts in this zone.

The reaction equation associated with the ankerite-sericite alteration can be summarized as:

$$3(Mg,Fe)_5Al_2Si_3O_{10}(OH)_8 + 14CaCO_3 + CaTiSiO_5 + 16CO_2 + 2K^+ \rightarrow$$

chlorite calcite titanite

$$2KAl_3Si_3O_{10}(OH)_2 + 15Ca(Mg,Fe)(CO_3)_2 + TiO_2 + 4SiO_2 + 9H_2O + 2H^+$$

sericite ankerite rutile

Despite the pervasive carbonate (and sericite) alteration, most samples contain portions of recrystallized, fine-grained, quartz-albite matrix and some of them (*e.g.* samples BN60-20) still have albite relics in thin section. The early albite is therefore presumed to be stable in Zone II and is not incorporated in the above reaction.

Towards the high-grade ore zone (Zone III), the carbonate alteration is less widespread and coarse albite is abundant. The albite occurs as subhedral, greyish-white grains that are locally as large as 7 millimetres in diameter and it may constitute up to 70% of the rock (*e.g.* samples BN60-37 and BN29-B1). This albite-rich assemblage is regarded as a marginal or transitional facies of the ankerite-sericite zone, towards the red albite-pyrite alteration. Despite the large grain-size and abundance of the albite in this zone, it is conspicuously different than that in the high-grade ore zone (see below), especially in terms of colour.

7.2.3 Zone III: Red albite-pyrite (+gold) zone

This zone represents the highest intensity of hydrothermal alteration and is characterized by substantial formation of new mineral phases replacing the pre-existing gabbro constituents. The most significant features of this zone are the widespread presence of hydrothermal red albite and the occurrence of gold-bearing pyrite.

In general, the red albite-pyrite (+gold) zone occurs as a series of discontinuous, anastomosing, lens-shaped intervals (veins?), in close

association and interleaved with the albite-dominated facies of Zone II (see above). Mineralized lenses as thick as 40 centimetres are commonly located in the central parts of the red albite-pyrite zone, bordered by minor and barren lenses at both sides (see Fig.7-1). The footwall contact of the zone is gradational and intercalated with the chlorite-magnetite zone (Zone IV).

Large albite grains up to 7 mm long are the main constituent of the red albite-pyrite zone. Albite typically comprises about 80% of the altered rock and is characterized by a prominent yellowish-red to reddish-orange colour (see Fig.7-2), though it is essentially colourless in thin section. Colour zoning of the albite is visible in a number of mineralized samples (*e.g.* sample BN60-34). Pyrite occurs as either small disseminated cubes or, more commonly, as localized patches of large, polygrain aggregates. Gold is invariably confined to the aggregates of pyrite. The red albite-pyrite zone also contains minor amounts of muscovite (sericite), ankerite and minor chlorite. Slender apatite prisms up to 2mm long are abundant in this zone. Coarse leucoxene grains, the only remnant of the gabbro, have been recrystallized into rutile pseudomorphs with crystals up to 0.5 mm in diameter. The rutile-dominated leucoxene is widespread throughout the mineralized intervals and appears to be in close textural association with the Au-bearing pyrite so that the latter has commonly overgrown and/or enclosed patches of leucoxene (Fig.7-6).

The following reaction equations summarize the mineralogic transformations from an ankerite-sericite altered gabbro to a red albite-pyrite (+gold) assemblage:

$$KAl_3Si_3O_{10}(OH)_2 + 3Na^+ + 6SiO_2 \rightarrow 3NaAlSi_3O_8 + K^+ + 2H^+$$

sericite quartz albite

$$FeTiO_3 + Ca(Mg,Fe)(CO_3)_2 + 4(HS)^- \rightarrow$$

titanomagnetite ankerite

$$2FeS_2 + TiO_2 + Ca^{2+} + Mg^{2+} + 2CO_2 + 2H_2O$$

pyrite rutile

7.2.4 Zone IV: Chlorite-magnetite zone

The red albite-pyrite (+gold) zone is bounded in the hanging wall by the ankerite-sericite alteration zone which should recur in the footwall to the mineralization if the alteration zonation is symmetrical. However, the immediate footwall of the high-grade ore zone in the Stog'er Tight deposit is characterized by a distinctive alteration (and deformation) style, different than that in alteration zones II and III. This zone is characterized by intensive chlorite alteration associated with cataclastic deformation (see Section 7.3). The uppermost part of the chlorite-magnetite zone interleaves with the red albite-pyrite alteration (replacement veins), whereas the lower contact is gradational with the footwall chlorite-calcite zone (see Fig.7-1).

The chlorite-magnetite zone is characterized by a notable dark-green appearance in both drill-core and outcrop (Fig.7-2). Relics of brecciated grey albite grains are commonly visible close to the high-grade zone (Zone III), similar

to those in the albite-rich facies of the hanging wall ankerite-sericite zone. The largest leucoxene grains (up to 1 cm in diameter) are observed in the chlorite-magnetite zone, suggesting that this zone generally coincides with the coarsest-grained gabbro at the centre of the sill(s). The altered gabbro of this zone is also strongly magnetic, containing up to 5% magnetite.

Albite occurs as single and/or polygrain porphyroclasts in the chlorite-magnetite zone. It is variably fractured or brecciated and is normally widely dispersed within a matrix of chlorite, carbonate and fine-grained quartz (Fig.7-7). Chlorite alteration is widespread and is closely associated with carbonate and locally, sericite. A prominent feature of many (but not all) samples of this zone (*e.g.* samples BN53-21 and BN60-40) is the coexistence of two different types of chlorite with distinctive optical properties and chemical compositions. The groundmass chlorite (type C) is characterized by a weak pleochroism, pale greenish-yellow colour and dark grey birefringence. It has progressively replaced the grey albite and especially, ankerite, along the cleavages and twin planes, such that these phases almost totally disappear in the advanced stages of alteration. The other generation of chlorite (type D) is strongly pleochroic, green in colour, and has indigo to purple-blue birefringence (Fig.7-8). The latter type is prevalent as interstitial stringers and fracture fillings in the rock, which suggests that chlorite (D) formed later than chlorite (C). SEM analyses on samples BN53-18 and BN60-40 have indicated that the two chlorite types can be differentiated from one another (and also from chlorite types A and B) based on their chemical compositions (see Appendix I). Chlorite (C) has Al_2O_3/SiO_2 and

FeO/MgO ratios of about 0.68 and 3.6 respectively, whereas those of chlorite (D) are 0.93 and 4.5, respectively. Both chlorite types locally contain variable amounts of sericite as disseminated inclusion.

The chlorite-magnetite zone is also characterized by the occurrence of Ti-free magnetite which is exclusive to the altered gabbro in this zone. Magnetite forms small octahedra up to 0.2 mm in diameter, that are locally visible in drill-core or otherwise can be detected by a hand magnet. There is generally a close textural relationship between euhedral magnetite and the skeletal gabbro leucoxene, which is analogous to the pyrite-leucoxene association in Zone III. Centimetre-long stretched leucoxene grains overgrown by magnetite can be observed in the chlorite-magnetite zone of trenches IIIM and VM, as well as in the drill-cores BN89-53 and BN89-60. The textural and mineralogic features of the magnetite in this zone (*e.g.* lack of inclusions and skeletal texture) suggests that it is hydrothermal in origin, as opposed to the igneous ilmenomagnetite (and metamorphic leucoxene) in the gabbro. It is notable that the strongly magnetic alteration facies of Zone IV is widespread in the study area and is by no means confined to the so-called Magnetic Zone, though the latter contains the largest leucoxene (and overgrown magnetite) grains found in the area.

Carbonate is variably abundant in the chlorite-magnetite zone and occurs mainly associated with chlorite in the matrix of the altered rock. SEM analyses and direct acid digestion tests on thin sections have shown that both calcite and ankerite exist in this zone, with calcite commonly occurring in fractures interstitial to the ankerite grains. This clearly indicates that the formation of

ankerite was followed by a late phase of calcite precipitation. Minor amounts of sericite and pyrite also occur locally in IV. The presence of sericite flakes with diffuse boundaries within chlorite (both C and D types) aggregates suggests that sericite is replaced by a late chlorite alteration.

The following is a suggested equation for the alteration reaction in the chlorite-magnetite zone:

$$15Ca(Mg,Fe)(CO_3)_2 + 2KAl_3Si_3O_{10}(OH)_2 + 3FeTiO_3 + 6H_2O \rightarrow$$

ankerite sericite titanomagnetite

$$3(Mg,Fe)_5Al_2Si_2O_{10}(OH)_8 + Fe_3O_4 + 3TiO_2 + 15CaCO_3 + 2K^+ + 15CO_2$$

chlorite magnetite rutile calcite

It is notable that the above alteration reaction has been incomplete, such that the coexistence of the reactants and products is typically observed.

Figure 7-3 Photomicrograph of the ankerite-sericite altered gabbro showing abundant ankerite (buff-grey), sericite (birefringent), albite (twinned) and leucoxene (opaque) (xpol. x25).

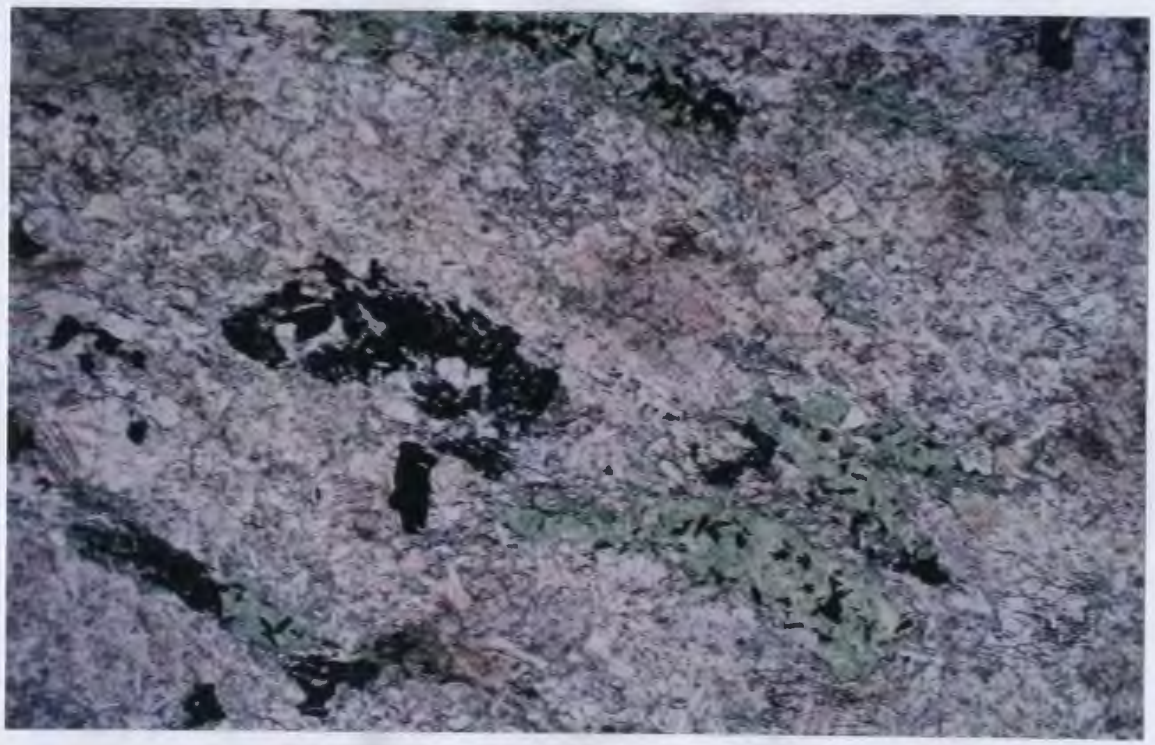

Figure 7-4 Photomicrograph from the ankerite-sericite alteration zone. Patches of chlorite (green) contain abundant rutile and ilmenite inclusions (x25).

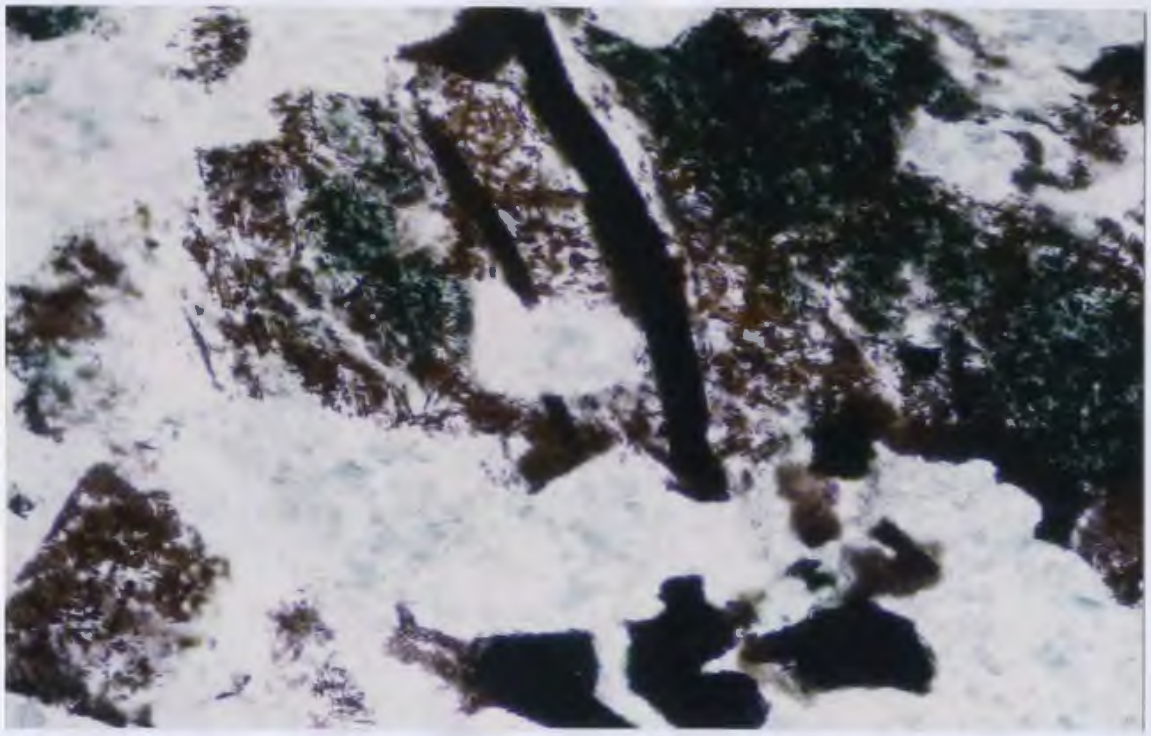

Figure 7-5 Photomicrograph of the ankerite-sericite altered gabbro showing the replacement of massive leucoxene lumps (opaque) by acicular rutile (translucent) (x100).

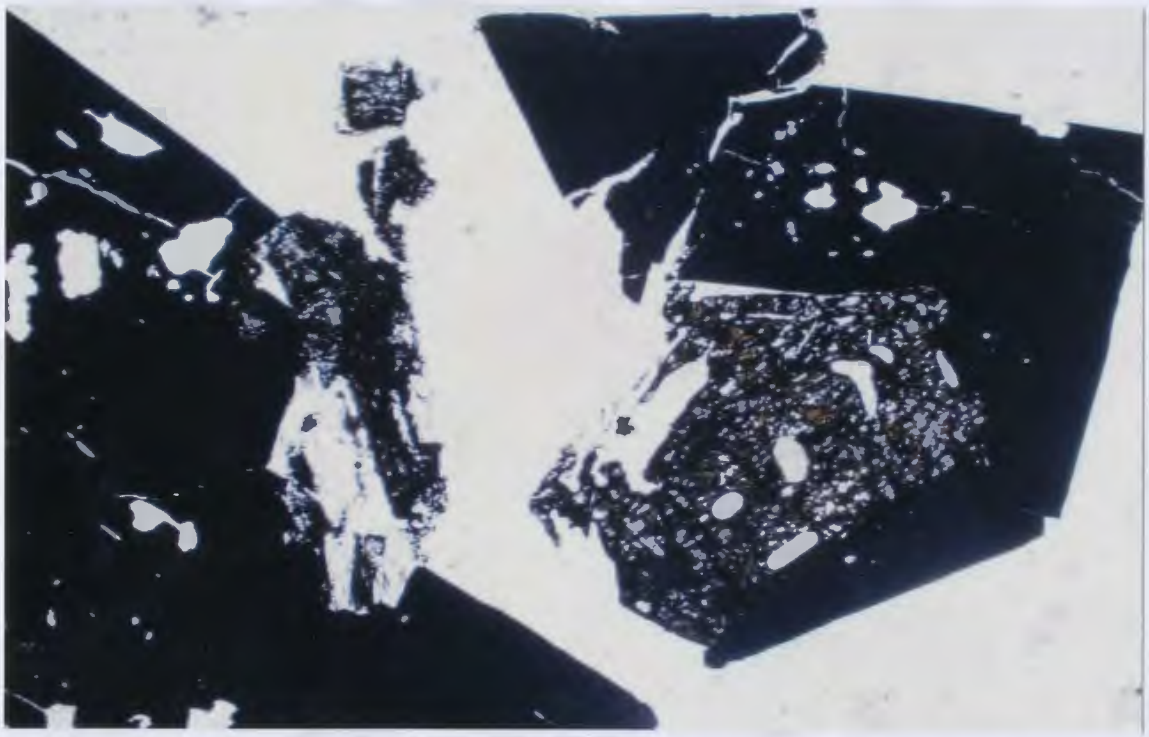

Figure 7-6 Photomicrograph from the red albite-pyrite zone illustrating patches of porous leucoxene partially enclosed by pyrite. White background is dominantly albite (x25).

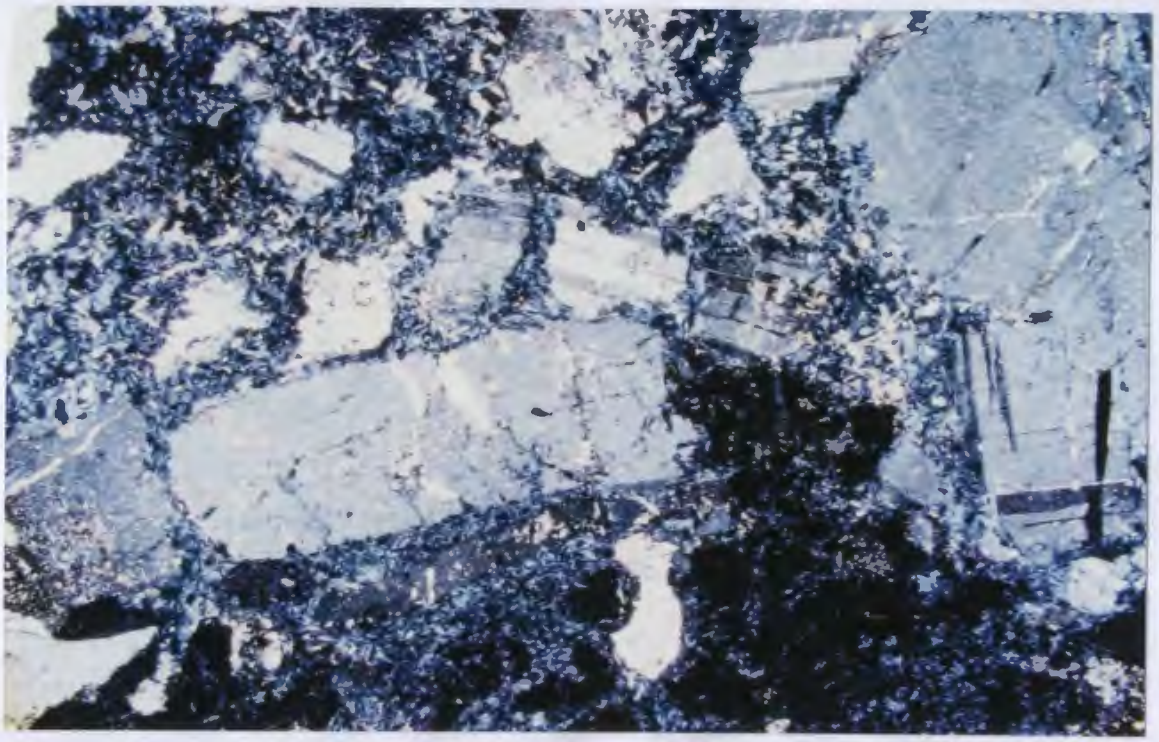

Figure 7-7 Photomicrograph of chlorite-magnetite altered gabbro showing fractured and brecciated albite (twinned) in a matrix of fine-grained chlorite (cataclastic deformation) (xpol. x14).

Figure 7-8 Photomicrograph of chlorite-magnetite altered gabbro illustrating two generations of chlorite. Note the early chlorite (yellow-green) replacing albite along twin planes (x100).

7.3 DEFORMATIONAL FABRICS IN THE ALTERATION SEQUENCE

Hydrothermal alteration in zones of high shear strain generally produces a variety of deformational fabrics and microstructures in the altered rocks. These fabrics are defined by the distribution and morphologies of the newly formed alteration phases (porphyroblasts or neocrysts), as well as of the pre-existing mineral grains (porphyroclasts). The texture of the altered rock depends on a number of parameters, including the nature of deformation (*e.g.* brittle versus ductile deformation), rate of strain recovery (*e.g.* recrystallization), intensity of alteration and the relative timing of alteration with respect to deformation. This section describes the textural characteristics of the altered rocks in the alteration sequence of the Stog'er Tight deposit. Articles by Bell and Etheridge (1973) and Wise *et al.*(1984) are useful references for the definitions and terminologies of the deformational fabrics used in this work.

The deformational microstructures in the alteration zone of the Stog'er Tight deposit are highly variable and range from purely ductile fabrics (*e.g.* mylonitic deformation) to brittle-ductile (semi-cataclastic) features. The calcite-chlorite alteration (Zone I) is commonly associated with a weak to moderate foliation fabric (*e.g.* sample 91821-C4). Albite laths contain internal dislocated subgrains and are locally recrystallized to fine-grained quartz and albite along the grain/subgrain boundaries (see Section 5.4). The foliation is mainly defined by the stretched wisps of chlorite and leucoxene.

The altered gabbro in the ankerite-sericite zone has been subjected to

strong mylonitic deformation, as revealed by the abundance of recrystallized quartz/albite aggregates and the local occurrence of albite porphyroclasts in the matrix. However, the pervasive carbonate (and sericite) alteration has widely obscured the resulting mylonitic foliation, such that the altered rock looks massive in hand sample. Stretched chlorite and leucoxene specks still define an anisotropic deformational fabric, which implies the syn- to post-tectonic formation of ankerite and sericite in the mylonitized host rock. In the albite-rich marginal facies of the ankerite-sericite zone, however, the foliation fabric is weakly developed, and the dominant, coarse-grained, grey albite laths define a semi-isotropic fabric (see below).

A variety of deformational microstructures occur in the red albite-pyrite zone, which include ductile and brittle-ductile fabrics. The dominant textural feature of this zone is an isotropic fabric that is composed mainly of large red albite grains. Commonly, the anhedral, perfectly twinned and strain-free albite grains with polygonal shapes define a crystalloblastic fabric that is characteristic of many metamorphic rocks (Fig.7-9, sample BN60-34). The isotropic fabric of the red albite neocrysts, along with the recrystallization of leucoxene into equant rutile aggregates, has obliterated any indication of shear strain in the corresponding rocks. However, the presence of a well-developed foliation in the adjacent, less intensely altered intervals of the shear zone is suggestive of a widespread mylonitic deformation in the entire alteration sequence.

Another group of samples from the red albite-pyrite zone preserve a variety of deformational features that are superimposed on the isotropic

recrystallized fabric (*e.g.* BN24-08). The red albite neocrysts locally have undulatory extinction, dislocated internal subgrains, and contorted polysynthetic twins (Fig.7-10), that are indicative of formation in a tectonically active environment. The pyrite aggregates and the albite neocrysts in a number of other samples are fractured and/or brecciated in an irregular fashion (Fig.7-11). Large pyrite grains formed during the peak of hydrothermal alteration, have been broken up into smaller subgrains as a result of this brittle-ductile deformation (Fig.7-12). Grain contortion and/or brecciation is also observed in leucoxene patches. The brittle failure of the rock is generally manifested by a series of microscopic to mesoscopic fractures that are filled by a variety of hydrothermal mineral phases, including fine-grained quartz, sericite and ankerite. Chlorite and calcite are prevalent in the advanced stages of brittle fracturing.

Brittle-ductile deformation in the form of rock fracturing (as opposed to uniform ductile shearing) is especially dominant in the chlorite-magnetite zone, compared to Zone III. Fractured and microbrecciated albite fragments typically lie in a fine-grained, chlorite-dominated matrix (Fig.7-7). Accordingly, the chlorite-magnetite altered gabbro has locally the texture of a cataclasite. Abundant slickensides are also visible in the outcrops of the chlorite-magnetite zone.

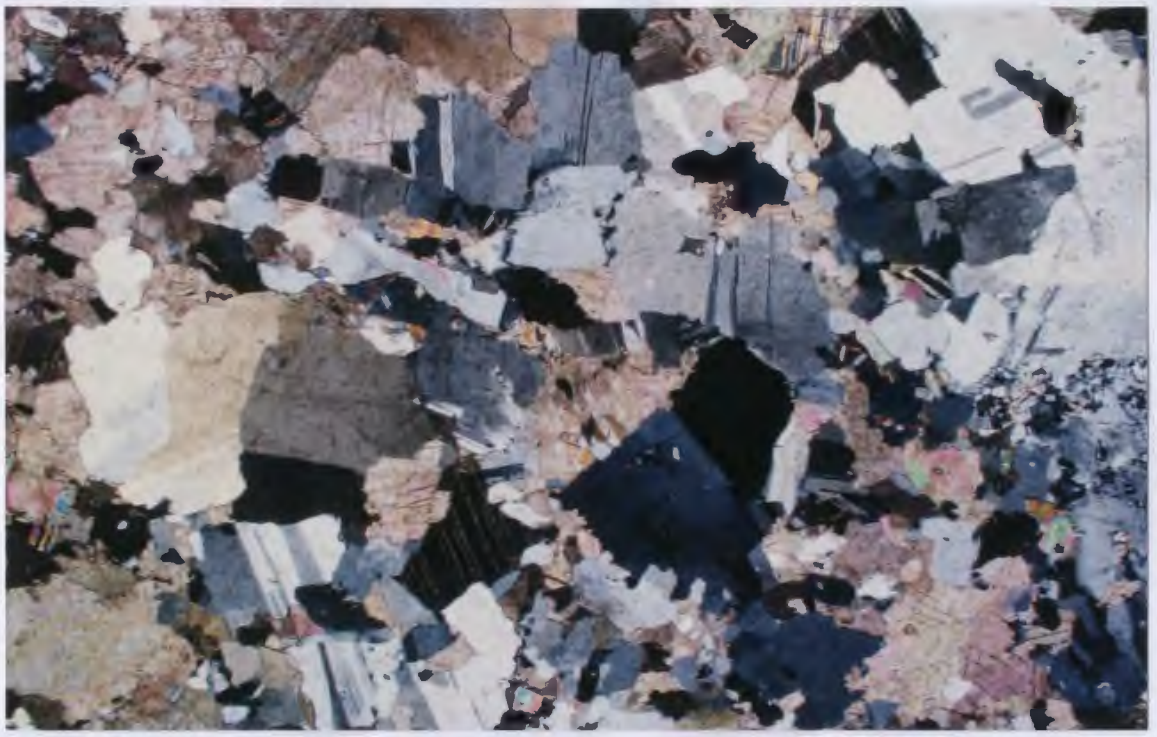

Figure 7-9 Photomicrograph showing the crystalloblastic fabric of albite and ankerite in the red albite-pyrite zone (xpol. x25).

Figure 7-10 Dislocated subgrains and contorted polysynthetic twins in large red albite grains (xpol. x25).

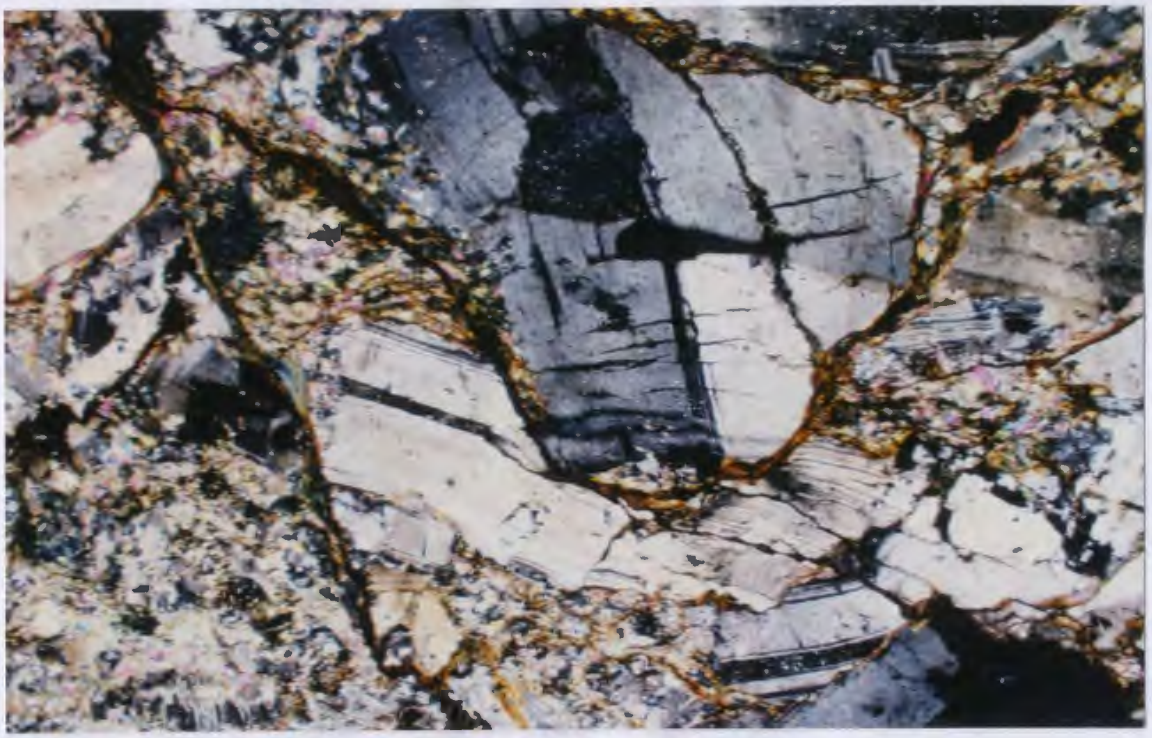

Figure 7-11 Photomicrograph of the red albite-pyrite altered gabbro showing the development of late cataclastic deformation in albite neocrysts. Note the occurrence of sericite in fractures (xpol. x25).

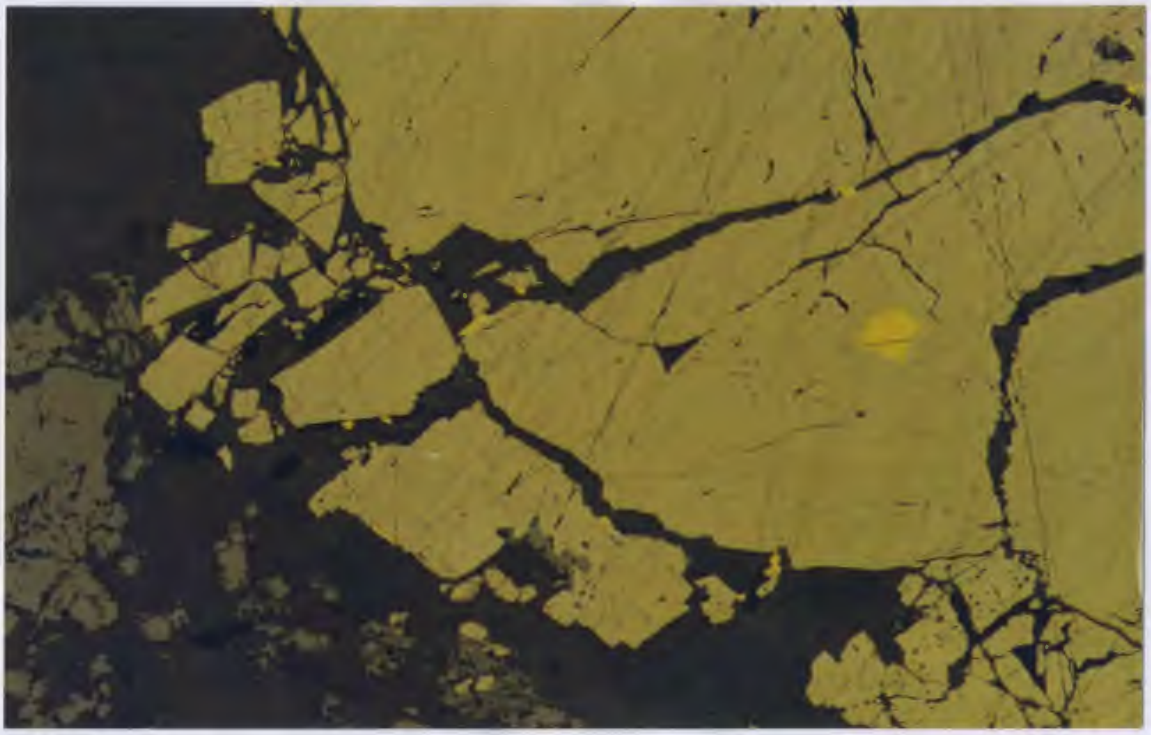

Figure 7-12 Reflecting-light photomicrograph showing the late brecciation of a large pyrite grain. Note the gold inclusion in the middle-right side of the picture (x25).

7.4 U/Th-BEARING MINERAL PHASES

A comparatively minor but important constituent of the hydrothermally altered rocks from the Stog'er Tight deposit are uranium-bearing accessory phases. Petrographic studies have revealed a number of minute inclusions up to 100 μm in diameter, surrounded by dark pleochroic haloes, especially in alteration zones III and IV. These radioactive inclusions were classified into two groups; a) dark angular inclusions with no evident optical properties (Fig.7-13) and, b) round transparent inclusions with high relief and high birefringence (Fig.7-14). SEM semi-quantitative analyses indicated that group (a) inclusions have the composition of zircon ($ZrSiO_4$) while group (b) inclusions consist of a variety of phosphates including monazite [$(Ce,La)PO_4$] and xenotime (YPO_4).

The U/Th-bearing inclusions are more easily recognized in samples from the chlorite-magnetite zone, where radiation damage resulting from decay of U and Th is best developed in the surrounding chlorite. Nevertheless, they are most abundant and have their maximum grain-sizes in the red albite-pyrite zone, associated with the high-grade ore (samples BN29-A31 and 91818-C4). It is notable that there are basic morphologic contrasts between the zircon inclusions associated with high-grade alteration and zircon prisms in the unaltered-gabbro (see Chapter 8). These observations indicate that the U/Th-bearing phases are of hydrothermal origin, and were generated by the same hydrothermal processes that were responsible for host rock alteration and Au-

mineralization.

SEM examination reveals that the majority of zircon and monazite inclusions found within chlorite in Zone IV samples are markedly fractured (Fig.7-15) or completely microbrecciated (Fig.7-16). These features have important bearing on the relative timing of hydrothermal alteration and Au-mineralization in the Stog'er Tight deposit (see Section 7.6 and Chapter 8).

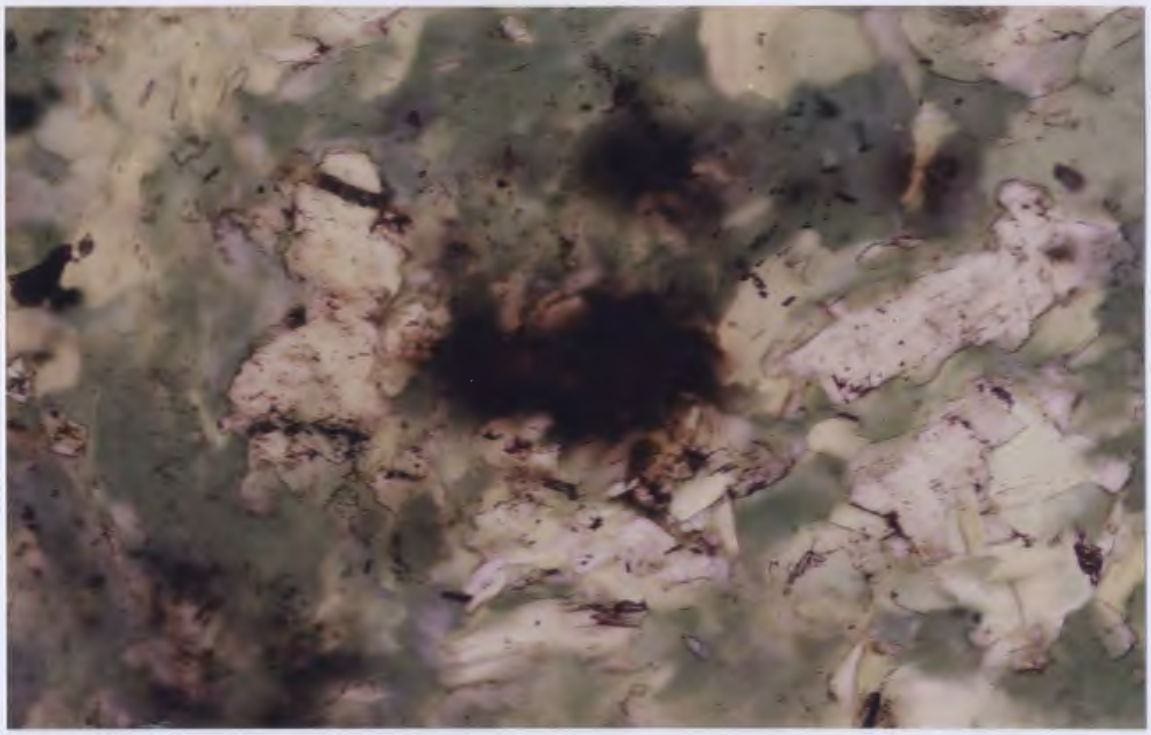

Figure 7-13 Photomicrograph of a hydrothermal zircon inclusion surrounded by dark pleochroic halo, in the chlorite-magnetite zone (x250).

Figure 7-14 Photomicrograph of hydrothermal monazite inclusions in the chlorite-magnetite altered gabbro (x250).

Figure 7-15 SEM photomicrograph of two hydrothermal zircon (ZR) and monazite (MO) inclusions. Note the development of microfractures in these inclusions.

Figure 7-16 SEM photomicrograph of the same zircon inclusion as in Figure 7-13. Note the microbrecciation in this hydrothermal zircon inclusion.

7.5 VEINS AND GOLD MINERALIZATION

A number of drill-cores recovered from different locations in the study area have exposed a variety of quartz-rich veins in the highly altered and mineralized zones. Many of these veins are tension structures characterized by the brittle fracturing of the previously altered rocks, and the deposition of quartz in the open spaces. No gold is found in direct association to these types of veins. The tension veins apparently occurred late in the alteration history of the deposit and have no genetic relationship to Au-mineralization. However, the red albite-pyrite alteration zone (replacement veins) is commonly (but not invariably) associated with a series of deformed, shear parallel, quartz-albite-ankerite veins which are normally less than 10 cm wide. These are distinct from the tension veins, especially in terms of textural relationships to the altered host rock. The vein-host rock interface is locally marked by a narrow strip of ankerite, though in most cases, the boundary is irregular and defuse, with the vein grading outwards into the altered gabbro without any sharp contact.

The host gabbro immediately adjacent to the shear-parallel veins is characterized by intensive red-albite alteration and by the local deposition of coarse, Au-bearing pyrite (Fig.7-17). The intensity of alteration tends to diminish gradually with increasing distance from the vein boundaries, over a scale of 5 to 15 cm. Despite the common association of Au mineralization with the shear-parallel veins in drill-core, no equivalent veins have been observed in

the mineralized outcrops of the Stog'er Tight and Magnetic Zones. In outcrop, Au-bearing pyrite occurs as coarse, polygrain aggregates within a uniform groundmass of red albite (Fig.7-18).

The mineralogy of the shear-parallel veins includes quartz, albite and ankerite, with subordinate and variable amounts of muscovite (sericite), chlorite and tourmaline. Quartz is the major constituent of the veins occurring as pale- to milky-white crystals of variable shapes and sizes, up to more than 1cm in diameter. Crystalloblastic quartz grains with undulose extinction, stylolitic grain boundaries and abundant internal subgrains are common in the veins.

Albite occurs in the veins as coarse-grained, colourless to pink crystals up to several millimetres in diameter. Its pink colour is invariably paler than that of the red albite in the adjacent mineralized host rock. In thin section it is characterized by polysynthetic twins that are markedly bent in most samples, without any indication of fracturing or mylonitization.

Ankerite is commonly found in the shear-parallel veins as white to rusty aggregates, lining the vein at the interface with the host rock. In thin section, it occurs as coarse euhedral to subhedral crystals with prominent cleavage and/or polysynthetic twins, and is locally intergrown with slender tourmaline needles. Textural relationships indicate that the early precipitation of ankerite was followed by the formation of quartz and albite. Muscovite and chlorite are formed along the fractures that cut the other vein minerals, and therefore, occur late in the vein crystallization sequence. Examples of vermicular growth of chlorite in quartz are also observed in a few vein samples (*e.g.* sample BN60-

A7, Fig.7-19). The progression of this process results in total replacement of quartz by chlorite and the formation of centimetre-sized chlorite pseudomorphs after quartz in the veins.

Gold occurs in the Stog'er Tight deposit as inclusions inside polygrain aggregates of pyrite. The Au-bearing pyrite is exclusive to the strongly altered and recrystallized gabbro (red albite-pyrite zone), and no gold is observed directly inside the quartz-albite-ankerite veins. Polished thin sections of samples from the high-grade ore zone display abundant gold inclusions in the form of minute blebs and seams up to 100 μm in diameter, disseminated in pyrite (Fig.7-20 and -21). Most of the gold occurs in fractures in pyrite though, in some cases, it forms small globular inclusions. Some gold is also found inside silicate phases near large pyrite grains, but these appear to have been released during fracturing and brecciation of pyrite. Minor chalcopyrite is locally found in association with gold and pyrite, though it is generally a rare constituent of the ore assemblage. A close textural association exists between Au-bearing pyrite and recrystallized, rutile-dominated leucoxene. Pyrite aggregates have typically overgrown and/or enclosed patches of skeletal leucoxene (see Fig.7-6) suggesting that the leucoxene (titanomagnetite) plays an important role in the precipitation of gold.

SEM analyses indicate that gold is relatively pure, with less than 10% Ag content. No As, Sb, Bi or Te have been detected.

Figure 7-17 Drill-core sample of a shear-parallel, quartz-albite-ankerite vein and its adjacent altered/mineralized wallrock, from the high-grade ore zone. Note the polygrain patches of Au-bearing pyrite to the left.

Figure 7-18 Aggregates of gold-bearing pyrite within a uniform groundmass of hydrothermal red albite in the trench outcrops of the Stog'er Tight Zone (trench IIIS).

Figure 7-19 Photomicrograph of a quartz-ankerite vein showing the vermicular growth of chlorite in quartz. Note the replacement of quartz by chlorite at the upper-left corner.

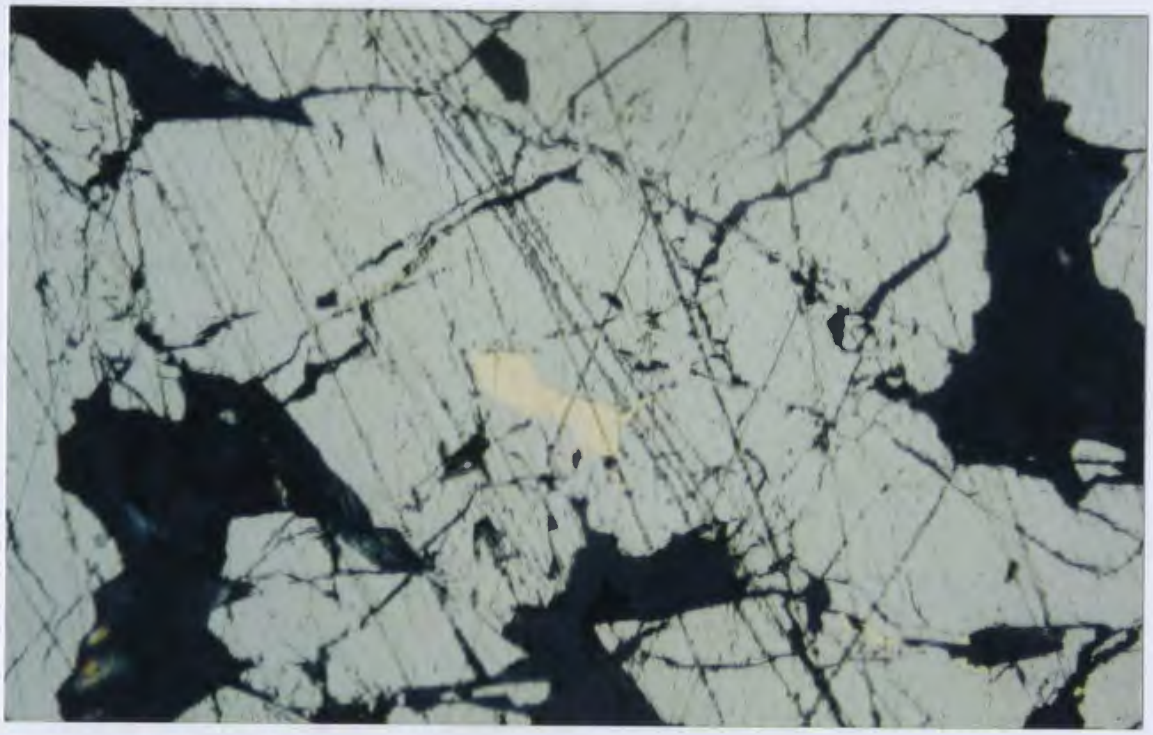

Figure 7-20 Reflected-light photomicrograph of gold inclusion in pyrite.

Figure 7-21 SEM photomicrograph of the same gold inclusion as in Figure 7-20. Note the abundance of gold seams and stringers in the pyrite.

7.6 SUMMARY OF ALTERATION HISTORY

The consistent mineralogic zonation and the distinct microstructural features of the Stog'er Tight deposit imply that the hydrothermal alteration and mineralization of the host gabbro was a progressive and evolving process, which was associated with significant shear deformation in the altered rocks.

The hydrothermal alteration of the Stog'er Tight gabbro started with chlorite-calcite alteration over a wide area, and was followed by a more concentrated ankerite-sericite alteration within the shear zones. Both alteration zones show variable degrees of mylonitic (ductile) deformation (D_E deformation, see Chapter 4), such as the syntectonic recrystallization of albite to a fine-grained quartz/albite matrix, though the massive ankerite (and sericite) deposition probably post-dated the main episode of mylonitic deformation.

By the progress of hydrothermal alteration, the carbonate-rich ankerite-sericite assemblage grades into an albite-dominated transitional facies, close to the red albite-pyrite zone. The presence of large albite porphyroblasts (larger than the original gabbro albite) with isotropic fabrics, together with the general absence of fine-grained mylonitic matrix in this marginal zone, reflects high rates of strain recovery in the form of advanced syndeformational crystal growth and/or post-tectonic annealing. The resulting isotropic fabric has apparently overprinted (and obliterated) the mylonitic foliation (D_E) of the altered rock.

The peak of intensity of hydrothermal alteration and gold mineralization occurs in the red albite-pyrite alteration zone. Overall, the red albite-pyrite (high-grade) alteration appears to be distinctive in terms of structure and mineralogy, as compared to the above-mentioned alteration zones. It occurs as lens-shaped and discontinuous, high-grade, alteration/mineralization intervals, in close spatial association with the albite-dominated facies of Zone II. Despite the mineralogic and textural similarities between the latter and the red albite-pyrite assemblage (*e.g.* dominance of albite and isotropic fabrics), the overall red colour of albite in Zone III indicates that it is not simply produced by the overgrowth of grey albite of Zone II. Rather, the red albite-pyrite assemblage is likely to have formed by the confined replacement of the previously altered (ankerite-sericite?) gabbro along the lenticular zones of fluid percolation and high-grade alteration. The discontinuous, Au-bearing, red albite-pyrite intervals can therefore be interpreted as a series of "replacement veins" within the altered and mylonitized gabbro.

The replacement veins are typically characterized by irregular and diffuse contacts with the host rock and appear to have formed by replacement of the host rather than by the filling of fractures and/or open spaces (Misik, 1971; Spang and Groshong, 1981). These characteristics are consistent with those of the altered gabbro in the red albite-pyrite replacement zone.

The chlorite-magnetite zone that occurs at the footwall of the red albite-pyrite replacement zone, seems to be out of sequence and does not coincide with the symmetry and the progressive nature of the hydrothermal alteration.

The dominance of brittle fractures and slickensides as the main deformational fabrics, along with the lack of a well-defined foliation in the rocks, are indicative of a semi-cataclastic (brittle-ductile) deformation in the chlorite-magnetite zone. Nevertheless, the presence of large albite porphyroclasts in this zone, similar to the recrystallized grey albite in Zone II (marginal facies), denotes an earlier phase of crystal growth preceding the late cataclastic deformation. Also, the sericite-chlorite and calcite-ankerite coexistence reflect disequilibrium among mineral phases. Considering the disequilibrium conditions and according to the textural relationships described above, the alteration assemblage of Zone IV can be interpreted in terms of an early ankerite-sericite (-albite) alteration which was subsequently overprinted by a late, retrograde, chlorite-calcite-magnetite alteration. The association of this retrograde alteration with cataclastic features in the rock suggests that Zone IV probably records a late episode of confined brittle-ductile deformation (D_L deformation, see Chapter 4) and concomitant penetrative fluid percolation within the main ductile shear zone of the study area.

The same alteration/deformation episode was probably responsible for the local brittle deformation in Zone III. The occurrence of microscopic to mesoscopic fractures filled with chlorite and calcite at the lower sections of the red albite-pyrite (+gold) zone (close to the footwall Zone IV) implies that the brittle-ductile (D_E) deformation and retrograde chlorite alteration post-dated the peak of hydrothermal alteration and Au mineralization in the sequence. This is further confirmed by the fractured and microbrecciated nature of zircon

inclusions in the chlorite-magnetite zone.

The shear-parallel, quartz-albite-ankerite veins associated with Au mineralization in the red albite-pyrite replacement zones are characterized by diffuse and gradational boundaries with the altered host rock (see Section 7.4). The gradational vein boundaries along with the particular orientation of the veins subparallel to the main foliation in the alteration sequence, suggest that vein formation was largely a syn- to late-tectonic process. Moreover, the observation of bent polysynthetic twins in unstrained vein albite implies that the mylonitic deformation (D_E) was active no later than vein formation.

7.7 GEOCHEMISTRY OF ALTERATION

The mineralogic transformations associated with the advanced stages of hydrothermal alteration are accompanied by substantial changes in the chemical composition of the rock. The degree of enrichment or depletion of a given element in the altered rock is a function of its concentration and mobility in the hydrothermal fluid. Most major elements, such as Si, Na and K, and the great majority of low field strength (trace) elements (*e.g.* Cs, Rb, Ba and Sr) tend to be mobile in hydrothermal systems and are concentrated in mineral phases which are highly susceptible to alteration reactions (*e.g.* feldspars, micas and amphiboles). Understanding the compositional variations of the altered rocks in the context of distinct alteration assemblages is of particular importance to assessing the composition of mineralizing fluids and the physicochemical

conditions of alteration.

7.7.1 Geochemical Data

The suite of samples selected for chemical analysis (total of 48) included 13 altered gabbro samples from the different alteration zones in drill-holes BN89-55, BN89-53 and BN88-24 (see Appendix V). These were analyzed for major and trace elements by AA and XRF methods. ICP-MS trace element analyses were performed on a subset of 6 of the 13 samples. The analytical techniques are described in Chapter 1. Drill-hole BN88-24, in particular, includes a complete section from the unaltered gabbro to the high-grade mineralized zone, with a well developed alteration zonation. Geochemical data for these altered samples and their immediate unaltered host gabbro are presented in Table 7-1.

Table 7-1 Chemical data for the samples of drill-hole BN88-24.

Lab No. Sample Zone	M1669 BN24-01 Gabbro	M1672 BN24-06 Zone II	M1673 BN24-09 Zone III	M1675 BN24-14 Zone IV
SiO_2 (%)	47.72	39.83	52.35	36.18
TiO_2	1.29	1.37	0.58	3.69
Al_2O_3	17.09	16.41	21.43	16.92
Fe_2O_3	11.85	9.66	8.02	24.93
MnO	0.18	0.16	0.05	0.25
MgO	7.83	4.40	1.21	4.72
CaO	11.12	11.53	1.79	5.26
Na_2O	2.72	1.15	6.30	3.28
K_2O	0.02	3.99	3.54	0.84
P_2O_5	0.19	0.10	0.30	0.60
Total	95.62	88.60	95.57	96.67
Cr (ppm)	608	86	11	4
Ni	99	24	ND	ND
Sc	41	37	10	34
V	244	272	127	373
Cu	30	11	ND	16
Zn	61	36	33	196
Rb	0.1	47.6	39.0	9.6
Ba	14.36	97.00	174.00	53.00
Sr	417.41	262.40	106.86	198.60
Ta	1.18	0.77	3.56	2.02
Nb	7.74	7.30	37.40	23.58
Hf	2.87	3.78	16.17	10.10
Zr	126.63	122.95	738.06	425.80
Ti	7743	8207	3483	22098
Y	22.70	17.62	85.44	63.93
Th	0.55	0.55	3.49	1.85

Lab No. Sample Zone	M1669 BN24-01 Gabbro	M1672 BN24-06 Zone II	M1673 BN24-09 Zone III	M1675 BN24-14 Zone IV
La	8.10	6.64	43.44	25.91
Ce	21.34	17.27	108.66	69.85
Pr	2.98	2.46	14.69	9.97
Nd	13.31	11.26	62.80	46.20
Sm	3.42	3.01	15.13	11.88
Eu	1.20	1.13	4.74	3.46
Gd	3.70	3.10	15.73	12.79
Tb	0.58	0.52	2.41	1.94
Dy	3.49	3.09	14.80	11.80
Ho	0.71	0.64	3.06	2.40
Er	1.98	1.81	8.70	6.70
Tm	0.27	0.26	1.24	0.92
Yb	1.67	1.70	8.14	5.65
Lu	0.25	0.27	1.29	0.86
Average REE enrichment relative to the unaltered gabbro.	0.00	0.94	4.81	3.49
Density	3.03	2.81	3.01	2.95

7.7.2 Composition-Volume Relationships

Hydrothermal alteration (and shear deformation) can involve significant volume changes in the rock which affects the apparent concentrations of elements in the analyzed samples (*e.g.* elemental enrichment and/or dilution). The composition-volume relationships must be assessed in order to determine the actual elemental gains or losses (mass balance) associated with the formation of the different alteration assemblages. This can be accomplished by means of appropriate mass balance calculations described in this section.

Gresens (1967) formulated a series of equations to calculate the elemental gains and losses associated with metasomatic or hydrothermal processes which involve volume changes. Whole rock chemical compositions can be used in Gresens' calculations (regardless of mineral structural formulae) in order to assess actual compositional changes, using the equation:

$$x_n = f_v (g_B/g_A) c_n^B - c_n^A$$

where x_n is the net change in the concentration of component n (grams/100 grams of parent rock), f_v is the volume factor (final volume/initial volume), g_A and g_B are the specific gravities of the parent and alteration product, and c_n^A and c_n^B are the concentrations of component n (wt%) in the parent and product, respectively. The parameters x_n and f_v are both unknowns in the above equation, therefore f_v has to be graphically estimated in order to be able to calculate x_n.

Mass balance calculations were performed on a suite of samples

representative of Zone II, Zone III and Zone IV alteration assemblages and their parent unaltered gabbro from drill-hole BN88-24 (see Table 7-1). The calculations were made in two different ways. First, the composition of each alteration assemblage was compared to that of the unaltered gabbro to determine separately the rate of compositional variations in each alteration zone (Fig.7-22a-d). Second, the composition of each alteration assemblage was compared to that of the preceding assemblage in the alteration sequence, in order to examine the progressive compositional changes with the advancement of hydrothermal alteration (Fig.7-23a-d). The data for two trace elements, La (a LREE) and Yb (a HREE), where available, were plotted on the diagrams to allow comparison between REE and major element behaviours in each assemblage. Figures 7-22 and 7-23 illustrates the results of mass balance calculations in the form of composition-volume (gain/loss versus volume factor) plots.

The composition-volume relationships in sample BN24-02 from the chlorite-calcite zone (Fig.7-23a) imply that at volume factors of slightly lower than one (*c.*0.96), there is no significant variations in Al, Ti and Mg contents (isochemical behaviour). Si, Ca, and Fe are variably depleted at this volume factor. The loss of Si, in particular, is consistent with the alteration reaction of actinolite and epidote (unaltered gabbro) to the chlorite-calcite assemblage (see Section 7.2.1).

The mass balance calculations on sample BN24-06 from the ankerite-sericite zone (Fig.7-23b) give a good volume factor constraint of $f_v = 1.12$ (12%

volume gain), based on the isochemical behaviours of Al and Ti, when the chemical compositions are compared to that of the preceding alteration assemblage (Zone I). This value is consistent with an increase in Ca, Fe and especially, K contents, and with significant Na, Si and Mg depletions. K, Na and Si variations, in particular, are in agreement with the formation of hydrothermal sericite and the partial break down of albite in this zone (see Section 7.2.2). The slight Fe and Ca gain is probably related to the loss of these elements in the preceding chlorite-calcite zone. The calculations also show that the ankerite-sericite altered rock is depleted in Na, Mg, Ca and probably Si, and is enriched in Fe and K relative to the parent gabbro.

Figure 7-23c illustrates the compositional variations in the red albite-pyrite zone (sample BN24-09), as compared to the preceding Zone II assemblage. Unlike those of the previous alteration zones, the composition-volume diagram of Zone III reflects the significant mobilization of the majority of elements including Ti. The isochemical behaviours of Si and Al at $f_v \approx 0.7$ (30% volume loss), however, would be the best estimation for the volume factor in this assemblage. K, Ti, Mg, Fe and Ca are variably depleted, whereas Na is significantly increased at this point. These chemical variations are fairly consistent with the pervasive replacement of the altered gabbro by the hydrothermal red albite (see Section 7.2.3).

The results of mass balance calculations on sample BN24-14 from the chlorite-magnetite zone (Zone IV) are illustrated in Figure 7-23d. Unlike those in the other alteration zones, no unambiguous constraints can be placed on the

rate of compositional variations and volume changes in the altered rocks of this zone. The clustering of data based on isochemical behaviours of elements occurs around volume factors of about 0.35 and 0.92 (65% and 0.8% volume loss, respectively). The former coincides with the isochemical behaviours of Ti, Fe, Na, and La, whereas the latter value is supported by those of Al and Mg. Neither of the two estimated volume factors are preferentially supported or rejected by the petrographic observations. The true volume factor most probably lies somewhere between the two estimated values.

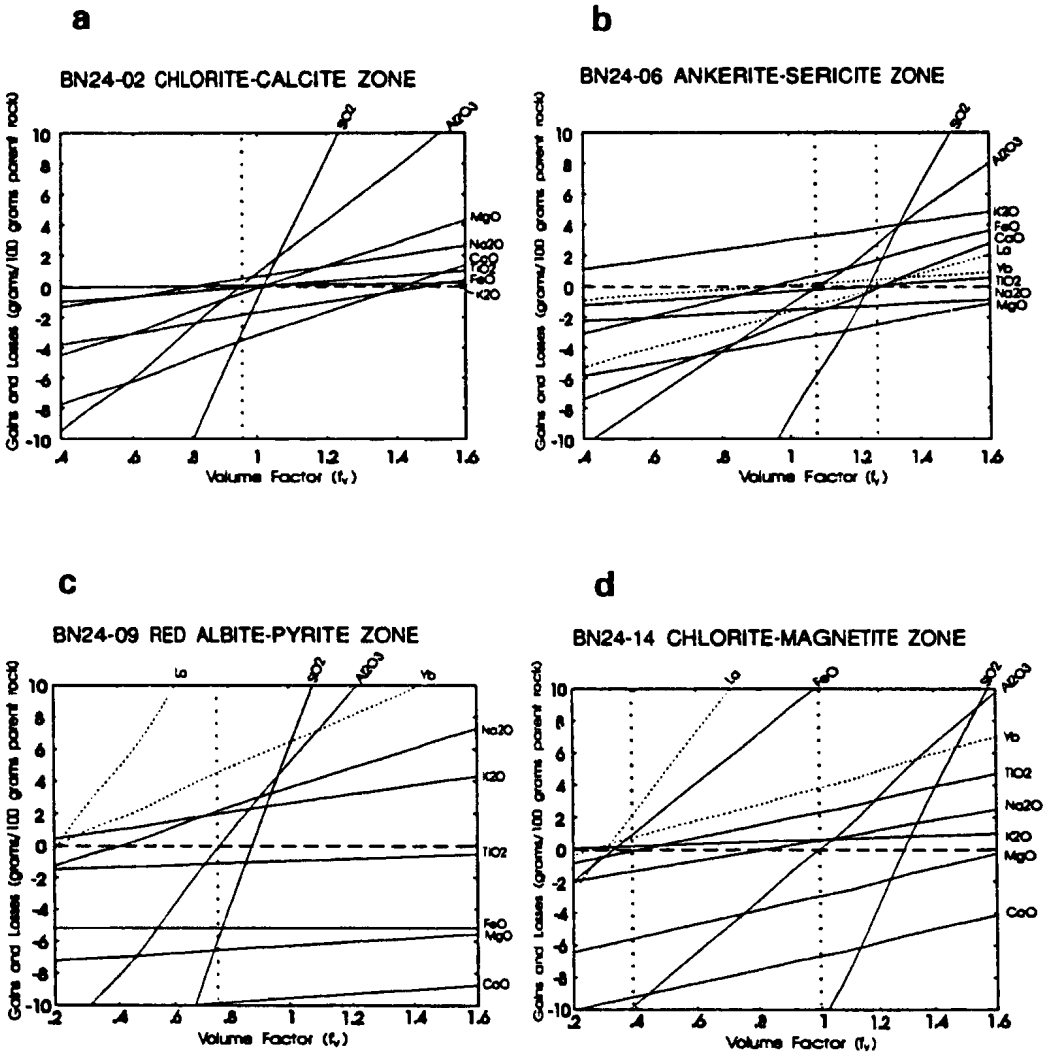

Figure 7-22a-d Mass balance calculations pertinent to the compositional variations in each hydrothermal alteration zone with respect to the unaltered gabbro, as a function of volume change.

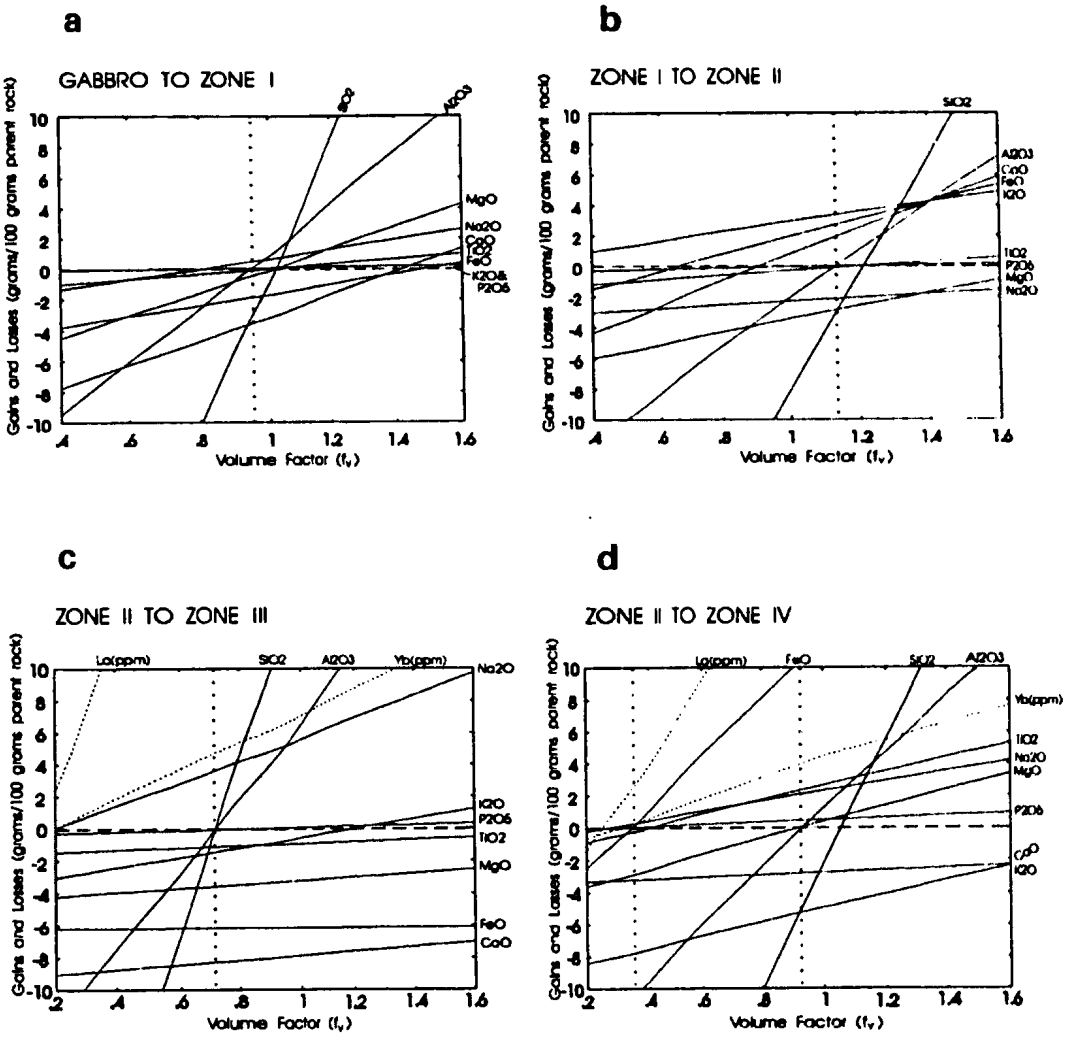

Figure 7-23a-d Mass balance calculations pertinent to the compositional variations in each alteration zone with respect to the preceding assemblage in the alteration sequence, as a function of volume change.

7.7.3 Al, Ti and LILE Variations

Potassium metasomatism is a characteristic alteration feature of the mesothermal Au-Ag deposits, as well as of many magmatic-related ore deposits (*e.g.* Kerrich, 1983 and 1989b,c). K, Rb and Ba (LILE) interelement relationships in magmatic systems, however, are controlled by crystal-melt fractionation processes and are distinct from those in the nonmagmatic hydrothermal systems (*e.g.* Kerrich & Fryer, 1988). Alternatively, elements such as Al, Ti and Th have been reported to be generally immobile, or behave isochemically, during alteration associated with mesothermal Au-Ag deposits (Fryer *et al.* 1979; Kerrich, 1983). The concentrations of the latter group in the altered rocks are believed to reflect those of the host lithologies.

The absolute concentrations and interelement ratios of K, Rb and Ba in the Stog'er Tight gabbro and its altered/mineralized counterparts are demonstrated in Figures 7-24a-c (see Appendices II and III for analytical data). The highest LILE enrichment is associated with the sericite-ankerite (Zone III) and red albite-pyrite (Zone IV) altered rocks, where hydrothermal sericite is a major constituent. K and Rb are highly correlated in both unaltered and altered gabbro samples. Their coherent behaviour is present over more than two orders of magnitude in K content (from <200 ppm to >20000 ppm, Fig.7-24a). K and Ba are generally well correlated (Fig.7-24b), but with a greater degree of scatter in the data, as compared to the K-Rb correlation. Large scatter in the unaltered samples is probably due to low analytical precision at low Ba concentrations.

There is also a general increase in K/Ba ratio with the intensity of alteration. Figure 7-24c shows the covariation of K/Rb and K/Ba ratios in the analyzed samples. The K/Rb ratios in the altered/mineralized rocks are fairly uniform and lie within the 600-800 range, whereas there is a significant and systematic increase in K/Ba ratio (from 70 to >200) with alteration. It is notable that the variations in these elemental ratios are independent of the probable alteration-induced volume changes discussed above.

The presumed alteration-insensitive elements Al and Ti are plotted against K (index of alteration) in Figures 7-25a and 7-25b for the above samples. Al behaves isochemically in the majority of altered rocks and has almost the same concentration range (10-20%, regardless of the volume changes) as in the unaltered gabbro. In contrast, Ti has a significantly wider range of variation in the altered rocks, as compared to Al. The large scatter in Ti contents (from <1 ppm to ≈4 ppm) is indicative of mobility of Ti, especially in the chlorite-magnetite zone.

7.7.4 REE, HFSE and Th Variations

In Chapter 6, immobile elements such as HFSE, REE and Th were used to discriminate between different rock suites in the study area. Figure 7-26 illustrates similar extended REE plots for the alteration sequence from two separate drill sections (see Table 7-1 and Appendix III for chemical data, Appendix IV for normalizing factors). The trace element profiles show that there is a general and uniform increase in elemental concentrations with increasing

intensity of alteration, such that Zone III (red albite-pyrite zone) may have been enriched by up to 600% in certain elements (*e.g.* Zr) relative to the host gabbro. This enrichment is far greater than that expected for compositional variation within the main gabbro body (shaded field in Figure 7-26a). Figure 7-26 also indicates coherent enrichments in REE and Th relative to the more variable HFSE (*i.e.* Zr, Hf, Nb and Y). A comparison between trace element profiles of drill-holes BN88-24 and BN89-53 (figures 7-26a and 7-26b) clearly indicates that samples of similar alteration zone but from separate localities (*e.g.* samples BN24-09 and BN53-13), have significantly different degrees of trace element enrichment, though enrichment patterns (subparallel REE, separate from HFSE) appear to be identical in both sequences. Figure 7-27 illustrates the trace element contents of the altered rocks from drill-hole BN88-24 which are normalized relative to their immediate host (unaltered) gabbro. The prominent flat patterns of these samples indicate that trace elements with different degrees of compatibility (K_Ds), such as HREE and LREE, have been enriched to almost the same extent in all of the alteration zones.

7.7.5 INTERPRETATION OF RESULTS

The LILE systematics and K, Rb and Ba covariations in the Stog'er Tight deposit appear to be similar to those of the other mesothermal gold deposits. Nevertheless, the K/Rb and K/Ba ratios in the alteration zone of the Stog'er Tight deposit are significantly higher than those in the Archean analogues.

Kerrich (1989b,c) noted that for the Archean greenstone gold deposits in the Abitibi Subprovince, the ranges of K/Rb and K/Ba ratios are 230-380 and 35-100, respectively. In the Stog'er Tight deposit the K/Rb ratio ranges from ≈600 to 816, and the K/Ba from ≈70 to 260. A comparison between analytical data for the Stog'er Tight deposit (Appendix IV) and those for the Archean lode gold deposits (*e.g.* Kerrich, 1989b-Table 1) clearly indicates that the K enrichment in the former has been significantly stronger, as compared to the Rb and Ba enrichments. Considering the suggested lack of a pronounced host rock control on the fractionation of K, Rb and Ba during the hydrothermal alteration associated with the Archean gold deposits (Kerrich & Fryer, 1988; Kerrich, 1989b,c), the high K/Rb and K/Ba ratios in the Stog'er Tight deposit can only be explained by the preferential enrichment of K relative to Rb and Ba.

The hydrothermal alteration associated with Au-mineralization in the Stog'er Tight deposit is characterized by pronounced REE, HFSE and Th enrichments. Two different explanations can be proposed for the presumed-immobile element variations in the altered rocks of the Stog'er Tight deposit: 1) the enrichment of REE, HFSE and Th occurred as a result of their concentration from a fluid phase into the wall rock during hydrothermal alteration, as manifested in the abundance of REE-rich inclusions (*e.g.* monazite) in the strongly altered gabbro, or 2) the enrichments are artifacts of volume loss effects (*e.g.* O'Hara & Blackburn, 1989) that accompanied strong shear deformation, as suggested by mass-balance calculations.

The first interpretation (hydrothermal enrichment) is broadly confirmed

by petrographic observations. The widespread presence of U- and REE-bearing mineral phases such as hydrothermal zircon, monazite, apatite and xenotime (Section 7.3), especially in the alteration zones III and IV, is solid evidence for the hydrothermal concentration of these elements into the altered host rocks. However, this model is unable to explain the subparallel patterns of progressive REE enrichment in the alteration sequence. REE as a group, are commonly transported in alkaline solutions as carbonate, fluoride or sulphate complexes, while HREE complexes are generally more stable than those of LREE and are the last ones to break down (Kerrich & Fryer, 1979 and references therein). Accordingly, LREE abundances are relatively unfractionated (or uniformly depleted) in the alteration zones of mesothermal Au-deposits, but REE heavier than Sm exhibit progressive depletion in the altered host rocks (concentrate in the fluid) with increasing atomic number (Kerrich & Fryer, 1979; Kerrich, 1983). These fractionated REE distributions are in contrast with those observed in the Stog'er Tight deposit.

The second explanation (volume loss) is consistent, to some extent, with the results of mass balance calculations on Zone II and Zone IV rocks. Table 7-1 shows the average REE enrichments for the three altered gabbro samples of drill-hole BN88-24. These values are in good agreement with the 1.12 and 0.3-0.4 (minimum estimation) volume factors estimated for samples BN24-06 and BN24-14, respectively. The volume loss model can also explain the coherent behaviours (parallel enrichment patterns) of REE in the altered rocks, assuming that these elements have been essentially immobile even at highest grades of

hydrothermal alteration. Nevertheless, the suggested rates of volume loss (up to 70%) requires intensive mylonitization and dehydration of the altered rocks. Presently, there is no evidence for such high degrees of shear deformation in the alteration zone of the Stog'er Tight deposit. The red albite-pyrite zone (the most enriched zone), in particular, exhibits widespread recrystallization and replacement of the gabbro by hydrothermal red albite, which can potentially dilute the trace element concentrations by significant amounts.

It can be concluded from the foregoing discussion that neither of the two end-member interpretations can exclusively integrate the petrographic and geochemical evidence into a model which can explain the systematic trace element variations with alteration. However, it is probable that the net variations in REE, HFSE and Th contents across the alteration sequence have been controlled by a combination of hydrothermal enrichment and volume loss. It is notable that this model, though suggestive, cannot precisely quantify the chemical variations associated with the hydrothermal fluid-rock interactions, unless the elemental ratios (as opposed to absolute concentrations) are considered.

Figure 7-28a demonstrates a mantle-normalized trace element plot for the same samples as in Figure 7-26a, that is extended to include low field-strength elements (LFSE) Rb, K, Ba and Sr, transition elements (TE) Sc, V, Ni, and Cr, as well as the base metals Cu and Zn (see Appendix IV for normalizing factors). In Figure 7-28b, the elemental concentrations are corrected for possible volume effects using the average REE-enrichment parameters of Table 7-1, and

assuming that all the REE variations were caused by volume loss. This shows that the enrichments in REE and HFSE (as *groups* of elements) can be well accounted for by volume adjustments alone, while the variations in LFSE, TE and base metal contents appear to be independent (or somewhat intensified) by volume corrections. These two plots serve as graphical representations of the discussed end-member models for chemical variations associated with alteration.

7.8 SUMMARY

Gold mineralization in the Stog'er Tight deposit is associated with extensive hydrothermal alteration of the host gabbro as manifested by systematic and zoned mineralogic and compositional variations throughout the alteration sequence. Four different alteration zones have been defined including the chlorite-calcite zone, ankerite-sericite zone, red albite-pyrite (+gold) zone and the chlorite-magnetite zone. The chlorite-calcite alteration and in part, ankerite-sericite alteration were concomitant with an episode of mylonitic (ductile) deformation in the shear zones. The red albite-pyrite replacement (high grade alteration) of the altered and deformed gabbro occurred by subsequent strain recovery in the form of advanced recrystallization and post-tectonic annealing. The footwall chlorite-magnetite alteration records a late episode of confined brittle-ductile deformation and retrograde alteration that post-dated the peak of hydrothermal alteration (and mineralization) in the sequence. Gold

occurs invariably in pyrite within the strongly albitized wall rock at the margins of syndeformational quartz-albite-ankerite veins. Gold-bearing pyrite is texturally associated with the titanomagnetite relics from the gabbro.

Hydrothermal alteration in the Stog'er Tight deposit is characterized by significant LILE, HFSE, REE and Th enrichments and by concomitant incorporation of a variety of U- and REE-bearing mineral phases in the altered rocks. The LILE systematics of the deposit are consistent with those of the Archean mesothermal gold deposits, though a higher degree of K-enrichment (relative to Rb and Ba) is observed in the former. The REE, HFSE and Th enrichments were probably induced by a combination of intensive alteration by enriched hydrothermal fluids and volume loss, while no unique explanation can be made for the subparallel REE enrichments in the alteration sequence.

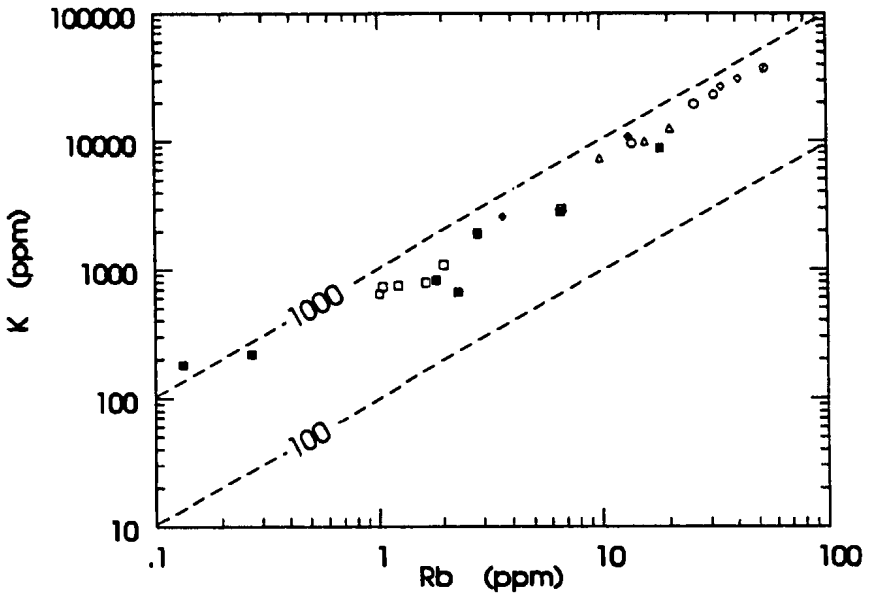

Figure 7-24a

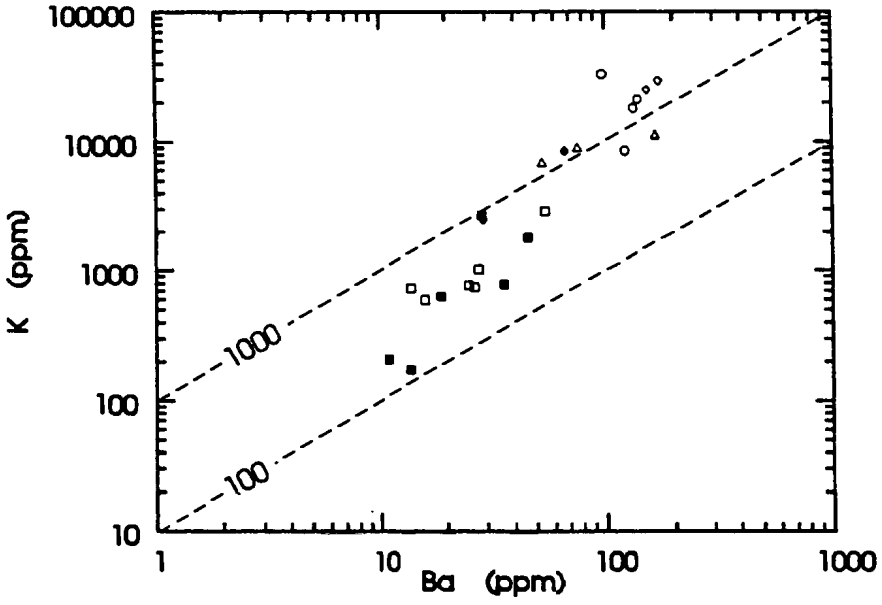

Figure 7-24b

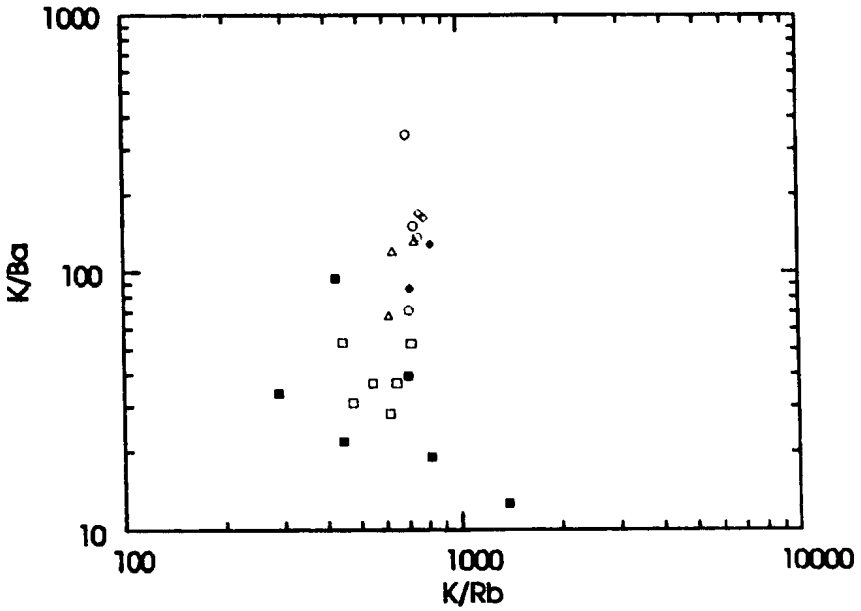

Figure 7-24c

LEGEND OF PLOT SYMBOLS

□ Low Fe-Ti gabbro
■ Main Stog'er Tight gabbro
○ Ankerite-sericite alteration
◇ Red albite-pyrite alteration
◆ High-grade ore
▵ Chlorite-magnetite alteration

Figure 7-24 K, Rb and Ba covariations in the unaltered gabbro and the alteration zones. See Appendices II and III for analytical data.

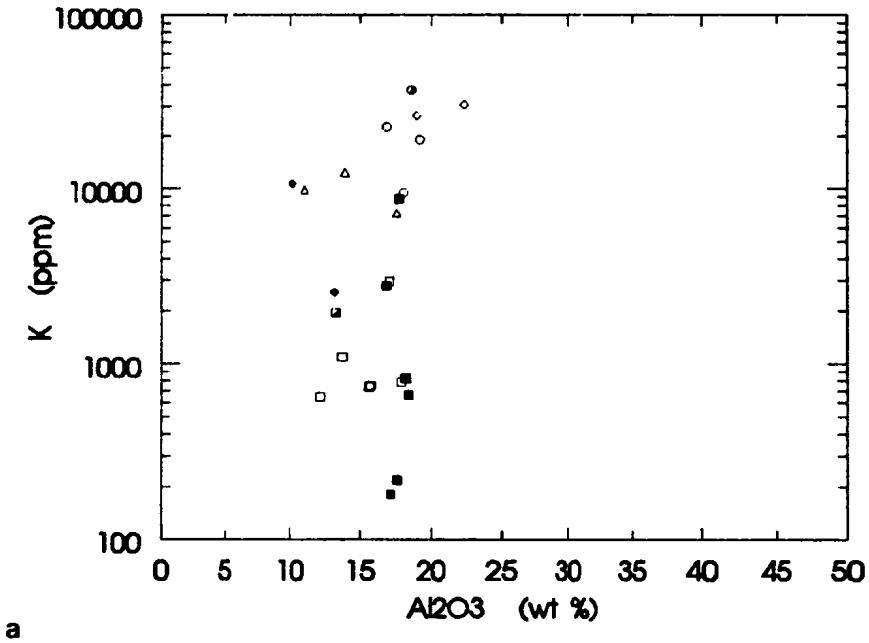

a

b

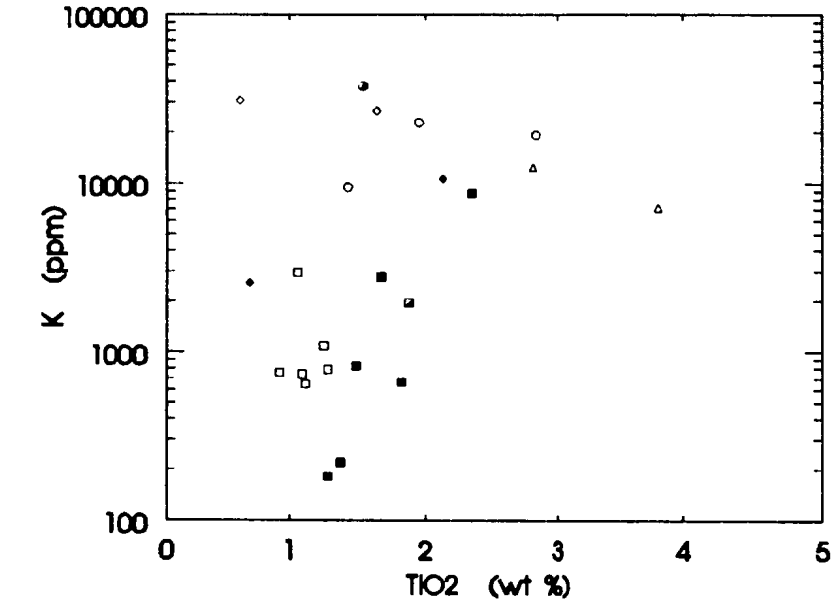

Figure 7-25 Al and Ti variations in the unaltered gabbro and the alteration zone. Symbols as in Figure 7-24.

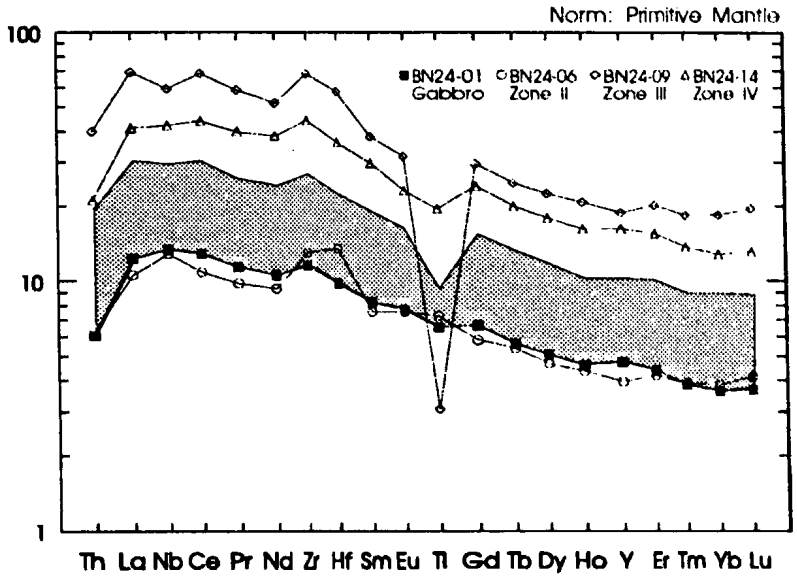

Figure 7-26a Extended REE profile for gabbro and alteration assemblages of drill-hole BN88-24. Shaded area represents the range of unaltered gabbro compositions in the area (see Table 7-1 for alteration zones).

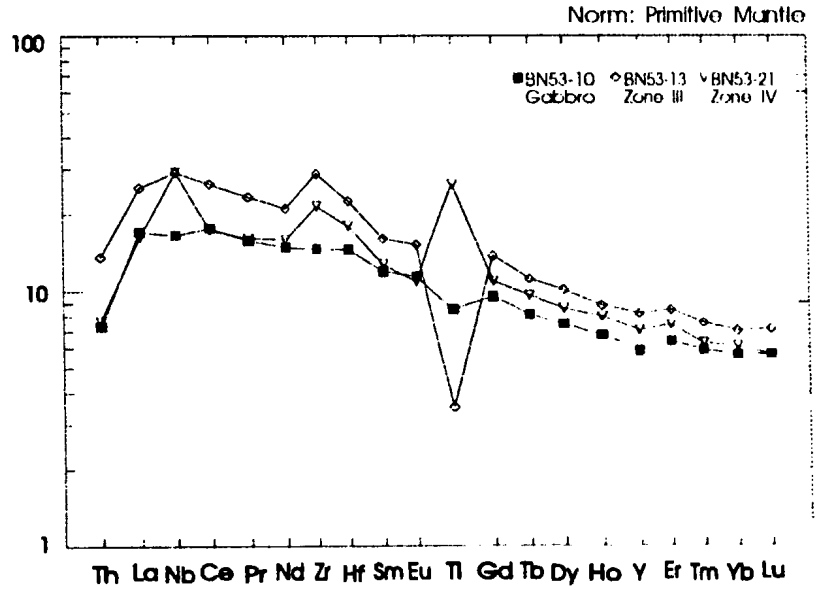

Figure 7-26b Extended REE profile for gabbro and alteration assemblages of drill-hole BN89-53.

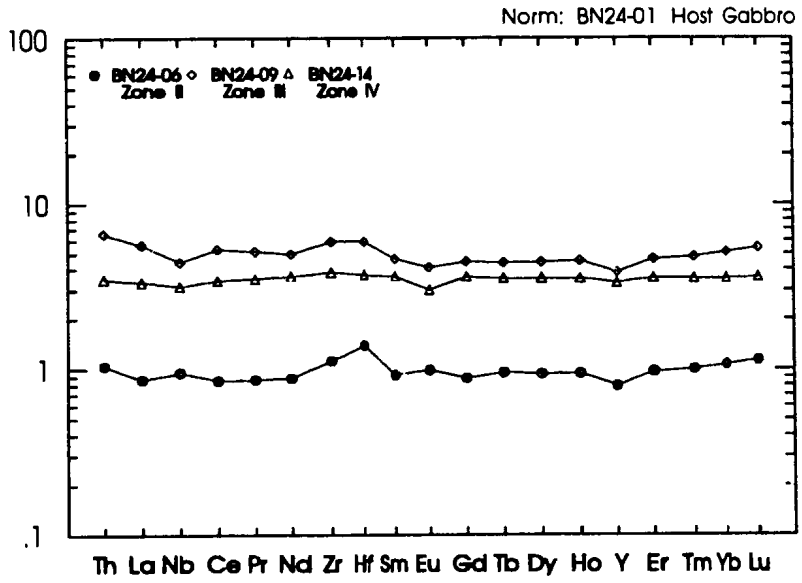

Figure 7-27 Extended REE profile of different alteration assemblages of drill-hole BN88-24, normalized to the unaltered gabbro composition.

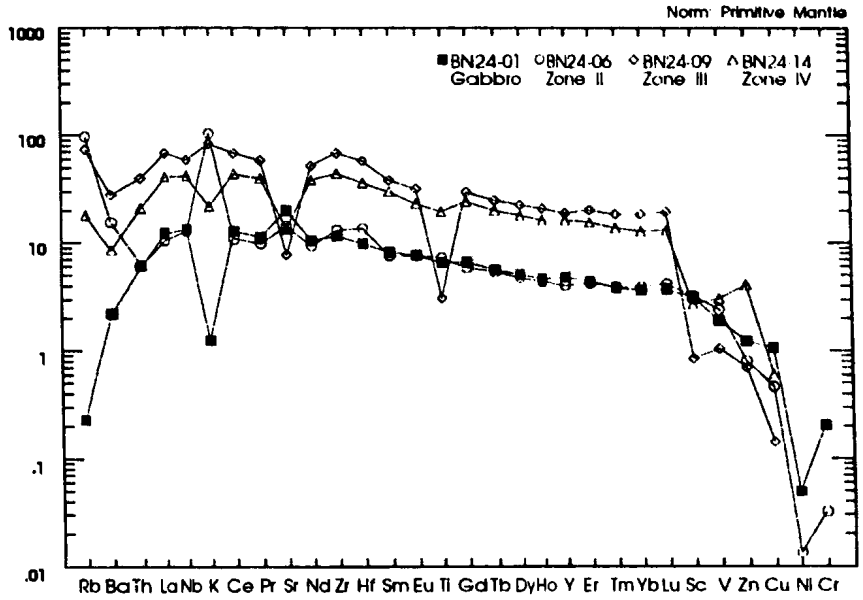

Figure 7-28a Extended trace element plot for the same samples as in Figure 7-26a.

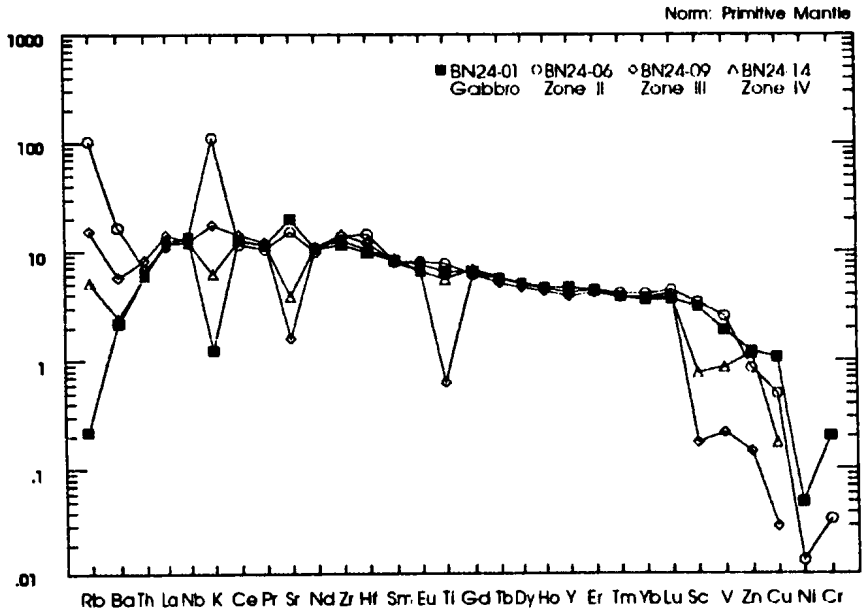

Figure 7-28b Extended trace element plot similar to (a), corrected for possible volume variations.

CHAPTER 8: GEOCHRONOLOGY

8.1 INTRODUCTION

It has been demonstrated, based on field (Chapter 3), structural (Chapter 4) and petrographic (Chapters 5 and 7) observations, that the D_I deformation, hydrothermal alteration and the associated gold mineralization clearly post-dated the igneous crystallization and sub-sea-floor metamorphism of the Stog'er Tight Gabbro. The crystallization age of the gabbro is constrained by the age of the Point Rousse Ophiolite Complex which is presumed to be the same as that of the Betts Cove Complex (Early Ordovician). There are, however, no radiometric ages reported from the Point Rousse Complex. The coincidence of the ductile-deformation/alteration event with the D_M thrusting in the Point Rousse Complex (section 4.2) places a speculative post-Early Ordovician to Acadian (Devonian) age limit on gold mineralization in the Stog'er Tight prospect (section 4.1). Nevertheless, these do not serve as direct and solid evidence for the age of mineralization event.

This chapter presents the results of U-Pb radiometric dating of the host rock and of the gold mineralization in the Stog'er Tight prospect. The geologic

setting, field relationships and the petrographic and geochemical characteristics of the dated rock types are described in the previous chapters. The specific features of the processed samples are described below.

8.2 DESCRIPTION OF SAMPLES

A 25 kg sample of pegmatitic gabbro (sample JR90915) was collected from trench IS, eastern Stog'er Tight prospect, for determination of the gabbro crystallization age. This sample contained large plagioclase and hornblende grains (4mm and 7mm, respectively) in a prominent ophitic texture. Small zircon and titanite inclusions were observed within hornblende grains in thin section. An identical sample from the same locality (sample JR91822-3) was analyzed for major and trace elements and is plotted together with other gabbro samples on the geochemical diagrams of Chapter 6.

Radiometric dating of the alteration associated with gold mineralization started with four altered gabbro samples from drill-core BN89-60 (samples BN60-A8, -45, -37 and -47). These samples were mainly from the chlorite-magnetite alteration zone, where the presence of the radioactive inclusions was first recognized by the observation of pleochroic haloes in chlorite in thin section. A 30 kg altered gabbro sample (sample JR91822-1) was later collected (field season of 1991) from the alteration/mineralization zone of trench IIIM and was processed for radiometric dating.

8.3 SAMPLE PREPARATION

8.3.1 Initial Separation

The large geochronology samples (JR90915 and JR91822-1) were smashed into cobble-size pieces with a sledge hammer and hydraulic splitter and were water-washed in order to remove all surface soil. Both samples were subsequently crushed in a jaw-crusher and were pulverized using a disk-mill. The sample powders were washed on the Wilfley Table twice to separate the heavy minerals from the rest of the sample. The heavy mineral fractions were washed with alcohol and dried before being sieved with 70 mesh sieves. The < 70 mesh fractions went through magnetic free-fall twice to remove magnetite as well as the iron contaminants resulting from the abrasion of the disks.

Sample JR90915 (pegmatitic gabbro) was then processed by Bromoform in a separatory funnel and its heavy fraction (sink) was passed through a Frantz magnetic separator at 10° and 0.5, 1.0 and 1.7 Amperes, respectively, in order to separate magnetic minerals such as the remaining amphibole and epidote. The non-magnetic fraction of sample JR91822-1 was not processed through the Bromoform and Frantz separation stages as it was not a sufficiently large fraction. Both samples were sieved with 100 mesh and 200 mesh sieves and their < 200 mesh fractions were put through Methylene Iodide liquid separation in order to remove impurities such as apatite. The obtained fraction of sample JR90915 was composed of pyrite, zircon and minor carbonate. Pyrite was

dissolved in hot HNO_3 and a semi-pure zircon fraction resulted. Zircon grains were subsequently hand-picked from both samples under a binocular microscope.

The four drill-core samples were split by the hydraulic splitter and were pulverized in a tungsten-bowl pulverizer. The rock powders were processed separately by Bromoform and Methylene Iodide in separatory funnels and the resulted heavy mineral fractions (sink) were sieved through 100 mesh and 200 mesh sieves.

8.3.2 Mineral Fractions

Unlike those in the pegmatitic gabbro, the accessory mineral species of the altered gabbro samples were not readily identifiable due to their small grain-sizes (20 to 80μm) and their fundamental morphologic dissimilarities to their common and well-known igneous (and metamorphic) equivalents. Therefore, the prospective mineral grains were hand-picked from the final fractions of each sample under the microscope and were grouped into morphologically similar populations. Selected grains of each population were mounted on carbon-coated, double-sided scotch tapes on small sample holders and were analyzed by SEM. These SEM-identified grains are recoverable and can be directly used for geochronology.

A total of 13 mineral fractions were identified, selected, processed and measured for their U and Pb isotopic ratios. These included zircon, rutile and monazite fractions.

Igneous Zircon

Clear, euhedral zircon grains with a simple prismatic habit and pyramidal terminations (Fig.8-1) were picked from the concentrated fraction of sample JR90915. About 100 zircon grains were selected and grouped into 4 fractions based on grain quality. These range from perfectly clear and intact prisms to cracked and slightly hematitized fragments. The 3 best fractions were abraded with pyrite in air-abrasion devices (cf. Krogh, 1982) under 2 psi pressure for 30 minutes to 5 hours, to remove altered surfaces of the prisms.

Hydrothermal Zircon

The hydrothermal zircon is morphologically distinct from the common igneous zircon. It is characterized by angular, stubby and porous grains with an opaque, pinkish- to dark-red colour, some of which have uncommon crystal twins (Fig.8-2). Some grains (sample JR91822-1) have pseudomorphous shapes after igneous zircon. Examples of optically clear, euhedral prisms (igneous zircon) partially replaced by red, turbid material (hydrothermal zircon) have also been found in the altered gabbro samples. Four hydrothermal zircon fractions were picked from samples BN60-37 and JR91822-1 and were abraded under 2 psi pressure for up to 6 hours.

Rutile

Hydrothermal rutile was hand-picked from the concentrated fractions of samples JR91822-1 and BN60-A8. The latter contains large (between 100 and

200 mesh), stubby rutile prisms with striated surfaces and a dark-brown colour (Fig.8-3). The most euhedral prisms were picked and were abraded for 1 hour under 3 psi pressure to remove chlorite from grain surfaces. Sample JR91822-1 contains abundant, yellow to orange, clear rutile with common elbow twins (Fig.8-4). Two fractions from the best quality rutile were picked for further processing.

Monazite

The hydrothermal monazite is characterized by small, round, colourless and clear grains with a notably high relief (Fig.8-5). It is indistinguishable from anhedral apatite under binocular microscope and therefore had to be analyzed by SEM (identified by its Ce and La peaks) before final selection. Two monazite fractions were selected from samples BN60-A8 and BN60-47.

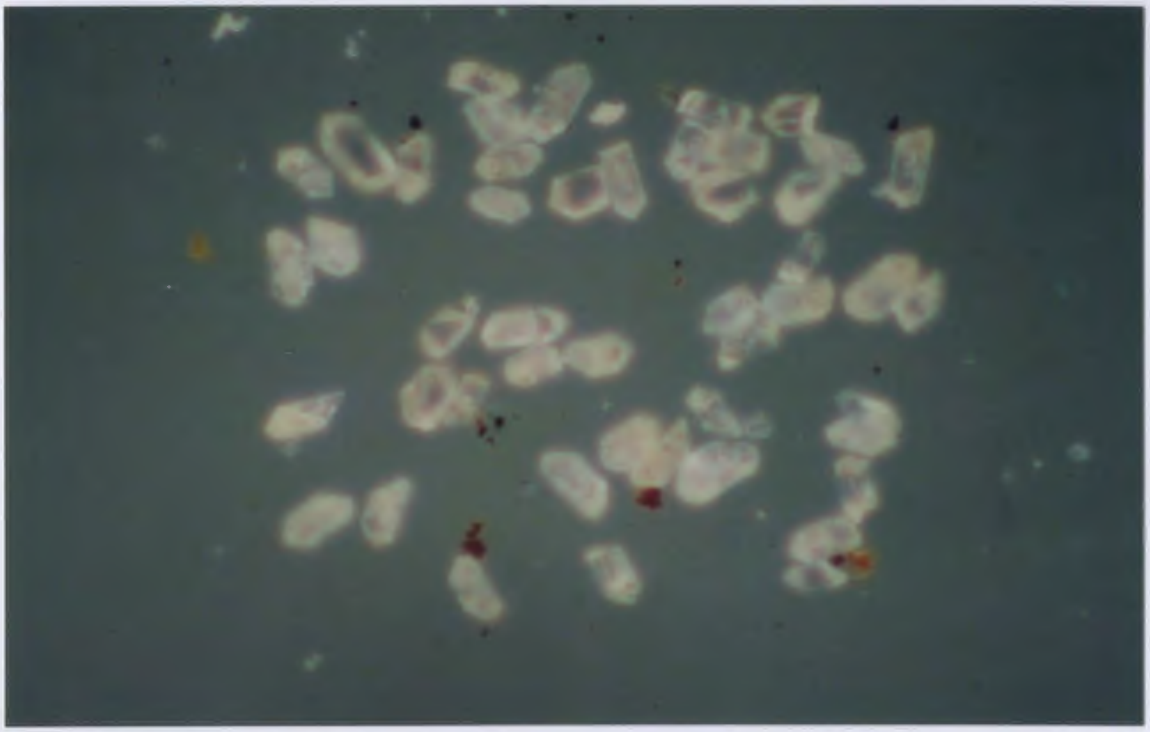

Figure 8-1 Separated fraction of igneous zircon prisms from the Stog'er Tight Gabbro (sample JR90915). (x100)

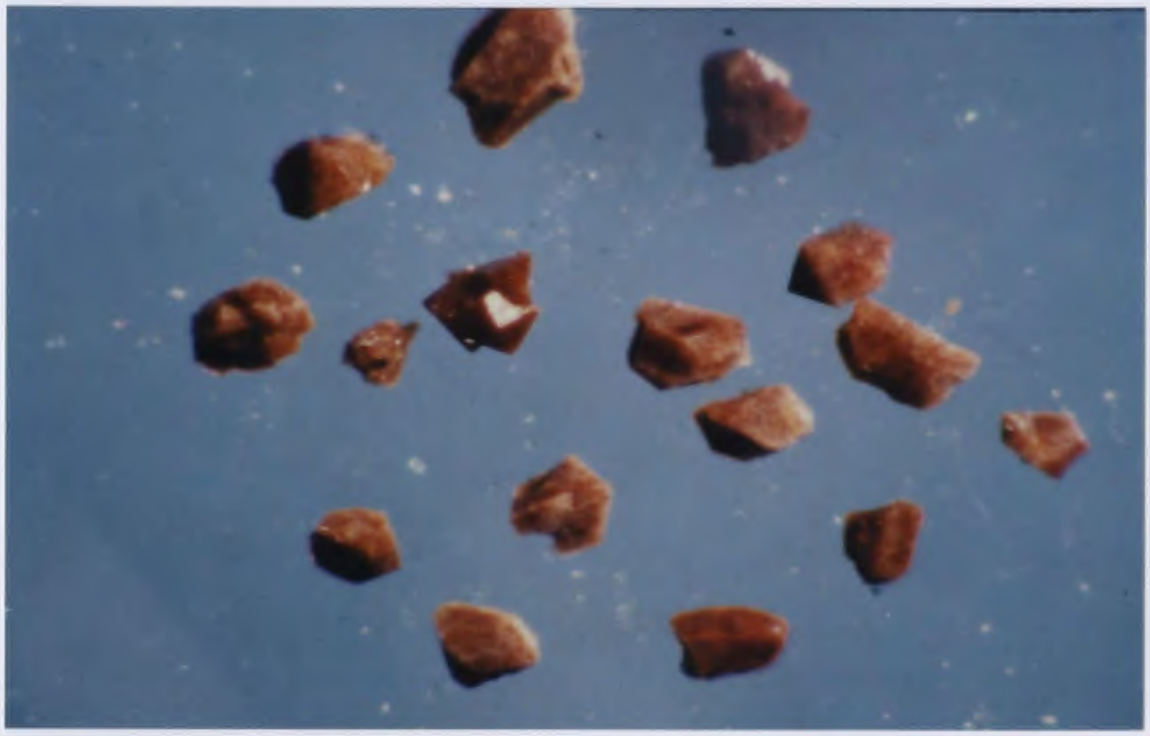

Figure 8-2 Separated fraction of red hydrothermal zircon grains from the altered gabbro (sample JR91822-1) (x150).

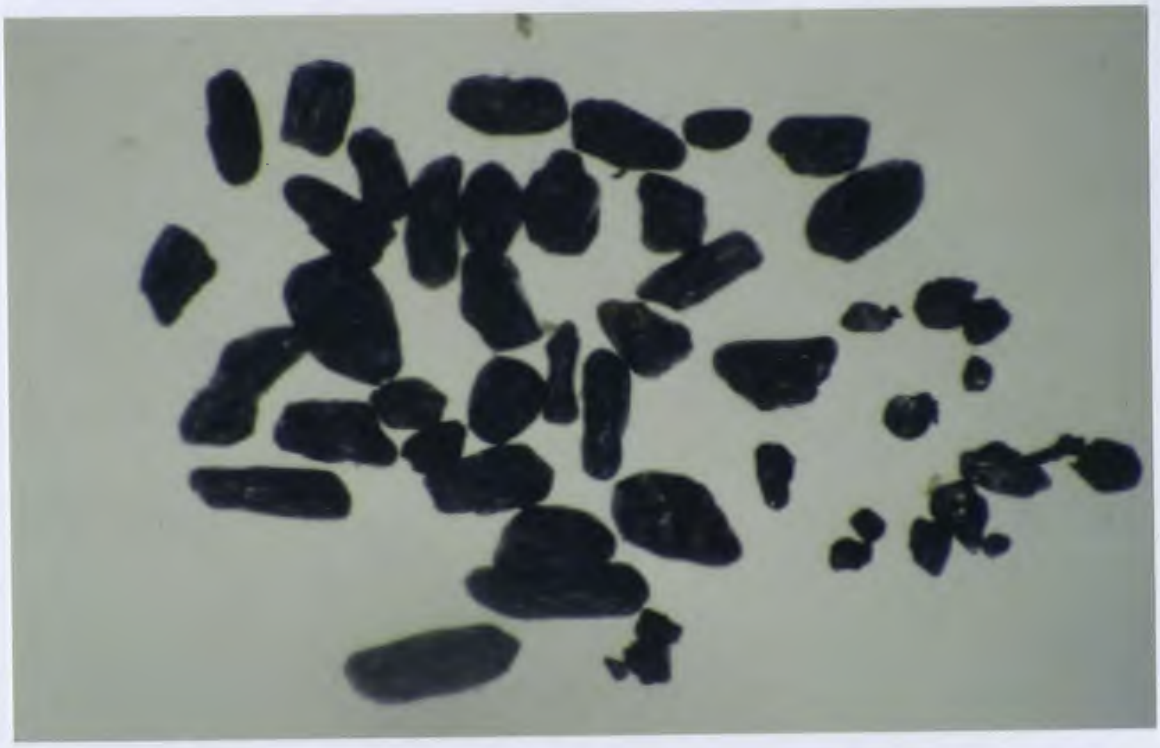

Figure 8-3 Separated fraction of dark hydrothermal rutile from the red albite-pyrite (+gold) zone, sample BN60-A8 (x100).

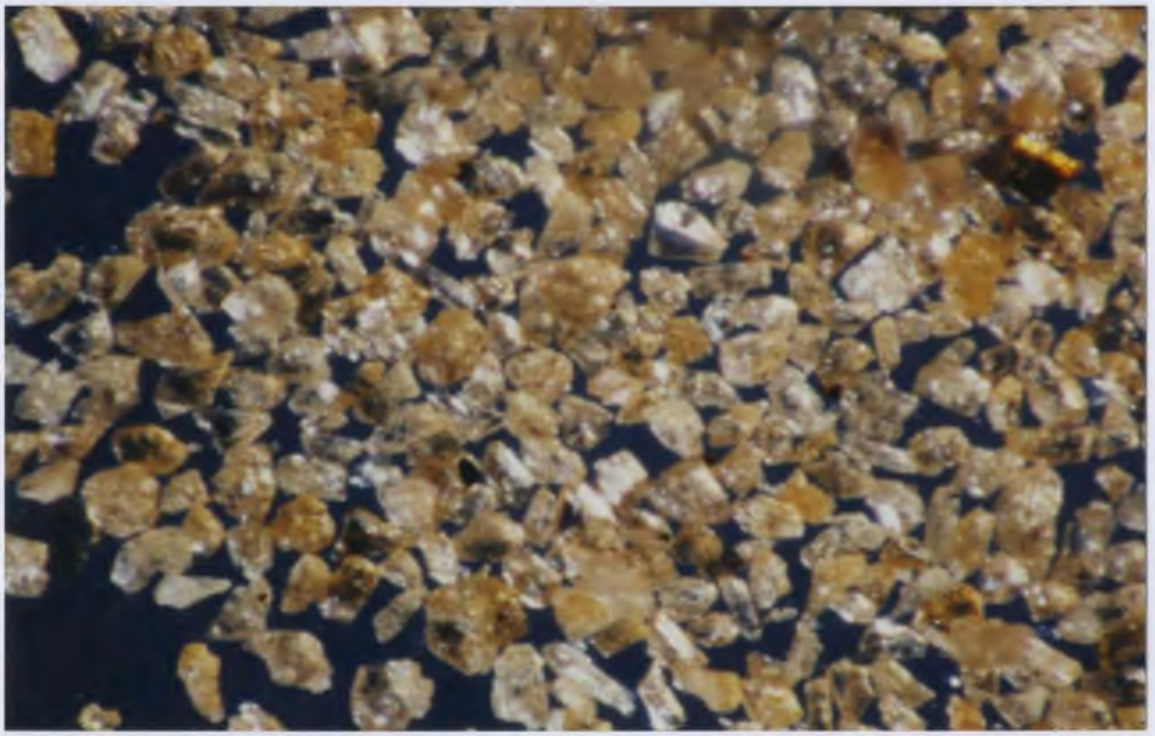

Figure 8-4 Separated fraction of yellow-orange rutile from sample JR91822-1 (x100).

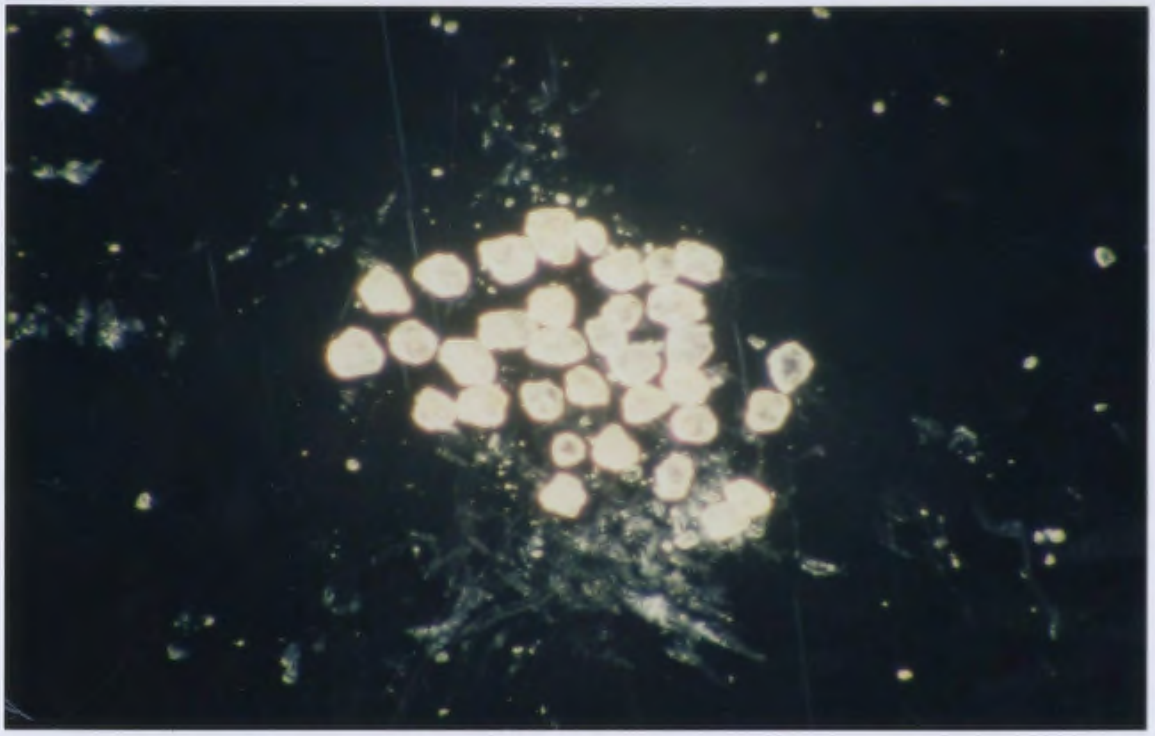

Figure 8-5 Separated fraction of hydrothermal monazite from the red albite-pyrite (+gold) zone, sample BN60-47 (x100).

8.4 ANALYTICAL PROCEDURES

The air-abraded mineral fractions were washed in nitric acid on a hot plate to remove the remaining pyrite. All samples were loaded into separately labelled glass beakers and were successively washed in nitric acid, water and acetone (distilled reagents) on the hot plate. The cleaned and dried fractions were carefully weighed, loaded in dissolution bombs and were spiked with a mixed ^{205}Pb-^{235}U spike. 0.5 cc HF and 2 drops of nitric acid were added to each teflon bomb for zircon and rutile fractions. Monazite fractions were dissolved with a 6N HCl solution in Savilex cap-screw bombs on a hot plate. The samples (bombs) stayed in the oven at 210°C for 5 days and then proceeded to ion-exchange chromatography.

The HF-dissolved samples were converted overnight to 3.1N HCl, then poured out of bombs into small ion-exchange columns (with the exception of the dark rutile sample which was loaded onto a large column). Pb and U were successively eluted using HCl-based chemistry for zircon, and HBr-based chemistry for rutile and monazite solutions, following the techniques of Krogh (1973) and Manhes et al.(1978). The elutants were subsequently evaporated on the hot plate and U and Pb were collected in the form of a single droplet in the PMP beakers by adding 1 drop of 0.5N H_3PO_4.

All samples were measured for U and Pb isotopic ratios on the Finnigan

MAT 262 multi-collector solid-source mass spectrometer at Memorial University. Samples were loaded on Re filaments with silica gel and H_3PO_4 and measurements were carried out in the 1400 to 1600°C temperature range The isotopic ratios were measured in ion-counter peak jumping and Faraday static modes with ^{204}Pb measured in the ion-counter. The U and Pb concentrations and the measured isotopic ratios are given in Table 8-1. The data are corrected for isotopic fractionation in mass spectrometer (0.1%/AMU), laboratory contamination (blanks, 10-15 pg total common Pb) and for Pb in the spike. The common Pb isotopic compositions at the time of crystallization were calculated from the model of Stacey and Kramers (1975). 2σ absolute uncertainties are calculated with an error propagation procedure modified after Ludwig (1980). This calculation procedure takes into account measurement precision and uncertainties involving U and Pb fractionation, sample and spike weights, and the amounts of U and Pb laboratory blanks. The 2σ uncertainties are reported after the ratios in Table 8-1 and refer to the final digits.

TABLE 8-1: U-Pb data

No.	Properties	Wt. [mg]*	U [ppm]	Pb rad	total comm. Pb(pg)	^{206}Pb / ^{204}Pb	^{208}Pb / ^{206}Pb	^{206}Pb / ^{238}U	+/-	^{207}Pb / ^{235}U	+/-	^{207}Pb / ^{206}Pb	+/-	AGES (Ma) ^{206}Pb / ^{238}U	AGES (Ma) ^{207}Pb / ^{206}Pb
STOG'ER TIGHT GABBRO (JR90915)															
1	20 euhed grains-abraded	0.012	568	64.9	29	1146	.6610	.07720	52	.6041	44	.05675	18	479	482
2	Best clear prisms-abraded	0.042	629	68.0	20	6283	.6006	.07563	46	.5921	33	.05678	20	470	483
3	Angular zircon fragments	0.058	961	102.6	85	3083	.6106	.07429	28	.5816	24	.05678	8	462	483
4	35 cracked prisms	0.015	767	82.3	21	2471	.6600	.07246	78	.5669	60	.05674	14	451	482
ALTERATION ZONE (DRILL-CORE)															
5	BN60-37: 5 red zircon-abraded	0.005	332	30.6	73	114	.5331	.06728	74	.5115	107	.05513	94	420	418
6	BN60-37: 3 red zircon-abraded	0.003	226	20.0	12	257	.5242	.06505	38	.4944	68	.05512	66	406	417
ALTERATION ZONE (OUTCROP) (JR91822-1)															
7	35 large red zircon-abraded	0.071	1235	105.8	253	1391	.5137	.06332	46	.4887	35	.05597	18	396	451
8	32 red zircon-abraded	0.027	562	52.8	92	685	.6329	.06451	40	.4980	34	.05599	22	403	452

NOTES * Uncertainty in weight +/-0.006 mg (2σ).

** Corrected for fractionation and blank, 10-15 pg laboratory blank and initial common lead calculated from the model of Stacey and Kramers (1975) and 1 pg U blank. Uncertainties on the isotopic ratios are calculated with the procedure of Ludwig (1980) and are reported as 2σ after the ratios and refer to the final digits.

8.5 RESULTS

8.5.1 Age of the Stog'er Tight Gabbro

The fraction of abraded, euhedral zircon grains (No.1) from sample JR90915 is concordant within uncertainties and yielded a $^{207}Pb/^{206}Pb$ age of 482 Ma associated with a $^{206}Pb/^{238}U$ age of 479 Ma. The three other zircon fractions produced variably discordant ages, though all of their $^{207}Pb/^{206}Pb$ ages are between 482 and 483 Ma, in accord with that of the concordant fraction. All four fractions plot along a discordia line on the U-Pb concordia diagram (Fig.8-6a). The best fit calculations (Davis, 1982) on the discordia line (88% probability of fit) yielded an upper intercept age of 483.1 +8.7/-4.8 Ma and a lower intercept age of 8 Ma for the sample. The lower concordia intercept has considerably wide limits as all four fractions plot close to the upper concordia intercept. This allows the discordia line to fluctuate considerably between the data points. If the lower intercept is constrained to pass through a point at 10 ±10 Ma, a significantly smaller uncertainty will be obtained for the upper intercept age which is largely influenced by the $^{207}Pb/^{206}Pb$ error on the points near concordia. With this constraint, the crystallization age of the Stog'er Tight Gabbro is determined to be 483 +3/-2 Ma which is in agreement with all $^{207}Pb/^{206}Pb$ ages as well as the concordant point.

8.5.2 Age of the Hydrothermal Alteration

A red (hydrothermal) zircon fraction of sample BN60-37 (No.5) is concordant with a $^{207}Pb/^{206}Pb$ age of 418 Ma and a $^{206}Pb/^{238}U$ age of 420 Ma. This fraction was composed of 5 abraded zircon grains (0.005 mg) and the total radiogenic Pb analyzed was only 216 pg. Therefore, the uncertainty on $^{207}Pb/^{235}U$ age (and also $^{207}Pb/^{206}Pb$ age) is relatively high because of the large relative common Pb contribution from the blank (Fig.8-6b). Accordingly, the $^{206}Pb/^{238}U$ age of 420 $\pm$5 Ma (2σ) is suggested to be the most reliable age for the sample. The second red zircon fraction from the same sample (No.6) was smaller than the former (0.003 mg, 64 pg radiogenic Pb) and yielded discordant ages of 406 $\pm$3 Ma ($^{206}Pb/^{238}U$) and 417 $\pm$26 Ma ($^{207}Pb/^{206}Pb$). This sample has a better radiogenic Pb : common Pb ratio and its $^{207}Pb/^{206}Pb$ age overlaps with that of the concordant fraction within uncertainties.

The large red zircon fractions from sample JR91822-1 (No. 9 and 10) yielded discordant ages which range from 396 ($^{206}Pb/^{238}U$) to 452 ($^{207}Pb/^{206}Pb$) Ma. These fractions neither fall on a line with the two red zircon fractions of sample BN60-37 (No.5 and 6) nor intersect with the gabbro discordia line. They are therefore interpreted as a mixed population of hydrothermal zircon and igneous zircon from the gabbro. This interpretation is consistent with the pseudomorphous shapes of these zircon grains, as well.

The 3 analyzed hydrothermal rutile fractions had very low U concentrations (all under 1ppm) with minor or no radiogenic Pb. The $^{206}Pb/^{204}Pb$ ratios in these fractions are about 19 which is essentially that of the common

Pb. This common Pb is a mixture of laboratory and sample common Pb's that cannot be uniquely resolved. No significant ages were therefore obtained from the hydrothermal rutiles and the isotopic ratios are not reported in the present work.

Highly discordant ages were yielded from the two analyzed monazite fractions. These fractions had low U and radiogenic Pb contents and tend to fall way above the concordia line. The ages measured from the monazite fractions, therefore, are of no value.

Presently, the only measured ages for the hydrothermal alteration are those from the red zircon fractions of sample BN60-37. The concordant U-Pb age of 420 ±5 Ma is therefore proposed for the alteration/mineralization event in the Stog'er Tight gold deposit.

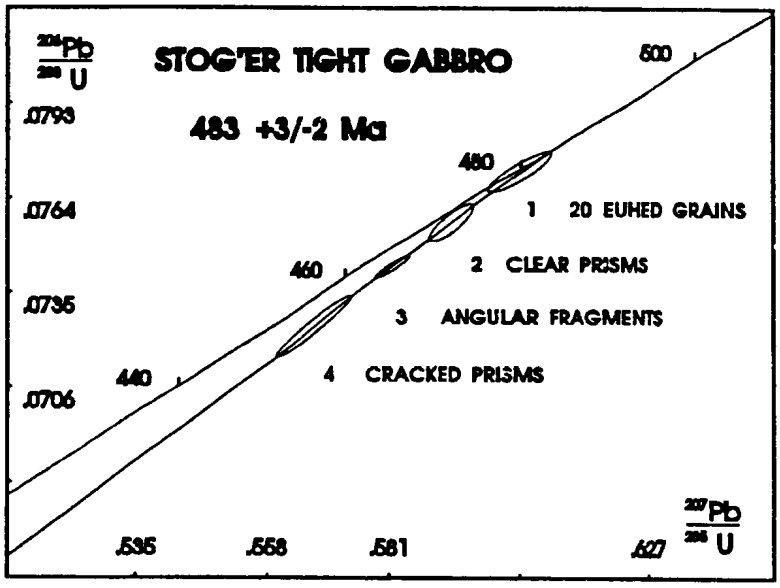

Figure 8-6a Concordia diagram for the age of the Stog'er Tight Gabbro.

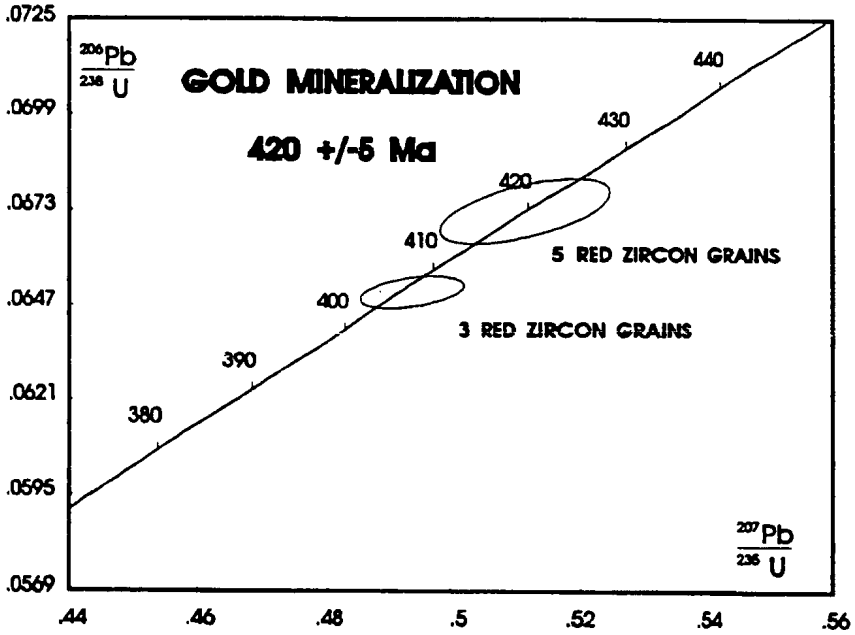

Figure 8-6b Concordia diagram for the age of hydrothermal alteration in the Stog'er Tight deposit.

8.6 INTERPRETATION

The Stog'er Tight host gabbro is stratigraphically included in the volcanic cover sequence of the Point Rousse Complex. The ophiolite complexes of the Baie Verte Peninsula, including the Point Rousse and Betts Cove Complexes, are believed to be parts of an oceanic crust of essentially the same age (Hibbard, 1983) and to be mutually correlative. Accordingly, the Point Rousse Cover Sequence has been correlated with the Arenigian Snooks Arm Group which conformably overlies the Betts Cove Complex (see Chapter 2).

The measured 483 +3/-2 Ma age of the Stog'er Tight Gabbro (and of the Point Rousse Cover Sequence) is entirely consistent with the Middle Arenigian fossil age of the Snooks Arm Group and confirms the correlation between these two lithologic units. The age of the underlying ophiolitic rocks of the Point Rousse Complex, by comparison, should be slightly older than the cover sequence and probably overlaps with the age of the Betts Cove Complex (488.6 +3.1/-1.8; Dunning & Krogh, 1985).

A number of mainly granitoid intrusions and extrusive rocks crosscut (and overlie) the ophiolite complexes (Baie Verte Belt) and the metamorphosed continental margin sedimentary rocks (Fleur de Lys Belt) of the Baie Verte Peninsula (see Chapter 2). U-Pb igneous crystallization ages have recently been measured from the Burlington Granodiorite, Dunamagon Granite, Cape Brule Porphyry and the Seal Island Bight Syenite, as well as the Wild Cove Pond

Igneous Suite and the Fleur de Lys migmatites (Dunning and Cawood, unpublished data). Coyle (1990) also reported U-Pb ages for the Cape St. John Group. Figure 8-7 is a schematic illustration of the radiometric ages from the Baie Verte Peninsula. The conspicuous clustering of igneous ages between 440 and 424 Ma indicates a major phase of Early to mid-Silurian magmatism on the Peninsula which is clearly distinct from the classical Taconian (Middle Ordovician) and Acadian (Devonian) orogenic phases of the Appalachian Orogen. It must be noted here that on the basis of biostratigraphic criteria, the Ordovician-Silurian boundary has traditionally been placed at ~438 Ma. Nevertheless, a recent time-scale calibration based on the precise U-Pb radiometric dating of the Ordovician and Lower Silurian stratotypes of Britain (Tucker et al., 1990) places the top of the Ashgill Series (Upper Ordovician) near 441 Ma suggesting placement of the boundary at this age. Attention must be paid to this new revision of the Paleozoic time-scale in considering the time period of orogenic activity in the Baie Verte Peninsula.

The metamorphosed continental margin sedimentary and volcanic rocks of the Fleur de Lys Supergroup to the west of the Baie Verte Line have a polyphase metamorphic history (see Chapter 2). Dallmeyer (1977) suggested, based on $^{40}Ar/^{39}Ar$ cooling ages of metamorphic mineral phases, that the peak of metamorphism in the Fleur de Lys Supergroup was reached before the Acadian Orogenic phase. Jamieson & Vernon (1987) and Jamieson (1990) provided structural and textural evidence in support of the isotopic ages and concluded that the main phase of metamorphism in the western Baie Verte

Peninsula pre-dated 420 Ma and occurred in the Early Silurian. U-Pb dating of monazites from the Fleur de Lys migmatites (Dunning & Cawood, unpublished data) gave an age of 427 ±2 Ma for the high-grade metamorphism (migmatitization), in agreement with the proposed Early Silurian ages of metamorphism in the Fleur de Lys Supergroup (Fig.8-7). Overall, the bulk of present age data indicates that the peak of metamorphism in the underlying metamorphosed continental margin rocks was synchronous with the main stage of magmatic activity (and tectonism) on the Baie Verte Peninsula.

The best estimated age of Au mineralization in the Stog'er Tight prospect (420 ±5 Ma) is also plotted on Figure 8-7 together with the latest measured igneous and metamorphic ages (Dunning & Cawood, unpublished data) from the Peninsula. It shows that Au mineralization occurred during the final stage of Silurian magmatic activity, coeval with or shortly after the peak of metamorphism in the underlying metamorphosed continental margin rocks. The crystallization age of the youngest dated granitoid intrusion in the Baie Verte Belt is 427 ±2 Ma (Seal Island Bight Syenite, Dunning & Cawood, unpublished data) that is approximately 7 Ma older than the mineralization event in Stog'er Tight, but overlaps within combined uncertainties. The age of Au mineralization also overlaps with that of the I-type granites from the Wild Cove Pond Igneous Suite (424 ±2) which intrudes the Fleur de Lys Supergroup to the west of the Baie Verte Line.

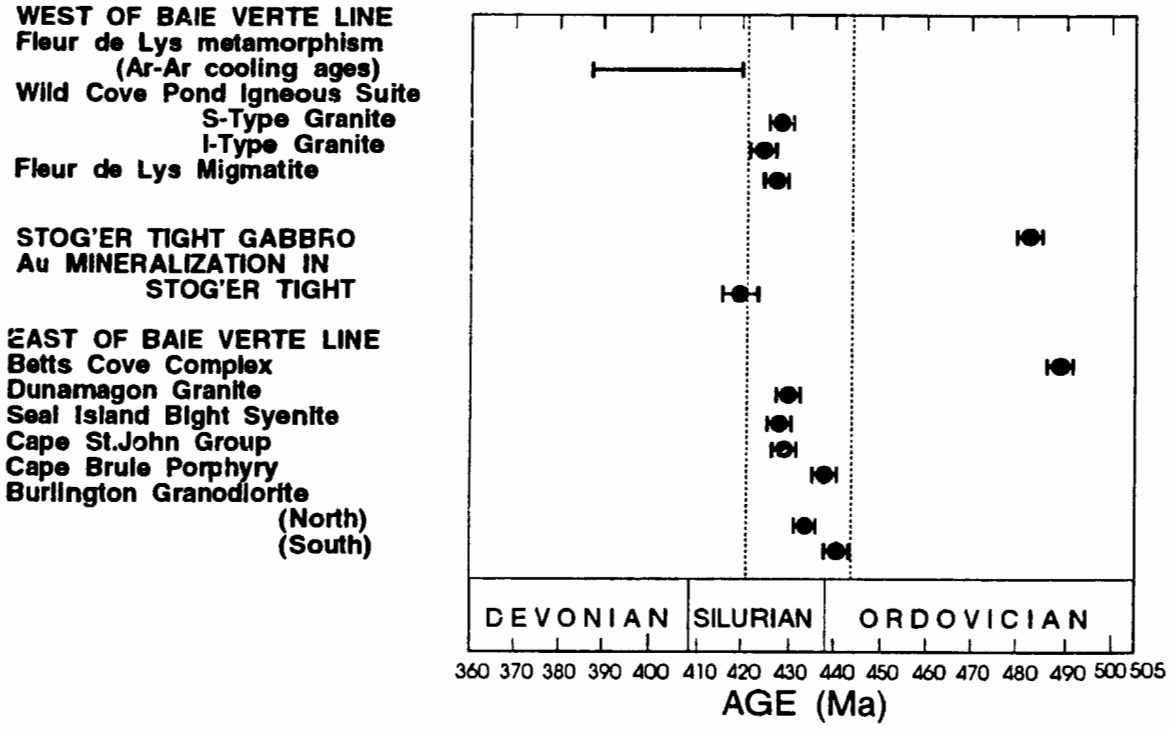

Figure 8-7 Compilation of radiometric ages from the Baie Verte Peninsula, from variable sources, including the measured U-Pb ages of this study.

CHAPTER 9: DISCUSSION

9.1 GEOLOGIC SETTING OF STOG'ER TIGHT GABBRO

The Dunnage tectonostratigraphic zone of the Appalachian Orogen represents the Cambro-Ordovician oceanic terranes, including the ophiolitic suites and island arc sequences (see Chapter 2), that were accreted to the North American continent in Ordovician time (Taconian Orogeny). The presumed-Taconian plate collision and ophiolite obduction along the western boundary of the Dunnage Zone at the Baie Verte Peninsula is manifested in the Baie Verte-Brompton Line, which separates the Dunnage oceanic terranes from the Laurentian continental margin (Humber Zone). The Stog'er Tight gold prospect is located on the Baie Verte Peninsula, to the east of the Baie Verte Line, within the Point Rousse Complex.

Stratigraphic relationships (Chapter 3) indicate that gold mineralization in the Stog'er Tight deposit is hosted by multiple gabbroic sills which have conformably intruded the stratified, mafic to intermediate, volcanic and pyroclastic rocks of the Point Rousse Complex. The chemical compositions of the gabbroic rocks in the study area (Chapter 6) have suggested that, a) these

high-level intrusive rocks have compositional trends similar to the oceanic tholeiites, b) different gabbro sills are geochemically distinctive and they probably originated from a geochemically evolving source, and c) the main host gabbro of gold mineralization features an E-MORB to OIB geochemical signature that is in contrast with the typical island-arc affinity of the enclosing volcanic/pyroclastic units (and most of the Point Rousse Complex). The stratigraphic and lithochemical characteristics of the Stog'er Tight gabbro are comparable to those of analogous rock units in other island-arc volcanic sequences of the Dunnage Zone (*e.g.* Snooks Arm Group and Wild Bight Group). These all share characteristics with the Fijian high-Ti alkali olivine basalts that are associated with recent arc-rifting processes in the southwest Pacific ocean (see Section 6.3).

The U-Pb age determinations of this study yielded an Early Ordovician age of 483 +3/-2 Ma for the crystallization of the Stog'er Tight gabbro (Chapter 8). This age is somewhat younger than the age of the ophiolitic rocks on the Baie Verte Peninsula (Betts Cove Complex, 488.6 +3.1/-1.8 Ma), and is consistent with the late intrusion of the gabbro into the ophiolitic volcanic cover rocks of the Point Rousse Complex. Although the precise age of emplacement of the ophiolitic suites on the Baie Verte Peninsula is not well constrained, the measured $^{40}Ar/^{39}Ar$ ages from the metamorphic aureoles of the Bay of Islands Complex (and the St. Anthony Complex) indicate that obduction of the oceanic crust in these areas occurred at least 14 Ma after the crystallization of the ophiolitic intrusive rocks (Chapter 2). These timing

constraints strongly suggest by analogy that the Stog'er Tight gabbro was formed in an oceanic environment, prior to the emplacement of the Point Rousse Complex (oceanic slab) onto the continental margin along the Baie Verte Line. The pre-collisional intrusion of the Stog'er Tight gabbro is also confirmed by its stratigraphic conformity with the enclosing ophiolitic volcanic rocks, and by its sub-seafloor style of metamorphism (Chapter 5).

According to the stratigraphic, geochemical and geochronological data, the Stog'er Tight gabbro is interpreted to have been emplaced during an episode of island-arc rifting, tholeiitic magmatism and, possibly, back-arc basin development, which occurred in the Early Ordovician, prior to Taconian collisional accretion of the oceanic terranes to the continental margin.

9.2 ENVIRONMENT OF GOLD MINERALIZATION

Gold mineralization in the Stog'er Tight deposit is structurally controlled by shear zones which are best developed in the gabbro sills. The close association of Au mineralization with shear deformation and, especially, hydrothermal alteration which has overprinted the greenschist metamorphic assemblage of the gabbro, are indicative of an epigenetic style of mineralization. The measured mid-Silurian age of hydrothermal zircon associated with mineralization (Chapter 8) supports this epigenetic origin.

It is suggested, based on structural relationships (Chapter 4), that the mineralization-related D_1 structures in the Stog'er Tight deposit are genetically

related to a major tectonic event on the Baie Verte Peninsula which involved large-scale folding of the Point Rousse Complex (F_M syncline), southward-directed emplacement of the Complex along the Scrape Thrust (D_M thrusting) and probably, strike-slip movements along the Baie Verte Line. The structures associated with this tectonic event are characterized by an eastward trend, that is in contrast with the general north-south trend of earlier structures such as the Baie Verte Line. This supports the notion that gold mineralization in the Stog'er Tight deposit post-dated the Ordovician collisional tectonism, though the precise age of the collisional event at the Baie Verte Peninsula is not well constrained.

The detailed study of the microstructural fabrics associated with hydrothermal alteration (and deformation) in the D_1 shear zones of the Stog'er Tight deposit (Chapter 7) reveals that the peak of alteration and gold mineralization (red albite-pyrite replacement) occurred at a late stage of D_E ductile deformation, and was essentially complete prior to the D_L brittle-ductile phase. Consequently, gold mineralization must have been related to a single alteration/deformation event and, moreover, the deposition of Au-bearing pyrite at the peak of hydrothermal alteration must have occurred in a relatively short time period, between the D_E and D_L deformation episodes. The occurrence of hydrothermal zircon inclusions (420 ±5 Ma, see Chapter 8) in the red albite-pyrite-Au zones and the microbrecciated texture of these inclusions in the chlorite-magnetite zone, have placed tight constraints on the timing of the peak hydrothermal alteration and gold deposition. This may also delimit the timing of

the widespread D_M deformation (S_M foliation, F_M folding and D_M thrusting) on the Baie Verte Peninsula to the mid-Silurian.

The relationship of gold mineralization to brittle-ductile style of deformation is characteristic of many shear-hosted, mesothermal Au-Ag deposits (*e.g.* Kerrich, 1990). It is suggested that under typical crustal conditions, the transition from ductile to brittle deformational regimes occurs at depths of 8 to 12 km, corresponding to vertical stresses of 2 to 3 kb, and temperatures of 240 to 360°C (Kerrich, 1999a). This suggests that although the Stog'er Tight gabbro was originally emplaced in the high stratigraphic levels of the Point Rousse Complex (*i.e.* the volcanic cover sequence), it was buried under a considerable thickness of rocks (probably thrust sheets) during the gold mineralization episode.

9.3 HOST ROCK CONTROLS ON GOLD MINERALIZATION

The hydrothermal alteration in the Stog'er Tight deposit is largely associated with zones of shear deformation which are preferentially developed in the gabbroic intrusive rocks (sills). The confinement of the ore shoots to the strongly altered, coarse-grained interiors of the gabbro sills, in particular, implies that mineralization, though clearly epigenetic, is largely stratabound. The possible rheological and/or chemical role(s) of the Stog'er Tight host gabbro in gold deposition, therefore, have been of key importance to this study.

The mode of deformation (brittle or ductile) of crustal material depends

on the intensive variables of the system, such as temperature, stress (confining and differential), fluid pressure, etc., as well as on the rheological properties of the rocks. Rheological properties are essentially governed by mineralogy and grain-size (Kerrich, 1989a), such that ductile (plastic) flow is enhanced in fine-grained, polycrystalline material, relative to the coarse-grained equivalents. Consequently, the fine-grained volcanic and pyroclastic rocks in the Stog'er Tight area have undergone a uniform ductile deformation, while discrete zones of confined shear deformation are preferentially developed in the coarse-grained gabbro, mainly because of the isotropic, competent lithology of the latter. Transgranular microfracturing associated with shear deformation in the gabbro enhanced confined fluid percolation through the shear zones, and facilitated the fluid-rock reactions. As a result, the hydrothermal alteration and its distinct zonation (and gold mineralization) is best developed in the sheared, coarse-grained gabbro, as opposed to the fine-grained, ductile volcanic/pyroclastic lithologies.

9.3.1 Gold Transportation and Precipitation

Romberger (1988), in a review of the solution chemistry of gold, proposed that gold is transported in hydrothermal systems most commonly as chloride ($AuCl_2^-$), bisulphide [$Au(HS)_2^-$, $Au_2S(HS)_2^{2-}$] and possibly, thioarsenide ($AuAsS_2^0$) complexes. Gold is soluble as the chloride complex in acid oxidizing solutions, whereas bisulphide complexes are favoured by reducing conditions in solutions where sulphur would occur as either H_2S or HS^-. The close

paragenetic relationship between gold and pyrite (and other sulphide phases) in the great majority of hydrothermal gold deposits indicates that gold is most likely transported as a bisulphide complex in these systems. Chloride complexes are stable at oxygen fugacities well above the stability conditions of sulphides, and therefore are considered unimportant in these sulphide-dominated, hydrothermal systems.

The relatively high solubility of gold-bisulphide complexes under hydrothermal conditions suggests that the mineralizing fluids are unlikely to have been saturated with respect to gold through most of their existence. In general, the contrasts between the geochemical environments of the source and host rocks are responsible for chemical changes causing ore deposition (Romberger, 1988). The mechanisms which can potentially result in the deposition of gold from the hydrothermal fluid at the site(s) of mineralization (at constant temperature), are a) oxidation, b) decrease in the activity of dissolved sulphur and, c) variations in pH of the fluid. However, oxidation is considered to be the most efficient mechanism for gold deposition, where bisulphide complexes are involved. Solution oxidation may result from a number of processes occurring in hydrothermal systems, the most important of which are boiling (fluid unmixing or effervescence), mixing with oxygenated ground waters and contact with an oxidizing host rock. Precipitation of sulphides can also reduce sulphur activity of the solution and enhance gold deposition.

Boiling or unmixing of fluids carrying CO_2, which also causes considerable changes in fluid chemistry, is considered by many to be the most important

factor in metal deposition (Murphy, 1989 and references therein). This mechanism is especially consistent with the style of mineralization in epithermal gold deposits. In shear-hosted mesothermal gold deposits, the brittle-ductile scheme of deformation within the host structures has been cited as an important control on the nature of fluid-rock interactions. Episodic brittle-ductile behaviour along shear zones can cause cyclic fluctuations in $P_{(fluid)}/P_{(total)}$, which allows the periodic escape of fluids along reactivated zones of mechanical weakness. The periodic decrease in fluid pressure leads to CO_2 immiscibility in water and the separation of CO_2 vapour from the fluid. During this process, trace gas species such as H_2, H_2S and CH_4 are partitioned into the vapour phase. Loss of these gas phases will act to oxidize the residual fluid and to lower the activity of reduced S-species, both of which induce coprecipitation of gold and pyrite (Kerrich, 1989a).

9.3.2 Gold Deposition Mechanism in Stog'er Tight Deposit

In the Stog'er Tight deposit, the highest grade of hydrothermal alteration and gold mineralization is characterized by massive replacement of the host gabbro (red albite-pyrite zone), during a late stage of ductile deformation (D_E). The late brittle-ductile deformation episode (D_L) apparently post-dated the mineralization event (see Chapter 7) and there is no evidence of cyclic brittle-ductile transition in the alteration sequence. These structural features, along with the notable paucity of tensional veins in the alteration/mineralization zone and the absence of gold in the veins, suggest that gold mineralization in the

Stog'er Tight deposit is unlikely to have been induced by pressure variations. Instead, the abundance of oxidizing mineral phases (titanomagnetite or leucoxene) in the host gabbro (Chapter 5), and their close textural association with the gold-bearing pyrite (Chapter 7), are indicative of direct chemical oxidation of the mineralizing fluid by the host gabbro.

The alteration reaction associated with the transformation of an ankerite-sericite assemblage to the red albite-pyrite assemblage (Section 7.2.3) can be modified to include deposition of gold from a soluble gold bisulphide complex:

$$FeTiO_3 + Ca(Mg,Fe)(CO_3)_2 + 2Au(HS^-)_2 \rightarrow$$

titanomagnetite ankerite

$$2FeS_2 + TiO_2 + Ca^{2+} + Mg^{2+} + 2CO_2 + 2H_2O + 2Au$$

pyrite rutile gold

It can be concluded from the above discussion that the relationship of the Stog'er Tight gabbro to gold mineralization is two-fold. First, the presence of a lenticular, rigid body of coarse-grained gabbro within a sequence of fine-grained, ductile volcanic/pyroclastic rocks favoured the differential development of discrete zones of shear deformation in the gabbro. The higher permeability of the strained gabbro along these shear zones focused the infiltration of hydrothermal fluids that were responsible for wallrock alteration and gold mineralization. Secondly, the chemical reaction between the hydrothermal fluid

containing gold bisulphide complexes, and the Fe-Ti oxide phases from the gabbro, induced the oxidation of the fluid and resulted in the coprecipitation of pyrite and gold in the strongly altered wallrock. The Stog'er Tight gabbro, therefore, acted not only as a mechanically suitable medium for fluid infiltration, but also as an equally important chemical sink for the gold dissolved in the mineralizing fluid.

9.3.3 Comparison of Alteration to Archean Deposits

Mechanical and chemical controls of host rock on gold mineralization, similar to those in the Stog'er Tight prospect, occur in a number of typical Archean mesothermal gold deposits, especially those hosted by gabbroic rocks. Dubé *et al.* (1987) described the alteration patterns and chemical processes associated with gold mineralization in the Chibougamau area, northeastern Abitibi Subprovince (Superior Province of Canada). In this area, gold mineralization is hosted by shear zones within differentiated, tholeiitic gabbro sills (Bourbeau sill) which have intruded the volcaniclastic and pyroclastic rocks of the Blondeau Formation. Magmatic differentiation has generated a variety of petrologic facies in the Bourbeau gabbro, ranging from pyroxenite-peridotite at the base, to soda granophyre at the top. They are all characterized by greenschist-facies metamorphic assemblages, primary igneous textures and the presence of titanomagnetite that is variably altered to leucoxene. The shear zones feature strong hydrothermal alteration that is characterized by the presence of carbonate, sericite, chlorite, fuchsite and pyrite. Dubé *et al.* (1987)

divided the alteration assemblages into four distinct facies, including the regional greenschist (A1), chlorite-calcite-magnetite (A2), ankerite-sericite-chlorite (A3), ankerite-fuchsite-chlorite (A4), and the ankerite-sericite-pyrite (A5) assemblages. Gold mineralization is associated with the A5 alteration facies. A close spatial relationship between titanomagnetite-leucoxene and pyrite (or secondary magnetite) is also noted. The authors concluded that the progressive hydrothermal alteration and the transition from a chlorite-calcite assemblage to an ankerite-dominated one is related to the CO_2/H_2O ratio in the hydrothermal fluid, such that the initial reduction of the metasomatized rock (*i.e.* oxidation of the fluid) at high CO_2/H_2O ratios (A5 facies, centre of the shear zone) was followed by a decrease in the ratio and the oxidation of the rock (A2 facies, away from the shear centre). According to this model, gold mineralization must have occurred as a result of oxidation of the hydrothermal fluid by the Fe-rich host rock, at high CO_2/H_2O conditions.

The San Antonio gold mine in the Rice Lake-Beresford Lake greenstone belt of the western Uchi Subprovince (Superior Province) was the subject of a detailed alteration study by Ames *et al.* (1991). The main host to gold mineralization in the San Antonio mine is a differentiated tholeiitic (Fe-rich) gabbro sill (San Antonio sill) which consists of a melagabbro base, a locally granophyric leucogabbro top, and gabbroic chilled margins, all characterized by a metamorphic (greenschist) mineral assemblage. The sill has intruded the felsic to intermediate volcaniclastic sequence of the Rice Lake Group (2729 ± 3 Ma). Gold mineralization is associated with quartz-albite-ankerite-pyrite stockwork

and shear veins within the sheared and altered leucogabbro. The hydrothermal alteration of the leucogabbro around the auriferous vein structures is subdivided into three zones (zones 1 to 3). Zone 1 is characterized by the association of calcite, chlorite and quartz, disappearance of actinolite, replacement of epidote by calcite, and an increase in the Fe content of chlorite. Zone 2 reflects an abundance of ankerite and paragonite, the absence of calcite and an increase in the Fe-content of chlorite. Zone 3 (adjacent to veins) is defined by the dominance of muscovite, hydrothermal albite and ankerite. Gold is associated with pyrite within the intensely altered leucogabbro, adjacent to the vein margins, while hydrothermal albite occurs at the interface between the vein and wallrock. Accordingly, Ames *et al.* (1991) suggested that the hydrothermal alteration assemblages were strongly controlled by the Fe-rich composition of the leucogabbro, through fluid-rock interaction. This interaction, which involved CO_2, K, S and Na metasomatism, changed the local chemical composition of the fluid to conditions suitable for gold deposition.

In the Archean Yilgarn block of Western Australia (see Section 9.5.2) and its gold-rich Eastern Goldfields province, the giant Kalgoorlie gold deposit (Phillips, 1986) is mainly hosted by a differentiated, tholeiitic, mafic sill (Golden Mile Dolerite) that is over 400 m thick and has a greenschist-facies metamorphic assemblage in the Golden Mile area. The Golden Mile Dolerite varies from a near-ultramafic basal portion to a granophyre of intermediate composition. Phillips (1986) subdivided the Golden Mile Dolerite into four general mappable units, based on an earlier, ten-fold subdivision of the sill,

south of Kalgoorlie. Gold mineralization (and hydrothermal alteration) is localized along a number of ductile shear zones within the dolerite sill. Three large-scale alteration zones are mapped within the Golden Mile Dolerite, mainly based on the mineralogy of the Fe-bearing phases (actinolite, chlorite, Fe-carbonate and pyrite). The gold lodes occur in the pyrite zone. It is indicated that shear zones and lithological variations within the dolerite influence the distribution of alteration zones, such that there is a strong correlation between the carbonate (including siderite and ankerite) alteration, and granophyre and plagioclase phyric parts of the Golden Mile Dolerite. Other portions of the sill are dominated by chlorite alteration. The pyrite zone is best developed within the ductile shear zones and becomes subordinate to carbonate alteration, within 5 m (or less) of the shear zone centre. Coarse pyrite grains locally replace skeletal ilmenite (leucoxene) grains. Overall, it is concluded that the alteration sequence of actinolite to chlorite, then to carbonate and finally, to pyrite represents a progressively more intense alteration, that involves addition of S, K, and Au, approaching the ductile shear zones. The great size of the Kalgoorlie deposit is attributed to the large volume of advected fluids, the chemically favourable nature of the host rocks, and the intense development of ductile shear zones in the area (Phillips, 1986).

A comparison between the Archean greenstone gold deposits discussed above and the Paleozoic Stog'er Tight prospect reveals numerous similarities. All of these gabbro-hosted gold deposits reflect a strong host rock control on the alteration zonation and gold mineralization. Although magmatic

differentiation in the Stog'er Tight gabbro is only weakly developed compared to that in the large, differentiated sills, there appears to be a notable lithologic correlation between the Stog'er Tight gabbro and the gold-bearing units of the Bourbeau sill (ferrogabbro and ferrodiorite facies), the San Antonio sill (leucogabbro) and the Golden Mile Dolerite (granophyre and plagioclase phyric). All these units are characterized by a high Fe content (especially as titanomagnetite) and appear to be the locus of snear deformation, pyrite alteration and gold concentration.

Besides the prominent lithologic similarities, the gabbro-hosted mesothermal gold deposits share many characteristics in terms of alteration zonation, as well. Figure 9-1 summarizes the alteration zonation features of the Archean gabbro-hosted gold deposits, and compares them to that of the Stog'er Tight prospect. It shows that there is a good correlation between Zone I and Zone II of the Stog'er Tight alteration sequence, and equivalent alteration facies in the other gabbro-hosted gold deposits. Zone III of the Stog'er Tight deposit, however, is distinct from other mineralization zones in terms of the modal abundance of hydrothermal albite ($\sim$80%). This zone is comparable to the metasomatic albite selvages that occur at the vein-wallrock interface in the San Antonio mine, though the intensity of albitization is significantly higher at Stog'er Tight. Consequently, Zone III of the Stog'er Tight alteration sequence may represent an increase in the activity of Na^+/K^+ in the system and also a decline in the CO_2/H_2O ratio of the hydrothermal fluid, during the red albite-pyrite replacement of the host rock and the deposition of gold.

The mineralogy of the Zone IV alteration assemblage (chlorite-magnetite-calcite) of the Stog'er Tight sequence seems to resemble that of the A2 facies in the Chibougamau deposit. However, the geometry of the alteration sequence, the paragenetic relationships and the microstructural fabrics (Chapter 7) clearly indicate that this alteration type was retrograde in nature and occurred late in the alteration history of the Stog'er Tight deposit. Zone IV, therefore, appears to be unique to the Stog'er Tight deposit, as it does not have any equivalent in the above mentioned deposits (the equivalent of A2 facies is Zone I). The retrograde characteristics of this alteration zone, therefore, reflect a change in fluid composition (and/or temperature) subsequent to the peak-alteration and gold mineralization.

Overall, the chemical control (in addition to mechanical control) of the host rock on gold mineralization in the gabbro-hosted mesothermal gold deposits appears to be a characteristic feature which is manifested by 1) their comparable alteration zonation due to progressive CO_2, S and K (± Na) metasomatism, 2) the association of mineralization with the Fe-rich lithologic units, 3) the progressive variations in mineralogic siting of Fe in the form of actinolite-chlorite-carbonate-pyrite transitions and, 4) the common occurrence of gold in the strongly altered wallrock, as opposed to the veins. These suggest that very similar hydrothermal processes have been responsible for host rock alteration and gold mineralization in the gabbro-hosted mesothermal deposits of different scales and ages.

9.4 TIMING OF GOLD MINERALIZATION

The absolute age of gold mineralization in the Stog'er Tight deposit is determined by U-Pb dating of hydrothermal zircon from the alteration zone of the deposit (Chapter 8). In general, the occurrence of zircon in geologic settings that are not directly related to magmatic crystallization, is uncommon. Rubin *et al.* (1988) described hydrothermal zircons associated with peraluminous F- and REE-rich rhyolites at Sierra Blanka Peaks, Texas. Metamorphic zircon overgrowths in a fluorite-bearing, granitic gneiss are reported by Wayne *et al.* (1992) from the Hope Valley Shear Zone, southeastern Massachusetts. The opaque brown colour, rounded grain-shapes and irregular, porous-appearing surface textures of these zircon overgrowths are especially comparable to those of the Stog'er Tight hydrothermal zircon. However, the fluid characteristics of most mesothermal precious metal deposits (*e.g.* low salinity and low ambient temperatures), would seem not to favour the mobility of Zr required for zircon dissolution and precipitation.

Claoue-Long *et al.* (1990) reported zircons from the mineralized veins and altered wallrock selvages of the Archean mesothermal gold deposits at Val d'Or, southern Abitibi Subprovince. They claimed that these zircons were in paragenetic association with other vein minerals such as tourmaline, and therefore were of hydrothermal origin. Claoue-Long *et al.* (1990) also suggested that the measured U-Pb (ion probe) ages of these "hydrothermal" zircons reflected the timing of the gold mineralization event at Val d'Or. However the accuracy of data acquisition and age calculation procedures involved in that

study, as well as the proposed hydrothermal origin for the analyzed zircons, have been the subject of great controversy (Corfu & Davis, 1991). In particular, the morphological features of the majority of the analyzed zircons (*e.g.* optical clarity, multifaceted shape) are identical to those of magmatic varieties in the host Bourlamaque batholith, suggesting the incorporation of wallrock zircon into the veins. Only the optically turbid (U-rich), metamict material which locally overgrows the clear zircon prisms of that study meet the criteria for secondary (hydrothermal) zircon. Unfortunately, the latter variety was not dated or yielded very discordant data.

The measured Silurian age of mineralization (420 ±5 Ma), based on the hydrothermal zircon data, is consistent with the epigenetic nature of the Stog'er Tight deposit and implies that mineralization post-dated intrusion of the host gabbro, by about 63 Ma. It has been suggested (Section 9.2) that the hydrothermal alteration and the associated shear deformation (D_I) in the Stog'er Tight area were conceivably coeval with an important phase of regional tectonism (D_M deformation) in the area. The available geochronologic data (see Chapters 2 and 8) demonstrates that the Early Silurian was also concomitant with a major episode of magmatism and metamorphism on the Baie Verte Peninsula. Establishing a feasible genetic model for the deposition of gold in the Stog'er Tight prospect, requires an understanding of the timing of gold mineralization with respect to these local and regional geologic events.

The radiometric ages of all the granitoid intrusive and felsic volcanic rocks of the Baie Verte Peninsula (Chapter 8), measured to date, lie within a

narrow age range, from Early to mid-Silurian (440 to 424 Ma). The closest of these intrusions geographically to the Stog'er Tight area is the Burlington Granodiorite which underlies a large area to the east of the Baie Verte Line. The Burlington Granodiorite intrudes both the Pacquet Harbour Group and the Betts Cove Complex (Hibbard, 1983). It is terminated by the Baie Verte Line and the Scrape Thrust at its northernmost exposure, about 3.5 km southwest of the Stog'er Tight area (Fig.3-1), suggesting that emplacement of the granodiorite was prior to the overthrusting of the Point Rousse Complex along the Scrape Thrust (D_M deformation). About 6 km to the south of this contact, a sample of the granodiorite gave a U-Pb zircon age of 432 $\pm$2 Ma (Dunning & Cawood, unpublished data). This indicates that gold mineralization post-dated the crystallization age of the Burlington Granodiorite, by ~12 Ma.

Large-scale, regional metamorphism on the Baie Verte Peninsula is mostly confined to the west of the Baie Verte Line, though a block of polydeformed and metamorphosed rocks is also situated at the northeastern part of the peninsula (Western and Eastern Orthotectonic Blocks, Hibbard, 1983). Metamorphism in these areas ranges from upper greenschist to lower amphibolite facies. It is suggested that metamorphism resulted from relaxation of a thermal anomaly following initial burial of the continental margin by overriding thrust sheets (Jamieson and Vernon, 1987). In contrast, the metamorphic features of rock units in the area around the Stog'er Tight prospect (Point Rousse Complex) are consistent with those of sub-seafloor metamorphism, and there is no evidence for post-emplacement regional

metamorphism in this area (see Chapter 5).

Despite the complex, polyphase tectonic history of the regionally metamorphosed rocks of the western Baie Verte Peninsula (*i.e.* Fleur de Lys terrane), the age of metamorphism is by and large constrained by the textural relationships and $^{40}Ar/^{39}Ar$ dating of the metamorphic minerals (see Chapter 2). However, the best age estimate for the peak of regional metamorphism is obtained by U-Pb dating of monazites from the migmatitic rocks of the Fleur de Lys Supergroup (427 $\pm$ 2 Ma, Dunning & Cawood, unpublished data). This age indicates that the peak of metamorphism in the overridden continental margin rocks was reached almost coeval with the major episode of Early Silurian magmatism, and between 40 to 60 Ma after the Ordovician collisional event (obduction of the ocean crust). Gold mineralization in the Stog'er Tight deposit, therefore, appears to be syn- to late-metamorphic (and magmatic), with respect to the Early Silurian Orogenic event in the Baie Verte Peninsula.

9.5 ARCHEAN ANALOGUES

The Stog'er Tight gold deposit shares many characteristics with some of the typical Archean lode gold deposits, in terms of structure, host rock control and wallrock alteration (Section 9.3), as well as the relative timing of gold mineralization. The following provides examples from some of the best-studied Archean mesothermal gold deposits in two major metallogenic provinces of the world, the Superior Province of Canadian shield and the Yilgarn Block of

southwestern Australia.

9.5.1 Superior Province of Canada

The Superior Province (Fig.9-2), one of the world's largest Archean cratons, is part of Laurentia or the Precambrian core of the North American plate. It is subdivided into subprovinces of high-grade gneiss, metasedimentary, greenstone-granite and plutonic types, which are interpreted as major tectonic components evolved and assembled during Archean polyphase orogenic events. Subprovince boundaries are complex zones of facies, metamorphic and structural transition, which are in many places marked by major faults with lengthy histories including late strike-slip movements. Abundant lode gold deposits are mainly related to these major fault systems and are confined to zones of late brittle-ductile deformation and rock alteration within greenstone-granite subprovinces (Card *et al.*, 1989).

In the southern Superior Province, the Abitibi Subprovince (Fig.9-2) is one of world's largest gold-producing greenstone belts. Extensive geochronologic studies on major lithologic units, as well as $^{40}Ar/^{39}Ar$ and U-Pb dating of hydrothermal minerals associated with gold, has implied that gold mineralization in the southern parts of the Superior Province consistently post-dated greenstone-belt magmatism and metamorphism. In the gold-rich area of the southern Abitibi Subprovince, U-Pb zircon data show that the major phase of greenstone volcanism ended at ~2700 Ma and was followed by deformation and intrusion of late plutons. Magmatic activity ended by ~2670 Ma (Corfu *et*

al.,1989). At the Camflo mine in the Malartic-Val d'Or gold camp (Jemielita *et al.*,1990 and references therein), a U-Pb zircon and titanite age of 2680 ±4 Ma is measured for a porphyritic quartz syenite that hosts the gold mineralization. The Pb-isotopic compositions of all of the concordant fractions of hydrothermal titanite and rutile, together with that of the vein scheelite, are collinear on a $^{207}Pb/^{204}Pb$ versus $^{206}Pb/^{204}Pb$ plot and give an isochron age of 2625 ±7 Ma. This is interpreted as the age of hydrothermal alteration associated with gold mineralization in the Camflo mine. The authors concluded that the alteration at Camflo significantly post-dated all Archean magmatism and metamorphism known in the Abitibi Subprovince. They suggested that fluids derived from devolatilization of the lower crust (*e.g.* Kapuskasing high-grade metamorphic rocks) may have been involved in the late hydrothermal activity and gold mineralization in the area.

In a similar study on the Sigma gold mine in the Val d'Or area, Wong *et al.*(1991) reported U-Pb zircon and rutile ages that constrain the timing of magmatism, metamorphism, deformation and mineralization in the mine area. The Colombiere rhyolite, part of the Val d'Or Formation (Malartic Group), represents the oldest rock unit in the vicinity of the Sigma Mine and is dated as 2705 ±1 Ma (zircon age). A U-Pb zircon age of 2700 ±1 Ma is given for the Bourlamaque batholith, the largest intrusive unit in the area which is also host to several gold deposits. Constraints on the age of hydrothermal alteration (and gold mineralization) have been made based on U-Pb ages of hydrothermal rutile (2599 ±9 Ma) from the vicinity of the gold-bearing quartz veins (Wong *et*

al.,1991). All reported ages are comparable to those obtained from rutile and titanite in the nearby Camflo Mine (Jemielita *et al.*,1990) and indicate that gold mineralization in the Sigma Mine post-dates the greenstone-belt magmatism and metamorphism by about 80 Ma.

To the west of the Abitibi Subprovince, the Late Archean Hemlo-Heron Bay greenstone belt was the subject of a detailed geochronologic study by Corfu and Muir (1989a,b) to elucidate the igneous evolution of the greenstone belt, as well as to resolve the timing of metamorphism, alteration and Au-Mo mineralization in the Hemlo deposit. The measured U-Pb titanite ages from the Hemlo area range from ~2678 to 2676 Ma and demonstrate a crude correlation of decreasing age with proximity to the ore deposit. These ages record the timing of the highest grade of metamorphism in Hemlo and also correlate with the age of the Gowan Lake Pluton (2678 ±2 Ma), the marginal phase of a large gneissic granitoid terrane, to the north of the Hemlo-Heron Bay greenstone belt. A distinctly younger group of titanite (2672-2670 Ma) occurring in the Hemlo ore zone, record lower-grade metamorphic processes which appear not to have affected the rocks outside the deposit. The ages of the most concordant rutile fractions along with that of a monazite fraction (2645 ±4 Ma) record a distinctly late episode of crystallization due to low-grade hydrothermal activity, which was independent from the ~2670 Ma titanite forming/resetting event.

The measured U-Pb ages of the metamorphic/hydrothermal phases, together with the paragenetic association of gold with low-temperature minerals

in the Hemlo deposit, suggest that the mineralization is linked to either the 2670 Ma phase of metamorphism or perhaps, to younger hydrothermal processes that formed rutile and monazite. The results indicate that the zone hosting the Hemlo Au-Mo deposit marks a complex Late Archean history of magmatism, metamorphism, deformation and prolonged hydrothermal activity, as an integral part of the overall process of crustal evolution and stabilization.

Although the precise geochronologic data from the southern Abitibi Subprovince rule out high-level magmatism and metamorphism as a source for gold mineralization, in the Hemlo Au-Mo deposit at least the early phase of gold mineralization was coeval with low-grade metamorphism. In the northwestern Superior Province, the contemporaneity of gold with regional magmatism and metamorphism is even more evident. Davis and Smith (1991) presented U-Pb geochronologic data from the northwestern Lake of Woods region, Wabigoon Subprovince (western Superior Province, Fig.9-2), documenting the temporal and tectonic relationships between late Archean greenstone accretion, pre- to post-tectonic magmatism, metamorphism and gold mineralization. The 2711-2708 Ma time period is characterized by late-tectonic plutonic activity in the western Wabigoon Subprovince as well as in the northerly Winnipeg River Subprovince. At the Duport Mine the timing of gold mineralization is bracketed between 2716 ±2 Ma, the age of a quartz-porphyry dike truncated by the gold lode, and 2709 ±2 Ma, the age of a dioritic dyke cutting the lode gold. Here, hydrothermal activity associated with mineralization overprints the amphibolite-facies contact metamorphic aureole of the Snowshoe Bay batholith.

Davis and Smith (1991) concluded that there is a close spatial and temporal relationship between gold mineralization and the associated D2 deformation, late felsic-intermediate plutons and the regional metamorphism, in the western Wabigoon Subprovince. They suggested that the tectonic juxtaposition of the Wabigoon and Winnipeg River Subprovinces by overthrusting, the age of which is constrained by a mylonitic granodiorite intrusion along their contact (2709 +4/-3, Corfu 1988), resulted in crustal thickening and a thermal anomaly which promoted metamorphism and partial melting within the overridden terrain (and in the lower crust). These accretionary tectonic processes were probably responsible for the generation of gold-bearing fluids and their mobilization along shear zones, which were active during collision. This interpretation is compatible with models involving magmatic derivation of hydrothermal fluids and/or metamorphic dewatering of the greenstone belt.

To the north of the Wabigoon Subprovince (northern Superior Province), the Red Lake greenstone belt of the Uchi Subprovince (Fig.9-2) is the locus of several gold mines and occurrences (*e.g.* Campbell and A.W. White Mines). Constraints on the timing of magmatism, deformation and gold mineralization in the Red Lake area were placed by the geochronologic studies of Corfu & Wallace (1986) and Corfu & Andrews (1986, 1987), using U-Pb ages of zircon, baddeleyite, titanite, rutile and monazite. All the major gold deposits in this area are spatially related to the hydrothermally altered rocks within both amphibolite- and greenschist-facies contact aureoles of surrounding batholiths. The

compilation of the U-Pb ages indicates that plutonism, deformation and metamorphism in the Red Lake belt were active over a period of ~30 Ma, between the end of greenstone volcanism at ~2730 Ma and the relatively abrupt termination of magmatism at ~2700 Ma. The U-Pb ages and the crosscutting relationships of the late-kinematic dikes constrain the timing of deformation, metamorphism, alteration and gold mineralization to the period between 2720 and 2700 Ma, that apparently post-dates volcanism and is coeval with much of the felsic plutonism in the area.

A comparison between the major gold producing greenstone belts of the Superior Province discussed above, indicates that despite their similar tectonic elements and comparable stratigraphic relationships, the spatial and temporal relationships between greenstone magmatism, metamorphism, regional deformation and gold mineralization in the southern Superior Province (*e.g.* Abitibi Subprovince) is distinct from that in the western and northern parts of the Province (*e.g.* western Wabigoon and Uchi Subprovinces). The major points of contrast between these subprovinces are; 1) the ages of volcanic, plutonic, metamorphic and mineralization events in the southern greenstone belts (Abitibi and Hemlo-Heron Bay) are significantly younger than those of the analogous events in the northern belts (Lake of Woods and Red Lake), 2) the exposed lithologic units in the northern belts record prolonged and polyphase magmatic, metamorphic and deformational episodes which are not detected in the Abitibi greenstone belt, 3) unlike the Abitibi belt that is characterized by a regional

greenschist facies metamorphism, the metamorphism in the Hemlo-Heron Bay, western Wabigoon and Red Lake belts ranges from amphibolite facies to greenschist facies, with the amphibolite-facies metamorphism apparently developed at the contact aureoles of large, late-tectonic intrusions, and 4) gold mineralization and the associated hydrothermal activity in the Abitibi belt post-date the regional magmatism and metamorphism by about 60 to 80 Ma, whereas in the northern greenstone belts these appear to have been contemporaneous with late episodes of plutonic and metamorphic activity; the timing of gold mineralization in the Hemlo deposit lie between these two end-member situations (syn- to post-metamorphic).

The diachronous nature of tectonic events (#1 above) in the southern and northern greenstone belts of the Superior Province can be explained by the progressive, southward growth of the Archean craton by successive, northward accretion of the greenstone belts (*e.g.* Corfu, 1988). Therefore the southern greenstone belts, such as the Abitibi belt, record later stages of greenstone formation and accretion. The dissimilarities in geologic record (#2 above), metamorphic grade (#3 above), and timing of gold mineralization (#4 above), however, are not readily explained by the successive accretion model. It is likely that the northern subprovinces of the Superior Province represent lower structural levels of the Archean crust, which are exposed as a result of a prolonged history of erosion (and/or uplift) in the older parts of the craton. This is particularly consistent with the higher metamorphic grades and the prominent diversity of lithologic units in the western Wabigoon and Uchi Subprovinces. If

this model is true, the syntectonic intrusive bodies which were responsible for high-grade metamorphism synchronous with gold mineralization, and also the post-kinematic, mafic to felsic dikes that crosscut the gold-bearing shear zones, might all be absent from the upper crustal levels represented by the Abitibi Subprovince.

9.5.2 Yilgarn Block of Western Australia

The Archean Yilgarn block of the Western Australian Shield (Fig.9-3) is a major gold-metallogenic province which broadly consists of high-grade gneiss terranes (Western Gneiss terrain) and granitoid-greenstone belts. Gold occurs primarily in the granitoid-greenstone terranes, with the highest abundance in the Norseman-Wiluna belt (*e.g.* Groves *et al.*, 1989). The greatest number of large gold deposits and the only giant gold deposit of Western Australia (Golden Mile, Kalgoorlie) are located in this belt.

Most large gold deposits of the Yilgarn block occur adjacent to the major lineaments of the block, which are manifested by dominantly strike-slip shear zones, and usually separate zones of contrasting stratigraphy and structural style, between or within greenstone belts (Vearncombe *et al.*, 1989). Mafic, Fe-rich rocks such as dolerites and basalts that are metamorphosed to greenschist to lower amphibolite facies, comprise the main host lithology of many of the gold deposits in the Norseman-Wiluna belt (*e.g.* Golden Mile deposit and Victory Mine). However, some large deposits, particularly in the Southern Cross (*e.g.* Copperhead) and Murchison (*e.g.* Big Bell) provinces, occur in amphibolite facies

domains (Groves *et al.*,1989). A number of small gold deposits (*e.g.* Griffin's Find) also occur in the granulite facies rocks of the Western Gneiss terrane and Southern Cross province (Barnicoat *et al.*, 1991).

Radiometric ages (*e.g.* Campbell & Hill, 1988; Hill & Compston, 1986; Claoue-Long *et al.*,1988) suggest that the onset of external plutonism in the Kalgoorlie-Norseman area coincides with the felsic volcanism in the greenstone belts, and both were followed by late-stage granitoid intrusions that cut the greenstone sequences. Gold mineralization occurred, apparently, late in the tectonic evolution of the Yilgarn Block, as the mineralization event has affected both 2.95- and 2.7-Ga greenstone belts. Furthermore, the mineralized structures tend to cut most of the granitoids and porphyries that intruded late in the greenstone belt evolution. Nevertheless, the precise timing of gold mineralization in the Yilgarn block is not well-constrained, as there are limited published radiometric ages that can positively bracket the mineralization event.

The Menzies-Kambalda area in the southcentral part of the Norseman-Wiluna belt (comprising also the Kalgoorlie area) includes a variety of gold deposits hosted by rocks which range in metamorphic grades from greenschist- (*e.g.* Golden Mile) to upper amphibolite (*e.g.* Twin Hills) facies. The largest gold deposit of the Norseman-Wiluna belt is Golden Mile which is hosted by a differentiated tholeiitic sill (Golden Mile Dolerite, Phillips, 1986). In a study of the different alteration styles associated with gold deposits of this area, Witt (1991) indicated that there are systematic paragenetic relationships between gold-related alteration and metamorphic grade. Gold mineralization in the

Menzies-Kambalda area occurs in structures generated during D_3 (regional shear) and D_4 (splay faulting) deformation episodes. High-grade metamorphism also occurs as thermal aureoles around syn-D_3 granites. It is suggested that, on a regional scale, the alteration assemblages and their zonation with respect to mineralized structures are not only controlled by the host rock lithology, but also by the grade of metamorphism. This is best demonstrated by the thermodynamically calculated phase equilibria between metamorphic and alteration assemblages (Fig.9-4). Figure 9-4 suggests that alteration zoning reflects an increase in X_{CO_2} and K towards the mineralization centres (Witt, 1991), whereas different alteration-metamorphic sets manifest variations in temperature, from <360 to 600°C. K-metasomatism is represented by muscovite, biotite, and microcline in domains of progressively higher metamorphic grade. Field and textural characteristics of the altered rocks also indicate that the crystallization of alteration assemblages, which occurred in thermal aureoles of syn-metamorphic plutons, was contemporaneous with shear deformation in the host structures. Accordingly, Witt (1991) concluded that the mineralizing event in the Menzies-Kambalda area was related to a greenstone-belt-scale hydrothermal system centred on cooling plutons, and the peak metamorphic conditions were attained later in the high-grade thermal aureoles than in lower-grade domains.

The increasing recognition of lode gold deposits in high-grade metamorphic terranes of the Yilgarn Block has revealed a continuum of mineralization types from greenschist- to granulite-facies metamorphic settings.

Barnicoat *et al.* (1991) presented data from the Fraser's mine wherein the amphibolite-facies ultramafic rocks and basic amphibolites are cut by gold-bearing shear zones that are characterized by biotite-rich alteration. Shear-hosted veins are bordered by alteration rims of diopside and calcic amphibole farther out, passing into biotite-dominated alteration of the whole shear zone. Gold occurs in both sulphides and silicates, and correlates with the abundance of diopside. Mineral assemblages in both host rocks and alteration zones suggest temperatures of 500-550°C and pressures of 3-5 kbar. The Griffin's Find deposit occurs in a sequence of metabasites and garnet-bearing metasedimentary rocks, within a granulite-facies, granitoid-gneiss terrane. Thermobarometry of garnet-bearing assemblages indicate metamorphic conditions of 700-750°C and 6 ±1 kbar, whereas garnet-clinopyroxene thermometry of the alteration gives a temperature of 740°C, that is indistinguishable from the peak metamorphic temperature. Here, the mineralized, quartz-clinopyroxene veins are adjacent to a quartz-clinopyroxene-grossular alteration.

The highly altered rocks of both the Fraser's mine and Griffin's Find are characterized by simple (mono- or bimineralic) assemblages, which imply that alteration was fluid-dominated rather than rock-buffered. Also, petrologic and textural evidence at both deposits are indicative of alteration and gold mineralization being syn-tectonic and syn-metamorphic. The age of metamorphism at the Griffin's Find was determined from a Pb-Pb mineral isochron for the weakly mineralized, footwall granulite. Metasedimentary

granulites next to the ore zone overlap this isochron, and together, they define an age of 2635.6 ±3.2 Ma for the peak metamorphism/alteration event (Barnicoat *et al.*, 1991). This age is indistinguishable from the U-Pb zircon ages of 2652 ±24 Ma for a porphyritic granitoid ~4 km south of the mine, and 2634 ±47 Ma for a calc-silicate gneiss adjacent to the mine.

In summary, recent studies on a number of typical Archean mesothermal gold deposits in the Superior Province of Canada and in the Yilgarn block of Western Australia have indicated that gold mineralization occurs in a variety of geologic environments corresponding to different crustal depths. In the greenschist-facies settings, there is a close temporal relationship between plutonism, deformation and the peak regional metamorphism, though gold mineralization is apparently younger than any of the geologic events recognized at the present erosional levels. In the high-grade (amphibolite- and granulite-facies) settings, in contrast, gold appears to be coeval with at least some episodes of plutonism, metamorphism and regional deformation. Any genetic model for mesothermal gold mineralization must therefore incorporate these contrasting timing features of the Archean lode gold deposits.

9.6 GENETIC MODEL FOR GOLD MINERALIZATION

Despite the many similarities between mesothermal gold deposits of all ages (*e.g.* structural setting, geochemistry, etc.) the origin of these important economic resources is one of the most controversial problems in gold

metallogeny. The distribution of mesothermal Au-Ag deposits in time, their spatial association with a variety of lithological types, and the functional relationships of mineralization to deformation, magmatism and metamorphism have been the subjects of substantial debate. These have given rise to a multiplicity of genetic models for these deposits (see Chapter 1). Herein, two of the most recently emphasized genetic models, the magmatic and the metamorphic model, that are also consistent with the geologic setting of the Stog'er Tight deposit, are briefly reviewed. Reviews by Kerrich (1989a,c, 1990) can be referred to for discussions and references on different genetic models.

The felsic magmatic model for the mesothermal gold deposits involves an orthomagmatic link between mineralizing fluids and some granitoid intrusions. The major lines of evidence in support of this model are the local spatial association, and possible geochemical relation, of mineralization with some syn- to late-kinematic intrusions (*e.g.* quartz-feldspar-porphyry intrusions in southern Abitibi belt, Cedar Lake Pluton at Hemlo), the contemporaneity between mineralization and magmatism at lower crustal levels (*e.g.* Tonalitic plutons in Kapuskasing Structural Zone), and the carbon isotopic compositions of some mesothermal Au-Ag systems (*e.g.* $\delta^{13}C_{carbonate}$ = ~-3.0 in Hollinger-McIntyre deposit). The orthomagmatic model, however, appears to be in conflict with the observed LILE (K, Rb and Ba) covariation trends, and the variably more radiogenic Sr and Pb initial isotopic ratios of the mesothermal gold deposits (compared to the mantle-like Pb and Sr isotopic compositions of the Archean tonalite-trondhjemite-granodiorites). Moreover, the $\delta^{13}C$ values of -5.0

±2‰ are considered to be difficult to interpret, as they fall within the ranges of magmatic, metamorphic and sedimentary rocks; $\delta^{13}C$ of -3.0‰ is therefore not uniquely diagnostic of a magmatic reservoir.

The structurally focused discharge of metamorphic fluids during subcretion of hydrated oceanic crust (and sediments) within accretionary tectonic settings has been proposed as a model for mesothermal Au-Ag mineralization. This model involves the release of structural water and volatiles (CO_2) from a hydrated rock of mafic composition, at the greenschist-amphibolite transition at 400-500°C. The generated metamorphic fluids are channelled along the terrane boundary structures at deep levels and are focussed into second or higher order splays at mid-crustal levels, where pressure-induced CO_2 unmixing and/or wallrock reactions promote Au and sulphide precipitation (Kerrich & Feng, 1992). This model explains the provinciality of O, Sr and C-isotopic systems in the mesothermal gold deposits in the context of lateral heterogeneity of crustal source regions. The main objection to this model, however, is the significant time lapse (up to ~80 Ma) between regional metamorphism and mineralization, which is characteristic of the majority of well-known deposits hosted by greenschist facies rocks. Also, the metamorphic dewatering model does not account for some deposits in amphibolite (*e.g.* Red Lake) and granulite (*e.g.* Griffin's Find) facies rocks.

The orthomagmatic and the metamorphic devolatilization models have been widely applied to the genesis of a variety of mesothermal gold deposits, especially those in Archean settings of the southern Abitibi Subprovince of

Canada and the Norseman-Wiluna belt of Australia. Nevertheless, controversy still exists over the applicability of these models to the broad spectrum of Archean to Phanerozoic, shear-hosted, mesothermal Au-Ag deposits. It is notable that the light stable isotopes (O, H, C and S), as the most reliable tracers of crustal fluids, have been generally unable to uniquely constrain the source(s) of hydrothermal fluids involved in mesothermal systems. The $\delta^{13}C$ of alteration assemblages and the $\delta^{18}O$ values of water in many mesothermal deposits, in particular, are consistent with either a magmatic or metamorphic origin and cannot distinguish between them (Kerrich, 1990).

Despite the existing paradox regarding the origin of mineralization in mesothermal Au-Ag deposits, the increasing recognition of more proximal gold deposits in high-grade (amphibolite- and granulite-facies) terranes, in continuum with higher level, greenschist-facies varieties (Section 9.5), has led to important insights as to the genesis of gold mineralization throughout the crust (Barnicoat *et al.*,1991; Witt, 1991). The presence of gold deposits in high-grade domains cogenetic with the greenschist-hosted mineralization rules out high-level sources, such as metamorphic devolatilization at the greenschist-amphibolite transition or magmatic fluids from high-level porphyries, as the origins of mineralizing fluids; a considerably deeper source is required for these fluids. Furthermore, the occurrence of syn-metamorphic, alteration associated with gold mineralization in thermal aureoles of syn-tectonic plutons (*e.g.*Red Lake area), indicate that both magmatic and metamorphic fluids could be involved in mineralization. Overall, it can be concluded that mesothermal gold deposits

represent a continuum of broadly cogenetic mineralization from depths of more than 20 km to less than 5 km. Mineralizing fluids that originated from coeval magmatism and high-grade metamorphism at deep crustal levels are strongly modified by wallrock interaction during their ascent. This also accounts for the provinciality of stable isotope values in the high-level deposits (Barnicoat *et al.*,1992).

The model of cogenetic gold mineralization at all crustal levels seems to be in contradiction with the observation that hydrothermal alteration in deposits hosted by greenschist-facies rocks post-dates the peak-metamorphism by several tens of millions of years. However, it has been suggested that this time delay is consistent with the time needed for a tectonically thickened crust to achieve thermal equilibrium following a collisional orogeny (*e.g.* Hodgson *et al.*,1990). According to this thermal model, the dehydration of the lower part of the crust during the early thermal evolution of the thickened crust results in the generation of tonalitic magmas which rise into the mid-crust. Upward intrusion of partial melts increases the rate of heat loss at surface, while leaves cooler mid-crustal rocks below and slows the rate of thermal equilibrium. Complete thermal equilibrium at depth will therefore be reached several tens of million years later than surface, during which time CO_2-rich hydrothermal fluids migrate upwards along major structural breaks, as the crust column comes into thermal equilibrium. Hodgson *et al.*(1990) suggested that the geological development of the Archean Abitibi belt, based on this model, is similar in many ways to that of the Bridge River area, British Columbia, and the Mother Lode

belt of California, which contain similar gold deposits.

9.7 CONCLUSION: GENETIC MODEL FOR GOLD IN STOG'ER TIGHT DEPOSIT

The epigenetic, shear-hosted, stratabound (gabbro-hosted) gold mineralization in the Stog'er Tight deposit occurs within the greenschist-facies ophiolitic rocks of the Point Rousse Complex, at the northern flexure of the Baie Verte Line on the Baie Verte Peninsula. The hydrothermal alteration associated with gold mineralization is characterized by the progressive chlorite-calcite and ankerite-sericite alteration, the red albite-pyrite replacement, and the late, retrograde chlorite-magnetite alteration of the host gabbro, within the D_I zones of shear deformation. Gold mineralization at the peak of hydrothermal alteration (Zone III) occurred at a late stage of D_E ductile deformation, prior to the D_L brittle-ductile transition.

The hydrothermal alteration in the Stog'er Tight deposit involved progressive CO_2, S and K (and/or Na) metasomatism, as well as significant LILE, REE, HFSE and Th enrichments (Chapter 7). The LILE systematics (K, Rb and Ba covariations) in the Stog'er Tight deposit are largely comparable to those in the other typical mesothermal gold deposits, and are consistent with the metamorphic devolatilization model for gold mineralization (Kerrich, 1989c). The hydrothermally altered rocks, especially those in the alteration zones of mesothermal gold deposits, are commonly characterized by a depletion in trace element contents which is more prominent in the HREE as compared to the

LREE. These trace element depletion trends, however, are in contrast with the observed systematic REE, HFSE and Th enrichments associated with the high-grade alteration in the Stog'er Tight deposit. Although the trace element enrichments in the alteration zone of Stog'er Tight cannot be precisely quantified due to poorly constrained volume effects, they imply that the hydrothermal fluids responsible for host rock alteration and gold mineralization were enriched in those elements. The significantly high REE, HFSE and Th contents of the mineralizing fluids suggest that they were in equilibrium with the enriched continental crustal material, as opposed to the commonly depleted oceanic rocks. Moreover, these elements are typically concentrated in mineral phases (*e.g.* zircon and monazite) which are not susceptible to low and medium grade metamorphism. This strongly implies that the local derivation of the mineralizing fluids from shallow-level, greenschist to amphibolite-facies, ophiolitic (supracrustal) sources is unlikely. Instead, larger-scale, high-grade processes (*e.g.* migmatitization and/or partial melting) at deep crustal levels are likely to have been involved in the generation of fluids. If this is true, and considering the tectonic evolution of the Baie Verte Peninsula which involved collisional orogeny and crustal accretion, the model of deep-seated magmatism and metamorphism in a tectonically thickened crust (see above) for the genesis of mesothermal Au-Ag deposits should apply to gold mineralization in the Stog'er Tight deposit.

The ophiolitic complexes of the eastern Baie Verte Peninsula (*e.g.* Betts Cove and Point Rousse Complexes) and their overlying, thick,

volcanic/volcaniclastic sequences (Snooks Arm Group, Point Rousse volcanic cover) represent supracrustal lithologies analogous to those of the Archean greenstone belts. To the west of the Baie Verte Line, the Fleur de Lys terrane (see Chapter 2) is composed of metaplutonic (and metasedimentary) basement (East Pond Metamorphic Suite), overlying metasedimentary cover (Fleur de Lys Supergroup) and post-tectonic granitoid batholiths (Wild Cove Pond Igneous Suite). The tectonic history of the Fleur de Lys terrane is especially comparable to that of the Archean metaplutonic belts (*e.g.* Winnipeg River, Superior Province; Western Gneiss terrane, Yilgarn block) and/or metasedimentary terranes (*e.g.* Pontiac Subprovince), which occur adjacent to the greenstone belts.

It has been suggested that high-grade metamorphism in the Fleur de Lys terrane resulted from relaxation of a thermal anomaly following the initial burial of the continental margin rocks by underthrusting (Jamieson and Vernon, 1987). The geochronologic data (Section 9.4) have indicated that the peak of metamorphism was reached almost coeval with the regional D_M deformation and the widespread intrusion of granitoid bodies (*e.g.* Wild Cove Pond Igneous Suite and Burlington Granodiorite) into both the Fleur de Lys terrane and the ophiolitic, supracrustal rocks. This sequence of events is especially comparable to that which led to gold mineralization in the northwestern Lake of Woods region (western Wabigoon Subprovince). The latter involved partial melting, metamorphism and deformation, as a result of tectonic juxtaposition of the Wabigoon and Winnipeg River Subprovinces by overthrusting (Davis & Smith,

1991). Overall, there appears to be an interesting match between the Early Silurian Orogeny in the Baie Verte Peninsula, and the ~2710 Ma tectonism in the northwestern Lake of Woods region.

An integration of the U-Pb zircon ages of this study with the available geochronologic data from the Baie Verte Peninsula (Fig.8-7) clearly demonstrates the temporal link of gold mineralization in the Stog'er Tight deposit to the deep crustal magmatism and high-grade metamorphism in the Baie Verte Peninsula. It shows that the mid-Silurian ages of migmatitization and granite emplacement (Wild Cove Pond Igneous Suite) within the basement lithologies of the Fleur de Lys terrane all overlap with the Early Silurian ages of magmatism (*e.g.* Burlington Granodiorite) in the supracrustal Baie Verte Belt. Most importantly, the gold mineralization event in the Stog'er Tight deposit overlaps in age with the basement plutonism and migmatitization, and in part, post-dates the widespread magmatism in the surrounding supracrustal rocks. Overall, these data indicate that deep-seated magmatism and high-grade metamorphism of the tectonically thickened crust, widespread magmatism in the supracrustal rocks, and gold mineralization in the Stog'er Tight deposit, all occurred in a relatively short period of time in the Early to mid-Silurian.

Besides the measured U-Pb age of metamorphism (migmatitization) in the adjacent Fleur de Lys terrane, there is also evidence for an Early Silurian syn-plutonic metamorphism in the eastern part of the Baie Verte Peninsula. The mafic to felsic volcanic and volcaniclastic rocks of the Pacquet Harbour Group are thermally metamorphosed to amphibolite grade peripheral to the Burlington

Granodiorite (Early Silurian), within approximately 1 km from the contact (Hibbard, 1983). This can be regarded as a near-surface indication of larger-scale, high-grade, metamorphic processes induced by voluminous plutons (such as Burlington Granodiorite) at deeper crustal levels. Consequently, it can be inferred that the bulk of magmatic and metamorphic activities on the Baie Verte Peninsula was related to the Early Silurian Orogeny, considering that there are presently no convincing evidence for an Ordovician (Taconian), obduction-related, metamorphism and/or deformation in the area.

Jamieson (1992) provided evidence from the eclogites in the East Pond Metamorphic Suite implying a rapid exhumtion of the Fleur de Lys terrane, subsequent to collisional tectonism and crustal thickening. The well-preserved high-pressure/low-temperature assemblage of these eclogites suggests that the post-tectonic exhumtion must have occurred rapidly, before thermal relaxation effects can completely obliterate the eclogite assemblage. The notion of a rapid relaxation of thermal anomaly in the tectonically thickened crust is especially consistent with the narrow Early Silurian age range of magmatism and metamorphism throughout the Baie Verte Peninsula.

Overall, the mineralogic, geochemical and geochronologic results of this study substantiate that the origin and nature of hydrothermal processes responsible for gold mineralization in the Stog'er Tight deposit are analogous to those in many of the typical Archean (and Phanerozoic) mesothermal gold deposits of accretionary tectonic settings. The recognition of magmatism at deep crustal levels as the main driving engine for the high-grade metamorphism

and generation of hydrothermal fluids, along with the wide distribution of Early Silurian plutons on the Baie Verte Peninsula, logically suggest the involvement of a crustal-scale plumbing system in the alteration/mineralization processes in the area. This can also explain the wide distribution of gold occurrences around the Baie Verte Line and its associated structures (*e.g.* Green Bay Fault) in the western Dunnage Zone. However, none of the occurrences discovered to date are of major economic significance, as compared to the large deposits of the Superior Province (*e.g.* Red Lake) and the Norseman-Wiluna belt (*e.g.* Kalgoorlie) in analcgous geologic settings. The absence of large ore reserves from the Baie Verte Peninsula, despite its proved favourable environment for mesothermal gold mineralization, might be due to short-term and insufficient exploration for epigenetic gold in the area. Alternatively, the relatively short duration of the plumbing system generated by magmatism and metamorphism over a limited period of time (Early Silurian), may explain the weak intensity of mineralization in the gold occurrences of the area. Further geologic research and exploration are undoubtedly required to tackle this problem.

Deposit	Chibougamau	San Antonio	Golden Mile	Stog'er Tight
Host Lithology	Bourbeau sill	San Antonio sill	Golden Mile Dolerite	Stog'er Tight gabbro
Alteration Facies	A2: chlorite-calcite-magnetite	Zone 1: calcite-chlorite-quartz	Chlorite zone	Zone I: chlorite-calcite
	A3: ankerite-sericite-chlorite	Zone 2: ankerite-paragonite-chlorite	Fe-carbonate zone	Zone II: ankerite-sericite (-albite)
	A4: ankerite-fuchsite-chlorite			
	A5: ankerite-sericite-pyrite	Zone 3: muscovite-albite-ankerite-pyrite	Pyrite zone	Zone III: red albite-pyrite (-sericite)
				Zone IV: chlorite-magnetite-calcite

Figure 9-1 Comparison between the alteration zonation of the Archean gabbro-hosted mesothermal gold deposits, and that in the Stog'er Tight deposit.

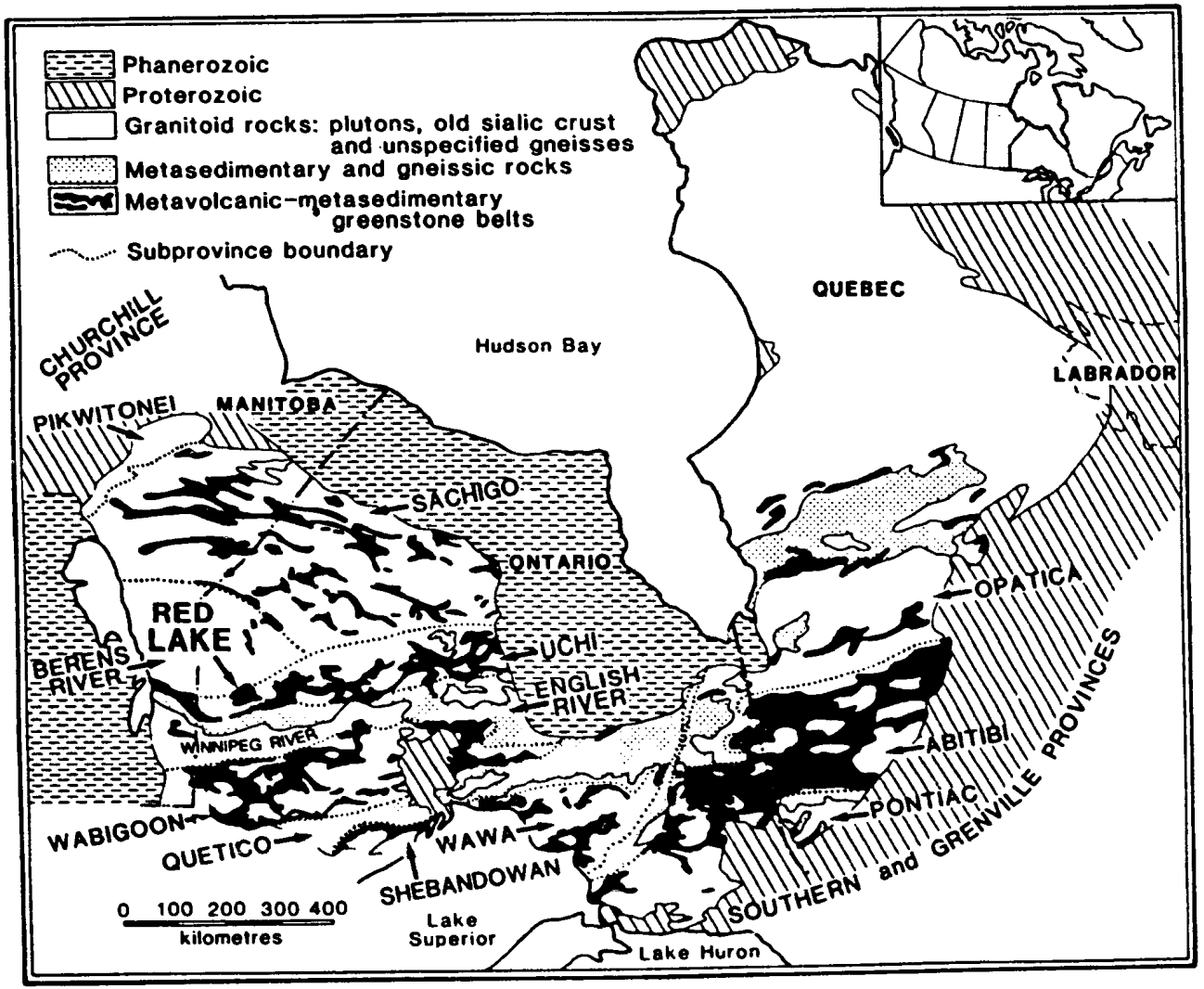

Figure 9-2 Tectonic map of the Superior Province and its subprovinces.

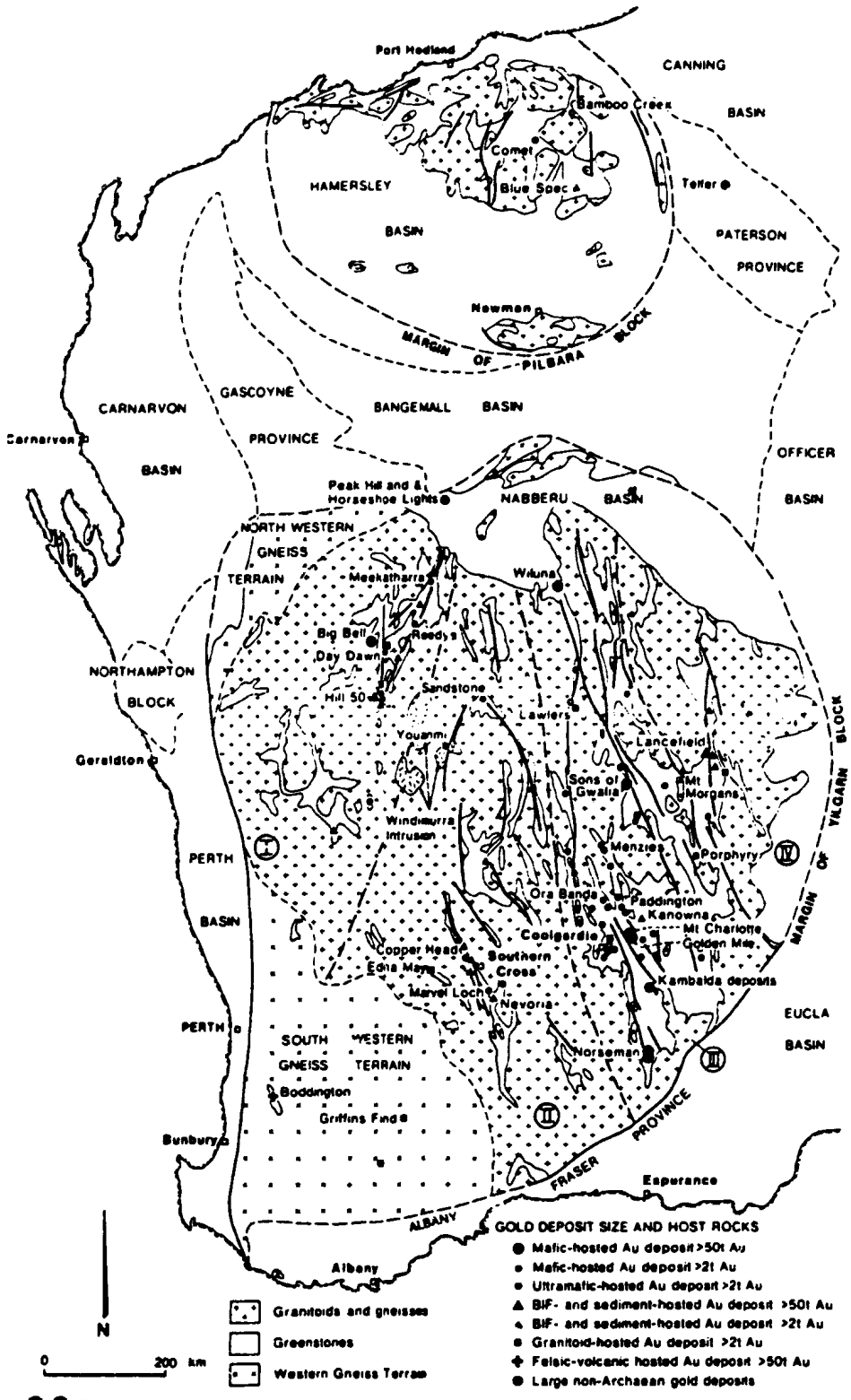

Figure 9-3 Tectonic map of the Archean Yilgarn Block of Australia and its gold deposits.

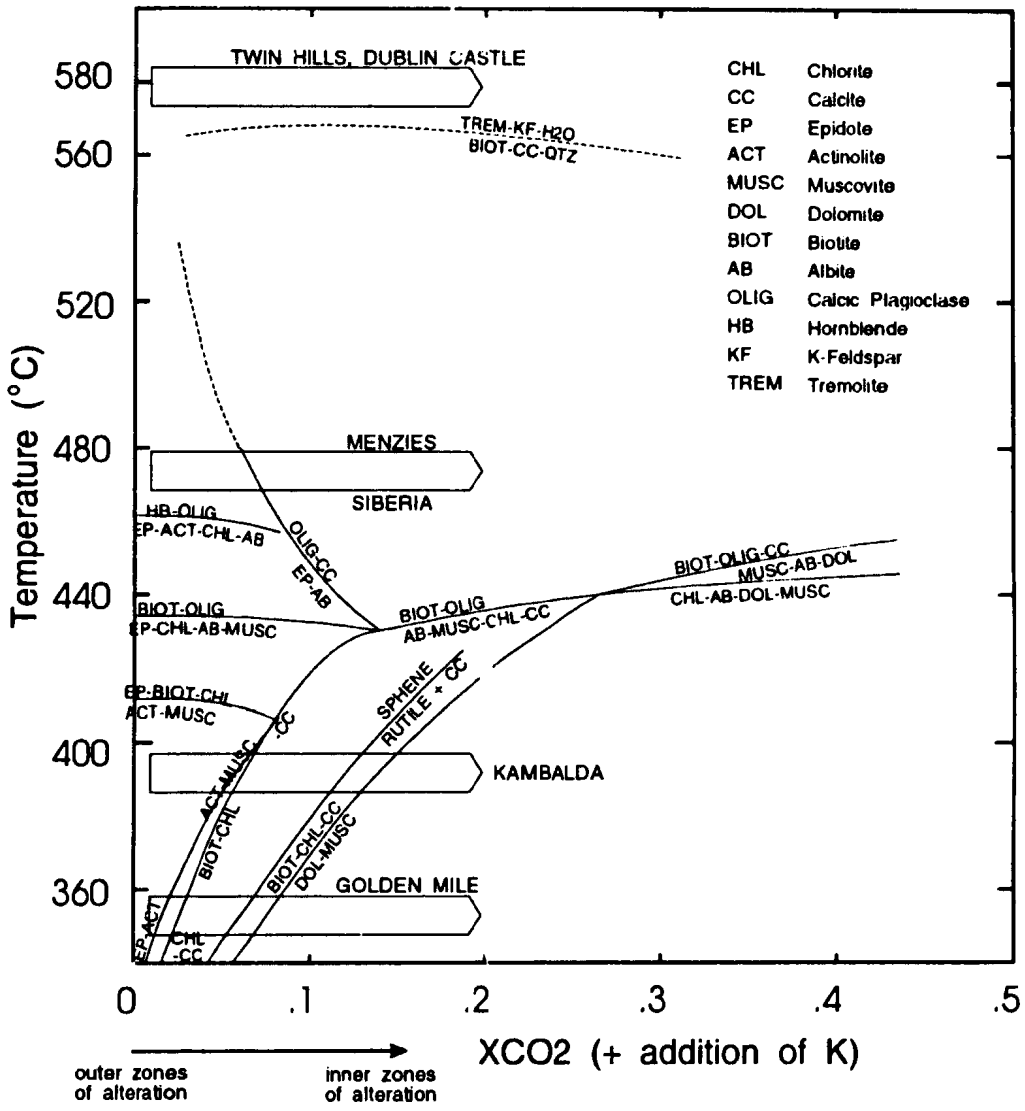

Figure 9-4 T-X_{CO_2} diagram for different mineral assemblages associated with gold deposits, at P_{total} = 3kbar. Arrows indicate the increase in X_{CO_2} and K towards the mineralization zones (after Witt,1991).

REFERENCES

Ames, D. E.; Franklin, J. M.; Froese, E., 1991, Zonation of hydrothermal alteration at the San Antonio Gold Mine, Bisset, Manitoba, Canada: Economic Geology, v.86, p.600-619.

Baird, D. M., 1951, The geology of Burlington Peninsula, Newfoundland: Geological Survey of Canada Paper 51-21, 70 pages.

Barnicoat, A. C.; Fare, R. J.; Groves, D. I.; McNaughton, N. J., 1991, Synmetamorphic lode-gold deposits in high-grade Archean settings: Geology, v.19, p.921-924.

Barovich, K. M.; Patchett, P. J., 1992, Behavior of isotopic systematics during deformation and metamorphism: a Hf, Nd and Sr isotopic study of mylonitized granite: Contributions to Mineralogy and Petrology, v.109, p.386-393.

Bell, T. H.; Etheridge, M. A., 1973, Microstructure of mylonites and their descriptive terminology: Lithos, v.6, p.337-348.

Best, M. G., 1982, Igneous and Metamorphic Petrology, W.H.Freeman & Co.

Bird, J. M.; Dewey, J. F., 1970, Lithosphere plate-continental margin tectonics and the evolution of the Appalachian Orogen: Geological Society of America Bulletin, v.81, p.1031-1060.

Bursnall, J. T., 1975, Stratigraphy, structure and metamorphism west of Baie Verte, Burlington Peninsula, Newfoundland: Unpublished Ph.D. thesis, Cambridge University, England, 337 pages.

Bursnall, J. T.; de Wit, M. J., 1975, Timing and development of the orthotectonic zone in the Appalachian Orogen of northwest Newfoundland: Canadian Journal of Earth Sciences, v.12, p.1712-1722.

Campbell, I. H.; Hill, R. I., 1988, A two-stage model for the formation of the granite-greenstone terrains of the Kalgoorlie-Norseman area, Western Australia: Earth and Planetary Science Letters, v.90, p.11-25.

Card, K. D.; Poulsen, K. H.; Francois, R., 1989, The Archean Superior Province of the Canadian Shield and its lode gold deposits, *in*, Keays, R. R.; Ramsay, W. R. H.; Groves, D. I. (eds), The geology of gold deposits: the perspective in 1988: Economic Geology Monograph 6, p.19-36.

Church, W. R., 1969, Metamorphic rocks of Burlington Peninsula and adjoining areas of Newfoundland and their bearing on continental drift in the North Atlantic, in, Kay, M., edr., North Atlantic Geology and Continental Drift: American Association of Petroleum Geologists, Memoir 12, p.212-233.

Claoue-Long, J. C.; Compston, W.; Cowden, A., 1988, The age of the Kambalda greenstone resolved by ion-microprobe: implications for Archean dating method: Earth and Planetary Science Letters, v.89, p.239-259.

Claoue-Long, J. C.; King, R. W.; Kerrich, R., 1990, Archaean hydrothermal zircon in the Abitibi greenstone belt: constraints on the timing of gold mineralization: Earth and Planetary Science Letters, v.98, p.109-128.

Cockburn, G. H., 1971, Peralkaline granite and associated plutonic rocks of the eastern division of the Fleur de Lys metamorphic complex of Newfoundland: Geological Society of America, Abstracts, Northeastern Section, p.22-23.

Coish, R. A., 1977, Ocean floor metamorphism in the Betts Cove Ophiolite, Newfoundland: Contributions to Mineralogy and Petrology, v.60, p.255-270.

Corfu, F., 1988, Differential response of U-Pb systems in co-existing accessory minerals, Winnipeg River Subprovince, Canadian Shield: implications for Archean crustal growth and stabilization: Contributions to Mineralogy and Petrology, v.98, p.312-325.

Corfu, F.; Andrews, A. J., 1986, A U-Pb age for mineralized Nipissing diabase, Gowganda, Ontarion: Canadian Journal of Earth Sciences, v.23, p.107-109.

Corfu, F.; Andrews, A. J., 1987, Geochronological constraints on the timing of magmatism, deformation, and gold mineralization in the Red Lake greenstone belt, northwestern Ontario: Canadian Journal of Earth Sciences, v.24, p.1302-1320.

Corfu, F.; Davis, D. W., 1991, Comment on "Archean hydrothermal zircon in the Abitibi greenstone belt: constraints on the timing of gold mineralization" by Claoue-Long, J.C.; King, R.W. and Kerrich, R: Earth and Planetary Science Letters, v.104, p.545-552.

Corfu, F.; Krogh, T. E.; Kwok, Y. Y.; Jensen, L. S., 1989, U-Pb zircon geochronology in the southwestern Abitibi greenstone belt, Superior Province: Canadian Journal of Earth Sciences, v.26, p.1747-1763.

Corfu, F.; Muir, T. L., 1989a, The Hemlo-Heron Bay grteenstone belt and Hemlo Au-Mo deposit, Superior Province, Ontario, Canada, 1. Sequence of igneous activity determined by zircon U-Pb geochronology: Chemical Geology (Isotope Geoscience Section), v.79, p.183-200.

Corfu, F.; Muir, T. L., 1989b, The Hemlo-Heron Bay greenstone belt and Hemlo Au-Mo deposit, Superior Province, Ontario, Canada, 2. Timing of metamorphism, alteration and Au mineralization from titanite, rutile, and monazite U-Pb geochronology: Chemical Geology (Isotope Geoscience Section), v.79, p.201-223.

Corfu, F.; Wallace, H., 1986, U-Pb zircon ages for magmatism in the Red Lake greenstone belt, northwestern Ontario: Canadian Journal of Earth Sciences, v.23, p.27-42.

Coyle, M., 1990, Geology, geochemistry and the geochronology of the Springdale Group, an Early Silurian caldera in central Newfoundland: Ph.D. thesis, Memorial University of

Newfoundland, p.310 pages.

Dallmeyer, R. D., 1977, 40Ar/39Ar Age Spectra of Minerals from the Fleur de Lys Terrane in Northwest Newfoundland: their Bearing on Chronology of Metamorphism within the Appalachian Orthotectonic Zone: Journal of Geology, v.85, p.89-103.

Dallmeyer, R. D.; Williams, H., 1975, 40Ar/39Ar ages from the Bay of Islands metamorphic aureole; their bearing on the timing of Ordovician ophiolite abduction: Canadian Journal of Earth Sciences, v.12, p.1685-1690.

Davis, D. W., 1982, Optimum linear regression and error estimation applied to U-Pb data: Canadian Journal of Earth Sciences, v.19, p.2141-2149.

Davis, D. W.; Smith, P. M., 1991, Archean gold mineralization in the Wabigoon Subprovince, a product of crustal accretion: evidence from U-Pb geochronology in the Lake of the Woods area, Superior Province, Canada: Journal of Geology, v.99, p.337-353.

DeGrace, J. R.; Kean, B. F.; Hsu, E.; Green, T., 1976, Geology of the Nippers Harbour map area (2E/13), Newfoundland: Newfoundland Department of Mines and Energy, Mineral Development Division, Report 76-3, 73 pages.

de Wit, M. J., 1976, Metamorphic textures and deformation: a new mechanism for the development of syntectonic porphyroblasts and its implications for interpreting timing relationships in metamorphic rocks: Geological Journal, v.11, p.71-100.

de Wit, M. J., 1980, Structural and metamorphic relationships of pre-Fleur de Lys and Fleur de Lys rocks of the Baie Verte Peninsula, Newfoundland: Canadian Journal of Earth Sciences, v.17, p.1559-1575.

Dewey, J. F., 1969, Evolution of the Appalachian/Caledonian Orogen: Nature, v.22, p.124-129.

Dimroth, E.; Lichtblau, A. P., 1979, Metamorphic evolution of Archean hyaloclastites, Noranda area, Quebec,Canada. Part I: Canadian Journal of Earth Sciences, v.16.

Dube', B., 1990, A preliminary report on contrasting structural styles of gold-only deposits in western Newfoundland: Geological Survey of Canada, Paper 90-1B, p.77-90.

Dube', B.; Guha, J.; Rocheleau, M., 1987, Alteration patterns related to gold mineralization and their relation to CO_2/H_2O ratios: Mineralogy and Petrology, v.37, p.267-291.

Dunning, G. R.; Kean, B. F.; Thurlow, J. G.; Swinden, H. S., 1987, Geochronology of the Buchans, Roberts Arm, and Victoria Lake groups and Mansfield Cove Complex, Newfoundland: Canadian Journal of Earth Sciences, v.24, p.1175-1184.

Dunning, G. R.; Krogh, T. E., 1985, Geochronology of ophiolites of the Newfoundland Appalachians: Canadian Journal of Earth Sciences, v.22, p.1659-1670.

Dunning, G. R.; O'Brien, S. J.; Colman-Sadd, S. P.; Blackwood, R. F.; Dickson, W. L.; O'Neill,

P. P.; Krogh, T. E., 1990, Silurian Orogeny in the Newfoundland Appalachians: Journal of Geology, v.98, p.895-913.

Dunning, G. R.; Swinden, H. S.; Kean, B. F.; Evans, D. T. W.; Jenner, G. A., 1991, A Cambrian island arc in Iapetus: Geochronology and geochemistry of Lake Ambrose Volcanic Belt, Newfoundland Appalachians: Geological Magazine, v.128, p.1-17.

Dunning, G. R.; Wilton, D. H. C.; Herd, R. K., 1989, Geology, geochemistry and geochronology of a Taconic batholith, Southwestern Newfoundland: Transactions of the Royal Society of Edinburgh: Earth Sciences., v.80, p.159-168.

Evans, D. T. W., 1992, Gold metallogeny of the Eastern Dunnage Zone, Central Newfoundland: Current Research, Newfoundland Department of Mines and Energy, Report 92-1, p.231-243.

Fisher, R. V.; Schmincke, H.-U., 1984, Pyroclastic Rocks, Springer-Verlag.

Friedman, G. M.; Sanders, J. E., 1978, Principles of Sedimentology, John Wiley & Sons.

Fryer, B. J.; Kerrich, R.; Hutchinson, R. W.; Peirce, M. G.; Rogers, D. S., 1979, Archean precious-metal hydrothermal systems, Dome Mine, Abitibi Greenstone Belt. I. Patterns of alteration and metal distribution: Canadian Journal of Earth Sciences, v.16, p.421-439.

Gale, G. H., 1973, Paleozoic basaltic komatiite and ocean floor type basalts from northeast Newfoundland: Earth and Planetary Science Letters, v.18, p.22-28.

Gill, J. B., 1984, Sr-Pb-Nd isotopic evidence that both MORB and OIB sources contribute to oceanic island arc magmas in Fiji: Earth and Planetary Science Letters, v.68, p.443-458.

Gresens, R. L., 1967, Composition-volume relationships of metasomatism: Chemical Geology, v.2, p.47-65.

Groves, D. I.; Barley, M. E.; Ho, S. E., 1989, Nature, genesis, and tectonic setting of Mesothermal gold mineralization in the Yilgarn block, Western Australia, *in*, Keays, R. R.; Ramsay, W. R. H.; Groves, D. I. (eds), The geology of gold deposits: the perspective in 1988: Economic Geology Monograph 6, p.71-85.

Hibbard, J., 1982, Significance of the Baie Verte Flexure, Newfoundland: Geological Society of America Bulletin, v.93, p.790-797.

Hibbard, J., 1983, Geology of the Baie Verte Peninsula, Newfoundland, Newfoundland Department of Mines and Energy, Memoir 2.

Hill, R. I.; Compston, W.; Cowden, A., 1986, Age of granite emplacement, southern Yilgran block, western Australia: Aust. Natl. Uni., Res. Sch. Earth Sci. Annu. Rep., p.70-71.

Hodgson, C. J.; Hamilton, J. V.; Hanes, J. A.; Piroshco, D. W., 1990, Late emplacement of gold in the Archean Abitibi and analogous Phanerozoic "greenstone" belts: a consequence of thermal equilibration following collisional orogeny, in, Robert, F.; Sheahan, P. A.; Green, S. B.,ed., Greenstone Gold and Crustal Evolution, p.171.

Hoffman, P. F., 1990, On accretion of granite-greenstone terranes: in, Robert, F.; Sheahan, P.A.; Green, S.B., Greenstone Gold and Crustal Evolution, Proceedings of a workshop held at Val d'Or, Quebec., p.32-46.

Huard, A. A., 1990, The Noranda/Impala Stog'er Tight deposit: International Association on the Genesis of Ore Deposits, 8th Symposium, Field Trip Guide, p.173-177.

Huard, A. A.; O'Driscoll, C., 1985, Auriferous specularite-alunite-pyrophyllite deposits of the Hickeys Pondarea, northern Burin Peninsula Newfoundland: Current Research, Newfoundland Department of Mines and Energy, v.85-1, p.182-189.

Jamieson, R. A., 1990, Metamorphism of an Early Paleozoic continental margin, Western Baie VertePeninsula, Newfoundland: Journal of Metamorphic Geology, v.8, p.269-288.

Jamieson, R. A., 1992, Exhumtion of eclogite, Western Baie Verte Peninsula, Microprobe meets Lithoprobe: The Tuzo Wilson Cycle, a 25th Anniversary Symposium, Geological Association of Canada (Newfoundland Section) Program with Abstracts, p.20.

Jamieson, R. A.; Vernon, R. H., 1987, Timing of porphyroblast growth in the Fleur de Lys Supergroup, Newfoundland: Journal of Metamorphic Petrology, v.5, 273-288.

Jemielita, R. A.; Davis, D. W.; Krogh, T. E., 1990, U-Pb evidence for Abitibi gold mineralization postdating greenstone magmatism and metamorphism: Nature, v.346, p.831-834.

Jenner, G. A.; Fryer, B. J., 1980, Geochemistry of the Upper Snooks Arm Group basalts, Burlington Peninsula, Newfoundland: evidence against formation in an island arc: Canadian Journal of Earth Sciences, v.17, p.888-900.

Karlstrom, K. E.; van der Pluijm, B. A.; Williams, P. F., 1982. Structural interpretation of the eastern Notre Dame Bay area, Newfoundland; regional pos.-Middle Silurian thrusting and asymmetrical folding: Canadian Journal of Earth Sciences, v.19, p.2325-2341.

Kean, B. F.; Dean, P. L.; Strong, D. F., 1981, Regional geology of the Central Volcanic Belt of Newfoundland: in, Swanson, E.A., Strong, D.F.; Thurlow, J.G., eds., The Buchans Orebodies, Fifty Year of Geology and Mining., p.65-78.

Keays, R. R.; Skinner, B. J., 1988, Introduction: in, Keays, R.R.; Ramsay, R.H.; Groves, D.I. (eds), The Geology of Gold Deposits, Economic Geology Monograph 6, p.1-8.

Kennedy, M. J., 1971, Structure and stratigraphy of the Fleur de Lys Supergroup in the Fleur de Lys area, Burlington Peninsula, Newfoundland: Geological Association of Canada Proceedings, v.24, p.59-71.

Kennedy, M. J., 1975, The Fleur de Lys Supergroup: stratigraphic comparison of Moine and Daldradian equivalents in Newfoundland with the British Caledonides: Geological Society of London, v.131, p.305-310.

Kerrich, R., 1983, Geochemistry of Gold Deposits in the Abitibi Greenstone Belt: The Canadian Institute of Mining and Metallurgy, Special Volume 27.

Kerrich, R., 1989a, Geodynamic setting and hydraulic regimes: shear zone hosted mesothermal gold deposits, *in*, Bursnall, J.T., edt., Mineralization and Shear Zones, Geological Association of Canada Short Coarse Notes, v.6, p.89-128.

Kerrich, R., 1989b, Source processes for Archean Au-Ag vein deposits: evidence from lithophile-element systematics of the Hollinger-McIntyre and Buffalo Ankerite deposits, Timmins: Canadian Journal of Earth Sciences, v.26, p.755-781.

Kerrich, R., 1989c, Lithophile Element Systematics of Gold Vein Deposits in Archean Greenstone Belts: Implications for Source Processes, *in*, Keays, R. R.; Ramsay, W. R. H.; Groves, D. I. (eds), The geology of gold deposits: the perspective in 1988: Economic Geology, Monograph 6, p.508-520.

Kerrich, R., 1990, Mesothermal gold deposits: a critique of genetic hypotheses, in, Robert, F.; Sheahan, P. A.; Green, S. B., ed., Greenstone Gold and Crustal Evolution: p.13-31.

Kerrich, R.; Feng, R., 1992, Archean geodynamics and the Abitibi-Pontiac collision, implications for advection of fluids at transpressive collisional boundaries and the origin of giant quartz vein systems: Earth Science Reviews 32, p.33-60.

Kerrich, R.; Fryer, B. J., 1979, Archean precious-metal hydrothermal systems, Dome Mine, Abitibi Greenstone Belt. II. REE and oxygen isotope relations: Canadian Journal of Earth Sciences, v.16, p.440-458.

Kerrich, R. W.; Fryer, B. J., 1988, Lithophile-element systematics of Archean greenstone belt Au-Ag vein deposits: Implications for source processes: Canadian Journal of Earth Sciences, v.25, p.945-953.

Kerrich, R.; Wyman, D., 1990, Geodynamic setting of mesothermal gold deposits; an association with accretionary tectonic regimes: Geology, v.18, p.882-885.

Kidd, W. S. F., 1974, The evolution of the Baie Verte Lineament, Burlington Peninsula, Newfoundland: Unpublished Ph.D. thesis, Cambridge University, England, 294 pages.

Kidd, W. S. F.; Dewey, J. F.; Bird, J. M., 1978, The Ming's Bight Ophiolite Complex, Newfoundland: Appalachian oceanic crust and mantle: Canadian Journal of Earth Sciences, v.15, p.781-804.

Kirkwood, D.; Dube, B., 1992, Structural control of sill-hosted gold mineralization: the Stog'er Tight Gold Deposit, Baie Verte Peninsula, Northwestern Newfoundland: Geological Survey of Canada, Current Research, 92-1D, p.211-221.

Krogh, T. E., 1973, A low-contamination method for hydrothermal decomposition of zircon and extraction of U and Pb for isotopic age determination: Geochem. Cosmochim. Acta, v.37, p.488-494.

Krogh, T. E., 1982, Improved accuracy of U-Pb zircon ages by the creation of more concordant systems using an air abrasion technique: Geochim. Cosmochim. Acta, v.46, p.637-649.

Longerich, H. P.; Jenner, G. A.; Fryer, B. J.; Jackson, S. E., 1990, Inductively coupled plasma-mass spectrometric analysis of geological samples: a critical evaluation based on case studies: Chemical Geology, v.83, p.105-118.

Ludwig, K. R., 1980, Calculation of uncertainties of U-Pb isotope data: Earth and Planetary Science Letters, v.46, p.212-220.

Manhes, G.; Minster, J. F.; Allegre, C. J., 1978, Comparative uranium-thorium-lead and rubidium-strontium study of the Saint Severin amphoterite; consequences for early solar system chronology: Earth and Planetary Science Letters, v.39, p.14-24.

Misik, M., 1971, Observations concerning calcite veinlets in carbonate rocks: Journal of Sedimentary Petrology, v.41, p.450-460.

Miyashiro, A.; Shido, F., 1975, Tholeiitic and calc-alkalic series in relation to the behaviors of Titanium, Vanadium, Chromium and Nickel: American Journal of Science, v.275, p.265-277.

Murphy, J. B., 1989, Tectonic evolution and metamorphic characteristics of shear zones, *in*: Bursnall, J.T., edt., Mineralization and Shear Zones, Geological Association of Canada Short Coarse Notes, v.6, p.24-29.

Neale, E. R. W., 1958, Baie Verte, Newfoundland: Geological Survey of Canada Map 10-1958.

Neale, E. R. W., 1959, Relationship of the Baie Verte Group to gneissic groups on the Burlington Peninsula, Newfoundland: Geological Society of America Bulletin, v.76, p.1650-1651.

Neale, E. R. W., 1967, Burlington (Baie Verte) Peninsula, Newfoundland: Geological Survey of Canada Paper 67-1A, p.183-186.

Norman, R. E.; Strong, D. F., 1975, The geology and geochemistry of ophiolitic rocks exposed at Ming's Bight, Newfoundland: Canadian Journal of Earth Sciences, v.12, p.777-797.

O'Brien, B. H.; O'Brien, S. J.; Dunning, G. D., 1991, Silurian cover, Late Precambrian-Early Ordovician basement, and the chronology of orogenesis in the Hermitage Flexure (Newfoundland Appalachians): American Journal of Science, v.291.

O'Hara, K.; Blackburn, W. H., 1989, Volume-loss model for trace-element enrichments in mylonites: Geology, v.17, p.524-527.

Pearce, J. A. and Cann, J. R., 1973, Tectonic setting of basic volcanic rocks determined using trace element analyses: Earth and Planetary Science Letters, v.19, p.290-300.

Pearce, J. A. and Norry, M. J., 1979, Petrogenetic Implications of Ti, Zr, Y, and Nb Variations in Volcanic Rocks: Contributions to Mineralogy and Petrology, v.69, p.33-47.

Phillips, G. N., 1986, Geology and alteration in the Golden Mile, Kalgoorlie: Economic Geology, v.81, p.779-808.

Robert, F.; Brown, A. C., 1986, Archean gold-bearing quartz veins at the Sigma Mine, Abitibi Greenstone Belt, Quebec: Part II. Vein Paragenesis and Hydrothermal Alteration: Economic Geology, v.81, p.593-616.

Romberger, S. B., 1988, Geochemistry of gold in hydrothermal deposits: U.S.Geological Survey Bulletin, v.1857-A, p.A9-A25.

Rubin, J. N.; Henry, C. D.; Price, J. C., 1988, Hydrothermal zircons and zircon overgrowths, Sierra Blanka Peaks, Texas: American Mineralogist, v.74, p.865-869.

Salters, V. J. M.; Hart, S. R., 1991, The mantle sources of ocean ridges, islands and arcs: the Hf-isotope connection: Earth and Planetary Science Letters, v.104, p.364-380.

Shervais, J. W., 1982, Ti-V plots and the petrogenesis of modern and ophiolitic lavas: Earth & Planetary Science Letters, v.59, p.101-118.

Smith, T. J.; Kesler, S. E., 1985, Relation of fluid inclusion geochemistry to wallrock alteration and lithogeochemical zonation at the Hollinger-McIntyre gold deposit, Timmins, Ontario, Canada: CIM Bulletin, v.78, p.35-46.

Snelgrove, A. K., 1931, Geology and ore deposits of Betts Cove-Tilt Cove area, Notre Dame Bay, Newfoundland: Canadian Mining and Metallurgical Bulletin, v.24, 43 pages.

Spang, J. H.; Groshong, R. H. Jr., 1981, Deformation mechanism and strain history of a minor fold from the Appalachian Valley and Ridge Province: Tectonophysics, v.72, p.323-42.

Stacey, J. S.; Kramers, J. D., 1975, Approximation of terrestrial lead isotope evolution by a two-stage model: Earth and Planetary Science Letters, v.26, p.207-221.

Sun, S. S.; McDonough, W. F., 1989, Chemical and isotopic systematics of oceanic basalts, implications for mantle composition and processes, *in*, Saunders, A.D. and Norry, M.J. (eds), Magmatism in the Ocean Basins: Geological Society Special Publications 42, p.313-345.

Swinden, H. C.; Jenner, G. A.; Fryer, B. J.; Hertogen, J.; Roddick, J. C., 1990, Petrogenesis and paleotectonic history of the Wild Bight Group, an Ordovician rifted island arc in central Newfoundland: Contributions to Mineralogy and Petrology, v.105, p.219-241.

Tuach, J.; Dean, P. L.; Swinden, H. S.; O'Driscoll, C. F.; Kean, B. F.; Evans, D. T. W., 1988, Gold Mineralization in Newfoundland: A 1988 Review: Current Research, Newfoundland Department of Mines and Energy, Report 88-1.

Tucker, R. D.; Krogh, T. E.; Ross, R. J.; Williams, S. H., 1990, Time-scale calibration by high-precision U-Pb zircon dating of interstratified volcanic ashes in the Ordovician and Lower Silurian stratotypes of Britain: Earth and Planetary Science Letters, v.100, p.51-58.

Upadhyay, H. D., 1973, The Betts Cove ophiolite and related rocks of the Snooks Arm Group, Newfoundland: Unpublished Ph.D. thesis, Memorial University of Newfoundland, 224 pages.

Vearncombe, J. R.; Barley, M. E.; Eisenlohr, B. N.; Groves, D. I.; Houstoun, S. M.; Skwarnecki,

M. S., 1989, Structural controls on mesothermal gold mineralization: examples from the Archean terranes of Southern Africa and Western Australia, *in*, Keays, R. R.; Ramsay, W. R. H.; Groves, D. I. (eds), The geology of gold deposits: the perspective in 1988: Economic Geology Monograph 6, p.124-134.

Wanless, R. K.; Stevens, R. D.; Lachance, G. R.; Delabio, R. N., 1972, Age determination and geological studies: K-Ar isotopic ages, Report 10: Geological Survey of Canada, Paper 71-2, p.89-93.

Wayne, D. M.; Sinha, A. K.; Hewitt, D. A., 1992, Differential response of zircon U-Pb isotopic systematics to metamorphism across a lithologic boundary: an example from the Hope Valley Shear Zone, southeastern Massachusetts, USA: Contributions to Mineralogy and Petrology, v.109, p.408-420.

Williams, H., 1978, Geological development of the northern Appalachians: its bearing on the evolution of the British Isles, in, Bowes, D.L. and Leake, B.E., eds., Crustal Evolution in Northwestern Britain and Adjacent Regions: Geological Journal, Special Issue 10, p.1-22.

Williams, H., 1979, Appalachian Orogen in Canada: Canadian Journal of Earth Sciences, v.16, p.792-807.

Williams, H.; Colman-Sadd, S. P.; Swinden, H. S., 1988, Tectonic-stratigraphic subdivisions of central Newfoundland: Current research, Part B. Geological Survey of Canada Paper 88-1B, p.91-98.

Williams, H.; Hatcher, R. D., 1983, Appalachian suspect terranes: *in*, Hatcher, R.D.; Williams, H.; Ziets, I., Contributions to the Tectonics and Geophysics of Mountain Chains, Geological Society of America Memoir 158, p.33-53.

Williams, H.; St-Julien, P., 1982, The Baie Verte-Brompton Line: Early Paleozoic continental interface in the Canadian Appalachians, in, St-Julien, P. and Beland, J., Major Structural Zones and Faults of the Northern Appalachians: Geological Association of Canada, Special Paper 24, p.177-207.

Wilson, J. T., 1966, Did the Atlantic close and then re-open?: Nature, v.211, p.676-681.

Wilton, D. H. C., 1983, The geology and structural history of the Cape Ray Fault Zone inSouthwestern Newfoundland: Canadian Journal of Earth Sciences, v.20, p.1119-1133.

Winchester, J. A. and Floyd, P. A., 1977, Geochemical discrimination of different magma series and their differentiation products using immobile elements: Chemical Geology, v.20, p.325-343.

Winkler, H. G. F., 1974, Petrogenesis of Metamorphic Rocks, Springer-Verlag.

Wise, D. U. et.al., 1984, Fault-related rocks: Suggestions for terminology: Geology, v.12, p.391-394.

Witt, W. K., 1991, Regional metamorphic controls on alteration associated with gold

mineralization in the Eastern Goldfields province, Western Australia: implications for the timing and origin of Archean lode-gold deposits: Geology, v.19, p.982-985.

Wong, L.; Davis, D. W.; Krogh, T. E.; Robert, F., 1991, U-Pb zircon and rutile chronology of Archean greenstone formation and gold mineralization in the Val d'Or region, Quebec: Earth and Planetary Science Letters, v.104, p.325-336.

Wood, D. A.; Joron, J. L.; Treuil, M., 1979, A reappraisal of the use of trace elements to classify and discriminate between magma series erupted in different tectonic settings: Earth and Planetary Science Letters, v.50, p.326-36.

APPENDIX I: Selected mineral composition data from SEM semi-quantitative analysis.

Sample	BN67-A22	BN67-A22	BN60-A9	BN19-03	BN61-03	BN60-37
Mineral	ACTINOLITE	HORNBLENDE	EPIDOTE	CHLORITE A	LEUCOXENE	WHITE MICA
SiO2	55.21	44.92	36.76	30.63	27.37	47.77
TiO2	0.07	2.94	0.02	-	42.45	0.17
Al2O3	1.91	7.84	23.26	23.05	0.97	34.22
FeO	13.75	21.69	13.70	28.91	0.27	4.57
MgO	12.94	8.89	0.68	16.10	0.11	1.14
CaO	15.04	11.77	24.70	0.05	28.28	0.01
Na2O	0.77	1.45	0.46	1.14	0.06	0.48
K2O	0.20	0.50	0.14	-	0.06	11.26

Sample	BN60-A6	BN60-37	BN60-40	BN60-40
Mineral	CHLORITE B	ANKERITE	CHLORITE C	CHLORITE D
SiO2	28.43	0.73	30.94	26.81
TiO2	-	-	-	-
Al2O3	24.37	0.91	21.59	24.67
FeO	34.25	37.15	34.50	37.93
MgO	11.69	12.34	9.80	8.48
CaO	0.03	46.97	0.26	-
Na2O	1.24	1.29	1.05	1.18
K2O	-	0.09	0.04	0.02

APPENDIX II: CHEMICAL DATA FOR THE MAIN ROCK UNITS IN THE STOG'ER TIGHT AREA.

Lab No.	M135†	M136*	M139†	M145†	M1657	M1658*
Sample	BN53-01	BN53-02	BN53-10	BN53-25	BN55-B1	BN55-B3
Suite	VPU	VPU	MGAB	VPU	LFTG	LFTG
Rock Type	ASH TUFF	ASH TUFF	GABBRO	VOLCANIC	GABBRO	GABBRO
SiO2	55.51	54.59	47.42	54.01	47.94	52.59
TiO2	1.08	1.05	1.67	0.93	1.30	0.92
Al2O3	16.97	16.77	16.81	13.65	17.84	15.71
Fe2O3	8.58	9.21	12.84	8.13	13.86	10.60
MnO	0.13	0.17	0.18	0.14	0.20	0.19
MgO	7.40	6.30	5.22	8.72	8.25	6.54
CaO	4.41	5.40	12.38	9.11	5.90	8.17
Na2O	3.06	5.66	2.91	4.90	4.48	5.07
K2O	2.73	0.72	0.34	0.05	0.10	0.09
P2O5	0.14	0.13	0.23	0.37	0.14	0.13
Total	97.82	100.76	96.38	99.62	97.47	98.68
Mg #	63.09	57.54	44.59	68.01	54.10	54.98
Cr	179	192	91	556	358	342
Ni	75	73	26	220	77	52
Sc	20	22	46	23	44	41
V	139	130	324	174	304	234
Cu	31	14	18	91	46	90
Zn	58	66	81	44	81	54
K	22649	6015	2799	375	792	757
Rb	46.6	9.0	6.6	0.6	1.7	1.2

Ba	252.45	117.31	29.65	51.82	25.61	26.92
Sr	137.74	179.38	363.10	443.87	158.63	217.35
Ta	1.00	-	1.05	1.10	0.50	-
Nb	6.73	6.93	9.16	8.51	3.98	3.45
Hf	3.29	-	4.22	3.90	2.59	-
Zr	127.68	125.71	151.30	176.97	102.76	91.10
Ti	6472	6272	10034	5578	7768	5510
Y	20.69	21.93	25.70	16.89	28.56	25.12
Th	3.85	2.83	0.66	8.63	0.97	0.34
La	13.39	-	11.14	41.65	7.04	-
Ce	30.63	62.83	29.10	87.76	17.10	61.39
Pr	3.58	-	4.11	10.24	2.41	-
Nd	15.14	-	18.62	38.11	11.62	-
Sm	3.49	-	4.95	6.00	3.34	-
Eu	1.05	-	1.77	1.73	1.20	-
Gd	3.65	-	5.28	4.54	4.35	-
Tb	0.58	-	0.82	0.54	0.71	-
Dy	3.69	-	5.12	3.07	4.58	-
Ho	0.74	-	1.04	0.60	1.01	-
Er	2.10	-	2.85	1.54	2.86	-
Tm	0.31	-	0.42	0.22	0.41	-
Yb	1.87	-	2.58	1.41	2.53	-
Lu	0.29	-	0.38	0.20	0.39	-

Lab No.	M1659	M1661	M1662	M1663	M1664	M1669
Sample	BN55-B6	BN55-B9	BN55-B10	BN55-B12	BN55-B15	BN24-01
Suite	LFTG*	LFTG	MGAB*	MGAB	MGAB	MGAB
Rock Type	GABBRO	GABBRO	GABBRO	GABBRO	GABBRO	GABBRO
SiO2	51.65	50.37	44.41	47.75	47.34	47.72
TiO2	1.10	1.06	1.92	1.39	1.82	1.29
Al2O3	15.60	17.02	16.73	17.55	18.36	17.09
Fe2O3	11.73	10.76	14.44	13.03	14.25	11.85
MnO	0.19	0.19	0.19	0.19	0.22	0.18
MgO	6.32	6.46	7.16	6.58	4.82	7.83
CaO	8.67	9.57	10.79	10.32	9.14	11.12
Na2O	4.48	4.08	3.00	2.97	3.66	2.72
K2O	0.09	0.36	1.17	0.03	0.08	0.02
P2O5	0.18	0.13	0.20	0.20	0.31	0.19
Total	98.65	97.94	95.43	94.83	95.90	95.62
Mg #	51.60	54.33	49.53	50.00	40.10	56.70
Cr	256	209	346	276	25	608
Ni	36	43	68	59	14	99
Sc	47	45	43	43	30	41
V	246	244	342	287	323	244
Cu	43	42	46	29	28	30
Zn	65	73	65	72	93	61
K	741	2958	9673	219	666	182
Rb	1.0	6.6	22.4	0.3	2.3	0.1

Ba	14.09	55.63	378.98	11.45	19.70	14.36
Sr	203.20	292.20	186.38	367.82	430.22	417.41
Ta	-	0.69	-	1.00	0.96	1.18
Nb	4.59	3.44	8.42	9.11	12.34	7.74
Hf	-	2.66	-	3.85	4.32	2.87
Zr	117.71	88.18	151.22	144.05	188.94	126.63
Ti	6582	6384	11503	8326	10927	7743
Y	32.06	25.83	23.65	26.27	31.23	22.70
Th	ND	0.92	1.02	0.69	0.82	0.55
La	-	5.62	-	10.18	12.14	8.10
Ce	41.82	14.36	59.26	26.70	31.48	21.34
Pr	-	2.08	-	3.75	4.47	2.98
Nd	-	10.10	-	16.83	20.39	13.31
Sm	-	2.95	-	4.18	5.07	3.42
Eu	-	1.12	-	1.41	1.75	1.20
Gd	-	3.83	-	4.32	5.31	3.70
Tb	-	0.65	-	0.67	0.81	0.58
Dy	-	4.30	-	4.13	4.87	3.49
Ho	-	0.92	-	0.85	1.01	0.71
Er	-	2.65	-	2.41	2.73	1.98
Tm	-	0.38	-	0.36	0.38	0.27
Yb	-	2.58	-	2.25	2.39	1.67
Lu	-	0.40	-	0.33	0.36	0.25

Lab No.	M1670	M1680	M2415	M2416	M2418	M2419
Sample	BN24-02	BN54-B5	BN18-B3	BN54-R	91821-A1	BN55-B2
Suite	MGAB*	VPU	VPU	VPU	VPU	LFTG
Rock Type	GABBRO	VOLCANIC	VOLCANIC	VOLCANIC	VOLCANIC	GABBRO
SiO2	47.03	54.65	50.66	51.35	49.94	47.59
TiO2	1.50	0.98	1.02	0.57	0.53	1.13
Al2O3	18.13	16.08	16.57	13.19	11.29	12.26
Fe2O3	12.60	7.82	8.26	11.80	8.07	11.21
MnO	0.15	0.21	0.12	0.22	0.15	0.19
MgO	7.77	6.23	9.68	9.93	10.78	12.84
CaO	9.11	9.03	8.41	9.56	15.23	11.17
Na2O	3.45	4.50	5.07	3.31	3.84	3.46
K2O	0.10	0.10	0.09	0.06	0.18	0.08
P2O5	0.17	0.39	0.12	0.01	ND	0.09
Total	95.26	97.21	92.49	92.39	93.52	91.90
Mg #	54.98	61.21	69.89	62.50	72.56	69.41
Cr	438	301	175	34	362	338
Ni	70	130	40	28	64	68
Sc	43	17	25	35	37	42
V	276	169	173	349	232	277
Cu	23	31	10	42	64	64
Zn	56	65	45	165	40	48
K	828	812	718	476	1482	651
Rb	1.9	0.6	1.1	0.6	1.7	1.0

Ba	37.64	27.02	111.23	11.16	21.71	17.55
Sr	245.45	433.07	344.03	141.00	99.83	349.59
Ta	-	1.42	1.33	0.37	0.48	0.45
Nb	7.61	9.63	5.60	1.02	0.67	3.38
Hf	-	3.73	5.08	1.00	0.96	2.51
Zr	129.09	144.37	119.23	29.31	24.07	87.97
Ti	8980	5895	6131	3432	3167	6752
Y	21.52	18.14	21.97	14.75	11.68	22.24
Th	1.58	5.78	4.14	0.32	0.45	0.83
La	-	31.59	17.02	1.81	1.45	5.46
Ce	47.16	68.15	40.28	4.60	3.71	14.43
Pr	-	7.82	5.09	0.67	0.59	2.08
Nd	-	29.30	21.50	3.41	3.05	10.04
Sm	-	5.09	5.62	1.26	1.21	3.00
Eu	-	1.50	1.99	0.39	0.47	1.18
Gd	-	4.27	6.49	1.76	1.66	3.82
Tb	-	0.53	1.06	0.34	0.29	0.60
Dy	-	3.01	6.50	2.45	1.96	4.16
Ho	-	0.60	1.36	0.55	0.44	0.85
Er	-	1.68	3.88	1.70	1.36	2.42
Tm	-	0.24	0.54	0.26	0.18	0.35
Yb	-	1.47	3.55	1.84	1.30	2.28
Lu	-	0.23	0.54	0.29	0.19	0.35

Lab No.	M2420	M2421
Sample	BN55-B5	91822-3
Suite	LFTG	MGAB
Rock Type	GABBRO	GABBRO (GEOCHRON.)
SiO2	42.77	49.23
TiO2	1.27	1.88
Al2O3	13.82	13.37
Fe2O3	15.23	13.93
MnO	0.25	0.20
MgO	13.02	7.89
CaO	11.17	9.29
Na2O	2.17	3.45
K2O	0.13	0.24
P2O5	0.18	0.53
Total	93.25	92.52
Mg #	62.87	52.86
Cr	223	21
Ni	55	15
Sc	47	35
V	324	247
Cu	49	86
Zn	93	82
K	1095	1956
Rb	2.0	2.8

Ba	29.66	49.52
Sr	289.58	294.66
Ta	0.55	1.77
Nb	4.91	18.10
Hf	3.58	6.85
Zr	125.31	275.19
Ti	7593	11255
Y	32.79	44.43
Th	1.31	1.86
La	8.39	20.54
Ce	21.74	51.69
Pr	3.08	6.98
Nd	14.77	31.42
Sm	4.40	8.15
Eu	1.77	2.65
Gd	5.52	8.85
Tb	0.90	1.38
Dy	5.82	8.52
Ho	1.19	1.64
Er	3.49	4.78
Tm	0.50	0.66
Yb	3.24	4.27
Lu	0.49	0.62

Notes:

† Si, Al, Mg and Na measured by AA method.

* Ba and Ce measured by XRF method.

Concentrations of major element (SiO_2 to P_2O_5) are in *wt%* and those of trace elements (Cr to Lu) are in *ppm*.

Major element concentrations are re-calculated to 100% (Total= total before recalculation).

ND= not detected.

APPENDIX III: CHEMICAL DATA FOR SELECTED ALTERED ROCKS.

Lab No.	M141†	M143†	M1665*	M1666*	M1667*	M1668*
Sample	BN53-13	BN53-21	BN55-B17	BN55-B18	BN55-B19	BN55-B20
Rock Type	MINERALIZE	CHL-MT	CHL-CC	ANK-SER	ALB-PYR	ANK-SER
SiO2	56.60	43.40	45.05	40.88	44.58	40.40
TiO2	0.66	4.96	2.30	1.80	1.54	2.65
Al2O3	12.90	10.30	17.21	15.50	17.80	18.00
Fe2O3	6.68	16.10	14.26	14.42	10.58	13.83
MnO	0.15	0.23	0.16	0.19	0.15	0.18
MgO	4.94	4.39	4.26	4.38	2.72	4.37
CaO	6.71	11.54	8.69	9.52	8.52	7.39
Na2O	7.60	0.51	4.27	2.89	5.01	4.66
K2O	0.30	1.10	1.03	2.55	3.02	2.18
P2O5	0.68	0.19	0.21	0.24	0.25	0.44
Total	97.23	92.72	97.44	92.35	94.17	94.10
Mg #	59.41	35.07	37.17	37.57	33.74	38.49
Cr	ND	ND	9	18	9	ND
Ni	ND	ND	9	8	ND	4
Sc	10	62	35	36	22	34
V	43	517	364	335	307	331
Cu	ND	13	24	13	36	ND
Zn	ND	113	76	93	40	71
S	18673.29	1870.92	186.08	125.73	1122.99	1267.11
K	2499	9140	8517	21127	25053	18105
Rb	3.5	14.5	17.9	29.1	32.1	24.2

Ba	29.00	76.00	270.29	140.10	154.58	133.04
Sr	205.38	76.11	206.43	179.88	218.40	193.18
Ta	3.65	1.41	-	-	-	-
Nb	17.07	17.11	11.06	10.86	12.73	12.92
Hf	6.30	5.04	-	-	-	-
Zr	283.73	210.88	184.08	187.24	235.38	227.62
Ti	3981	29747	13794	10791	9262	15887
Y	33.70	29.92	27.68	29.10	30.89	35.53
Th	1.19	0.67	-	-	-	-
La	15.99	10.27	-	-	-	-
Ce	41.77	27.66	70.61	65.94	58.17	65.64
Pr	5.85	4.04	-	-	-	-
Nd	25.45	19.27	-	-	-	-
Sm	6.39	5.07	-	-	-	-
Eu	2.28	1.63	-	-	-	-
Gd	7.31	5.83	-	-	-	-
Tb	1.09	0.94	-	-	-	-
Dy	6.68	5.66	-	-	-	-
Ho	1.30	1.17	-	-	-	-
Er	3.63	3.19	-	-	-	-
Tm	0.51	0.42	-	-	-	-
Yb	3.09	2.69	-	-	-	-
Lu	0.47	0.37	-	-	-	-

Lab No.	M1671*	M1672	M1673	M1674*	M1675	M1676*
Sample	BN24-04	BN24-06	BN24-09	BN24-11	BN24-14	BN24-17
Rock Type	ANK-SER	ANK-SER	ALB-PYR	MINERALIZE	CHL-MT	CHL-MT
SiO2	41.58	39.83	52.35	27.93	36.18	43.95
TiO2	1.30	1.37	0.58	1.70	3.69	2.56
Al2O3	16.18	16.41	21.43	8.09	16.92	12.80
Fe2O3	10.14	9.66	8.02	24.26	24.93	14.23
MnO	0.16	0.16	0.05	0.21	0.25	0.25
MgO	4.75	4.40	1.21	1.57	4.72	3.95
CaO	10.73	11.53	1.79	9.80	5.26	8.56
Na2O	4.09	1.15	6.30	3.25	3.28	3.50
K2O	1.03	3.99	3.54	1.03	0.84	1.37
P2O5	0.13	0.10	0.30	1.82	0.60	0.41
Total	90.09	88.60	95.57	79.65	96.67	91.59
Mg #	48.13	47.41	23.01	11.36	27.27	35.47
Cr	126	86	11	24	4	17
Ni	31	24	ND	13	ND	ND
Sc	38	37	10	19	34	33
V	270	272	127	73	373	313
Cu	47	11	ND	ND	16	13
Zn	37	36	33	10	196	105
S	151.73	690.10	13373.43	147991.59	744.33	706.82
K	8567	33106	29420	8517	7006	11406
Rb	12.2	47.6	39.0	10.4	9.6	18.6

Ba	121.22	97.00	174.00	66.49	53.00	167.70
Sr	314.95	262.40	106.86	224.21	198.60	229.14
Ta	-	0.77	3.56	-	2.02	-
Nb	6.47	7.30	37.40	37.94	23.58	18.26
Hf	-	3.78	16.17	-	10.10	-
Zr	116.12	122.95	738.06	437.86	425.80	248.89
Ti	7793	8207	3483	10203	22098	15317
Y	18.32	17.62	85.44	71.31	63.93	43.84
Th	-	0.55	3.49	-	1.85	-
La	-	6.64	43.44	-	25.91	-
Ce	73.84	17.27	108.66	97.82	69.85	97.01
Pr	-	2.46	14.69	-	9.97	-
Nd	-	11.26	62.80	-	46.20	-
Sm	-	3.01	15.13	-	11.88	-
Eu	-	1.13	4.74	-	3.46	-
Gd	-	3.10	15.73	-	12.79	-
Tb	-	0.52	2.41	-	1.94	-
Dy	-	3.09	14.80	-	11.80	-
Ho	-	0.64	3.06	-	2.40	-
Er	-	1.81	8.70	-	6.70	-
Tm	-	0.26	1.24	-	0.92	-
Yb	-	1.70	8.14	-	5.65	-
Lu	-	0.27	1.29	-	0.86	-

Notes:

† Si, Al, Mg and Na measured by AA method.

* Ba and Ce measured by XRF method.

Concentrations of major elements (SiO_2 to P_2O_5) are in *wt%* and those of trace elements (Cr to Lu) are in *ppm*.

ND= not detected

APPENDIX IV: Average primitive-mantle elemental concentrations (ppm) used as normalizing values for the extended REE plots (spider diagrams). Data from G.A. Jenner (personal commun.,1991).

Rb	0.555	Gd	0.533
Ba	6.270	Tb	0.097
Th	0.088	Dy	0.661
La	0.630	Ho	0.148
Nb	0.650	Y	3.900
K	267	Er	0.432
Ce	1.590	Tm	0.067
Pr	0.251	Yb	0.442
Sr	18.9	Lu	0.066
Nd	1.210	Sc	13.00
Zr	9.800	V	128
Hf	0.280	Zn	50
Sm	0.399	Cu	28
Eu	0.150	Ni	2000
Ti	1134	Cr	3000

APPENDIX V: Drill-Core Logs and Cross-Sections.

The results of lithologic core-logging and petrographic examinations of selected samples from 22 diamond drill-holes in the eastern Stog'er Tight prospect area pertinent to this study are described in the following geologic cross-sections. The drill-holes are located along 5 parallel drill-sections (101 + 00W to 105 + 00W) with NNE-SSW orientation. The drill-hole positions, depths and bearings are compiled from Noranda Exploration Company's unpublished reports and maps. Sections illustrate lithology as well as the distribution of alteration/mineralization zones. The alteration zonation and the deformational features of rocks are not represented in the sections because of scale and graphic limitations. Nevertheless, regardless of few exceptions, the hanging wall and the footwall of the ore zones are dominated by ankerite-sericite alteration and chlorite-magnetite alteration, respectively.

The lithologic correlations between adjacent drill-holes in the same section are represented by dashed lines. The goodness of correlation is not uniform throughout the drill-sections and is highly variable between different drill-holes. Correlation is generally poor in drill-section 101 + 00W while the best correlation is manifested by drill-sections 102 + 00W and 105 + 00W. Correlations have also been made between drill-sections and surface trenches, as much as possible.

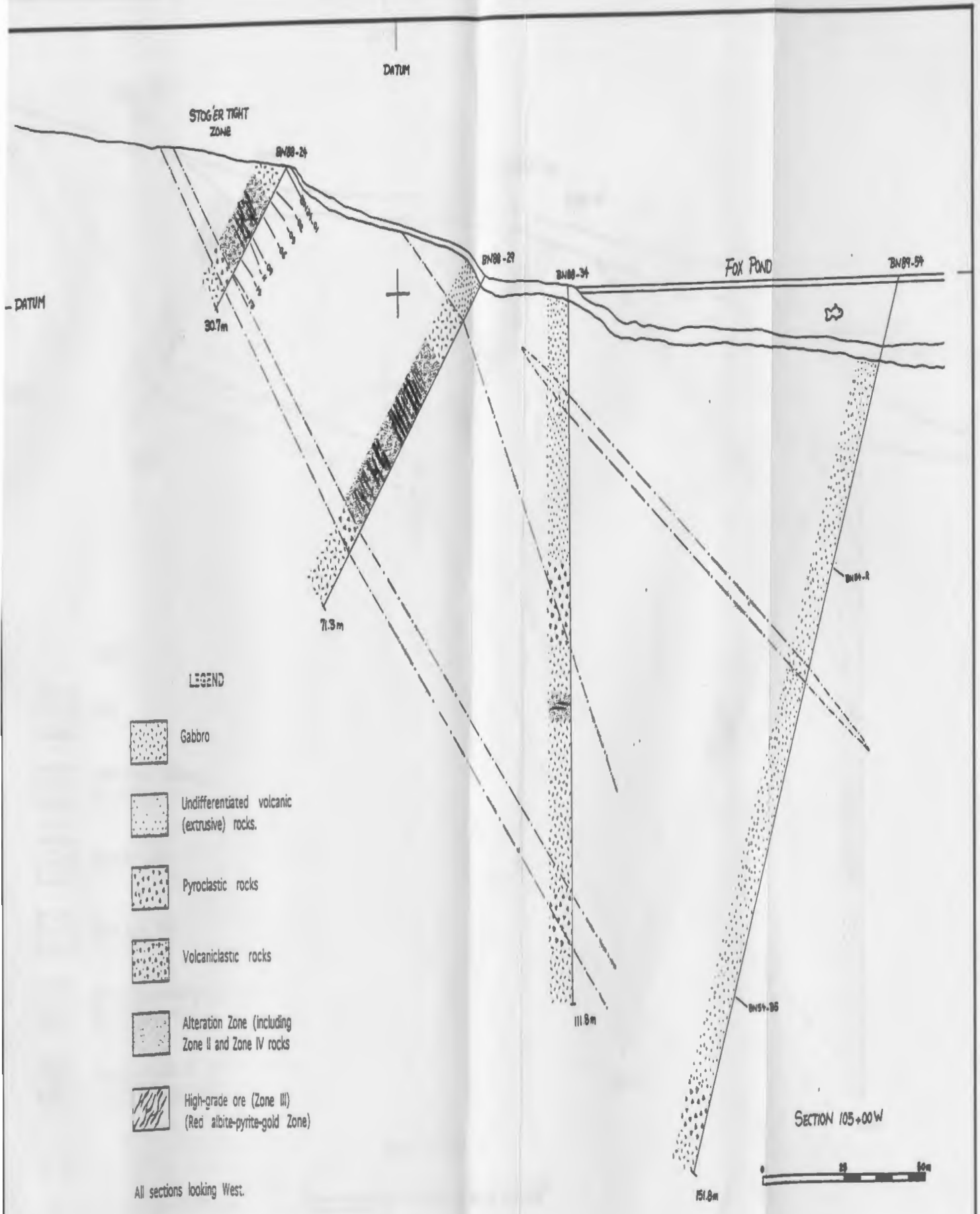
DATUM
STOG'ER TIGHT ZONE
BN88-24
BN88-29
BN88-34
FOX POND
BN89-54
DATUM
30.7m
71.3m
111.8m
151.8m
BN89-R
BN89-35
SECTION 105+00W
0
25
50m
LEGEND
Gabbro
Undifferentiated volcanic (extrusive) rocks.
Pyroclastic rocks
Volcaniclastic rocks
Alteration Zone (including Zone II and Zone IV rocks
High-grade ore (Zone III) (Red albite-pyrite-gold Zone)
All sections looking West.
Note that cross-sections have different scales.

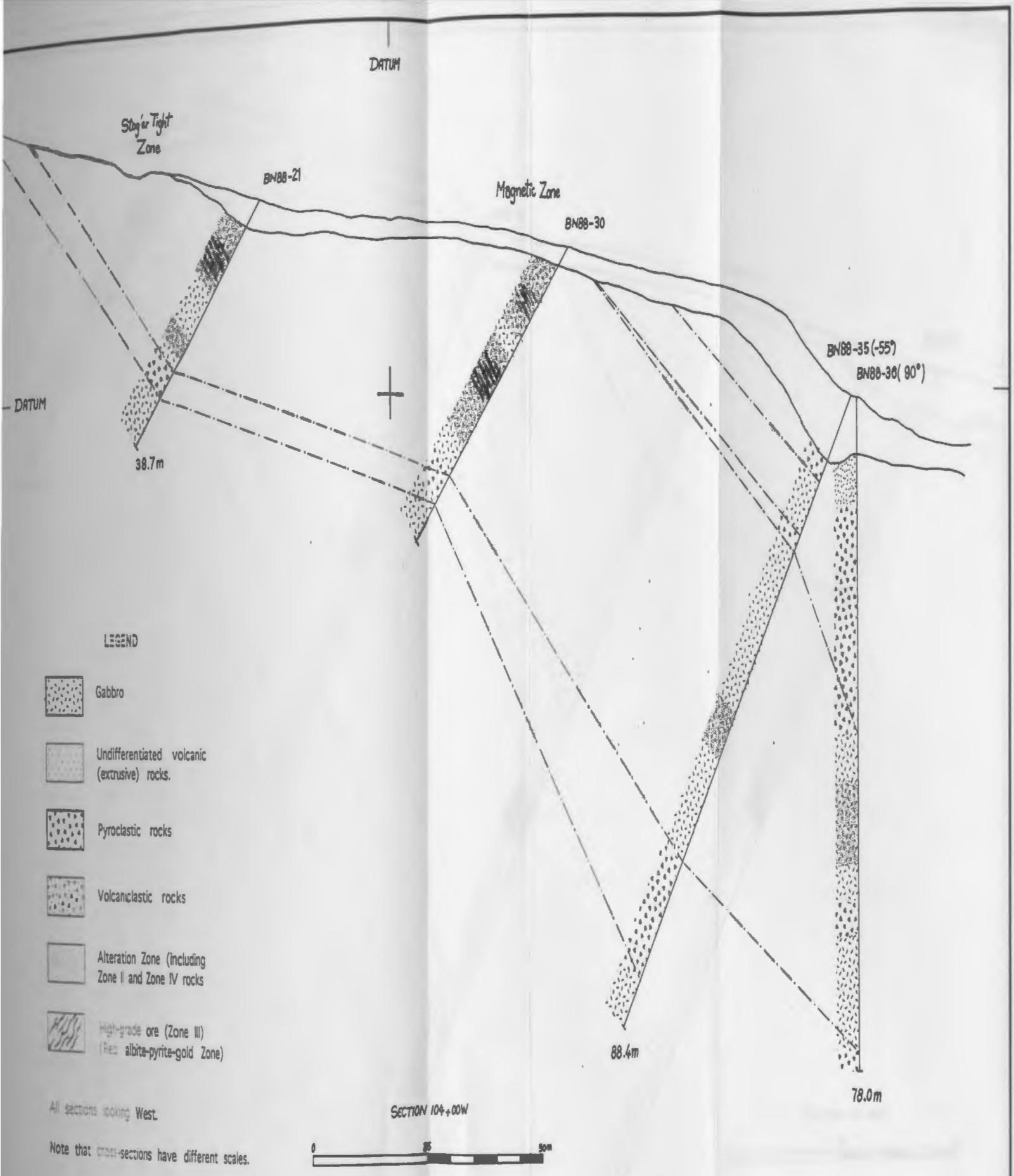
DATUM
Stag'er Tight Zone
BN88-21
Magnetic Zone
BN88-30
BN88-35(-55°)
BN88-36(90°)
DATUM
38.7m
88.4m
78.0m
LEGEND
Gabbro
Undifferentiated volcanic (extrusive) rocks.
Pyroclastic rocks
Volcaniclastic rocks
Alteration Zone (including Zone I and Zone IV rocks
High-grade ore (Zone III) (Fe albite-pyrite-gold Zone)
All sections looking West.
Note that cross-sections have different scales.
SECTION 104+00W
0
25
50m

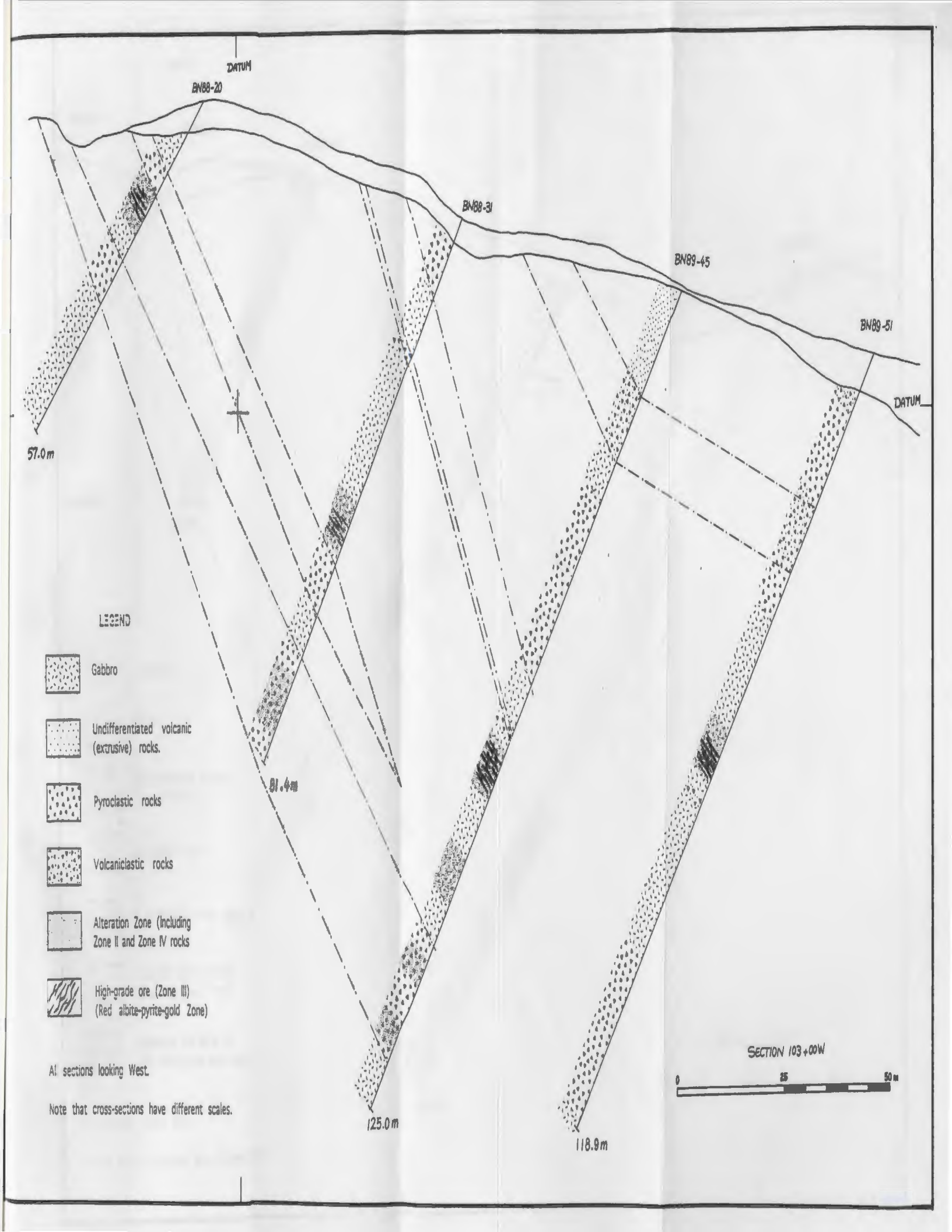
DATUM
BN88-20
BN88-31
BN89-45
BN89-51
DATUM
57.0m
81.4m
125.0m
118.9m
LEGEND
Gabbro
Undifferentiated volcanic (extrusive) rocks.
Pyroclastic rocks
Volcaniclastic rocks
Alteration Zone (Including Zone II and Zone IV rocks
High-grade ore (Zone III) (Red albite-pyrite-gold Zone)
All sections looking West.
Note that cross-sections have different scales.
SECTION 103+00W
0
25
50 m

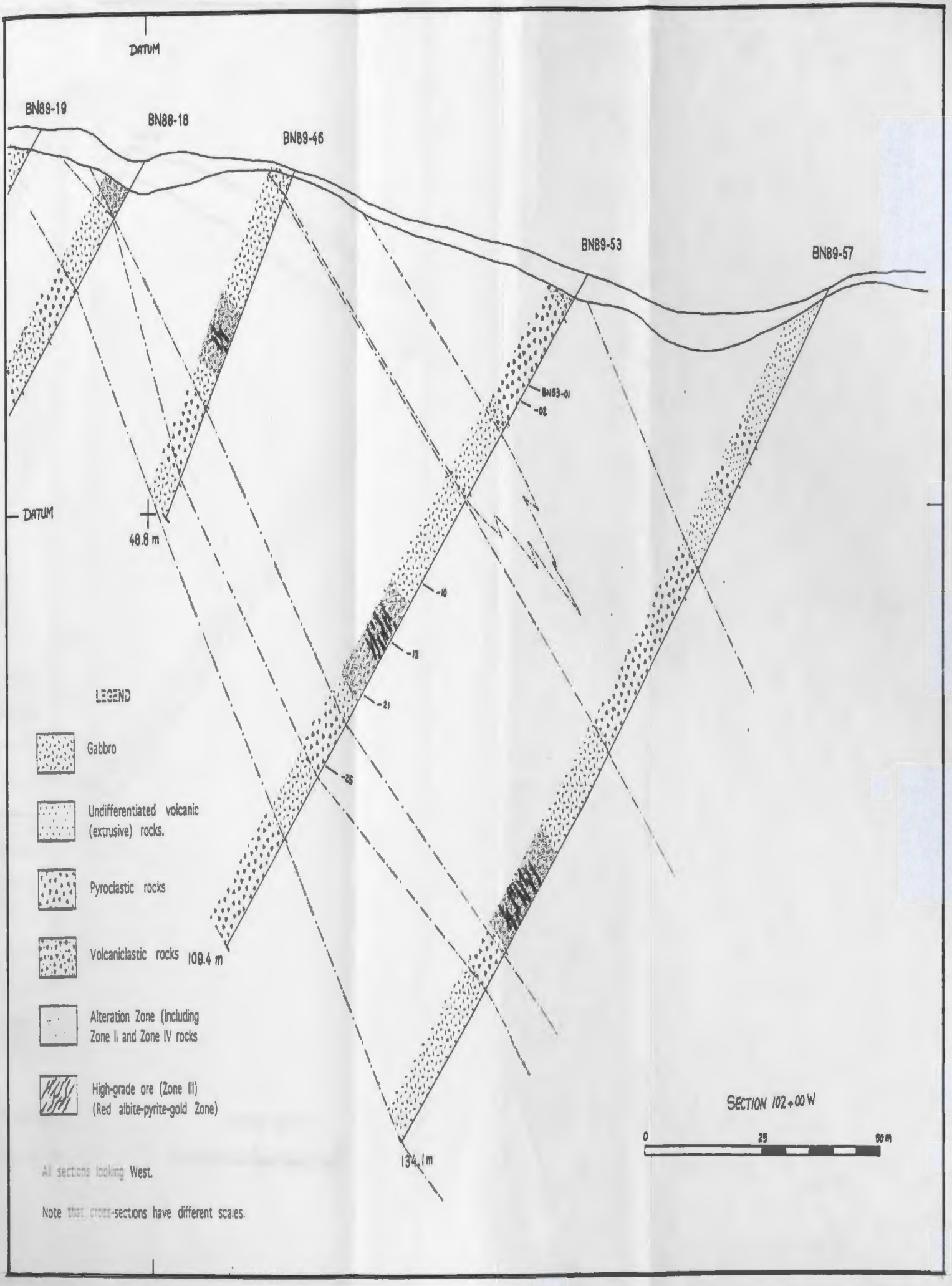
DATUM
BN89-19
BN88-18
BN89-46
BN89-53
BN89-57
BN53-01
-02
DATUM
48.8 m
-10
-18
-21
-25
109.4 m
134.1m
LEGEND
Gabbro
Undifferentiated volcanic (extrusive) rocks.
Pyroclastic rocks
Volcaniclastic rocks
Alteration Zone (including Zone II and Zone IV rocks
High-grade ore (Zone III) (Red albite-pyrite-gold Zone)
SECTION 102+00 W
0
25
50 m
All sections looking West.
Note that cross-sections have different scales.

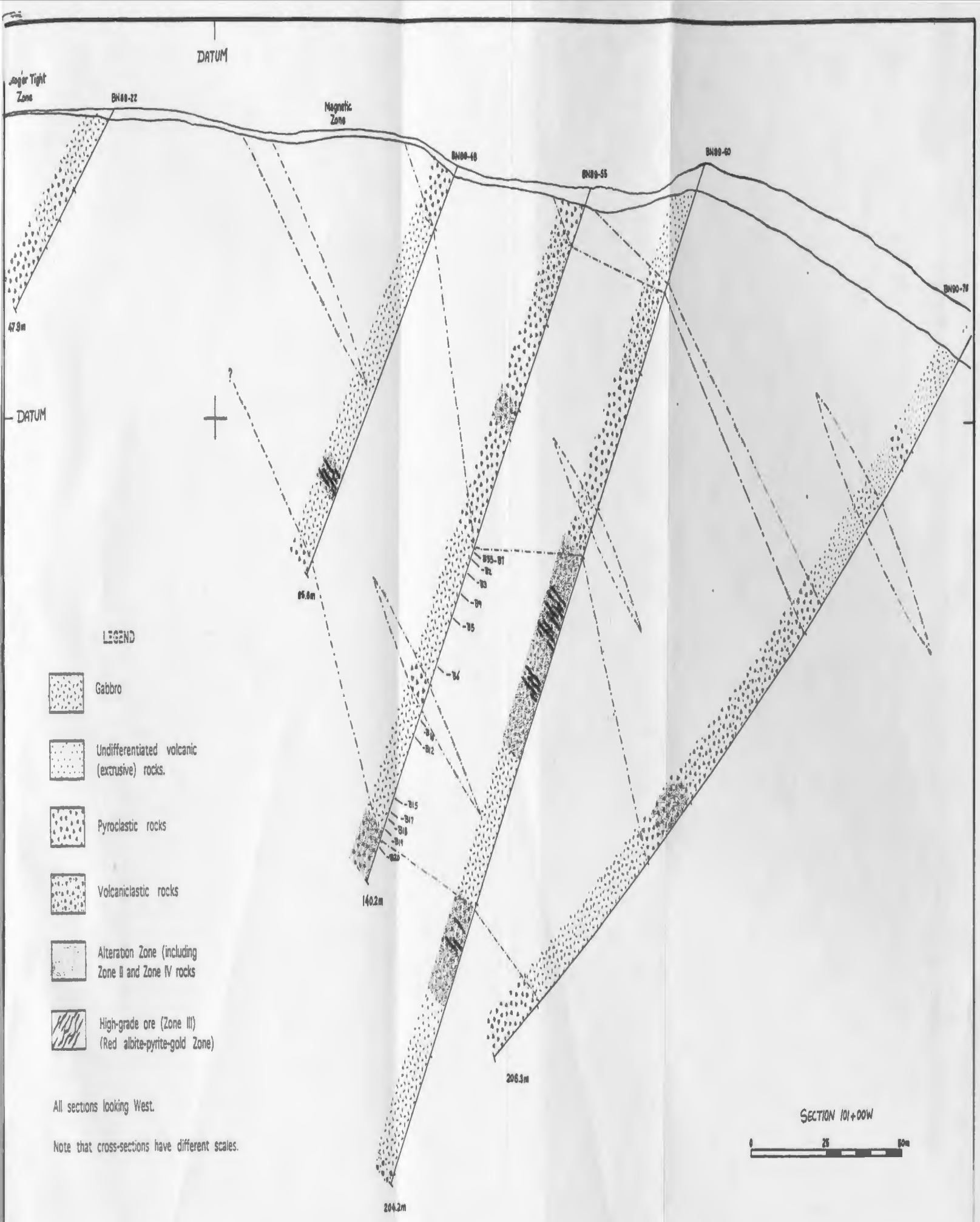
DATUM
Magnetic Zone
BN88-55
BN88-60
47.9m
DATUM
95.6m
140.2m
206.3m
204.2m
LEGEND
Gabbro
Undifferentiated volcanic (extrusive) rocks.
Pyroclastic rocks
Volcaniclastic rocks
Alteration Zone (including Zone II and Zone IV rocks
High-grade ore (Zone III) (Red albite-pyrite-gold Zone)
All sections looking West.
Note that cross-sections have different scales.
SECTION 101+00W
0
25
50m